Expanding Agromining to the Rare-Earth Elements : Key elements of success from a chemical engineering perspective

Bastien Jally

Thèse

Présentée et soutenue publiquement pour l'obtention du titre de

DOCTEUR DE L'UNIVERSITÉ DE LORRAINE

Mention: **GÉNIE DES PROCÉDÉS ET DES PRODUITS ET DES MOLÉCULES**

par **Bastien JALLY**

Expanding Agromining to the Rare-Earth Elements: Key elements of success from a chemical engineering perspective

Soutenance prévue le 22 février 2022

Membres du jury :

Mme Lucie COUDERT	Professeure, UQAT	Rapportrice
M. Laurent CASSAYRE	Directeur de recherche, CNRS	Rapporteur
Mme Isabelle BILLARD	Directrice de recherche, CNRS	Examinatrice
M. Alexandre CHAGNES	Professeur, Université de Lorraine	Examinateur, président du jury
M. Dominique HORBEZ	Docteur, Solvay	Examinateur
Mme Marie-Odile SIMONNOT	Professeure, Université de Lorraine	Directrice de thèse
M. Yetao TANG	Professeur, SYSU	Co-directeur de thèse
M. Baptiste LAUBIE	Maître de conférences (HDR), Université de Lorraine	Invité
M. Jean Louis MOREL	Professeur émérite, Université de Lorraine	Invité
M. Rongliang QIU	Professeur, SYSU	Invité

Acknowledgements

Ce document - fruit d'un long travail – est également l'occasion de remercier toutes les personnes qui ont contribué à la réussite de cette thèse. Je pense tout d'abord à ma directrice de thèse Marie-Odile Simonnot, dont le soutien a été indéfectible du début (et même avant), à la fin de ces travaux (et encore après). Son empathie combinée à son exigence m'a permis de réaliser un grand bond en avant, en tant que scientifique, mais aussi en tant que personne. Je pense également à mon co-directeur Yetao Tang, pour son soutien constant, sa gentillesse inconditionnelle et pour son accueil en Chine. Je remercie vivement Baptiste Laubie, pour son encadrement actif, son humour, son soutien, et ses conseils.

Réaliser une partie de son doctorat en Chine n'est pas une mince affaire, et cela n'aurait jamais été possible sans Jean Louis Morel pour un très grand nombre de raisons. Je tiens à le remercier pour m'avoir inclus dans ce Laboratoire International Associé, et ainsi bénéficier des toutes ces rencontres et expériences en Chine. Grand merci pour les nombreux conseils et le suivi. Et merci enfin pour les plantes.

Merci également au membres de mon jury de thèse pour leur relecture active du manuscrit, tout particulièrement Lucie Coudert et Laurent Cassayre comme rapporteurs, et Alexandre Chagnes et Isabelle Billard comme examinateurs. Et merci pour l'échange très constructif que nous avons eu, les perspectives discutées étaient fort enrichissantes. Je remercie également Dominique Horbez pour son suivi et sa vision industrielle précieuse. Merci aussi à Laurence Muhr qui a constitué mon comité de suivi avec bienveillance.

J'adresse aussi ma reconnaissance à toutes les personnes qui m'ont aidé et accueilli en Chine. Sans Meina je n'aurais jamais eu de visa. Sans Yanglaoshi, Hongxiang et Shichen, il n'aurait jamais été validé. Merci également à Qiu Rongliang, et Wang Shizhong pour leur accueil au LEPCRT. Je ne saurais remercier assez Wenshen Liu, pour les plantes certes, mais aussi les bons moments et les aventures sur le terrain qui ont égayé mon séjour. Merci à Wenshen, Meina et son mari qui ont organisé le rapatriement de mes affaires personnelles après qu'il ait fallu quitter le pays en urgence à cause de la pandémie. Merci enfin aux amis du bureau 612 pour votre accueil, le basket et les repas partagés.

Je remercie sincèrement les financeurs : le 111 project pour la partie chinoise, Carnot ICEEL pour le support, tout particulièrement le Labex Ressources 21, qui a permis de poursuivre la thèse dans des conditions très favorables alors que la pandémie présageait du contraire.

Merci également à Hermine Huot, pour tes nombreux conseils sur la vie en Chine, le fonctionnement du laboratoire, les conseils scientifiques aussi, et merci aussi pour ta gentillesse. Merci à Damien Blaudez pour les plantes cultivées en hydroponie.

Merci à ceux qui m'ont formé sur les appareils tout au long de mon parcours, en particulier Steve Pontvianne, mais aussi Emilien Girot, Sarah Bena et Philippe Arnoux. Merci pour votre patience, votre gentillesse et vos précieux savoirs. Merci aussi à Claire Hazotte pour l'enseignement des ficelles du métier alors que j'étais en stage. Et merci à Marie-Noëlle Pons et Emmanuel Mousset, j'étais ravi de travailler à vos côtés.

Merci à tous les collègues avec qui j'ai partagé d'excellent moments au laboratoire (ou pas loin). Je pense à mes prédécesseures sur l'agromine Mathilde G., Zeinab C., Romane T., et Dulce N. Je pense également à la grande chanteuse Pauline et la si sympathique Maia. Merci au BJC pour m'avoir accueilli comme membre actif. Pensée pour Mathilde F., Matteo et Stéphanie, on a bien rigolé. Merci à mes voisins de l'équipe SAFE, Olivier, Dominique, et Augustin et Léa pour la bonne humeur partagée au

coin café (ceci-dit, merci pour le café aussi !). Je remercie également les stagiaires qui ont croisé ma route dans ce bureau et qui ont partagé leur bonne humeur, Amandine, Claire S., Mathilde R. ; et plus récemment Gaétan et Aurélien. Un grand merci à Morgane pour m'avoir fait confiance dans l'encadrement de son stage. Merci aussi à Etienne, pour toutes ces interruptions, questions, et discussions scientifiques qui aiguisaient ma curiosité ravivaient ma motivation. Merci aux deux Thomas qui ont pris le relai de ce côté-là.

Je suis fier d'avoir eu comme compagnons de voyage doctoral Faidzul et Nicolas, fier d'avoir partagé de nombreux moments avec eux, de vrais coups durs comme des joies immenses et j'espère en partager d'autres par la suite. Merci aussi aux amies Chloé, Fanfan et Armande pour ces moments partagés à Nancy, dans les Vosges et en Albanie, qui ont marqué cette époque de ma vie.

Merci à tous ceux qui étaient là pour la soutenance et pour partager cette grande fête. Vous avez incontestablement fait mon bonheur.

Merci Betty, pour m'avoir fait confiance, redonné le sourire dans les moments les plus difficiles, pour avoir ri et pleuré ensemble, même éloignés de 9256 km, et fait de moi une meilleure personne.

Merci enfin à mes parents et ma grand-mère qui m'ont toujours soutenu inconditionnellement.

Table of contents

List of abbreviations

TR	Terre rare
LRGP	Laboratoire Réactions et Génie des Procédés
LSE	Laboratoire Sols et Environnement
LIEC	Laboratoire interdisciplinaire des environnements continentaux
GIEC	Groupe d'experts intergouvernemental sur l'évolution du climat
ANSH	Ammonium nickel sulfate hexahydrate
CFA	Coal fly ash
DoE	Design of experiment
DSP	Desilication product
DVB	Divinyl benzene
ECOLAND	Ecosystem Services provided by Contaminated Land
EDS	Energy dispersive spectroscopy
EDTA	Ethylenediaminetetraacetic acid
EU	European Union
FCC	Fluid-cracking catalyst
FTIR-ATR	Fourier transform infrared analysis, attenuated total reflectance
GHG	Greenhouse gas
GWP	Global warming potential
HA	Hyperaccumulator
HHV	Higher heating value
HREE	Heavy rare-earth element
IAC	Ionic adsorption clay
ICP-OES	Inductively-coupled plasma emission spectroscopy
IPCC	Intergovernmental Panel on Climate Change
IX	Ion-exchange
LCA	Life-cycle assessment
LD	Limit of detection
LHV	Lower heating value
LQ	Limit of quantification
LREE	Light rare-earth element
PE	Polyethylene
PTFE	Polytetrafluoroethylene
RE	Rare-earth
REE	Rare-earth element
REO	Rare-earth oxide
S/L	Solid-to-liquid (ratio)
SD	Standard deviation
SEM	Scanning electron microscopy
SX	Solvent extraction
TGA	Thermogravimetric analysis
US	United States
XRD	X-ray diffraction
XRF	X-ray fluorescence
HEDTA	Hydroxyethylethylenediaminetriacetic acid
DTPA	Diethylenetriaminepentaacetic acid
TBP	Tributyl phosphate

Table of contents

Résumé en français

Depuis un certain temps déjà, et en raison des avertissements, notamment du Groupe d'experts intergouvernemental sur l'évolution du climat (GIEC), de nombreux pays se mobilisent pour limiter l'augmentation de la température, et s'empresser d'atteindre la neutralité carbone.

Des objectifs tangibles ont été fixés : à l'été 2021, l'Union européenne (UE) s'est fixé comme objectif pour 2030 de réduire ses émissions de gaz à effet de serre (GES) de 55% par rapport à 1990 (programme " Fit for 55 "). À plus long terme, l'objectif neutralité carbone de l'UE est affiché pour 2050. Les autres grands pays ne sont pas en reste, la Chine a également fixé des objectifs importants au cours de l'automne 2021, comme le passage du pic des émissions de carbone avant 2030 et la neutralité carbone pour 2060.

Pour faire face à cet immense défi, de nouvelles technologies ont récemment vu le jour, permettant l'exploitation ou le stockage d'énergies renouvelables avec des émissions de CO_2 quasi nulles. Des éoliennes aux voitures électriques, des solutions prometteuses existent pour adapter nos modes de vie. Si ces technologies constituent une partie de la solution, elles exercent également une pression sur d'autres ressources non renouvelables.

Leur approvisionnement est conditionné par leur disponibilité, la présence d'installations d'extraction et de raffinage, et des aspects politico-économiques (par exemple, embargos, quotas). Certaines instances politiques ont proposé une liste de matières premières "critiques", qui ont une grande importance économique et présentent en même temps un risque d'approvisionnement insuffisant. Les États-Unis (depuis 2017), et plus récemment l'UE (2020), ont publié une liste de ces matières "critiques", parmi lesquelles figurent, en tête de liste, les terres rares (TR).

Les TR comprennent dix-sept éléments, les quinze lanthanides auxquels s'ajoutent l'yttrium (Y) et le scandium (Sc). Les technologies de la communication (écrans de smartphones, fibres optiques), mais aussi la défense et l'armement, désormais considérées comme essentielles, contribuent largement à la demande croissante en terres rares.

Ces éléments, malgré leur nom, ne sont pas rares, mais aujourd'hui, leur production mondiale est principalement localisée dans un seul pays, la Chine, qui elle-même utilise largement cette ressource. En outre, certaines TR sont particulièrement recherchées en raison de leurs propriétés. Par exemple, le dysprosium (Dy) est un additif quasiment irremplaçable pour maintenir la stabilité à température (>160 °C) des aimants à haute performance. Ces aimants sont présents dans les éoliennes et les véhicules électriques.

Actuellement, moins de 1% des TR est recyclé, car elles sont en très faibles concentrations et intimement mélangées à d'autres matrices, que ce soit dans les objets en fin de vie ou dans les déchets industriels, ce qui les rend difficiles à séparer et à valoriser. Les TR proviennent donc presque exclusivement de l'exploitation minière.

Cette demande a un coût. Leur extraction au cours des cinquante dernières années lègue un paysage morcelé, notamment dans le sud de la Chine. Désormais interdite, la pratique de l'excavation suivie de la lixiviation en tas, a laissé des centaines de kilomètres carrés de résidus miniers. Initialement des forêts tropicales, ces milieux dégradés sont soumis à une érosion intense. Le sol restant nu, les poussières s'envolent et se répandent dans les cours d'eau voisins, menaçant les écosystèmes et la santé humaine.

La biodiversité peine à se reconstituer. Le stockage naturel du carbone dans le sol, assuré par l'écosystème précédent, y est à l'arrêt (Figure 1).

Figure 1 : Zone de récolte des hyperaccumulateurs de TR, indiquée par le pointeur bleu. Elle se situe dans le comté de Dingnan, dans la province du Jiangxi. Crédit photo satellite : Google Earth, CNES / Airbus, 2018. Carte : Wikimédia Commons.

Dans un contexte où ces services écosystémiques sont plus que jamais indispensables, est apparue la volonté de refonctionnaliser ces sols délaissés. Des aides gouvernementales chinoises ont été déployées pour leur revégétalisation à grande échelle, et des programmes de recherche ont été lancés, visant à mieux comprendre ces écosystèmes dégradés et envisager leur restauration. Ces stériles miniers, pauvres en nutriments, sont peu propices à l'installation de plantes et l'utilisation, coûteuse, d'amendement est inévitable.

Pour pallier cela, une des clés de la réussite de cette restauration pourrait être le recours à des plantes adaptées localement, et présentant un intérêt économique. Par exemple, de la biomasse à vocation énergétique, apte à la production de fibres, ou encore, source de composés d'intérêt. Ainsi, les coûts de revégétalisation seraient compensés par la valeur économique produite en récoltant une partie des plantes.

L'agromine est une filière qui combine la culture de plantes hyperaccumulatrices et la récupération de métaux à partir de ces plantes. Elle peut jouer ici un rôle déterminant. En effet, les espèces *Dicranopteris linearis* (précédemment connue sous le nom de *Dicranopteris dichotoma*) et *Phytolacca americana*, sont deux espèces candidates identifiées pour cette filière (Figure 2). Ces deux espèces extraient les TR du sol et les concentrent dans leurs parties aériennes, jusqu'à des valeurs supérieures à celles caractéristiques des minerais exploités.

Figure 2 : La fougère *Dicranopteris linearis* (à gauche), et l'herbacée *Phytolacca americana* (à droite).

La récupération des TR, via des procédés (hydro)métallurgiques, permettrait alors de concrétiser la valeur économique de ces plantes. De plus, elle contribuerait partiellement à l'approvisionnement en TR, nécessaire au déploiement des technologies modernes. Elle s'inscrirait ainsi dans le contexte de l'économie circulaire.

La mise en œuvre de l'agromine des TR soulève de nombreuses questions scientifiques. En ce qui concerne les procédés de valorisation, il s'agit d'extraire les TR à partir des tissus végétaux, avec pour but de minimiser les coûts en réactifs et en énergie et d'avoir un impact le plus faible possible sur l'environnement.

Plus précisément, les questions auxquelles il faut répondre sont les suivantes :

- Comment rendre plus durables les procédés de valorisation des TR à partir de plantes hyperaccumulatrices ?
- Le traitement des cendres, plutôt que de la biomasse sèche, apporte-t-il plus de bénéfices que d'inconvénients ?
- Existe-t-il des critères applicables aux matières premières pour prédire l'applicabilité de l'agromine des TR ?
- Quels sont les points de vigilance à considérer dans les processus amont (sélection des espèces, culture) pour permettre/faciliter la récupération des éléments cibles en aval ?

Pour répondre à ces questions, ce travail de thèse a été réalisé dans le cadre du laboratoire international associé ECOLAND (Ecosystem Services provided by Contaminated Land), créé en 2015. Ce laboratoire commun est le résultat de relations établies entre le Laboratoire Sols et Environnement (LSE, Université de Lorraine-INRAE, UMR 1120) et le Laboratory of Environmental Pollution Control and Remediation Technologies (LEPCRT) de l'Université Sun Yat-sen de Guangzhou. ECOLAND implique également des membres d'autres laboratoires de l'Université de Lorraine, comme le Laboratoire Réactions et Génie des Procédés (LRGP, Université de Lorraine-CNRS, UMR 7274).

Ce travail de recherche a bénéficié du soutien financier de l'Université Sun Yat-sen, du Labex Ressources 21 et du projet Carnot ICEEL "REEcovery project" associant les membres du LSE, du LRGP et du LIEC (Laboratoire Interdisciplinaire des Environnements Continentaux, Université de Lorraine-

CNRS, UMR 7360). L'ambition de cette thèse est d'explorer la mise en œuvre de procédés innovants pour la récupération de ces éléments à partir de végétaux, et tout particulièrement des cendres.

Ses objectifs sont donc de:

- déterminer la faisabilité de l'agromine des TR, dans un contexte de restauration écologique des stériles miniers du sud de la Chine ;
- développer de nouveaux procédés de transformation qui prennent en compte les mécanismes limitants spécifiques aux minéraux bio sourcés ;
- minimiser la consommation de réactifs et d'énergie, afin d'obtenir les procédés les plus sobres.

Cette recherche est fondée sur l'acquisition de données scientifiques par l'expérimentation et le développement d'un procédé pyro/hydrométallurgique à l'échelle du laboratoire. Elle s'inscrit dans la continuité des travaux entrepris dans la thèse de Zeinab Chour (Université de Lorraine, décembre 2018).

La spécificité de la présente thèse porte sur l'approfondissement et l'optimisation du procédé de récupération des TR à partir des cendres de *D. linearis*. Elle comprend également l'étude d'une autre plante hyperaccumulatrice, *P. americana*, présentant des caractéristiques botaniques et physicochimiques différentes. En outre, elle comprend l'inventaire et l'extrapolation de la consommation de réactifs et des coûts associés, en vue d'une montée en échelle (échelle pilote).

Ainsi, au niveau applicatif, l'objectif de cette thèse est de donner une idée précise de la faisabilité de l'agromine des TR de manière quantitative en termes de procédés, et d'identifier en termes de composition du bio-ore les conditions de sa réussite.

Le premier chapitre propose un état de l'art sur les terres rares, les méthodes de production, et l'agromine. Il met en lumière les enjeux actuels et futurs et décrit la tension du marché mondial pour ces éléments. Les TR se distinguent par leurs propriétés magnétiques, optiques et électroniques uniques. Ces propriétés sont à l'origine de leur utilisation dans des technologies modernes et de pointes, concernant de nombreux secteurs à forts enjeux (énergie, communication, armement). Le marché est tourné vers la Chine, qui fournit plus 90% des besoins mondiaux depuis les années 2000, et ce malgré une demande toujours grandissante. A cela s'ajoute la faible occurrence de gisements concentrés, augmentant encore plus la tension sur ces éléments, désormais considérés comme « critiques ».

La métallurgie des TR repose principalement sur le traitement de trois minerais, traditionnellement excavés de mines à ciel ouvert: les fluorocarbonates de TR (bastnaésite), et les phosphates de TR (xénotime et monazite). Ces derniers sont plus riches en TR lourdes mais sont également porteurs d'éléments radioactifs (thorium, et dans une moindre mesure uranium). Les procédés actuels consistent à convertir les TR vers des formes solubles (par exemple craquage à la soude de la monazite, grillage à l'acide sulfurique d'un mélange des minerais), puis de les lixivier. Des étapes intermédiaires sont parfois nécessaires pour séparer les éléments radioactifs (Th, U), et des variations sont possibles en fonction des acides utilisés pour l'extraction, ou des éléments ciblés (par exemple, le cérium, Ce, est isolé rapidement via le procédé Molycorp).

Une partie importante de la production mondiale est également assurée via l'extraction des TR depuis les argiles ioniques, un type de gisement unique et spécifique du Sud de la Chine. Ici, les TR sont facilement extractibles par échange ionique. La circulation d'une solution saline (par ex., sulfate d'ammonium) suffit à lixivier les TR, qui sont ensuite précipitées sous forme de carbonate, permettant au passage le recyclage de la solution. L'excavation et la lixiviation en tas des minerais, étant désormais interdites, laissent place à la lixiviation in-situ.

Après l'étape d'extraction, et de mise en solution des TR, vient celle de la séparation et du raffinage. L'extraction liquide-liquide est aujourd'hui la voie la plus industrialisée, car elle permet l'opération en continu. Leur différence d'affinité pour les extractants - très faible du fait des propriétés chimiques très similaires des TR – est mise à profit pour leur séparation entre elles, via l'utilisation de centaines de cellules de mélange-décantation.

Il apparait que si les impacts des TR elles-mêmes sur l'environnement sont faibles (principalement du fait de leur faible mobilité, leur écotoxicité restant peu étudiée), les impacts des procédés d'extraction et de raffinage sont majeurs.

De nouveaux procédés visant l'exploitation de sources secondaires ont donc émergé à l'échelle du laboratoire, limitant partiellement ces impacts. En effet, le recyclage des produits en fin de vie, ou la valorisation des TR contenues dans des déchets industriels produits à très grande échelle (boues rouges, phosphogypse, cendres de centrales à charbon), ont émergé comme des solutions innovantes et susceptibles de contribuer à l'approvisionnement mondial. Ces procédés se confrontent à des matrices complexes où les éléments cibles sont dilués, et se cantonnent, pour l'heure, à la recherche académique.

L'agromine apparait comme une alternative prometteuse. Elle est une solution basée sur la nature, permettant la réalisation de nombreux services : végétalisation, production de biomasse, production de composés métalliques. Son évolution récente, et les derniers essais à l'échelle de plusieurs parcelles agricoles réparties dans le monde entier, attestent son caractère prometteur, d'ores et déjà pour le nickel.

La route est encore longue pour obtenir le même succès avec les TR. Cependant, les capacités d'accumulation des plantes *Dicranopteris linearis* et *Phytolacca americana* sont encourageantes. La voie reste à tracer, notamment concernant l'élaboration de procédés de valorisation des TR contenues dans leurs parties aériennes et l'évaluation de la viabilité de la filière.

Les outils et les approches, théoriques comme expérimentales, mises en œuvre dans cette thèse sont décrites dans le **deuxième chapitre**. L'analyse d'échantillons environnementaux (les deux plantes et leurs cendres) constitue une part majeure du travail réalisé. La chaine analytique commence avec le broyage de la biomasse, puis la minéralisation, qui est la mise en solution de l'intégralité des analytes par une digestion par de l'acide nitrique à pression et température par chauffage micro-onde. Enfin, l'analyse par spectroscopie d'émission de plasma à couplage inductif (ICP-OES) permet de mesurer la concentration des solutions. Pour les cendres, leur caractère réfractaire ne permet pas la digestion par l'acide nitrique. La fusion alcaline est alors conduite à très haute température en présence de fondants (sels alcalins), pour permettre leur solubilisation.

Ces travaux ont également recouru à l'analyse élémentaire du carbone, azote, hydrogène, oxygène, soufre, et chlore dans les solides par l'utilisation d'un analyseur multi-élémentaire. Diverses autres techniques classiques sont venues compléter la caractérisation des solides (analyse thermogravimétrique ATG, analyse infrarouge en réflectance totale atténuée FTIR-ATR).

Une palette d'outils est utilisée pour guider la production de données scientifiques, comme la méthode des plans d'expériences (Design Expert) ou la simulation d'équilibres chimiques en solution (JCHESS). La variété d'outils utilisés témoigne du caractère nouveau de la démarche, pour s'adapter au mieux, aux caractéristiques uniques des « bio-minerais » que sont les plantes et leurs cendres.

Enfin, les dispositifs expérimentaux classiquement utilisés en chimie minérale à l'échelle du laboratoire ont permis le développement et l'exploration d'un procédé de récupération des TR. Ces

équipements ont compris un four à moufle, des montages de chauffage à reflux, des dispositifs automatiques de contrôle et de réglage du pH (METTLER Toledo).

Au cours du troisième chapitre, les « bio-minerais » sont caractérisés de façon comparée, pour les deux espèces considérées : *D. linearis* et *P. americana*. Ces caractérisations mettent en lumière des propriétés différentes, voire opposées, des deux plantes.

La fougère *D. linearis* est très riche en silicium (Si) - ce qui n'est pas le cas de *P. americana* - ce qui confère à ses cendres une stabilité particulière, notamment face à l'attaque acide (en vue de l'extraction des TR). Le Si apparaît également problématique en termes de traitement hydrométallurgique : des problèmes de gélification, ralentissant les filtrations et encrassant les parois, peuvent survenir.

En dehors de cet aspect, *D. linearis* semble plus prometteuse que *P. americana*, du fait de sa teneur plus élevée en TR (au moins 2 $mg.g^{-1}$ contre environ 0.250 $mg.g^{-1}$ $\sum$TR). Sa capacité calorifique est comparable à celle du bois (19 $MJ.kg^{-1}$), ce qui est un atout majeur pour sa valorisation énergétique. En revanche l'herbacée *P. americana* présente une teneur élevée en chlore (Cl), soufre (S) et azote (N), potentiellement sources de gaz acides lors de sa combustion.

Dans les deux cas, la quantité d'aluminium (Al) présent est discutée. Cet élément forme un cation trivalent en solution, de la même manière que les TR. Il est donc généralement considéré comme une impureté plus ou moins préoccupante. Si les feuilles de *P. americana* sont moins concentrées en Al que les frondes de *D. linearis*, le ratio molaire Al/TR y est plus élevé, ce qui complique leur séparation.

Pour déterminer la meilleure plante candidate, les quantités de TR qu'il serait possible de produire à l'hectare doivent être prises en compte. Le rendement annuel en biomasse à l'hectare, fondé sur des données de littérature, combiné aux caractérisations physico-chimiques précédemment décrites, permettent d'estimer le rendement en métal en kilogrammes de TR produites annuellement par hectare. Pour *P. americana*, ce rendement atteindrait au mieux 3 $kg_{TR}.ha^{-1}.an^{-1}$, tandis que pour *D. linearis*, il atteindrait 12 $kg_{TR}.ha^{-1}.an^{-1}$.

Pour consolider l'ensemble, ces résultats sont convertis en termes de revenus économiques potentiels, en détaillant individuellement les prix de chaque TR. En effet, les deux plantes ont une répartition distincte en TR, et le prix de ces dernières varie sur plusieurs ordres de grandeurs. Du fait de sa forte teneur en néodyme (Nd) et en praséodyme (Pr), qui sont des éléments recherchés, la fougère se démarque favorablement une fois de plus, avec un revenu potentiel pouvant atteindre 385 $USD.ha.an^{-1}$ contre au mieux 130 $USD.ha.an^{-1}$ pour *P. americana*. Ces résultats, et les autres détaillés dans le chapitre, sont synthétisés dans un tableau, reproduit et traduit en français ici (Tableau 1).

Le quatrième chapitre s'attache à décrire l'élaboration d'un procédé de récupération des TR à partir des cendres de *D. linearis*, sur la base d'expérimentations à l'échelle du laboratoire. Ce procédé peut être découpé en trois grandes étapes : lixiviation alcaline des cendres, mise en solution des TR, puis isolation par précipitation (Figure 3).

Tableau 1: Synthèse des caractéristiques des bio-minerais considérés.

		D. linearis	***P. americana***
Production de biomasse	Caractéristiques	– Sauvage – Pionnière	– Domestique – Irrigation nécessaire
	Récolte	Tous les 2 ans	Bisannuelle
	Rendement annuel	3,00 $t.ha^{-1}.an^{-1}$	3,25 $t.ha^{-1}.an^{-1}$
Valeurs clés pour l'Agromine	[TR]	2,0 $mg.g^{-1}$ Jusqu'à 3,9 $mg.g^{-1}$	0,25 $mg.g^{-1}$ Jusqu'à 1,0 $mg.g^{-1}$
	Rendement en métal	6,0 $kg_{TR}.ha.an^{-1}$ Jusqu'à 11.7 $kg_{TR}.ha.an^{-1}$	0,8 $kg_{TR}.ha.an^{-1}$ Jusqu'à 3,4 $kg_{TR}.ha.an^{-1}$
	Revenus potentiels	200 $USD.ha.an^{-1}$ Jusqu'à 385 $USD.ha.an^{-1}$	30 $USD.ha.y^{-1}$ Jusqu'à 130 $USD.ha.an^{-1}$
Perspectives de procédé	Eléments cibles	Nd, Pr	Nd, Dy
	Combustion et valorisation de chaleur	– Faible teneur en Cl, N, S – Haute teneur en Pb – HHV *ca.* 19,3 $MJ.kg^{-1}$	– Haute teneur en Cl, N, S – Faible teneur en Pb – HHV *ca.* 18,3 $MJ.kg^{-1}$
	Cendres	Stables	Stables (550 °C) ou fondues et réactives (900 °C)
	Sous-produits possibles	Al	Mn

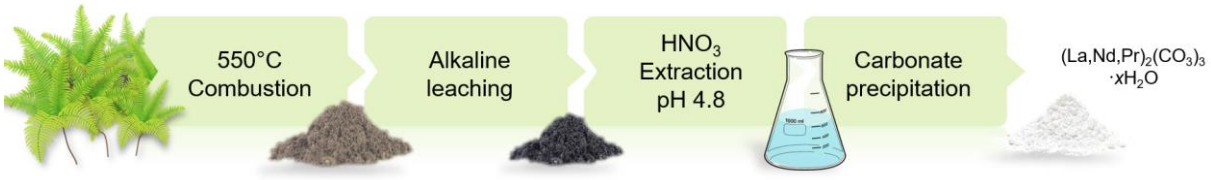

Figure 3 : Procédé de récupération des terres rares à partir des cendres de *D. linearis* développé dans cette thèse

La première étape de lixiviation alcaline permet la décomposition de la matrice alumino-silicatée vitreuse que constituent les cendres, et qui piège les TR. C'est également une étape de séparation car elle permet d'isoler jusqu'à 90 % de l'Al des cendres. Elle repose sur le fait que la silice (SiO_2), comme l'Al, sont solubles dans la soude concentrée. En revanche, les TR restent dans la phase solide et sont donc concentrées.

Différentes conditions opératoires sont explorées à l'aide de la méthode des plans d'expériences, en utilisant le logiciel Design Expert. Les meilleurs résultats sont obtenus pour les concentrations les plus

hautes en soude (jusqu'à 6 mol.L^{-1}), et les températures les plus élevées (90 °C). La durée d'extraction optimale est relativement courte (<10 min) dans les conditions opératoires testées.

Puis, les mécanismes limitant la solubilisation de l'Al sont étudiés, guidés par l'expérimentation et la simulation des équilibres thermodynamiques en solution. Au terme de ces études, il apparait que les cations alcalins comme le calcium (Ca), le magnésium (Mg) et le potassium (K), sont solubilisés puis reprécipitent sous forme d'aluminosilicates. La formation d'aluminosilicates de sodium n'est pas non plus à exclure. Il s'avère que dans l'industrie de l'aluminium, et particulièrement dans le cas du procédé Bayer, ces solides sont couramment appelés produits de désilication (desilication products, DSP).

Le rinçage des cendres traitées a également reçu une attention particulière, pour minimiser les quantités d'eau mises en jeu. Les produits de désilication étant très alcalins et partiellement solubles, ils engendrent une augmentation des quantités d'eau nécessaires au rinçage. Le rinçage est une étape importante car elle permet une neutralisation partielle du solide, destiné par la suite à une extraction en milieu acide.

Libérées de leur matrice vitreuse, les TR sont disponibles pour une étape d'extraction. Elle est conduite ici avec de l'acide nitrique. La méthodologie employée a pour objectif de solubiliser un maximum de TR sans mobiliser l'aluminium solide résiduel. L'extraction optimale est finalement conduite à pH modérément acide (*ca.* 4,7) à température ambiante (20 °C), durant 6 h.

Pour isoler les éléments cibles, à la solution porteuse des TR, on ajoute progressivement une solution de bicarbonate d'ammonium (de concentration 1 M). Les carbonates de TR sont alors précipités, et après maturation des suspensions à 40 °C durant 24 h, des rendements de précipitation supérieurs à 99 % sont obtenus. La stœchiométrie du précipité a été déterminée comme étant $Ln_2(CO_3)_3 \cdot 2{,}1\ H_2O$ (avec Ln représentant un élément TR). L'analyse des impuretés après dissolution des carbonates dans un acide de très haute pureté (acide nitrique, qualité Optima ®), révèle une pureté en carbonate de TR supérieure à au moins 99,5% pour tous les précipités produits. L'impureté principale est l'Al, ce qui vient conforter la stratégie de séparation de cet élément.

Enfin, des améliorations pour réduire les quantités de réactifs consommés sont mises en place. Une attention particulière est portée à la soude utilisée pour la lixiviation alcaline des cendres. L'augmentation du ratio solide-liquide permet d'en diminuer la consommation. La contrepartie est un rendement d'extraction de l'Al plus faible, et une consommation d'acide plus importante lors de l'étape d'extraction des TR. Le pH d'extraction joue également un rôle majeur concernant la qualité des précipités finaux : un pH légèrement inférieur à 4,6 implique une augmentation mesurable de la quantité d'impureté.

L'ensemble de ces résultats expérimentaux sont mis à contribution lors du **cinquième chapitre.** L'étude de la viabilité de la filière agromine appliquée aux TR, est envisagée sur la base des précédentes données expérimentales produites lors de cette thèse ainsi que de la thèse de Z. Chour. Des données de la littérature et des données économiques viennent compléter l'argumentaire. Il s'agit dans ce chapitre de projeter à l'échelle de la parcelle (1 ha), la production annuelle en TR à partir de *D. linearis* (soit 3 000 kg.an^{-1}).

Deux procédés sont envisagés : le procédé de lixiviation par l'acide sulfurique des frondes broyées, suivi d'une précipitation d'oxalate de TR (procédé SULF) (issu des travaux de thèse de Zeinab Chour) ; et le procédé basé sur les cendres, précédemment décrit (procédé ASH).

L'établissement des bilans matières des deux procédés, illustrés par des diagrammes de flux met en lumière de nouvelles améliorations possibles. Les principales améliorations doivent permettre le recyclage des solutions et des réactifs en excès (acide sulfurique, carbonate d'ammonium, oxalate). L'éventuelle utilisation des solides résiduels (déchets) est également considérée. Enfin plusieurs substitutions de réactifs sont à envisager pour diminuer les coûts (*e.g.*, remplacer l'acide nitrique par de l'acide sulfurique dans le procédé ASH).

La mise en équation de ces procédés, et leur version améliorée (ASH2 et SULF2) permet d'évaluer leurs coûts de fonctionnement, et le chiffre d'affaire possible, en se plaçant dans un contexte économique chinois. Grâce à la valorisation de la chaleur produite lors de la combustion de la fougère, le procédé ASH est le plus rentable. En revanche, le procédé SULF est moins coûteux mais génère moins de revenus.

La rentabilité des deux procédés dépend d'un paramètre crucial : la concentration en TR dans les frondes (Figure 4). Pour des valeurs de concentrations en TR totales en dessous de 2.1 $mg.g^{-1}$ dans les parties aériennes, les procédés de récupération décrits ici seront déficitaires. L'établissement de cette valeur permet de mieux guider la sélection de plantes à l'échelle du terrain, en vue de leur valorisation par des procédés métallurgiques.

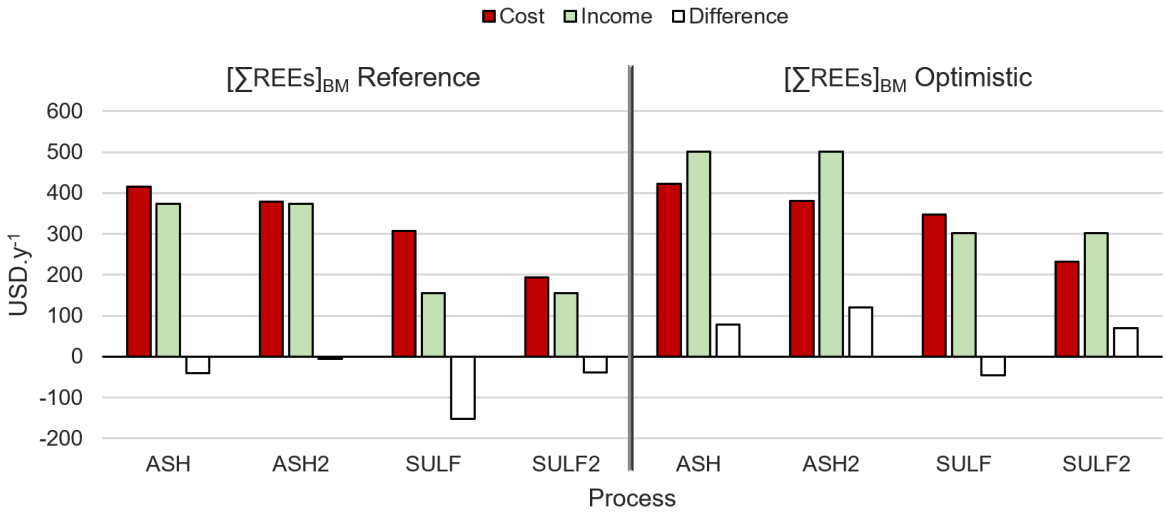

Figure 4: Coûts (cost), revenus (income), et différence en $USD.an^{-1}$ des différents procédés décrits dans le chapitre 5, pour deux concentrations en TR dans les parties aériennes. A gauche (Reference), $[TR]_{frondes}$ = 2 $mg.g^{-1}$, et à droite (Optimistic) $[TR]_{frondes}$ = 3.9 $mg.g^{-1}$.

Des valeurs de concentrations encore supérieures (jusqu'à 7 $mg.g^{-1}$ ∑TR, dans les frondes), sont rapportées dans la littérature. Bien que peu courantes, elles sont encourageantes et prometteuses. Sur la base de l'expérience de l'agromine du nickel, la mise en place de pratiques agronomiques à l'échelle de la parcelle est pressentie pour augmenter les quantités de TR produites à l'hectare.

Les objectifs de la thèse, fixés dans l'introduction ont été atteints. Tout d'abord, l'exploitation agricole des TR dans un contexte de restauration des résidus miniers a été déterminée comme étant plus que faisable, puisque des profits émergent de la production des composés. La combustion de la biomasse pour récupérer l'énergie, est cruciale pour maximiser les profits, et minimiser les déchets produits.

Un nouveau procédé de transformation a été conçu, qui tient compte de la spécificité des cendres de la biomasse. Le procédé développé permet de surmonter la stabilité de la matrice vitreuse aluminosilicatée et de produire un composé commercialisable de haute pureté (>99,5 %).

En même temps, la diminution des réactifs nécessaires a été mise en pratique, et des améliorations supplémentaires ont été identifiées pour l'échelle pilote. Les procédés développés antérieurement n'ont pas été négligés, puisque le procédé SULF a été évalué en termes de déchets produits par unité de produit (facteur E) et de viabilité économique.

Les questions scientifiques établies pour ce travail ont trouvé une réponse. Un nouveau procédé a été conçu, par une approche expérimentale. Une approche par bilans massiques, combinée à une étude économique, a permis de rendre deux procédés de récupération plus efficaces et d'évaluer les conditions nécessaires à leur soutenabilité.

La stabilité des cendres de *D. linearis* est apparue initialement comme un obstacle à la récupération des TR. Cependant, l'intégration de la récupération de chaleur, en combinaison avec la production d'un composé de haute pureté, en fait un procédé plus efficient (facteur E plus faible) et plus économique que le traitement de la biomasse sèche par l'acide sulfurique.

Pour les procédés sélectionnés, la concentration en TR des plantes est apparue comme le critère le plus crucial, dictant la viabilité. Une concentration minimale a été établie à environ 2,1 $mg.g^{-1}$ ∑TR. Ce critère pourrait être revu, en fonction de la matière première à traiter, car il repose sur une répartition en TR typique pour *D. linearis*. Le critère serait par exemple plus élevé si des éléments moins onéreux constituaient la majeure partie du contenu en TR (par exemple, La, Ce, Y). Pour *D. linearis*, il fournit une valeur guide pour sélectionner les individus, et orienter les pratiques agronomiques vers un objectif tangible.

Cette valeur constitue un premier point de vigilance, mais un second point de vigilance a été identifié. Si possible, les espèces candidates hyperaccumulatrices doivent éviter de co-accumuler de l'Al dans leurs parties aériennes. La consommation de réactifs (soude) et la pureté du produit final sont en jeu. La prise en compte du rapport molaire Al/TR est un nouveau critère qui pourrait changer la donne concernant la recherche de nouvelles espèces candidates.

De cette thèse, il ressort que le procédé mis en œuvre pour la valorisation des TR depuis les cendres *D. linearis* est non seulement possible, mais aussi très certainement rentable. Une attention particulière doit être portée cependant, à la réduction des réactifs utilisés et à la minimisation des déchets, notamment dans un contexte où l'industrie minérale a laissé des marques visibles sur l'environnement.

Introduction

Humanity has entered an era of major ecological and energy transitions. It is facing major difficulties, the most obvious consequences of which are climate change and the collapse of biodiversity.

Since the industrial revolution of the 19th century, man has used more and more energy from fossil resources. He has thus built a comfortable lifestyle, to which everyone aspires. This consumption of fossil energy results in a decrease of resources, and an increasing need for energy to exploit resources that are more and more difficult to reach. In addition, the release of greenhouse gases (GHG) into the atmosphere, of which CO_2 is certainly the best known, although not the only one, leads to the acidification of waters and soils, as well as to global warming.

For a while now, and because of the warnings, notably from the Intergovernmental Panel on Climate Change (IPCC), many countries have been mobilizing to limit the increase in temperature, and recommend reaching net zero CO_2 emissions, both in industrial production and in households, with heating and transport.

Tangible targets have been established: in the summer 2021, the European Union (EU) set as a goal for 2030 to reduce its emissions of GHG by 55% compared to 1990 (“Fit for 55” plan). In the long term, the goal of EU of net zero emissions is set for 2050. China has also recently (fall 2021) set important goals, such as peaking carbon emissions before 2030, and reaching carbon neutrality by 2060.

To face this immense challenge, new technologies have recently emerged, allowing the exploitation or storage of renewable energies with almost no CO_2 emissions. From wind turbines to electric cars, promising solutions exist to adapt our lifestyles. While these technologies are part of the solution, they also add pressure on other non-renewable resources.

The supply of these resources is conditioned by their availability, the presence of extraction and refining facilities, and politico-economic aspects (*e.g.*, embargos, quotas). Policy makers around the world proposed a list of “critical” raw materials, which are of highly economic importance and at the same time, presenting a risk of insufficient supply. The United States (since 2017), and more recently the EU (2020), published a list of these “critical” materials, among which figure, at the top of list, the rare-earth elements (REEs).

These are 17 elements, constituted of the 15 lanthanides in addition to yttrium (Y) and scandium (Sc). Communication technologies (smartphone screens, optical fibers), but also defense and armament, now considered essential, greatly contribute to the increasing demand for REEs.

These elements, despite their name, are not all rare, but currently, the production is mainly located in one country, China, which itself uses this resource extensively. In addition, some REEs are in particular demand because of their properties. For example, dysprosium (Dy) is a mandatory and almost irreplaceable additive to maintain the stability of high-strength magnets at temperatures (present in wind turbines and electric vehicles).

At present, less than 1% of rare earths (RE) are recycled, because they are found in very low concentrations and intimately mixed with other matrices, whether in end-of-life objects or in industrial waste, which makes them very difficult to separate and recover. Rare-earths therefore come almost entirely from mining.

Such demand comes at a cost. Their extraction over the last 50 years has left behind a fragmented landscape, particularly in South China. Now forbidden, the practice of excavation followed by heap leaching has left hundreds of square kilometers of mine tailings. Initially tropical forests, these degraded environments are subject to intense erosion. As the soil remains bare, the dust flies and spreads to nearby waterways, threatening ecosystems and health. Biodiversity struggles to re-establish itself. The natural storage of carbon in the soil, provided by the previous ecosystem, is halted.

In a context where these ecosystem services are more indispensable than ever, the will to refunctionalize these degraded soils has emerged, using nature-based solutions. The restoration of these environments by planting vegetation offers many benefits, such as the development of biodiversity, carbon storage, regulation of water flows, limitation of pollutant runoff into waterways, *etc.*, not to mention landscape improvement. Chinese government support has been deployed for their massive revegetation, and research programs have emerged to better understand these damaged ecosystems and plan their restoration.

However, given the low fertility of these former mining areas, revegetation requires a lot of effort, and one of the keys to the success of this restoration could be the use of locally adapted and economically interesting plants. Thus, the costs of revegetation would be compensated by the economic value produced by harvesting part of the plants. Possible solutions include the cultivation of plants for energy, plants to produce fibers, and plants to recover REEs from the tailings.

The latter option involves agromining: a phytotechnology designed to recover metals using plants. Agromining is defined as the combination of the cultivation of hyperaccumulator plants (HA) and the recovery of metals from these plants. In this context, agromining appears as a promising solution. The species *Dicranopteris linearis* (previously known as *Dicranopteris dichotoma*) and *Phytolacca americana*, are REE hyperaccumulator plants that grow spontaneously on these residues, and appear as potentially interesting candidates for this process. The recovery of the REEs from these plants via hydrometallurgical processes, would then concretize the economic value of these plants. In addition, it would partially contribute to the supply of these critical elements, necessary for the deployment of modern technologies. Thus, RE agromining could be a means of giving value to unused residues, which is in line with a circular economy logic.

The implementation of RE agromining raises many scientific questions. The first part concerns soils and plants, in order to better understand the parameters that govern soil fertility, the mechanisms of transfer of RE to plants, the transport and storage of these elements in plant tissues, and the role of microorganisms. It will then develop agronomic processes to achieve high yields of plants and RE. These issues are addressed by specialists in soil science, plant science, and agronomic processes. The second part deals with processes to extract RE from plant tissues, with the aim of minimizing material and energy costs and having the lowest possible impact on the environment.

More precisely, for this second part, the questions to be answered are:

- How to render the recovery processes of REEs from hyperaccumulating plants sustainable?
- Are there more advantages than disadvantages to processing ash rather than dry biomass ?
- Are there criteria applicable to raw materials to predict the applicability of RE agromining?
- What are the vigilance points to be considered in the upstream processes (species selection, cultivation) to allow/facilitate the recovery of target elements downstream?

To answer these questions, this thesis work was carried out in the framework of a perennial partnership, which is the joint laboratory ECOLAND (Ecosystem Services provided by Contaminated Land), created in 2015. This joint laboratory is the result of relationships established between the Laboratoire Sols et Environnement (LSE, Université de Lorraine-INRAE, UMR 1120) and the Laboratory of Environmental Pollution Control and Remediation Technologies (LEPCRT) of the Sun Yat-sen University of Guangzhou. ECOLAND also involves members of other laboratories at the University of Lorraine, such as the Laboratoire Réactions et Génie des Procédés (LRGP, Université de Lorraine-CNRS, UMR 7274). This research work has benefited from the financial support of Sun Yat-sen University, of Labex Ressources 21 and of Carnot ICEEL "REEcovery project" associating members of LSE, LRGP and LIEC (Laboratoire Interdisciplinaire des Environnements Continentaux, Université de Lorraine-CNRS, UMR 7360). The research work was planned to take place in four 9-month periods, alternating between the LRGP in Nancy and the LPCRT in Guangzhou. Due to the pandemic, most of it had to take place at the LRGP, and only a six-month period in Canton (September 2019 to January 2020) was possible.

The main objective of this thesis is to explore the implementation of innovative processes for the recovery of these elements from plants, and particularly from ashes.

Its specific objectives are therefore:

- to determine the feasibility of RE agromining, in the context of the restoration of mine tailings in South China;
- to develop new transformation processes that consider the limiting mechanisms specific to bio sourced minerals;
- to minimize the consumption of reagents and energy, to achieve the most efficient processes.

This research is based on the acquisition of scientific data through experimentation and the development of a pyro/hydrometallurgical process on a laboratory scale. It is a continuation of the work undertaken in the thesis of Zeinab Chour (University of Lorraine, December 2018).

The specificity of the present thesis focuses on deepening and optimizing the REE recovery process from the ash of *D. linearis*. It also includes the study of another hyperaccumulator plant, *P. americana*, with different botanical and physicochemical characteristics. Additionally, it will comprise the inventory and the extrapolation of the consumption of reagents and the associated costs, in view of a scale-up (pilot scale).

Thus, at the application level, the objective of this thesis is to give a precise idea of the feasibility of RE agromining in a quantitative way in terms of processes, and to identify in terms of bio-ore composition the conditions for its success.

This manuscript is organized in five chapters.

- Chapter 1: a review of the literature concerning the targeted elements: REEs. It is intended to be general in order to understand the current and future issues specific to these elements whose exploitation is relatively recent. The current transformation processes of conventional ores are described, as well as the processes currently under development for alternative sources.

- Chapter 2: the description of the equipment and methods used during this work, as well as the calculation tools and experimental setups.

- Chapter 3: the physico-chemical characterization of the bio-minerals (ash and biomass of the two HAs) is described in a perspective of exploitation. It is thus naturally completed by calculations to predict the quantity of REEs that it would be possible to obtain per hectare per year (metal yield). In the perspective of a chemical transformation, as well as in that of their agricultural exploitation, the two bio-minerals are compared.

- Chapter 4: the process of recovery of REEs from *D. linearis* ashes. The limiting physico-chemical mechanisms are investigated. The reduction of the use of reagents, and its influence on the final product are discussed on the basis of experimental data.

- Chapter 5: the study of the technical and economic feasibility of the two most promising processes. It gathers the establishment of material balances, the costs associated with the processes, the improvements to be implemented on a larger scale. On the basis of a minimal sensitivity study, it establishes a criterion on the minimal concentration of REEs in the plants.

Chapter 1:
Literature review

This chapter provides the reader with the fundamental properties of the rare-earth elements (REEs) and their application. The challenges at stake regarding global production and demand are discussed, as well as the production processes. Finally, the reader is introduced to the principles of agromining, and how it could be applied to the REEs.

1.1 The Rare Earth Elements (REEs)

1.1.1 Definition and properties

The Rare Earth Elements (REEs) are the 15 lanthanide elements of the periodical table of elements, as well as the elements Sc and Y (Table 2) (Leveque and Maestro, 1993).

The element promethium (Pm) does not have a stable isotope and is therefore not often listed in the REEs. Thus, in this thesis, we'll define the REEs as 16 elements. Being in a close group of the periodic table, they form a homogeneous group of elements with similar chemical and physical properties. Two types of distinctions are often found in literature, the first being between light (LREEs) and heavy REEs (HREEs). The LREEs are La, to Nd, while HREEs are Sm to Lu with the addition of Y.

Table 2: The Rare Earth Elements (Leveque and Maestro, 1993)

Element symbol	Element Name	Atomic Number	Atomic mass ($g.mol^{-1}$)
Sc	Scandium	21	44.96
Y	Yttrium	39	88.91
La	Lanthanum	57	138.91
Ce	Cerium	58	140.12
Pr	Praseodymium	59	140.91
Nd	Neodymium	60	144.24
Pm*	Promethium	61	(145)
Sm	Samarium	62	150.35
Eu	Europium	63	151.96
Gd	Gadolinium	64	157.25
Tb	Terbium	65	158.92
Dy	Dysprosium	66	162.50
Ho	Holmium	67	164.93
Er	Erbium	68	167.26
Tm	Thulium	69	168.93
Yb	Ytterbium	70	173.04
Lu	Lutetium	71	174.97

* Does not have any stable isotope

The chemical similarities among the series are mainly due to the unsaturated 4*f* and 5d^1 electron shells and the saturated 6s^2 shell. This particular structure enables unique electronic transitions that are characterized by narrow absorption and emission bands, as well as by a strong magnetic moment. These properties are used in numerous applications in optics and electronics (Leveque and Maestro, 1993). Yttrium (Y: [Kr] 4d^1 5s^2) and scandium (Sc: [Ar] 3d^1 4s^2) possess similar electron shell structures, and hence chemical properties, and are thus included in REEs.

Because of their abundance in the Earth's crust, REEs are not the rarest elements (Leveque and Maestro, 1993). Ce is the most abundant of the REEs and the abundancy decreases along the sawtooth profile along the atomic number, with Lu being the scarcest.

The sawtooth profile (Figure 5, Figure 6) is due to the Oddo-Harkins rule: elements with an even atomic number (*e.g.*, cerium: element 58) are more abundant than elements with the adjacent larger and smaller odd atomic numbers (La, element 57 and Pr, element 59) (Harkins, 1917; Oddo, 1914).

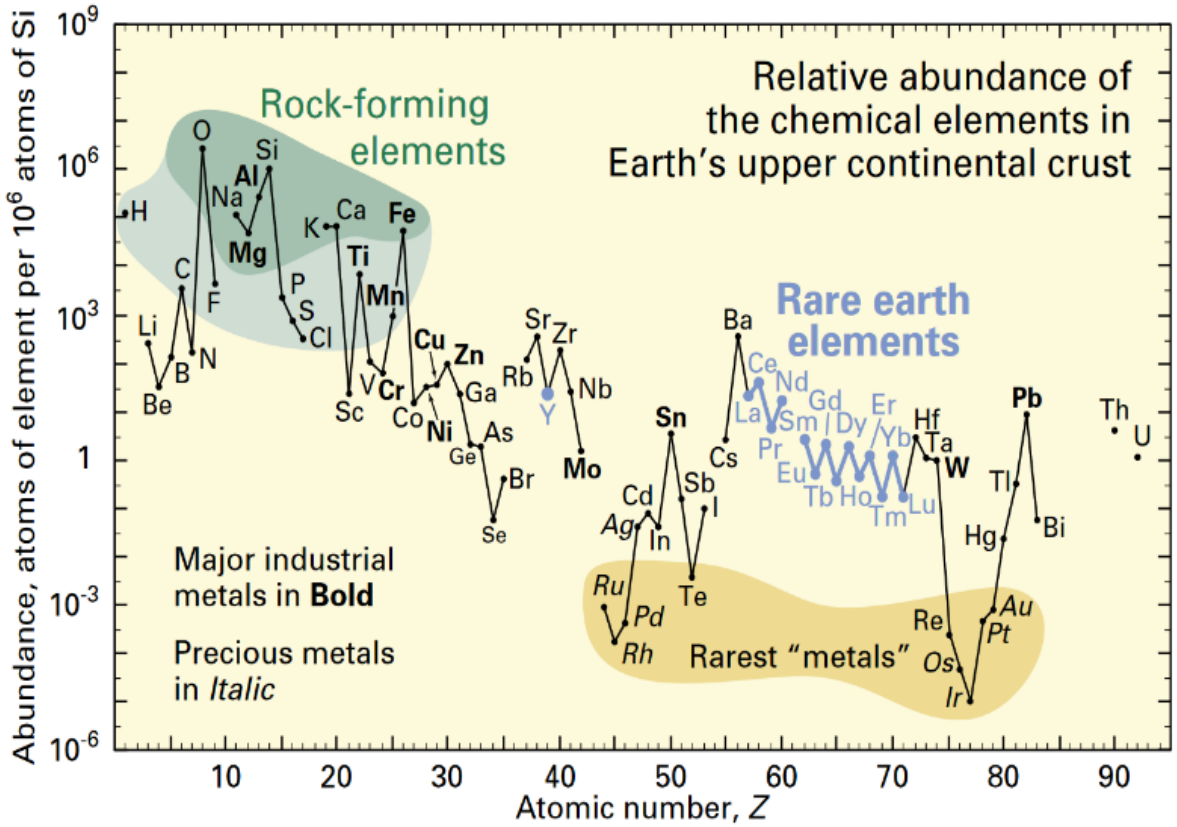

Figure 5: Relative abundance of the chemical elements in the Earth's upper continental crust (Haxel *et al.*, 2002)

This systematic variation often leads authors to normalize REE concentrations in environmental samples with the concentrations found in standard samples (*e.g.*, standard chondrite, meteoritic rocks, Post Archean Australian Shale) (Bea, 2015). Normalization smoothens the RE concentration diagrams (Figure 6B).

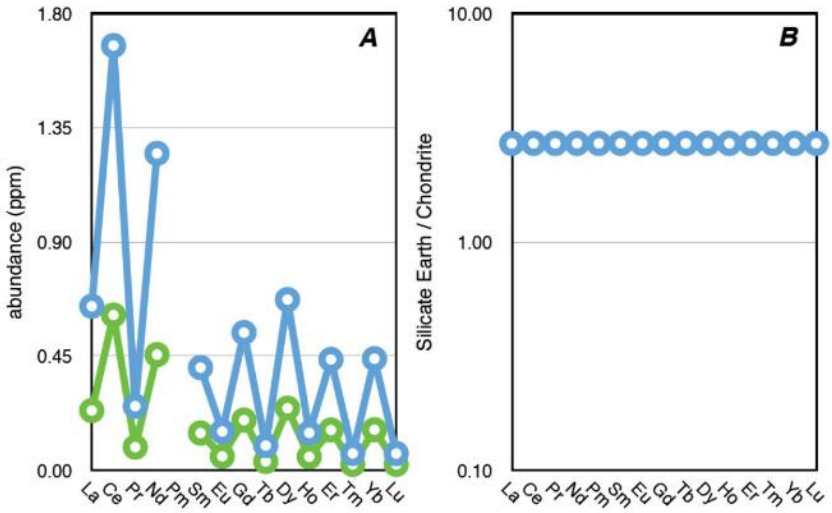

Figure 6: A) Absolute REE abundances in C1-chondrites (green) and Silicate Earth (blue). Note the sawtooth profile due to the Oddo-Harkins Rule. B) Normalization to chondrites smoothens the graph which is now horizontal at a constant of 2.7 x chondrite (Bea, 2015)

Regarding the physical properties of these metals, they are poor electrical conductors but exhibit superconductivity at low temperatures (below 30 K). In fact, metallic La is reportedly one of the best elemental superconductors like lead and niobium (Gupta and Krishnamurthy, 2005).

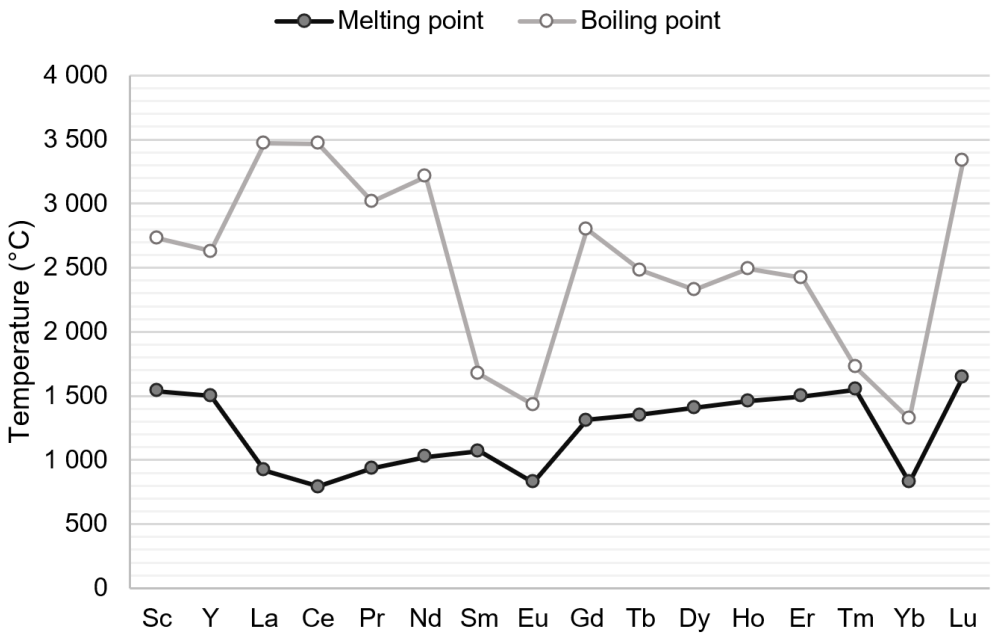

Figure 7: Boiling and melting points of RE metals

Their melting and boiling points are displayed in Figure 7. The boiling points show no trend along the series and are relatively variable, whereas the melting points increase along the series, except for Eu and Yb. The production of RE metals involves the use of RE chlorides for the electrolytic reduction of lower melting point elements (La, Ce) and fluorides for the reduction of heavier RE such as Gd or Y (Chour, 2018; Gschneidnerjr and Daane, 1988). Metals with a higher melting point cannot be reduced electrolytically because of electrode degradation at such temperatures. Sm, Eu, Yb, and Tm show lower

boiling points and are therefore mainly produced by sublimation and vacuum distillation methods (Gupta and Krishnamurthy, 2005).

1.1.2 REE chemistry

The most stable oxidation state is +III for all elements (5*d* and 6*s* electronic shells are empty) and is characteristic to REEs. In aqueous media, they often behave similarly as Al(+III). The standard oxidation potentials are listed in Table 3.

The +II state occurs naturally (Eu, Yb, and Sm) and +IV as well (Ce, Pr, and Tb), however, only Ce(+IV) is stable in aqueous solution. These differences can be exploited for separation between the REEs (Leveque and Maestro, 1993). They have an impact on natural (geochemical) processes and can be observed in environmental measurements. For example, because Eu can be divalent, its chemistry in magmatic conditions is different from that of other REEs. It incorporates into plagioclases by substituting Ca^{2+}, thus enriching the solid phase (crystals) and depleting the magma (Duschene, 1983). Thus, a relative enrichment of Eu can be observed in the sample with regard to other REEs (Figure 8), this enrichment is called anomaly.

Table 3: Characteristics of REE ions (Leveque and Maestro, 1993). E_0/SHE is the standard potential of oxidation of the couple relative to the standard hydrogen electrode.

Element Symbol	Ionic radius (Å)		E_0 / SHE (V)		
	REE^{3+}	other ion	III → II	III→0	III→IV
Sc	0.730	–	–	-2.08	–
Y	0.892	–	–	-2.37	–
La	1.061	–	–	-2.37	–
Ce	1.034	0.97 (Ce^{4+})	–	-2.34	-1.74
Pr	1.013	0.99 (Pr^{4+})	–	-2.35	-2.90
Nd	0.995	–	–	-2.32	–
Sm	0.964	1.19 (Sm^{2+})	-1.55	-2.30	–
Eu	0.950	1.17 (Eu^{2+})	-0.35	-1.99	–
Gd	0.938	–	–	-2.29	–
Tb	0.923	0.88 (Tb^{4+})	–	-2.30	–
Dy	0.908	–	–	-2.29	–
Ho	0.894	–	–	-2.33	–
Er	0.881	–	–	-2.31	–
Tm	0.869	–	–	-2.31	–
Yb	0.858	0.93 (Yb^{2+})	-1.15	-2.22	–
Lu	0.848	–	–	-2.30	–

In this case, the Eu anomaly is a well-known phenomenon in geochemistry and often noted as Eu* (Bea, 2015). A common expression for the Eu anomaly is:

$$Eu^* = \frac{Eu_N}{\sqrt{(Nd_N * Gd_N)}} \quad (1)$$

In this formula Eu* is a dimensionless number. Eu_N is the concentration of Eu in the sample divided by the Eu concentration in a standard sample (*e.g.*, standard chondrite). Gd_N and Nd_N are computed following the same method. After the calculation, the Eu* value is compared to 1 to assess relative enrichment (>1) or depletion (<1) (Bea, 2015).

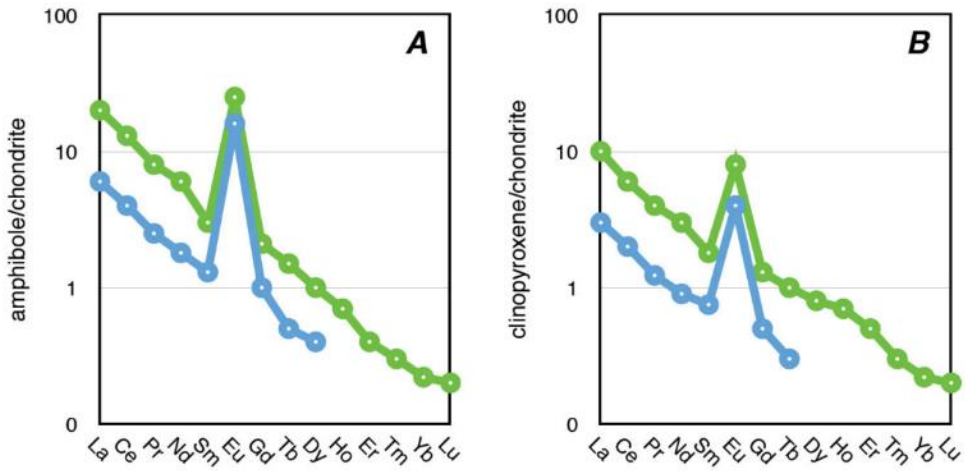

Figure 8: Chondrite-normalized REE patterns for feldspars (A) and plagioclases (B) (Bea, 2015). Normalization highlights a positive (>1) Eu* anomaly, denoting mineral enrichment, as described above

Regarding the tetravalent state, Pr(+IV) and Tb(+IV) are strong oxidants that are not stable in water (oxidizing water itself). Ce(+III) is oxidized by O_2 (atmospheric or dissolved), and CeO_4 partially precipitates (Tostevin *et al.*, 2016). The Ce* anomaly is also found in the literature and a comparable expression is used.

The metal forms of REEs are strong reducing agents. They can dissolve in water, liberating hydrogen. Trivalent cations are able to form complexes with a wide range of anions and other ligands. The solubility of the corresponding salts varies extensively as do the complex formation constants (Gupta and Krishnamurthy, 2005).

The relative affinity of REEs cations for inorganic ligands can be compared using the stability constants of complexes. Millero reported numerous inorganic complex formation constants, computed from experimental data and extrapolated to infinite dilution (Table 4). Carbonates, followed by phosphates, form the most stable complexes: $K_f \approx 10^{12}$ for $[REE(CO_3)_2]^{2-}$; $K_f \approx 10^{9}$ for $[REE(HPO_4)_2]^{-}$ (no ionic strength, 25 °C). The values of the equilibrium constants increase systematically along the lanthanide series with decreasing ionic radius.

Organic ligands form the most stable complexes, *e.g.*, EDTA (ethylenediaminetetraacetic) and more generally polyamine polyacetates like HEDTA (hydroxyethylethylenediaminetriacetic acid) or DTPA (diethylenetriaminepentaacetic acid). The formation constants of organic complexes are several orders of magnitude higher than the formation constants of inorganic complexes. Typical values for REE-EDTA constant of formation range from 10^{15-18} whereas for the most stable inorganic complex ($[REE-(CO_3)_2]^{-}$) typical values are 10^{10-13}. The acetate and oxalate anions also form notable complexes, with the former being involved in the REE transport inside organisms such as hyperaccumulator plants (Yuan *et al.*, 2017). Selective precipitation of oxalate is also widely used in dilute nitrate solutions (Gupta and Krishnamurthy, 2005).

Regarding water solubility, the most soluble salts are chlorides, bromides, nitrates, bromates, and perchlorates (*e.g.*, $La(NO_3)_3$ solubility exceeds 1 500 $g.L^{-1}$ in water at 25 °C), and increases with temperature (Rumble, 2019). On the contrary, sulfate solubility is relatively lower (20 $g.L^{-1}$ for $La_2(SO_4)_3$ at 25 °C) and decreases as temperature increases (Das *et al.*, 2019; Spedding and Jaffe, 1954). Oxides, sulfides, carbonates, oxalates, and phosphates are insoluble in water, and fluoride precipitation is one of the characteristic tests of REEs in solution (Gupta and Krishnamurthy, 2005).

Table 4: Stability constants of REE complexes (Ionic strength = 0 ; 25 °C) (Millero, 1992)

Log K: REE^{3+} + p A^{n-} = $[REE, A_p]3^{-p*n}$											
A:	OH^-	NO_3^-	Cl^-	F^-	HCO_3^-	$H_2PO_4^-$	SO_4^{2-}	CO_3^{2-}	HPO_4^{2-}	$(CO_3^{2-})_2$	$(HPO_4^-)_2$
La	5.1	0.58	0.29	3.12	2.02	2.50	3.21	6.82	4.87	11.31	8.17
Ce	5.6	0.69	0.31	3.28	1.95	2.43	3.29	6.95	7.98	11.50	8.34
Pr	5.6	0.69	0.32	3.48	1.89	2.37	3.27	7.03	5.08	11.65	8.50
Nd	5.67	0.79	0.32	3.56	1.83	2.31	3.26	7.13	5.18	11.80	8.66
Pm	5.77	0.88	0.31	3.63	1.79	2.27	3.34	7.22	5.27	11.96	8.81
Sm	5.81	0.78	0.30	3.58	1.75	2.23	3.28	7.30	5.35	12.11	8.96
Eu	5.83	0.83	0.28	3.63	1.60	2.21	3.37	7.37	5.42	12.24	9.10
Gd	5.79	0.47	0.28	3.75	1.72	2.20	3.25	7.44	5.49	12.39	9.24
Tb	5.98	0.51	0.27	3.85	1.71	2.19	3.20	7.50	5.54	12.52	9.37
Dy	6.04	0.15	0.27	3.89	1.72	2.20	3.15	7.55	5.6	12.65	9.49
Ho	6.01	0.25	0.27	3.95	1.73	2.21	3.16	7.59	5.64	12.77	9.62
Er	6.15	0.15	0.28	3.98	1.76	2.24	3.15	7.63	5.68	12.88	9.73
Tm	6.19	0.20	0.27	3.99	1.79	2.27	3.07	7.66	5.71	13.00	9.84
Yb	6.22	0.25	0.16	4.02	1.84	2.32	3.06	7.67	5.73	13.08	9.95
Lu	6.24	0.56	-0.03	4.05	1.90	2.38	3.01	7.70	5.75	13.20	10.05

According to Gupta, double salts of REEs are often encountered, and the most common ones are $2REE(NO_3)_3 \cdot 3MgNO_3 \cdot 24H_2O$ and $REE(NO_3)_3 \cdot 2NH_4NO_3 \cdot 4H_2O$, and the double sulfates $REE_2(SO_4)_3 \cdot 3Na_2SO_4 \cdot 12H_2O$ and $REE_2(SO_4)_3 \cdot MgSO_4 \cdot 24H_2O$ (Gupta and Krishnamurthy, 2005). The double sulfate salts of HREEs are water-soluble whereas LREEs double sulfate salts are significantly less soluble.

EDTA and other (polyamine) (poly)carboxylates of REEs are water soluble. Other molecules with functional groups like phosphate, phosphine, and other functional chelators involving ammonium groups have been specifically designed to chelate REEs. These molecules are generally hydrophobic and diluted in the organic phase to act as the extractant. Examples will be developed later on, please refer to section 2.2.

1.1.3 Applications

REEs have an ever-growing wide range of applications, but most of them concern modern technologies. The first industrial-scale application of REEs was in lighter flints, which production started in 1907. Lighter flints were composed of 30% iron (by mass) and 70% mischmetal. Mischmetal is an alloy of La-Ce with also Nd and Pr in the same proportion as the monazite mineral (Gupta and Krishnamurthy, 2005).

With time and technological development, numerous other applications have appeared, the main ones being catalysts, polishing powders, and glass additives. Later, new applications appeared with the development of phosphors (“energy saving” lamps), high-performance alloys, batteries, permanent magnets, and ceramics. The current repartition of rare earth oxides (REO) applications by volume is displayed in Figure 9.

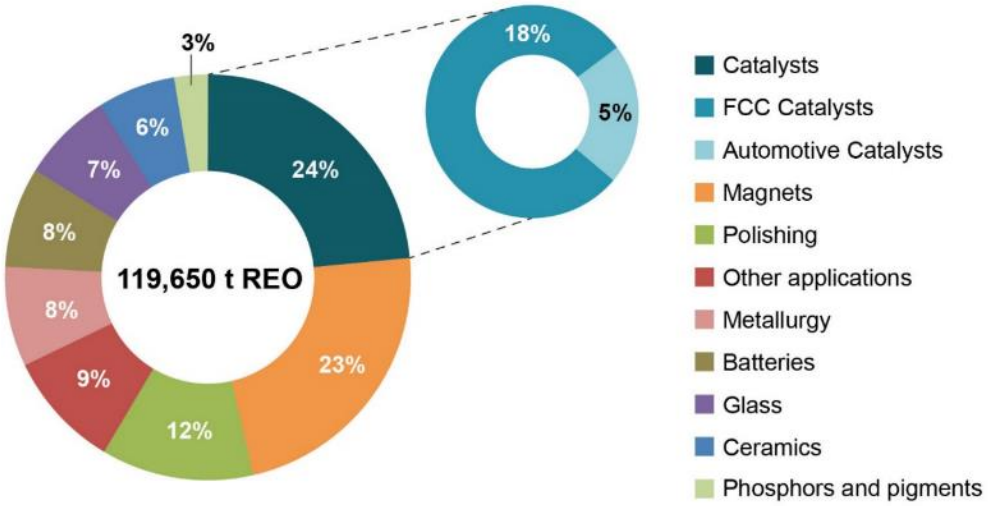

Figure 9: Estimated global REO consumption in 2015, reproduced from (Machacek and Kalvig, 2016) with data from (Roskill, 2016). FCC stands for fluid catalytic cracking. REO stands for rare earth oxides

Today, the predominant usage concerns catalysts with the use of La, Ce, and Nd in zeolites for fluid catalytic cracking (FCC) of petroleum in refineries (*i.e.*, obtaining lighter fractions from long-chain hydrocarbon fractions). REE-doped catalysts strongly enhance the efficiency of the process, reducing the amount of heat consumed compared to thermal cracking. Chloride mixtures are typically rich in La (80% of the REEs) with Ce (6% to 10%) and Nd (15%) and used to cover the support material at a mass ratio of 0.5% to 5% (Gupta and Krishnamurthy, 2005; Machacek and Kalvig, 2016). Regarding automotive catalysts, the main REE used is Ce, it significantly boosts stability and performance of precious metals (Pd, Rh), reducing their decomposition and release in the environment. Ce also acts as an "oxygen storage component", when air fails in the exhaust. Automotive catalysts are essential components of modern transportation technology because they drastically reduce emissions of gaseous hydrocarbons, nitrogen oxides, and carbon monoxide, converting them to water, carbon dioxide, and nitrogen (Binnemans *et al.*, 2013; Gupta and Krishnamurthy, 2005).

The second application in terms of volume is the production of permanent magnets. NdFeB magnets are one of the strongest conventional magnets today. Clean technologies rely heavily on them with the ever-growing use of wind turbines. However, the magnets inside electric vehicles (motors, but also all sorts of on-board equipment) are also a significant source of consumption. Electric bicycles are another modern application, as they require small and performant magnets for reasons of space and weight. The typical composition of electric vehicle magnets is 31 %Nd – 4.5 %Dy – 2 %Co –61.5 %Fe – 1 %B (mass fraction) (Binnemans *et al.*, 2018). Dy addition helps to keep magnetic activity at higher working temperatures (up to 160 °C).

Other significant applications involve the production of phosphors: in this case, most of the REEs used are HREEs (Eu, Tb, Y), notably in the red lamp phosphor Y_2O_3:Eu^{3+} (Binnemans *et al.*, 2018; Binnemans and Jones, 2015; Ronda, 1995). Phosphors are used to absorb UV light (typically from a Hg plasma) and re-emit visible light. They are used in fluorescent lamps and compact fluorescent lamps (energy saving lamps). Other subdomains of application are X-ray phosphors (Machacek and Kalvig, 2016). While this application is not significant in volume, it holds a serious share of the market because the scarcest elements are used (HREEs) with a high purity requirement (> 99.9%) (Gupta and Krishnamurthy, 2005). However, the trend is decreasing as other efficient lighting technologies are more and more widespread (LED) (Binnemans *et al.*, 2018).

Another application that needs to be mentioned here is the glass coloring industry (as well as decolorization), glass polishing (involving semi-purified Ce), optical fibers, batteries (anodes of NiMH are $LaNi_5$), metallurgy with high performance alloys, ceramic coloring, surgical lasers, neutron absorber. The applications and the corresponding elements are classified in Table 5.

Table 5: Application of the various REEs depending on the sector

Sector	Application	Most used elements
Catalysts	FFC catalysts, Automotive catalyst	La, Ce, Nd
Magnets	high-performance magnets	Nd, Dy
Polishing	Polishing powders for glass	Ce, La
Phosphors	Display, lighting	Y, Eu
Metallurgy	High-performance alloys	All / application dependent
Batteries	Electrode	La, Ce

Additionally, REEs have been widely used as micro-fertilizers since the 1990s. Positive effects have been observed on crop yield and plant quality. The inclusion of REEs as feed additive for cattle and poultry has shown positive effects on growth. In both cases, the lighter REEs were used (La, Ce, Pr, and Nd) (Redling, 2006).

1.1.4 The REE market

A remarkable market survey for European REEs was published by European EURARE project (Machacek and Kalvig, 2016). Annual global production has increased from 30 kton of rare earth oxides (REO) in 1983 to 130 kton in 2010. The production and country of production are plotted in Figure 10. It can be observed that after 1995, China started to dominate the market until the last few years with around 95% of global production.

The total annual demand for REO is plotted in Figure 11. A drastic rise can be observed from 55 kton in 1995 to 146 kton in 2015. The user countries have also changed: while Japan and the US were the main demanders in 1995, China is now the primary user of REEs.

A notable event, also known as the “rare earth crisis” in the RE economy is the appearance of Chinese export quotas, temporarily limiting the Chinese REEs exports in 2010. Shortages and a large gap between supply and demand led to a spike in REO prices. The crisis also led to the late development of production sites outside of China, with Australian mines and RE compound production in Malaysia (exploited by Lynas).

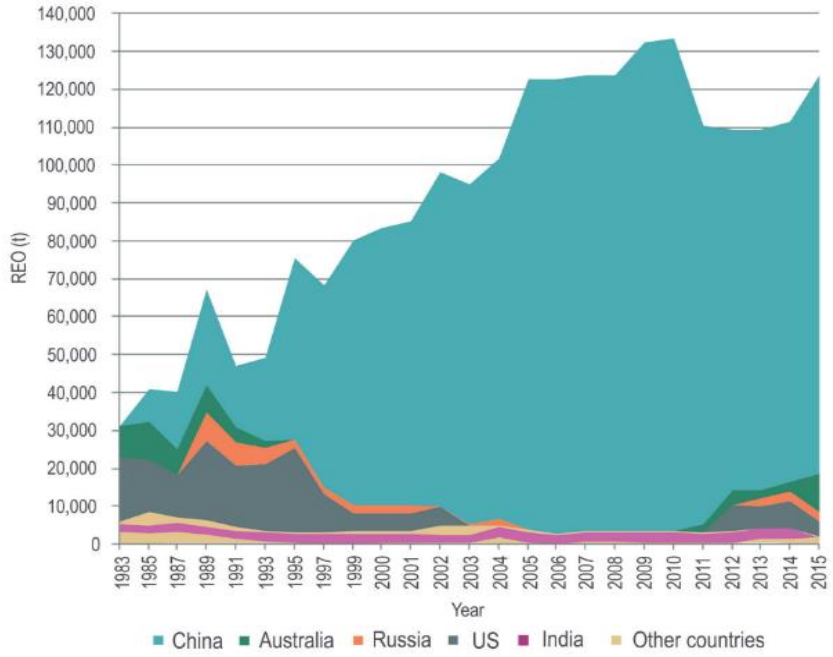

Figure 10: Evolution of global REO production since 1983 and producing countries (Machacek and Kalvig, 2016)

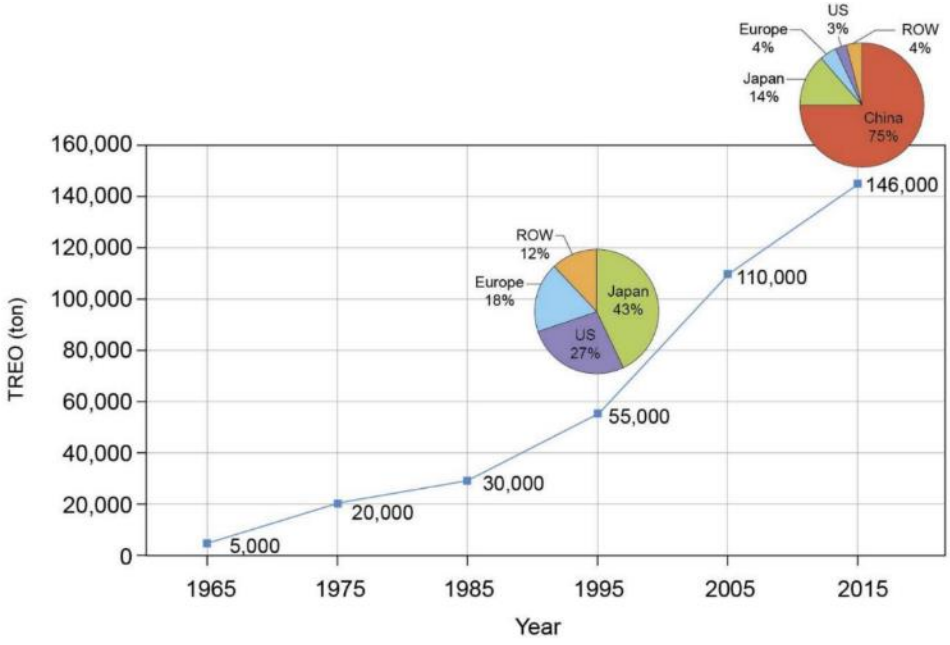

Figure 11: Evolution of global REO demand since 1965 and repartition of the demanding countries (Machacek and Kalvig, 2016). ROW standing for "rest of the world"

It is not easy to track prices per ton of REEs. They are not traded on public stock markets like other metals (*e.g.*, Au, Ni): buyers and sellers agree on the price. Authors often use United States Geological Survey (USGS) data as a reference for price trends (Bauer *et al.*, 2010; Machacek and Kalvig, 2016; National Science and Technology Council, 2018), but not all REEs are included. The Shanghai Steel Home market and the German Institute for Rare Earth and Metals (Institut für Seltene Erden und Metalle, ISE) can also be considered good indicative databases. Today, the prices are roughly at the same level since 2015, and the indicative prices are given in Table 6.

Table 6: Indicative prices for REEs in the form of metals or oxides, retrieved from the Institut Seltene Erden website (http://www.institut-seltene-erden.de/) as of 18 December 2020.

Light Rare Earth Elements	Purity	USD.kg^{-1}	Heavy Rare Earth Elements	Purity	USD.kg^{-1}
Lanthanum (La)	>99%	4.1	Europium Oxide (Eu_2O_3)	>99.999%	31.5
Lanthanum Oxide (La_2O_3)	>99.999%	3.4	Gadolinium Oxide (Gd_2O_3)	>99.5%	27.9
Cerium (Ce)	>99%	4.5	Terbium (Tb)	>99.9%	1305
Cerium Oxide (CeO_2)	>99.5%	1.5	Terbium Oxide (Tb_4O_7)	>99.9%	1025
Praseodymium (Pr)	>99%	95	Dysprosium (Dy)	>99.5%	387
Praseodymium Oxide (Pr_2O_3)	>99.5%	58.5	Dysprosium Oxide (Dy_2O_3)	>99.5%	295
Neodymium (Nd)	>99%	96.5	Holmium Oxide (Ho_2O_3)	>99.5%	89.9
Neodymium Oxide (Nd_2O_3)	>99.5%	79.0	Erbium Oxide (Er_2O_3)	>99.5%	26.5
Samarium (Sm)	>99.5%	13.3	Ytterbium Oxide (Yb_2O_3)	>99.99%	15.8
Samarium Oxide (Sm_2O_3)	>99.9%	1.8	Lutetium Oxide (Lu_2O_3)	>99%	744
Scandium (Sc)	>99.99%	3 302	Yttrium (Y)	>99.9%	28.5
Scandium Oxide (Sc_2O_3)	>99.99%	992	Yttrium Oxide (Y_2O_3)	>99.99%	3.3

The lightest REEs (La and Ce) are available at lower prices, compared to the other LREEs, and to HREEs. Only thulium (Tm) prices were not available on the sites consulted. Prices found on online retail sites range up to 1 000 USD.kg^{-1} Tm (metal). Scandium has the highest price per kilogram due to its most limited availability and niche markets.

The relatively high overall price reflects a significant growing demand for REEs. In fact, certain elements are considered critical materials by both Europe and the US (Bauer *et al.*, 2010; Machacek and Kalvig, 2016), considering their mandatory use in clean technologies components (permanent magnets, batteries, phosphors). Use, supply, and risk of shortage have been extensively studied, and the report of the European Commission clearly demonstrates the importance of REEs (European Commission, 2020). Out of all strategic materials, REEs appear to be the most critical in terms of supply risk (Figure 12). In detail, the supply risk for all REEs is equivalent for each REEs, while their economic importance is the highest for Sm, Nd and Pr.

1.1.5 Health and environmental risks

Demand for REEs is growing exponentially and releases to the environment (water bodies, soils) are likely to increase simultaneously. The related damage to ecosystems and human health should raise concerns.

1.1.5.1 Origin of REE releases to the environment

The three main sources of anthropogenic REE releases to the environment include: production (mining), use, and waste disposal. Production during mining is significant anthropogenic source of REE release due to specific mining techniques including heap and in-situ leaching (refer to section 1.2.1.4) (Hao *et al.*, 2016; W.-S. Liu *et al.*, 2019). Although heap leaching is now prohibited, the release of leachate to the environment is thus unavoidable, and the proportion of leachate lost varies depending on the technique used (Schulze *et al.*, 2017).

As for use, the agricultural application of REEs (feed additive, fertilizer) is also significant (Redling, 2006). In particular, in China, an estimated amount of 50 to 100 million tons of REO enters the Chinese agricultural system every year (Gonzalez *et al.*, 2014; Liang *et al.*, 2005).

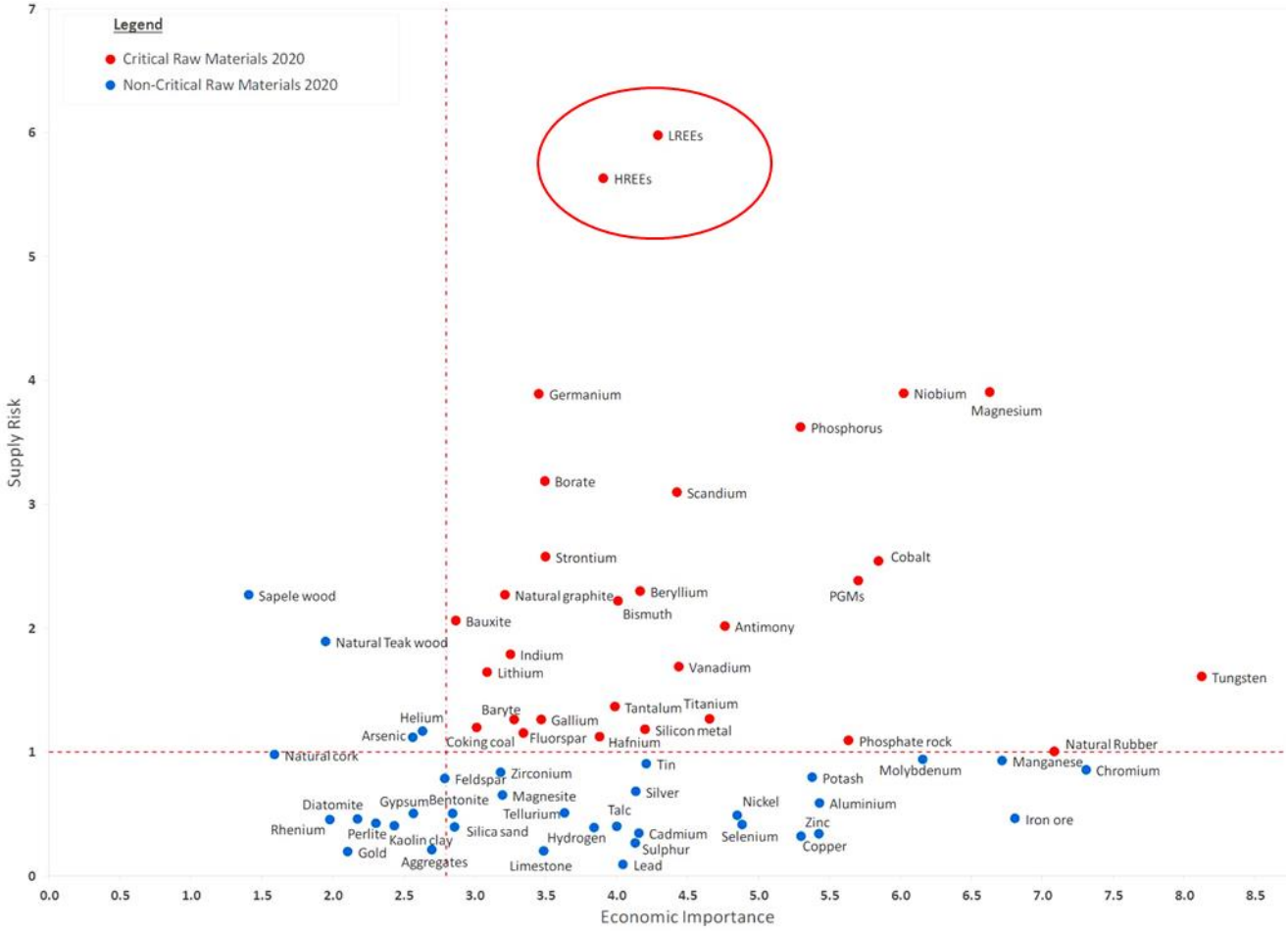

Figure 12: Critical assessment results of raw materials for EU (European Commission, 2020)

Phosphate fertilizer production is another source of REE release (Volokh *et al.*, 1990). When produced from igneous phosphate rocks and certain sedimentary deposits, a by-product is phosphogypsum which contains REEs (Emsbo *et al.*, 2015; Rychkov *et al.*, 2018).

Additionally, Gd is used as a contrasting agent in magnetic resonance imaging (MRI), and is released in urine, and thus into water bodies near cities. Lakes, estuaries, coastal waters, groundwater and tap water have been reported to be enriched in anthropogenic Gd (Gonzalez *et al.*, 2014; Lerat-Hardy *et al.*, 2019; Louis *et al.*, 2020).

Finally illegal deposits of e-wastes, and releases from catalyst producing industries are sources of anthropogenic REEs (Sneller *et al.*, 2000).

1.1.5.2 Fate in the environment

Regarding their fate in the environment, they show relatively a low mobility related to their strong adsorption on soils and sediments (Cao *et al.*, 2000; Sneller *et al.*, 2000). Indeed, they readily form insoluble carbonates, phosphates, and hydroxides in aquatic environments (please refer to section 1.1.2REE chemistry). However a small fraction (10%) remains water-soluble and is thus bioavailable (Pang *et al.*, 2001). The spread of REEs has been observed in the surroundings of mines in South China, and an accumulation in the sediments was observed (Liu *et al.*, 2019).

1.1.5.3 Toxicity and eco-toxicity

Ecotoxicological effects and mechanisms of actions are still poorly understood (Gonzalez *et al.*, 2014). Recent studies assessed the toxicity of some REEs to *E. coli* and marine bacteria (Kurvet *et al.*, 2017; Técher *et al.*, 2020). Studies seem to agree that, "for the present, environmental risks deriving from lanthanides should be limited to some hotspots (*e.g.*, downstream of wastewater treatment plants)"(González *et al.*, 2015).

REE toxicity is less than other trace metals or metalloids (*e.g.*, Cd or As) (Redling, 2006). However, long term adverse effects on human health are suspected. Harmful effects can occur on humans as REEs can accumulate in bones (Zaichick *et al.*, 2011) and cause harm to the circulatory and immunological systems (Zhang *et al.*, 2000). Measurable effects on digestive functions were observed in populations living in high REE areas compared to control areas (Zhu *et al.*, 2005). Adverse effects on the intellectual quotient of children living in the same areas have also been observed (Zhu *et al.*, 1996). It should be mentioned that, apart from these reports, literature is scarce on REE toxicity. Additionally, the aforementioned studies were conducted on small population groups (less than 150 individuals). Thus, the adverse effects of long-time exposure remain relatively unknown.

Nevertheless, the surrounding extraction and refining processes require attention. Indeed, the manufacture of REE compounds involves several steps, each associated with the release of contaminants and energy consumption. A comprehensive approach is therefore necessary to assess the impact of the production of a REE compound. The following section aims at describing the usual and alternative production processes and the associated impacts are discussed.

1.2 Resources and production

The objective of this section is to present the main resources as well as the conventional production methods of REEs.

1.2.1 Primary resources

In opposition to precious metals, which are generally less abundant in the earth's crust (Au, Co, Cu) REEs do not occur in large and concentrated deposits. More than 200 minerals are known to contain REEs but most of them are rare, or have a very low REE content. Today, 95% of all global RE resources are found in only three minerals: bastnaesite, monazite, and xenotime (Gupta and Krishnamurthy, 2005) (Figure 13).

Other commonly reported minerals in the literature are listed in Table 7. Bastnaesite and monazite mainly contain LREEs, whereas xenotime is the primary source of HREEs (mainly yttrium).

(a) (b) (c)

Figure 13: Different crystals of REE-bearing minerals. (a) Monazite crystal from the Savoy region, France. Photo: Frederic Hede. (b) Xenotime crystal from Austria. Photo: Matteo Chinellato. (c) Bastnaesite crystal from Pakistan. Photo: Thames Valley Minerals

Table 7: Rare earth minerals commonly reported in the literature (Gupta and Krishnamurthy, 2005; Habashi, 2013; Leveque and Maestro, 1993)

Mineral name	Formula
Monazite	(LREEs,Th)PO_4
Xenotime	(Y,HREEs)PO_4
Bastnaesite	(Ce,La)$(CO_3)F$
Gadolinite	$(Ce,La,Nd,Y)_2FeBe_2Si_2O_{10}$
Euxenite	$(Y,Ce,Ca,U,Th)(Ti,Nb,Ta)_2O_6$

1.2.1.1 Bastnaesite: (REE)$(CO_3)F$

Bastnaesite is a fluorocarbonate of LREEs (70 wt% of REO). It mainly contains Ce, La, Nd, and Pr (respectively, 50 – 30 – 15 – 5% of the total REEs in the mineral). This is the major part of the Chinese mine of Bayan Obo. This mine is situated in Inner Mongolia and its capacity is estimated at approximately 800 million metric tons of mineral at 6 wt% REO. Another significant deposit worth mentioning is the Mountain Pass mine in the United States (3.3 million metric tons, 7.7 wt% REO). Bastnaesite deposits are more subject to weathering than phosphate minerals (Leveque and Maestro, 1993).

1.2.1.2 Monazite (REE, Th)PO_4

Monazite is a phosphate of LREEs, associated with thorium (Th) and variable concentrations of uranium (U). Its REE content can vary from 35% to 70 wt% of REO and thorium content varies from 4% to 12 wt%. The typical REE repartition is similar to bastnaesite, (main REEs are Ce, La, Nd, Pr), however, it generally contains slightly more Y (1% to 2% of the REEs in the mineral). It is the most abundant mineral. It accumulates in beach sands (placers) all over the world, in generally small deposits. It constitutes the bulk of Australian Mount Weld mine, and a large deposit is also present in the Bayan Obo mine. The treatment of this mineral is problematic because of the radioactivity of uranium and thorium.

1.2.1.3 Xenotime (Y/HREEs)PO_4

Xenotime is also a REE phosphate, but its typical composition makes Y the main element (60% of the total RE content). Other HREEs are significantly represented (Dy: 9% to 10%, Gd: 4% to 8%, Yb: 6%, Er: 5% of the total RE content). Xenotime follows monazite in the deposits and generally represents 5% of the deposit (Gupta and Krishnamurthy, 2005).

1.2.1.4 Ionic adsorption clays from southern China

Another source of HREEs are the unique clay deposits in southeast China (they were only discovered in this region). They are sometimes called “ionic sands”, “ionic clays”, or “regolith deposits” (Figure 14) (Chi *et al.*, 2005; Gupta and Krishnamurthy, 2005; Leveque and Maestro, 1993). In these deposits, REEs are adsorbed onto clay minerals: *e.g.*, kaolinite $Al_2Si_2O_5(OH)_4$ (Gupta and Krishnamurthy, 2005).

Chi *et al.* reported that 80-85% of the REEs are present in the ion-exchangeable phase of the soil (Chi *et al.*, 2005). The mineral phase contains 9 to 13% of the total REE content and colloids account for 3 to 5%. The water-soluble fraction of REEs in the soil is negligible (< 1%) compared to the above-mentioned phases.

Figure 14: The rare earth-rich ionic sands in Southern China. Photo Wenshen Liu

These clays are the result of a unique and intense tropical weathering. The partitioning of REEs depends on the parent rock. The Xunwu clays contain notable amounts of La and Nd (75%) with lower amounts of HREEs (25%). However, the Longnam clays are very rich in Y (64%) and other HREEs, with La, Ce, Nd and Pr accounting for less than 8% of the total REE content (Gupta and Krishnamurthy, 2005). All types of these ionic clays are characterized by significant Ce depletion.

1.2.1.5 Scandium

Scandium concentrations are always very low and do not exceed several µg per g (ppb) in the minerals mentioned above. Because Sc does not combine with ore-forming anions, Sc minerals are uncommon, and deposits are thus scarcer. Sources of scandium include some of the Bayan Obo mine deposits, uranium ores, tungsten-bearing mineral wolframite, and bauxite residue produced during Al extraction (Binnemans *et al.*, 2015; Davris *et al.*, 2016).

1.2.1.6 Other primary resources

Other minerals in Russia, Greenland and in the Scandinavian area are also exploitable. However, they contain significantly smaller amounts than the ones present in China and Australia. Recently, two types of new possible sources of REEs were discovered in the deep waters (4 000 to 6 000 m). The first one consists of polymetallic nodules as an alternative source of REEs, where valuables elements (platinum group elements, Ni, Co, Cu) are associated with REEs at 1 000 $\mu g.g^{-1}$ (Guan *et al.*, 2017; Parhi *et al.*, 2015; Zhang *et al.*, 2012). More recently (2013), deep marine mud in the western North Pacific Ocean near Minamitorishima Island (Japan), was found to contain more than 5 000 $\mu g.g^{-1}$ before physical treatment (Takaya *et al.*, 2018). In both cases, tremendous amounts are available (16 Mt of REO), and the development of large-scale units at these depths is underway.

1.2.2 Production from primary resources

As with the processing of common ores, physical beneficiation is possible for the treatment of bastnaesite, monazite and xenotime ores. Gravimetry, flotation, and magnetic enrichment are conventionally used. The specificity begins with the chemical treatment of the above-cited minerals. Beneficiated ore is often referred to as a REE concentrate.

The concentrates are then “cracked” or “attacked” to render the REEs available for solubilization. Leaching of the cracked material is the actual solubilization of the REEs using strong acids (nitric or hydrochloric). Purification, separation of the REEs from each other, neutralization and further refining (selective precipitation, oxide preparation, metal preparation) are the finishing steps. The most common processes can be described by the same sequence (Figure 15).

Figure 15: General process scheme for conventional REE hydrometallurgy (Sadri *et al.*, 2017)

1.2.2.1 Ore cracking methods

On an industrial scale, two main processes dominate the cracking step: alkaline cracking and acid baking. Both are suitable for monazite and xenotime treatment. Acid baking is preferred for bastnaesite treatment.

Alkaline cracking is most likely carried out in an autoclave at 150 °C with 50 wt% NaOH at a solid to liquid ratio (S:L) of 1:1 (wt:wt) (Sadri *et al.*, 2017). Higher temperatures (*e.g.*, 170 °C) are reported (Gupta and Krishnamurthy, 2005; Habashi, 2013), and cracking at 120 °C with 70 wt% NaOH at ambient pressure could also be possible (Kim and Osseo-Asare, 2012; Sadri *et al.*, 2017). Habashi reported that the optimal conditions for alkaline cracking are “40–50% NaOH, 160 °C, NaOH to concentrate 2:1, time of reaction about 3 h” (Habashi, 2013). Other alkali materials can be used such as $CaCO_3$, CaO, or $CaCl_2$ but they are less common and more process-specific. The goal is to convert RE phosphates into RE hydroxides (equation (2)).

$$(\mathrm{REE})\mathrm{PO}_{4(s)} + 3\mathrm{NaOH}_{(aq)} \rightarrow (\mathrm{REE})(\mathrm{OH})_{3(s)} + 3\mathrm{Na}^{+}_{(aq)} + \mathrm{PO}^{3-}_{4(aq)} \quad (2)$$

Phosphate is released into solution and can be recovered and commercialized. The phosphate-rich leachate is cooled to 60 °C and $Na_3PO_4 \cdot 10\ H_2O$ crystallizes. Then, the solution still contains 47.4 wt% NaOH, 0.5 wt% Na_3PO_4 , 1.5% Na_2SiO_3 which allows it to be recycled (Habashi, 2013). A thick paste is obtained, which is then washed with water and dried. Th and U are also converted to hydroxides. Because they are soluble in carbonate media, they can be selectively leached using a Na_2CO_3 solution (Sadri *et al.*, 2017).

Bastnaesite can also undergo alkaline cracking, managing a preliminary step (Sadri *et al.*, 2017). Bastnaesite ((LREE)(CO_3)F) needs to be previously converted to a mix of chlorides and fluorides using hydrochloric acid (equation (3)). The chlorides are soluble, whereas the fluorides must undergo alkaline treatment (equation (4)).

$$\begin{aligned}(\mathrm{REE})\mathrm{F}_3 - (\mathrm{REE})_2(\mathrm{CO}_3)_{3(s)} + 9\mathrm{HCl}_{(aq)} \rightarrow \\ (\mathrm{REE})\mathrm{F}_{3(s)} + 2(\mathrm{REE})\mathrm{Cl}_{3(aq)} + 3\mathrm{HCl}_{(aq)} + 3\mathrm{H}_2\mathrm{O}_{(l)} + 3\mathrm{CO}_{2(g)}\end{aligned} \quad (3)$$

$$(\mathrm{REE})\mathrm{F}_{3(s)} + 3\mathrm{NaOH}_{(aq)} \rightarrow (\mathrm{REE})(\mathrm{OH})_{3(s)} + 3\mathrm{NaF(aq)} \quad (4)$$

Acid baking is the Chinese process used in Baotou with Bayan Obo ore (mainly bastnaesite but also monazite). With concentrated sulfuric acid in an oven, REE phosphates and fluorocarbonates can be converted to solid RE sulfates that can later be leached out in water. The calcination temperature is higher for bastnaesite (400 - 560 °C) than for monazite (200 - 250 °C) (Sadri *et al.*, 2017).

The Molycorp process is an alternative that consists of roasting the bastnaesite ore at 600 °C in an oxidizing atmosphere. Ce is oxidized to its tetravalent form as insoluble CeO_2 and purified from other elements by leaching the residue with concentrated HCl. The CeO_2 is ready to be used as a polishing powder.

1.2.2.2 Leaching methods for cracked ore

The cracked ore can be leached with nitric, sulfuric, or hydrochloric acid. When the acid baking method is used, water can leach out the RE sulfates. Extraction kinetics can be modelled by the shrinking core model (Feng *et al.*, 2013; Kim *et al.*, 2014; Sadri *et al.*, 2017). More broadly, this model also fits extraction kinetics from the ionic clays (Sadri *et al.*, 2017; Tian *et al.*, 2010; Y. Xiao *et al.*, 2015; Y.-F. Xiao *et al.*, 2015).

The model, described in Figure 16, consists of considering solid particle as a sphere of substrate and rich in solid reactant (in our case REEs). The leaching compound diffuses through the external film surrounding the particle and through the pores (external diffusion followed by internal diffusion) and liberates into the solution the element of interest (reaction) inside the sphere. By back diffusion, the element of interest is released into the primary solution. This model considers the presence of the inert remaining solid phase (ash) that can slow down the diffusion of the reagents and products, as well as the shrinking of the unreacted core particle.

This model has been used to successfully fit the leaching kinetics of various types of ores (monazite, bastnaesite, ionic clays). The internal diffusion of leaching reactants through the porous layer was determined as the controlling step (Table 8) where variable values of energy of activation were computed.

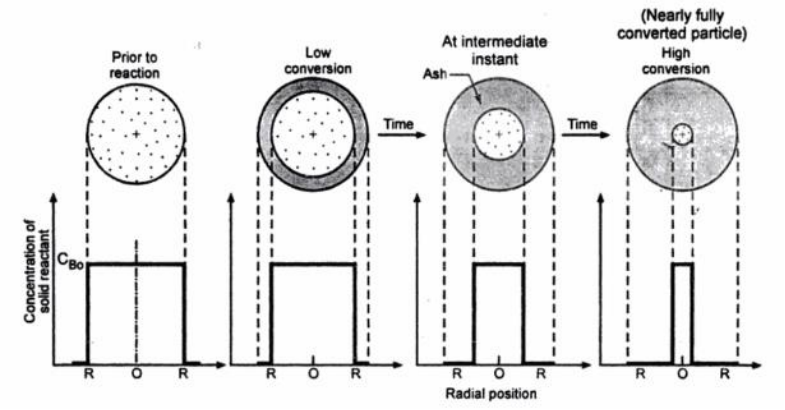

Figure 16: The shrinking core model (Gavhane, 2009)

Table 8: Studies of the leaching kinetics of various REEs ores. All studies report that internal diffusion of the reactants through the porous layer is the rate controlling step.

Mineral	Matrix	Extractant	Activation Energy	Ref
Monazite	Magnetite ore slag	H_2SO_4	24.8 kJ.mol^{-1}	(Kim *et al.*, 2014)
Bastnaesite	Roasted Calcines	H_2SO_4	10.0 kJ.mol^{-1}	(Feng *et al.*, 2013)
Bastnaesite	Concentrates	HCl	59.4 and 66.1 kJ.mol^{-1} $(REE)_2(CO_3)_3$ and $(REE)F_3$	(Bian *et al.*, 2010)
Ionic clays	Ionic clays	$(NH_4)_2SO_4$	-	(Tian *et al.*, 2010)
Bastnaesite	Fluorine fixed concentrates	HCl	-	(Zhu *et al.*, 2003)

1.2.2.3 Leaching methods for ionic clays

To extract REEs from the ionic clays in South China, no ore cracking is required as the REEs are physisorbed onto the aluminosilicate clay. Heap leaching was the main extraction technique until 2010 when it was banned due to environmental concerns (Schulze *et al.*, 2017; Yang *et al.*, 2013). In situ leaching has become the mandatory technique (Figure 17). Extracting methods are based on cation exchange reactions, using either NH_4SO_4, NH_4NO_3, or NH_4Cl solutions (He *et al.*, 2017, 2016; Huot *et al.*, 2018) where three ammonium cations replace one trivalent rare earth cation (Equation (5)).

$$[Al_2(Si_2O_5)(OH)_4]_m \cdot nREE^{3+}_{(s)} + 3nNH^+_{4(aq)} \rightleftharpoons [Al_2(Si_2O_5)(OH)_4]_m \cdot 3nNH^+_{4(s)} + nREE^{3+}_{(aq)} \quad (5)$$

Here, the model equation is for kaolinite ($Al_2Si_2O_5(OH)_4$), but other alumino-silicate minerals are found, such as halloysite ($Al_2Si_2O_5(OH)_4$) and montmorillonite ($(Na,Ca)_{0,3}(Al,Mg)_2Si_4O_{10}(OH)_2 \cdot n\ H_2O$) and mechanisms are most likely the same (Chi *et al.*, 2005). The most commonly used reagent is NH_4SO_4.

After drilling holes for injection on the top of a hill of ore, the leaching solution impregnates the ore for a period of 150 to 400 days (Navarro and Zhao, 2014; Vahidi *et al.*, 2016). The leachate is collected at the bottom of the hill in ponds, the REEs are precipitated and the leachate is recirculated.

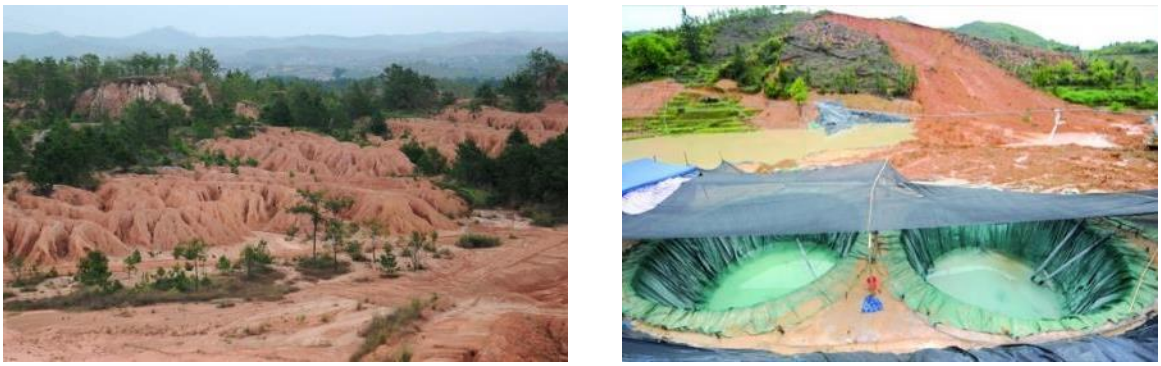

(a) (b)

Figure 17: Photographs of Southern China ionic clays mines. (a) Photograph by Zhou KE, Xinhua Press/Corbis. (b) Mine in Ningde, Fujian Province. Photo by China Foto Press (CFP)

1.2.2.4 Purification/ Separation: precipitation

After the REE solution is obtained, several options are available. It is possible to precipitate all the REEs with either oxalate, strong bases, or carbonate addition (oxalate being the most selective). For the direct leaching of the ionic clays, the most common precipitating agents are oxalic acid and NH_4CO_3 (Liu *et al.*, 2017).

A small fraction of Al is generally unintentionally leached with REEs, and co-precipitation happens leading to an impure solid (route 1 in Figure 18). By adjusting the pH and using NH_4CO_3, it is possible to selectively precipitate Al as a preliminary step at pH 5 (route 2 on Figure 18) (Luo *et al.*, 2015). However, while most of the aluminum can be precipitated during this step, the operation is quite difficult to control as 5 to 15% of the REEs coprecipitate, especially if their concentration is low compared to Al (Liu *et al.*, 2017; Schulze *et al.*, 2017).

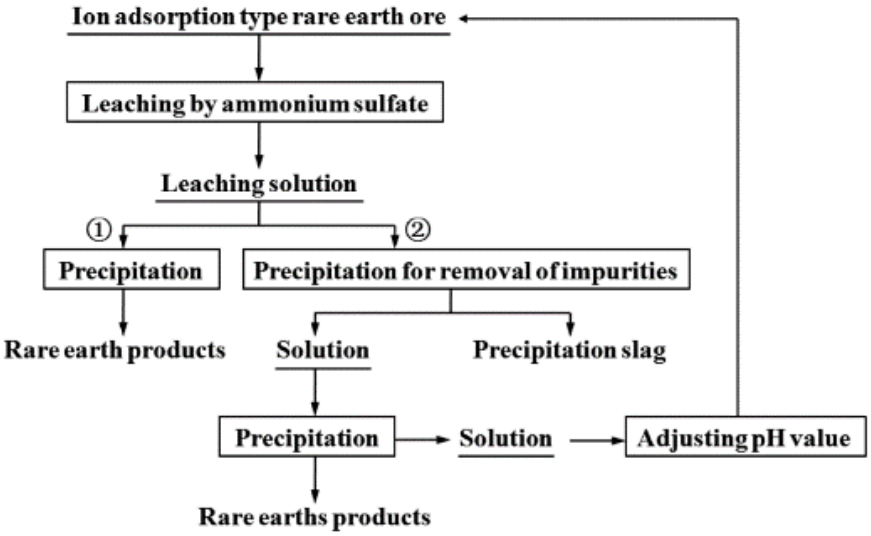

Figure 18: Traditional precipitation method for rare earth extraction from in-situ leaching solutions of ion-adsorption ores (Liu *et al.*, 2017)

Aluminum separation can also be conducted downstream, on the precipitate itself, by adding caustic soda (NaOH) to form highly soluble sodium aluminate: $NaAlO_2$ or in its ionic form: $[Al(OH)_4]^-$, Na^+ (Qi, 2018).

The precipitation step is not selective regarding individual REEs, precipitates are sold as carbonates or oxalates of the REE mixture and sold for further refining. Oxalate or carbonate precipitates can also be calcinated at 900 °C to produce oxides (Chi *et al.*, 2003; Leveque and Maestro, 1993).

1.2.2.5 Purification/ Separation

It is possible to separate REEs from each other using either solvent extraction (SX) or ion-exchange techniques (IX). The use of ion-exchange resins was abandoned in the late 1960s as the development of SX enabled continuous operation and larger scale production. SX has become the standard method for industrial production of REEs (Gupta and Krishnamurthy, 2005).

1.2.2.5.1 Solvent extraction (SX)

The SX process involves the use of a series of mixer-settler batteries. An organic phase (typically kerosene) carries an extractant or extracting agent, an organic molecule with a chelating function (*e.g.*, phosphonic, acetic, tertiary amine) which has a high affinity for the REEs.

Table 9: Common extractants used in solvent extraction of REEs (Leveque and Maestro, 1993)

Extractant common name	Formula	Type	Application
Tri-n-butyl-phosphate (TBP)	$(C_4H_9O)_3PO$	Solvating	All REEs in nitrate media
Di-2,4,4,-trimethylpentyl phosphonic acid (Cyanex 272 ®)	$(C_8H_{19})_2POOH$	Cationic	All REEs in nitrate media
Di(2-éthylhexyl) phosphonic acid (EHEHPA or Ionquest 801®)	$(C_8H_{17}O)C_8H_{17}POOH$	Cationic	Dy and Tb in chloride media
Trialkyl-methyl-ammonium-chloride (Aliquat 336®)	$R_3CH_3N^+Cl^-$	Anionic	All lanthanides but Ce in chloride media

They are classified as cationic (acid), anionic (alkali) or solvating (neutral). The common extractants are listed in Table 9. Equations (6) – (8) describe the possible mechanisms of extraction, where $\overline{RH}$ is the extracting agent in the organic phase (Leveque and Maestro, 1993).

cationic $$3\overline{RH} + REE^{3+} \rightleftharpoons \overline{R_3REE} + 3H^+ \quad (6)$$

anionic $$\overline{R_4N^+, NO_3^-} + 3REE^{3+} \rightleftharpoons \overline{R_4N^+, REE(NO_3)_4^-} \quad (7)$$

solvating $$3\overline{R} + REE^{3+} + 3NO_3^- \rightleftharpoons \overline{R_3REE(NO_3)_3} \quad (8)$$

For a given extractant and REE, and at a defined temperature, the partitioning between the aqueous phase and the organic phase is described using an equilibrium constant $K_{\overline{REE_i}/REE_i}$. Distribution coefficients are then defined by:

$$\alpha_{ij} = \frac{K_{\overline{REE_i}/REE_i}}{K_{\overline{REE_j}/REE_j}} \quad (9)$$

If α_{ij} is greater than one, it is theorically possible to separate REE_i and REE_j. The extractants reported in Table 9 all have a strong affinity for REEs, but not all of them fulfill this requirement *i.e.* having a differentiated affinity. Indeed, depending on the nature of the extractant, the distribution coefficients vary along the lanthanide series. Distribution coefficients of the REEs toward Yttrium are plotted in Figure 19 for various extractants.

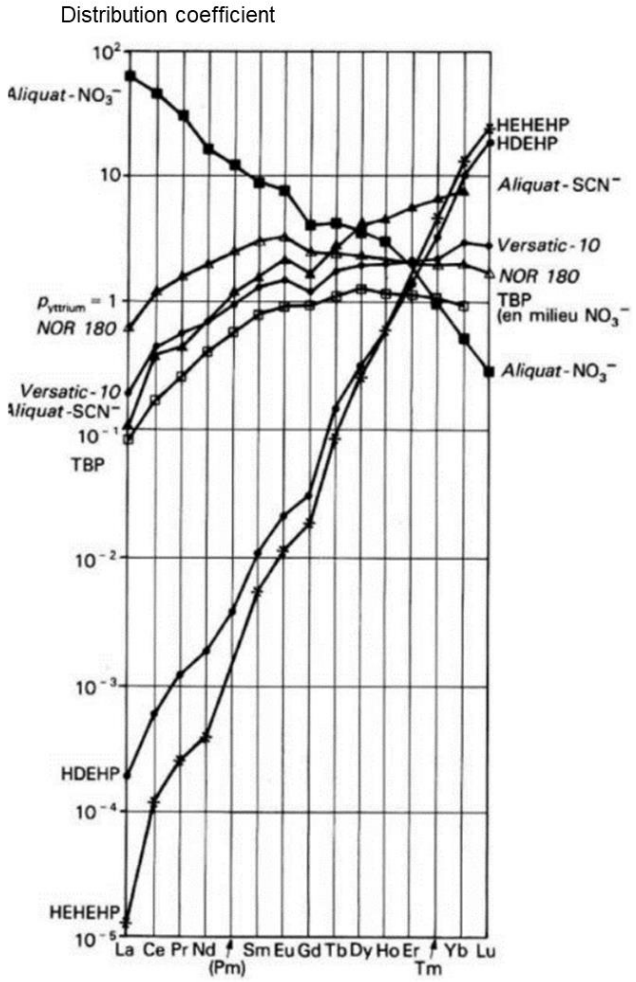

Figure 19: Distribution coefficient of the REEs for various extractants (Leveque and Maestro, 1993)

For one extractant, the steeper the curve, the more differentiated the affinity of the extractant for REEs (*e.g.*, HEHEHP, HDEHP, Aliquat). An extractant with a steep curve can be used for the separation of the REEs in-between them (*e.g.*, LREEs // HREEs). In contrast, an extractant with a flat curve (*e.g.*, TBP, NOR 180 and Versatic10), will preferably be used for the separation of REEs and non-REEs (*e.g.*, impurities such as Ca, Fe, or Pb). With different cuts along the series, it is possible to produce single-element solutions of high purity (>99.9%).

The nature of the anion in the aqueous media (nitrate, chloride, thiocyanate) has a strong impact in the extraction equilibria. Generally, nitrate anions are preferred among the others to generate high distribution coefficients between the two phases (Leveque and Maestro, 1993).

Industrially, SX separations are carried out using kerosene and batteries of hundreds of mixer-settlers. The Rhône-Poulenc (now Solvay) process for extraction and purification of REEs from monazite concentrates have been considered the industry standard (Gupta and Krishnamurthy, 2005). The flowsheet in Figure 20 sums up the main operations described so far.

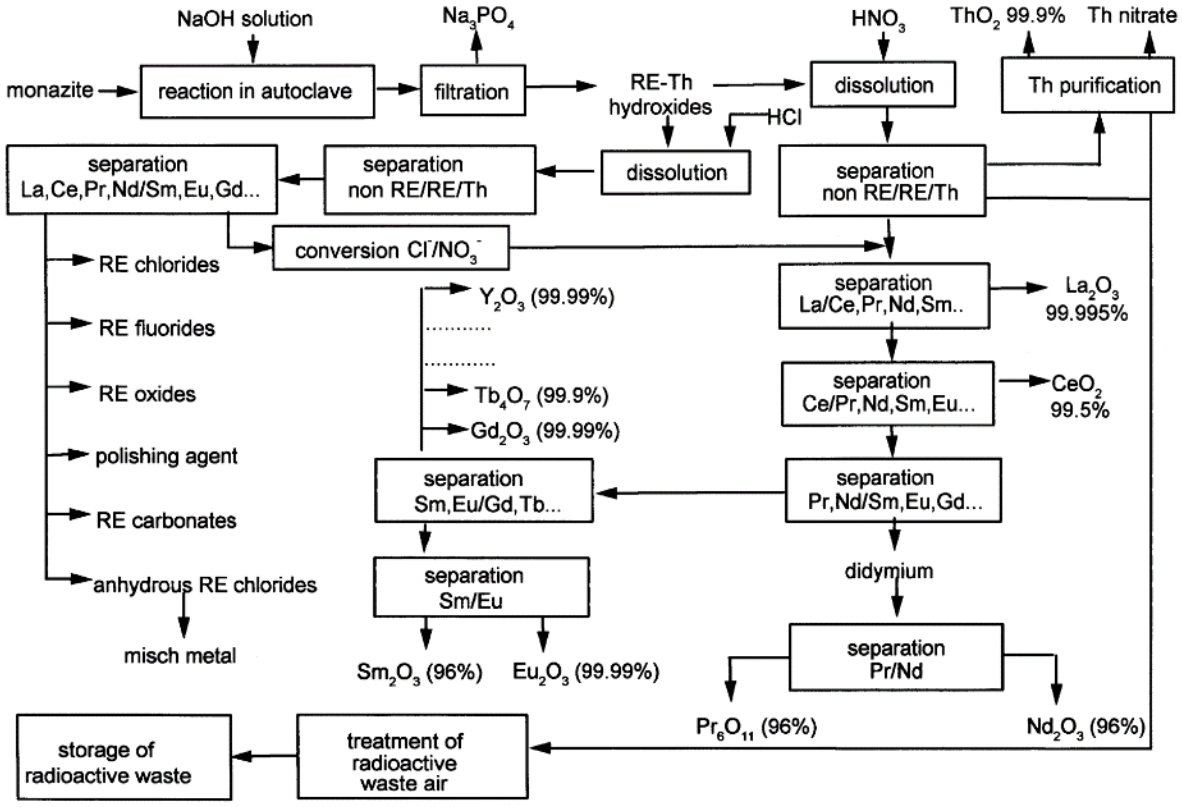

Figure 20: Rhône-Poulenc process for the treatment of monazite (1993) (Gupta and Krishnamurthy, 2005)

First of all, monazite undergoes alkaline cracking (with NaOH) in an autoclave and the aqueous phosphates are recovered in the filtration step, while the REEs remain solid (hydroxides) (please refer to the above part 2.2.1 for the ore cracking operating conditions). The remaining solid is dissolved with nitric or hydrochloric acid, the solution is purified of radioactive thorium and other impurities. The thorium is treated for purification (it can be used as nuclear fuel in particular fission power plants) and the contaminated waste is stored after the radioactive waste treatment.

After dissolution of the hydroxide by hydrochloric acid, the REEs lighter than Sm are isolated and can be used to produce a mix of REE chlorides, fluorides, oxides, carbonates, or mischmetal. The remaining REEs (heavier than Nd) in the chloride solution are converted to their nitrate form and undergo the nitrate route.

In the nitrate pathway, pure La is produced first followed by Ce. Solvent extraction in nitrate medium also enables the separation of REEs heavier than Nd. The separation between Nd and Pr leads to the production of pure Pr and Nd as oxides. For the remaining REEs, separation cuts are between Eu and Gd, followed by the separation of Sm and Eu. The HREEs are also isolated by SX and pure oxide compounds are produced.

This flowsheet illustrates the effectiveness of SX. However, it is no longer relevant because monazite is no longer processed. In order to simplify safety management (Th being radioactive), today, only bastnaesite concentrates are processed.

1.2.2.5.2 Ion-exchange separation

For the ion exchange process, the idea behind the separation is similar. The REEs are in aqueous solution as trivalent cations, they can be adsorbed onto resins coated with chelating molecules. An ion exchange resin consists of porous beads of inert polymer matrix (*e.g.*, polystyrene cross-linked with divinyl-benzene (DVB)), with functional groups attached (*e.g.*, phosphonic acid, iminodiacetic acid, sulfonic acid, amines). As with extractants, resins can be classified depending on the valence of the ion they can exchange: cationic (acid), anionic (alkali), chelating or solvating (neutral). The functional group is balanced with an exchangeable ion to respect electroneutrality. When the resin is saturated with one ion, the resin is said to be "conditioned" or "pre-equilibrated" with this ion.

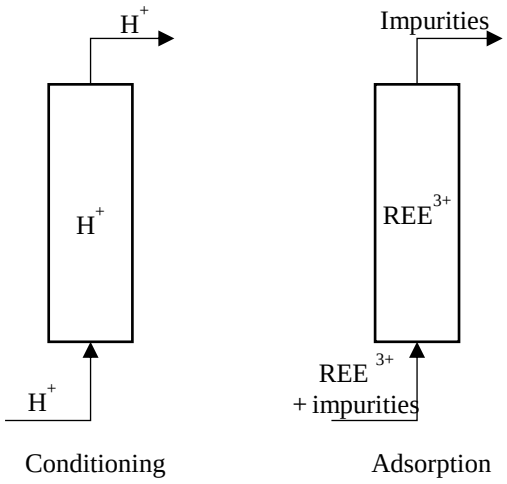

Figure 21: Preliminary stage of conditioning in H^+ form and adsorption of REEs onto a resin

To operate a separation with a resin, two main steps are required: (i) adsorption (or loading) and (ii) elution (or regeneration). During the adsorption step, a saline solution comes into contact with the resin (Figure 21). The mobile ion initially present on the resin matrix can be displaced by another (other) ion(s) in the solution (here mainly REE^{3+}). The other cations, considered as impurities, are likely to be adsorbed as well; the weaker their valence, the less likely they are to bind (divalents, monovalents).

Generally, three rules apply (Gupta and Krishnamurthy, 2005): "(1) an ion of higher charge displaces an ion of lower charge, (2) between similarly charged ions, the one with a larger hydrated radius displaces the one with a smaller radius, and (3) the displacement occurs according to the mass action law." In the elution step, a change of condition (*e.g.*, drastic change of concentration due to the injection of an eluent) causes the desorption of the ion from the resin and its replacement by an ion from the eluent solution.

Two elution strategies can be implemented (Figure 22 and Figure 23). The first method, but the least common in REE purification, is "elution chromatography" (Spedding *et al.*, 1947). The idea is to "push" the adsorbed REEs with an eluent. The eluted compounds move through the resin in broad concentration peaks separated by the eluent. Each REE travels at a different speed along the resin allowing them to be separated. The typical configuration is a sulfonic resin and the eluent alpha-hydroxybutyrate. However, according to Moore, this process "separates a small amount of REEs for the amount of capital and skilled labor invested" (Moore, 2000).

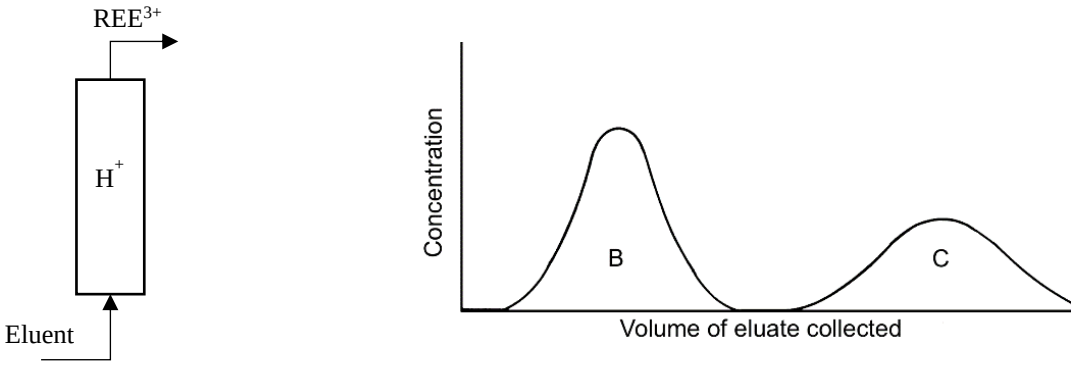

Figure 22: Principle of elution chromatography

The most widely used elution strategy for producing isolated REEs is "band displacement chromatography". Advances in the separation of individual REEs using this technique are credited to Spedding and his team in the mid-1950s (Leveque and Maestro, 1993; Spedding and Powell, 1960; Spedding and Voigt, 1951). A series of columns containing an ion exchange resin are connected in series. The solution containing a mixture of REEs is loaded onto the first column, which is called the "loading column" until saturation. In the first column the resin bears sulfonic groups. The subsequent columns are the separation columns. The eluents which have been used are citric acid and lactic acid (Habashi, 2013; Spedding and Voigt, 1951), EDTA or HEDTA (Moore, 2000; Morton, 1969; Spedding and Powell, 1960).

The separation columns are initially conditioned with a special cation: either Cu^{2+}or Zn^{2+} when using EDTA, or H^+ when using HEDTA), also called "retaining ion". During elution, this sorbed cation is exchanged against the REEs chelated with EDTA, thus acting as a "chemical barrier" to prevent the HREEs from travelling at the speed of EDTA. The LREEs in solution are preferentially sorbed onto the resin, while the HREEs are pushed out into the solution by forming strong chelates with EDTA. Hence, bands of high purity develop, according to the molecular weight (Moore, 2000).

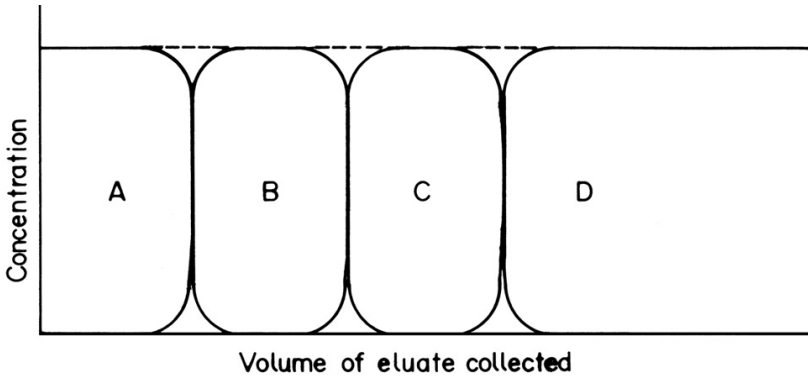

Figure 23: Principle of displacement chromatography (Habashi, 2013)

Habashi (2013) precisely described the industrial process using ion exchange resins. Six columns of resins were placed in series. After loading, and band development using citrate and pH control using lactic acid, the lightest REEs (La, Ce) are sorbed in the first two columns while the heaviest are sorbed onto the last one. While the majority of yttrium, terbium, and dysprosium are concentrated on the middle two columns. Each set of two columns was further fractionated through a series of eight smaller columns

(Figure 24). After the final elution, monoelement rare earth oxalates of high purity are obtained. The oxalates then go through a calcination step to obtain pure oxides.

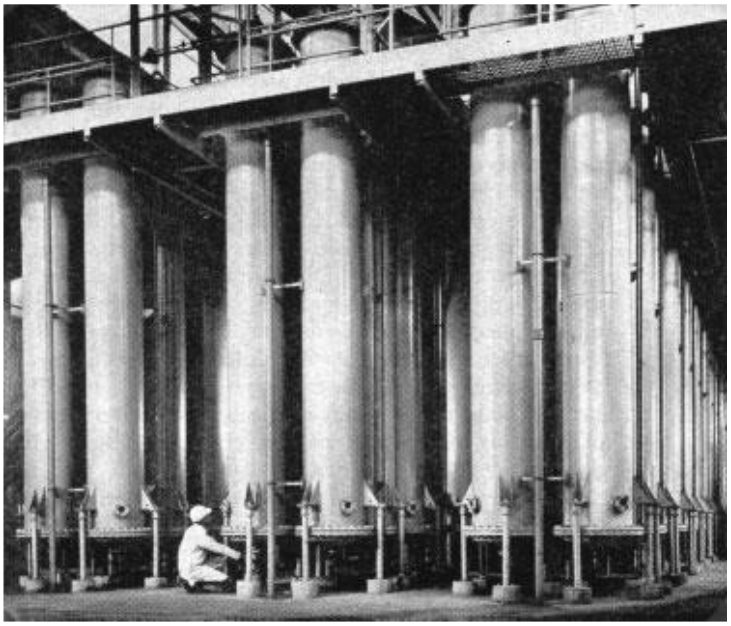

Figure 24: Ion exchange columns for separation of lanthanides at Michigan Chemical Corporation, St. Louis, Michigan (Habashi, 2013)

The main drawback of ion exchange techniques is the long operating time before fully separating a batch of REEs (about several months) (Moore, 2000). Today, solvent extraction has taken over IX techniques for industrial scale production. Solvent extraction enables higher productivity and continuous operation but its drawbacks reside in the purchase and management of series of hundreds of mixers-settlers.

1.2.3 Secondary resources and associated processes

There has been a growing interest in searching for alternative sources of REEs, considering the imbalance between production and demand, high prices, and non-negligible supply risk (please see 1.4 Market for REEs). Secondary sources include the end-of-use recycled products, pre-consumer scrap, and industrial process residues (Binnemans *et al.*, 2015, 2013). The processes for recovering REEs from these matrices differ from conventional ore processing, as matrices are diverse, REEs are diluted and accompanied by significant amounts of other unwanted elements (Fe, Al, Si, plastics).

1.2.3.1 Recycling

Only a tiny portion of REEs is recycled (less than 1% in 2011) (Binnemans *et al.*, 2013). However, the literature on REE recycling is rich, and lab-scaled recovery experiments have shown numerous routes that could be undertaken to effectively recycle these high-value elements. Efficient collection, increased public incentive, and the development of identified recycling pathways are the main gaps that need to be overcome for effective REE recycling.

Regarding the recycling of REE-containing products, the main secondary sources include pre-consumer magnet scrap and end-of-use magnets (Binnemans *et al.*, 2013; Ellis *et al.*, 1994; Lyman and Palmer, 1992) (NdFeB alloy, with a significant portion of Dy depending on the application), nickel-metal-hydride batteries (LREEs) (Luidold and Antrekowitsch, 2012; Müller and Friedrich, 2006), and lamp phosphors (high HREE content) (Braconnier and Rollat, 2010; De Michelis *et al.*, 2011).

Regarding the latter, the recycling industry seems compromised due to the progressive replacement of REE phosphors by other efficient lighting technologies (*e.g.*, LED).

Recycling of batteries and magnets can be done through either pyrometallurgical or hydrometallurgical route. However, hydrometallurgy is always needed as REEs are often found in furnace slags. The processing always follows the same scheme: an acid leaching followed by a purification. Solutions of HCl, HNO_3, H_2SO_4, and NH_4Cl have been studied for various magnets, magnet scraps and battery electrodes (Binnemans *et al.*, 2013). Depending on the matrix, HCl or H_2SO_4 is reported to be the most effective. The nature of the acid used also depends on the downstream purification process: nitric or hydrochloric acid is preferred for solvent extraction and ion exchangers, while sulfuric acid is more suitable for oxalate selective precipitation or sulfate double salt.

The aforementioned technique is used in the process developed by Lyman and Palmer (Lyman and Palmer, 1992) after the complete dissolution of NdFeB magnet in sulfuric acid. It consists of adding an alkali (KOH, NaOH or NH_4OH) to the sulfuric acid leachate containing the REEs. At pH 1.5, $REE_2(SO_4)_3M_2SO_4 \cdot 6H_2O$ (M = Na, K, NH_4) precipitates (Lyman and Palmer, 1992). It can be later converted to $REEF_3$ using HF.

1.2.3.2 Industrial process residues

According to Binnemans *et al.* (2013), phosphogypsum, bauxite residue (red mud), mine tailings, metallurgical slags, coal ash, incinerator ash, and wastewater streams are potential secondary sources of REEs. They present dilute concentrations but are available in large volumes (Binnemans *et al.*, 2015).

Phosphogypsum is the main by-product of the phosphoric acid production process. Phosphate ore is attacked by sulfuric acid (H_2SO_4); phosphoric acid is formed as well as gypsum ($CaSO_4$) called phosphogypsum. The phosphate ore can come from sedimentary deposits (85 to 90% of the world's reserves) with low REE contents (0.01 to 0.1% in mass), or from igneous rocks (accounting for 15% of the world's reserves). The re content in such rocks can reach 1-2%. During the reaction step, the majority of the REEs (70 to 85% of them) end up in the phosphogypsum residue. While the concentrations in the residue are low, tremendous amounts are produced every year (270 Mt in 2018 (Jasinski, 2019)). Rychkov described a recovery process sulfuric acid for the leaching step, a strong acid resin for the purification (sulfonic acid functions) and REE precipitation was conducted with NH_4CO_3 (Figure 25) (Rychkov *et al.*, 2018).

Bauxite residue, or "red mud" is the main by-product of aluminum oxide production. Bauxite is the raw ore of aluminum hydrated oxide. In the Bayer process, it is treated by NaOH to form soluble $NaAlO_2$ and the solid residue is called "red mud". The residue contains everything that could not be solubilized in the strongly alkaline solution, including the REEs associated with iron and titanium. The composition of the red mud varies with the composition of the parent bauxite ore, but the scandium content is notable, and unusually consists of an essential fraction of the total REEs present. The Jamaican bauxite residue can contain up to 390 $\mu g.g^{-1}$ (out of 2 000 $\mu g.g^{-1}$ of total REE). Greek bauxite residue exhibits a concentration of 130 $\mu g.g^{-1}$ Sc, while Suriname red mud contains up to 1 700 $\mu g.g^{-1}$ of Sc. Compared to the earth's crust (22 $\mu g.g^{-1}$ (Binnemans *et al.*, 2015)) or even other REE ores (few $\mu g.g^{-1}$ (Gupta and Krishnamurthy, 2005)), these concentrations are significantly higher.

Due to the inefficiency of ore beneficiation, RE mine tailings themselves can contain large amounts of REEs. This is the case for the two biggest mines in the world - Mountain Pass and Bayan Obo. At Mountain Pass, the tailings still contain up to 5% rare earth oxide, and Zhang *et al.* stated that only 10% of the REEs were actually recovered from the ore at Bayan Obo (Zhang *et al.*, 2014).

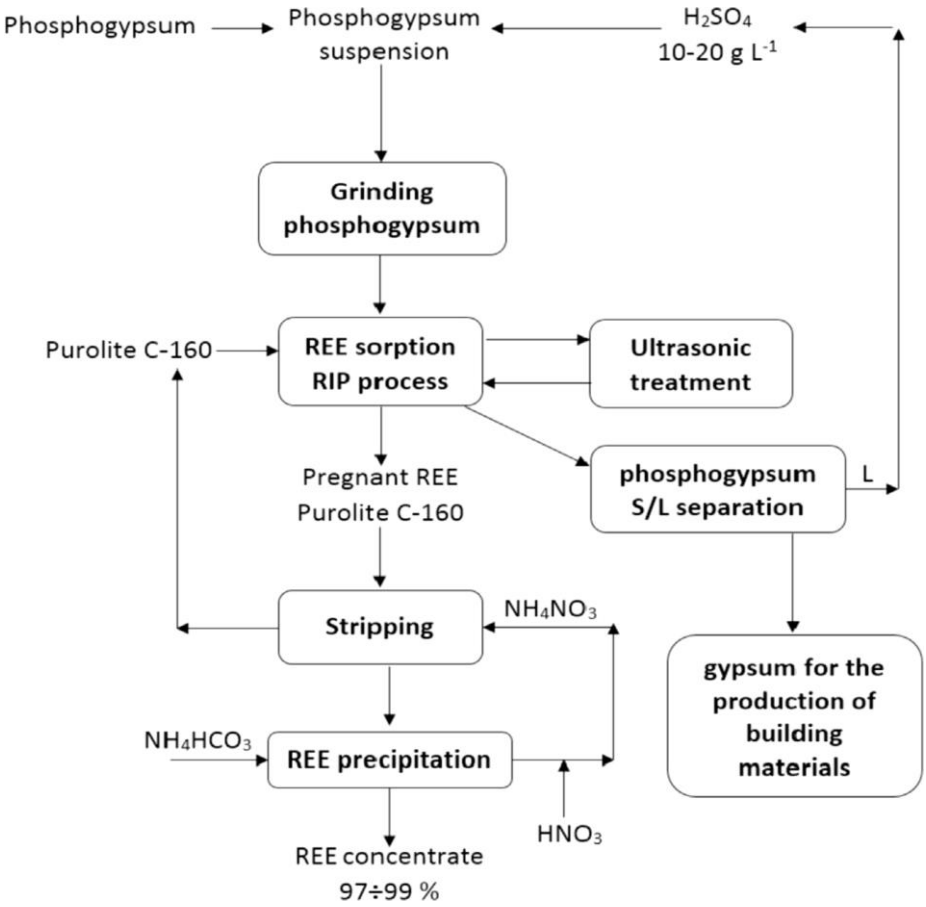

Figure 25: Conceptual flow sheet for REE recovery from phosphogypsum by leaching by sulfuric acid (Rychkov *et al.*, 2018).

Tailings from different types of mines (iron, titanium, uranium, niobium) have been studied as a potential secondary source of REEs (Binnemans *et al.*, 2015). Acid mine drainage from metal or coal mines is also reported as a potential source of rare earth. Several studies have aimed to recover the REEs with solid materials such as resins (Page *et al.*, 2017; Ramasamy *et al.*, 2017), but also inert materials such as cement dust (Ali *et al.*, 2011), nanoparticles (Li *et al.*, 2013), bio-nanocomposites (Iftekhar *et al.*, 2018, 2017a, 2017b), and even biosorption (on bacteria such as *Pseudomonas* sp., fungi such as *Ganoderma lucidum*, and sea algae such as *Sargassum*) (Binnemans *et al.*, 2015; Das and Das, 2013).

Finally, coal ash and oil shales also contain a wide variety of metals that could be recovered according to Binnemans, while incinerator ashes are not concentrated enough (Binnemans *et al.*, 2015).

1.2.4 The need for a less impacting industry

At present, harm derived from the REEs themselves do not appear preoccupying due to their low mobility and toxicity. Oppositely, the extraction and refining process is of prime concern.

Extensive mining, in-situ or heap leaching, have direct environmental impacts (land erosion, eutrophication). Indirect impacts stem from energy usage (ore cracking, roasting, calcination) and chemicals (acid and base, solvents) as part of the RE refining. Discharge of fluorides or radioelements are other negative impacts associated with the extraction of bastnaesite and monazite, respectively.

To quantitatively realize the extent of those impacts, a systematic analysis is required. Life cycle assessment (LCA) is a standardized method (International Standard Organization (ISO), 14040-14049 series) which is commonly accepted to evaluate and compare the environmental impacts of a process or a product. Briefly, the framework can be described by four stages (Figure 26):

- Defining the goal and scope of the study sets the boundaries of the system, the functional unit (this can be defined in terms of mass of product, or the required service the product provides).
- The inventory analysis lists all the materials and energy used in production, as well as emissions and by-products generated by the process.
- Impact assessment attributes environmental impacts to the use of the inventoried materials and energy *e.g.*, global warming potential (in kg of CO_2 per functional unit), water consumption (in kg of water per functional unit) or land use (in ha per functional unit), among others.
- Interpretation or data analysis enables the identification of the steps of the production process that generate the most impact, or the comparison with the same functional unit, but processed differently. Impacts can be benchmarked against the contribution of a single person (in a specific country, or worldwide) (Zapp *et al.*, 2018). For example, "ReCiPe" is a method to convert impacts to "person equivalents (PE)" and enables impacts to be summed.

As with other process of production, the LCA method can be applied to REEs. Publications related to the LCA of rare earth compounds only started to appear in 2014. One of the first studies was proposed by Koltun and Tharumarajah, with the estimation of the Global Warming Potential (GWP) associated with the production of 1 kg of a single REE in China, using the Bayan Obo mixed ore (bastnaesite and monazite) with the Chinese process (acid baking) (Koltun and Tharumarajah, 2014).

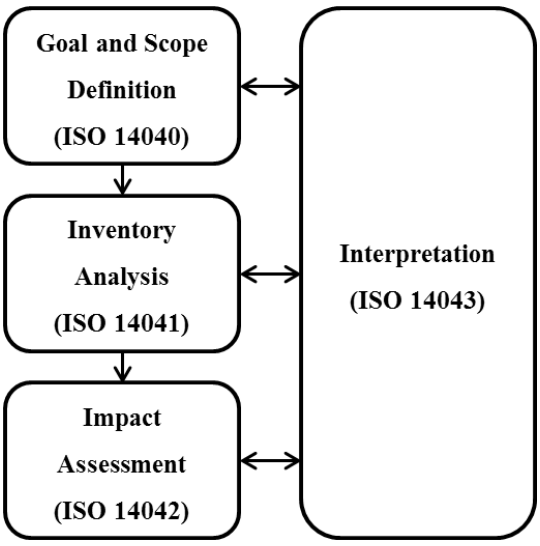

Figure 26: The LCA framework as defined in ISO 14 040

The computed CO_2 equivalent per kilogram of REO is depicted in Figure 27. Hence, in this assessment, the production of 1 kg of La generates around 10 kg of CO_2 equivalent. Contributions to this impact are mainly attributed to the chemical reagents used (HCl, solvent disposal).

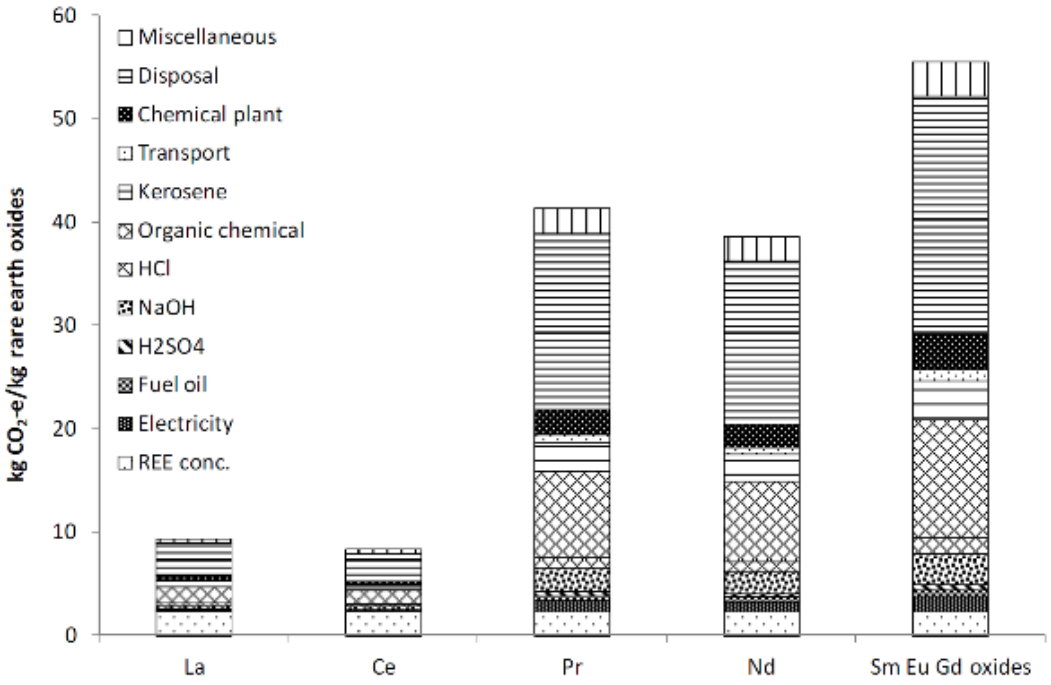

Figure 27: Greenhouse gas footprint of selected RE products (Koltun and Tharumarajah, 2014). Disposal includes hazardous solvent incineration. Mine rehabilitation is among the miscellaneous activities (Koltun and Tharumarajah, 2014; Weng *et al.*, 2013)

It can also be observed that GWP values are higher for heavier REEs than for La and Ce. This effect is due to the naturally higher abundances of the LREEs in bastnaesite and monazite mineral. The authors also showed that the distribution of impacts on the various REEs was affected by the allocation method used: the equal repartition of impacts using the mass composition of an ore is called "mass allocation". An alternative allocation suggested is a combination of mass, concentration, and price, to consider the fact that the REEs are always found together and will be processed together anyway. This fact also generates the so-called "balance problem": all REEs are produced whether they are wanted or not. This phenomenon implies the possible creation of stockpiles of unwanted elements (*e.g.*, an oversupply of La and Ce), or a failure of supply of particularly demanded elements that are not abundant, *e.g.*, a potential shortage of Dy or Lu (Binnemans *et al.*, 2018; Binnemans and Jones, 2015).

Apart from these considerations, LCA studies have been limited due to out-of-date (Mountain Pass processes from the '90s), or incomplete and inconsistent data sets (Chinese process), as demonstrated by Navarro and Zhao, until very recently (Navarro and Zhao, 2014).

Vahidi *et al.* have helped to fill these gaps by proposing comprehensive studies along the REE processing steps: ion-adsorption clay leaching (Vahidi *et al.*, 2016), solvent extraction separation (Vahidi and Zhao, 2017), and neodymium metal production via molten salt electrolysis (Vahidi and Zhao, 2018). Schreiber *et al.* proposed a LCA of the Dy and Nd metals that would be produced in Sweden (Nora Kärr) and compared it to the same metals that would be produced using Bayan Obo ore and the Chinese process (Schreiber *et al.*, 2016). The latter study was expanded to apply to ionic adsorption clays as a primary source of REEs (Figure 28) (Zapp *et al.*, 2018). Schulze *et al.* further developed and extended this study with more precise data using industrial insights, adding the solvent extraction separation step (Schulze *et al.*, 2017).

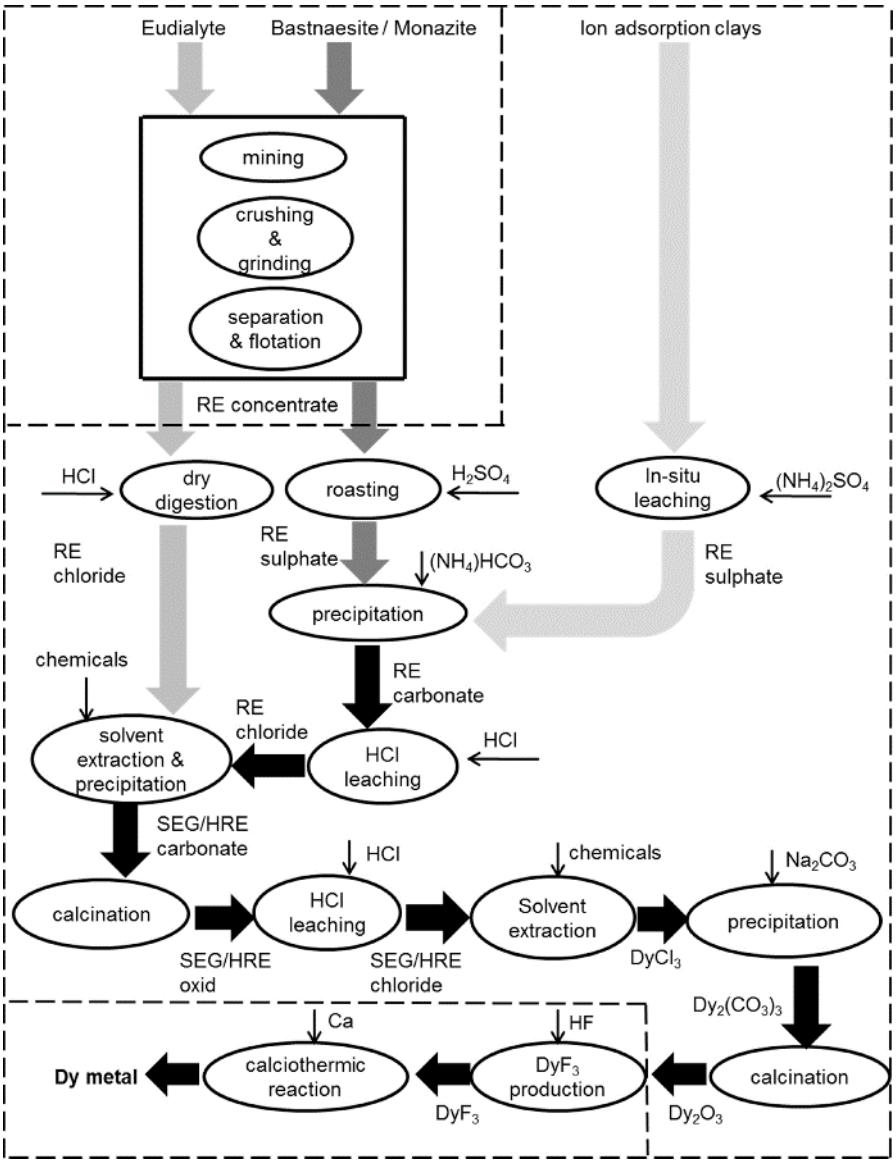

Figure 28: Flowsheet considered for the production of 1 kg of Dy metal with three possible resources (Zapp *et al.*, 2018)

Schreiber *et al.* considered the extraction of eudialyte from the Swedish Nora Kärr mine, the production process is dry digestion with HCl of the mineral (later called "eudialyte"). They also considered the conventional Chinese production process from bastnaesite/monazite. Because of two possible variations of the process, two scenarios were drawn "B/M" and "B/M sensitiv" (the second considering phosphate removal in wastewater). Finally, for ionic adsorption clays (IAC), three leaching scenarios were considered. The scenarios "IAC low", "IAC middle", and "IAC high" represent different leaching yields: respectively 9.9 kg, 24 kg, and 80.6 kg of ammonia sulfate per kg of REO. For each scenario, the steps following solvent extraction of the REEs, were the same. The final results were computed using the "ReCiPe world" impact normalization method (Figure 29).

The traditional processes ("B/M" "B/M sensitive", "IAC low", and "IAC middle") are comparable in terms of total impact. A significant difference can be observed when considering the high losses of ammonia in the environment for the "IAC high" scenario. In this case, the impact of marine eutrophication is the most significant, accounting for approximately two-thirds of the total impact. Zapp *et al.* report that 99% of the marine eutrophication impact were generated directly at the mining site. For

the remaining impacts, 78 to 95% of the total in-situ leaching impacts were generated in upstream ammonium sulfate production (Zapp *et al.*, 2018).

The "Eudialyte" scenario has the lowest total impact. However, emphasis should be put on the fact that this process has only been implemented on at laboratory scale. Hence, the production of Dy with European ore looks promising but as with any LCA study, data quality is crucial and scaling up may significantly influence the final results.

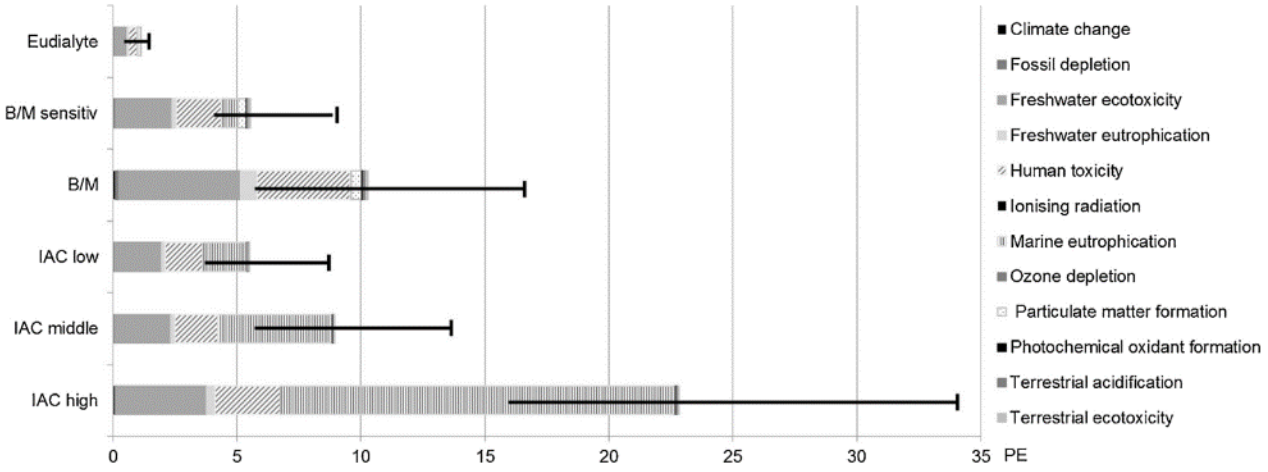

Figure 29: Impacts of the production of 1 kg Dy in person equivalents (PE) with deviation (Zapp *et al.*, 2018)

Considering the remaining studies, there is overall agreement that REE extraction and refining has more impact than other commonly mined trace metals (Browning *et al.*, 2016; Haque *et al.*, 2014). For example, the GWP of titanium from the standard process (Becher and Kroll) is 35.7 kg CO_2e.kg^{-1} (Norgate *et al.*, 2007), Browning *et al.* results indicate an average (on all REEs) of GWP value of 65.4 kg CO_2e.kg^{-1} with monazite processing (Browning *et al.*, 2016), and Koltun and Tharumarajah estimate GWP associated with Pr and Nd at 39 kg CO_2e.kg^{-1} (Koltun and Tharumarajah, 2014).

These studies constitute a strong basis, enlighten and delineate flaws of the process. Additionally, the inventory of reagents and energy consumed, as well as the contaminants emitted, sets grounds for process comparison and optimization.

These data are crucial when designing a new process, in this case, the agromining of the REEs. The novel process implicates a different scenario (to be described later) and the associated impacts must be assessed to ensure that the impacts are mitigated compared to traditional processes.

Complementary to LCA, indicators can be computed from mass inventories and balances for a given process. The E factor (E standing for environmental), was one of the first developed for chemical processes, primarily for pharmaceuticals (Sheldon, 1992). Its definition is straightforward: the E factor is defined as mass ratio of waste to desired product.

$$\mathrm{E} = \frac{\mathrm{mass}_{\mathrm{waste}}}{\mathrm{mass}_{\mathrm{product}}} \quad (9)$$

The other most recognized tool to assess the environmental acceptability of chemical process is the "atom economy", (sometimes referred to as "atom efficiency") proposed by Trost in 1991 (Sheldon, 2007; Trost, 1991). The atom economy focuses on a specific chemical reaction. It is calculated by dividing the molecular weight of the product by the sum total of the molecular weights of all substances formed in the stoichiometric equation for the reaction involved.

$$E_{At} = \frac{(\nu_{product} M_{product})}{\sum_i |\nu_i| (M_{product})_i} \quad (10)$$

The atom economy is often expressed in percentage, 100 % E_{At} would mean that all the atoms from the reagents are incorporated in the product, and there is no by-product (*e.g.*, additions in organic chemistry). In fact, most the reactions (acid-base, oxidation-reduction, substitutions, etc.) generate by-products and yield E_{At} far below 100%.

The atom economy is theoretical because it relies on a stoichiometric reaction. In practice, reagents are often introduced in stoichiometric excess for various purposes (kinetics, equilibrium displacement). Those practical considerations are taken into account when computing the E factor, which accounts for the all kind of waste generated by the process (Sheldon, 2007). Hence, only the E factor will be addressed in this thesis.

Orders of magnitude for this metric vary depending on the sector of chemistry (Table 10). In those calculations solvent and water are assumed to be recycled and most often than not, are excluded from calculations. When actual recycling rates are known and included, the complete E factor (cEf) can be computed (Sheldon, 2017).

Table 10: Orders of magnitude for the E factor in different chemical industry segments (Sheldon, 1992).

Industry segment	Tons per annum	E factor (kg waste per kg product)
Oil refining	10^6–10^8	<0.1
Bulk chemicals	10^4–10^6	<1–5
Fine chemicals	10^2–10^4	5–50
Pharmaceuticals	10–10^3	25 – >100

Regarding mineral and metal processing, these indicators (E factor, atom economy) are not commonly reported in the literature. Orders of magnitude can be estimated for a specific process. For example, the production of alumina through the Bayer process generates 0.7 to 2 tons of bauxite residue ("red mud") per ton of alumina produced (International Aluminium Institute, 2015). The production of one ton of phosphoric acid generates 4.5 – 5.5 t of phosphogypsum (Chuan *et al.*, 2018). For the recovery of metals, the amount of waste will greatly depend on the amount of gangue mineral treated, increasing with decreasing grade.

1.3 RE agromining

How the use of plants can help limit the impacts of mining and provide a viable secondary source of REEs

1.3.1 Phytoremediation: definitions and practical applications

Phytoremediation can be defined as the use of plants and their associated microorganisms to contain, inactivate, degrade or eliminate soil contaminants (Morel *et al.*, 1999; Sterckeman *et al.*, 2011). More marginally, it may also refer to the decontamination of other environmental compartments such as air or water. Phytoremediation aims to address some organic pollutions (pesticides, phenolic compounds) and trace metal elements (heavy metals such as Cd, Hg, Zn or metalloids such as As). It has the advantages of being an in-situ process, fixing atmospheric carbon, restoring soil and site properties altered, not altering soil morphology, and enhancing visual aspect. Restoration of some ecosystem services of the degraded field is also a valuable asset (Burges *et al.*, 2018; Cundy *et al.*, 2016). It is reputed to be a low-cost process compared to processes based on mechanical extraction followed by either thermal or chemical treatment. This is especially true for moderately polluted extensive surfaces. Additionally, thermal and chemical treatment may prevent further reuse of the soil, whereas the use of plants tends to restore soil functions and promotes the return of ecosystems. In some instances, biomass valorization is possible, which reduces the overall cost.

Generally, sub-processes are defined for phytoremediation: (i) phytostabilization, (ii) rhizodegradation, (iii) phytodegradation, (iv) phytovolatilization, and (v) phytoextraction.

In **phytostabilization**, a vegetation cover simply limits the availability and spreading of the contaminant by stabilizing the soil, retaining contaminating soil particles that wind or precipitations could transport, and limiting contaminant leaching by meteoric water.

Rhizodegradation involves the activation of microorganisms in the plant's rhizosphere to degrade the pollutant. On the other hand, **phytodegradation** involves the metabolic mechanism of the plant. In both cases, it can only address organic pollution (xenobiotics).

Phytovolatilization corresponds to the absorption of pollutants from the soil by the plant, their conversion into a volatile form and their subsequent release into the atmosphere. It can be applied to treat organic pollution but also to certain elements such as Hg or Se. Generally, the volatile form of these elements is methylated. The drawback of this technique is that the pollution is only transferred from one environmental compartment to another (from soil to air).

Phytoextraction is the technique of interest here. The plant absorbs the contaminant from the soil with its roots and translocates it to its aerial parts (leaves, fruits, seeds) through the stem. The roots can even secrete exudates to enhance the availability of the contaminant. Only a small number of plants can extract uncommonly high amounts of metals; they are called "hyperaccumulators" (HAs). Phytoextraction is at the core of agromining.

The scientific community is well aware of the fact that effectiveness must be evaluated by experiments in plots, under real conditions, and not only under controlled conditions at the laboratory scale. Like all soil remediation methods, it is situation-specific and cannot be compared to highly intrusive methods such as excavation, thermal methods, etc. The main limiting factors for the expansion and large-scale development of phytoremediation are the appropriate selection of adapted species and the availability

of their seeds, the rather slow speed of the process, and the reluctance of industries, among others. However, the integration of the production of valuable biomass (*e.g.*, fibers, highly-concentrated metal in the plant) offers opportunities for phytoremediation at an industrial scale (Morel *et al.*, 1999). In addition, these methods have excellent societal acceptability.

1.3.2 Hyperaccumulating plants (Hyperaccumulators)

The term hyperaccumulator (HA), which was first used by Brooks *et al.*, refers to a plant species that can accumulate unusually high amounts of an element (Brooks *et al.*, 1977). For example, for nickel, concentrations in plants above 1 000 $\mu g.g^{-1}$ on a dry weight basis are extremely rare and can be referred to as hyperaccumulator (Brooks *et al.*, 1977). In contrast, the concentration of Mn in plants is higher, resulting in a higher threshold value of 10 000 $\mu g.g^{-1}$. Van der Ent *et al.* set the hyperaccumulation criterion to be "at a minimum of 2–3 orders of magnitude higher than the range of foliar concentrations on normal soils, and at least one order of magnitude greater than the range in foliar concentrations on metalliferous soils" (van der Ent *et al.*, 2013).

Hence, over the years, a threshold value of foliar concentration (dry mass) has been defined for several elements to delineate hyperaccumulation:

- 100 $\mu g.g^{-1}$ for Cd, Se, and Tl
- 300 $\mu g.g^{-1}$ for Cu, Co, and Cr
- 1 000 $\mu g.g^{-1}$ for Ni, As, and Pb
- 3 000 $\mu g.g^{-1}$ for Zn
- 10 000 $\mu g.g^{-1}$ for Mn.

For a series of elements, the hyperaccumulation threshold has not been established and published (*e.g.*, REEs, Al, Sb) (van der Ent *et al.*, 2013) but the nominal value of 1 000 $\mu g.g^{-1}$ is commonly suggested by various authors (Liu *et al.*, 2021).

Nickel HAs have been by far the most studied type. When the concentration of Ni reaches ten times the hyperaccumulation value, the plant is said to be hypernickelophore. Zn and Cd HA have also been studied extensively. In 2013, Van der Ent *et al.* reported the number of hyperaccumulating species by element: " Ni (450), Cu (32), Co (30), Se (20), Pb (14), Zn (12), Mn (12), As (5), Cd (2), Tl (2)". Values for Co and Cu hyperaccumulators could be revised because of probable contamination during sampling (Faucon *et al.*, 2007; van der Ent *et al.*, 2013). Examples of species known as HAs are given in Table 11.

Since then, on-site investigations in ultramafic areas (Bouman *et al.*, 2018), and systematic scanning of world's herbaria have led to the discovery of new species of HAs (Purwadi *et al.*, 2021). In fact, systematic scanning can be conducted using a portable X-ray fluorescence spectrometer with high throughput thanks to the recent development of this technology and equipment (van der Ent *et al.*, 2019).

Usually, plants do not tolerate high amounts of heavy metal or other toxic metalloids in the soil. However, in the case of hyperaccumulators, the plant is able to survive on such a toxic environment. The toxic element is extracted from the soil by the plant roots and translocated into its aerial parts (leaves/fronds/fruits/seeds). The roots are able to withdraw the metal from the bioavailable compartment of the soil, but they also secrete exudates to convert unavailable metal for further extraction (Merlot *et al.*, 2021). Additionally, rhizosphere microorganisms are known to play a key role in enhancing metal availability (Benizri *et al.*, 2021). Hyperaccumulating plants found at the site generally accumulate one

element, but off-site studies have shown that often more than one element could be accumulated (Merlot *et al.*, 2021).

Table 11: Examples of hyperaccumulator plant species reported first (Chaney *et al.*, 2021).

Element	Species	Concentration (µg.g^{-1})	Reference
Cd	*Noccaea caerulescens*	3 000	(Reeves *et al.*, 2001)
Co	*Haumaniastrum robertii*	10 200*	(Brooks *et al.*, 1977)
Cu	*Haumaniastrum katangense*	8 356*	id
Pb	*Thlaspi rotundifolium*	8 200	(Reeves and Brooks, 1983)
Mn	*Macadamia neurophylla*	55 000	(Jaffré, 1979)
Ni	*Alyssum bertolonii*	13 400	(Minguzzi and Vergnano, 1948)
Ni	*Berkheya coddii*	17 000	(Morrey *et al.*, 1992)
Se	*Astragalus pattersoni*	6 000	(Cannon, 1960)
Tl	*Iberis intermedia*	3 070	(Leblanc *et al.*, 1999)
U	*Atriplex confertifolia*	100	
Zn	*Noccaea caerulescens*	10 000	(Reeves *et al.*, 2001)

* Often cited as a hyperaccumulator, it turns out that the actual Cu concentration in *Haumaniastrum katangense* leaves (and other supposed Cu hyperaccumulators) is significantly lower (*ca.* 200 µg.g^{-1} in this case). The formerly high reported value is due to metal dust deposited on the surface of the sticky leaves (Faucon *et al.*, 2007).

1.3.3 Agromining

1.3.3.1 Concept and agronomy

In 1983, Chaney proposed the use of metal hyperaccumulators to remediate polluted soil, and he also introduced the concept of "phytomining" (Chaney, 1983). In phytomining, HA harvesting could constitute a viable source of metal. A few decades later, the practical experience of nickel phytomining in the Balkans (Bani *et al.*, 2015a) added more perspective. The necessary use of adapted agronomic practices for optimal Ni uptake and biomass production led Morel and the experts of the field to propose the term "agromining" to broaden the scope of phytomining (van der Ent *et al.*, 2015).

1.3.3.2 Ni agromining

In 2019, several plot experiments of nickel agromining were conducted in Albania, France, Spain, United States, Malaysia. The most noteworthy trial is probably in Pogradec (Eastern Albania) (Figure 30) using *Odontarrhena chalcidica (*syn. *Alyssum murale*) field trial in Pogradec started in 2005 (Bani *et al.*, 2015a, 2015b, 2007). Agronomic trials involving NPK fertilization, plant density, and weed control, among others, increased Ni yield from 25 kg.ha^{-1} in 2007 (Bani *et al.*, 2007) to 105 kg.ha^{-1} (Bani *et al.*, 2015a). Plot experiments, involving co-culture trials, and plant growth-promoting rhizobacteria (PGPR) trials, have also been conducted on serpentine soils in Spain (Kidd and Monterroso, 2005; Saad *et al.*, 2018), Eastern Austria (Rosenkranz *et al.*, 2019), and in Greece (Kidd *et al.*, 2018).

The most recent field experiment is conducted in Malaysia (Figure 31) (Tisserand *et al.*, 2018). The grown HAs belong to the *Violaceae* family *(Rinorea bengalensis)* and the *Phyllanthaceae* family (*Phyllanthus rufuschaneyi*) (Nkrumah *et al.*, 2019). The perspectives appear to be promising as measured concentrations of Ni in grown shoots range up to 20 000 µg.g^{-1}.

Figure 30: Large-scale demonstration of agromining of Ni with *Odontarrhena chalcidica* growing on ultramafic substrate in the Balkans (Albania), and harvesting and baling operations (Nkrumah *et al.*, 2021)

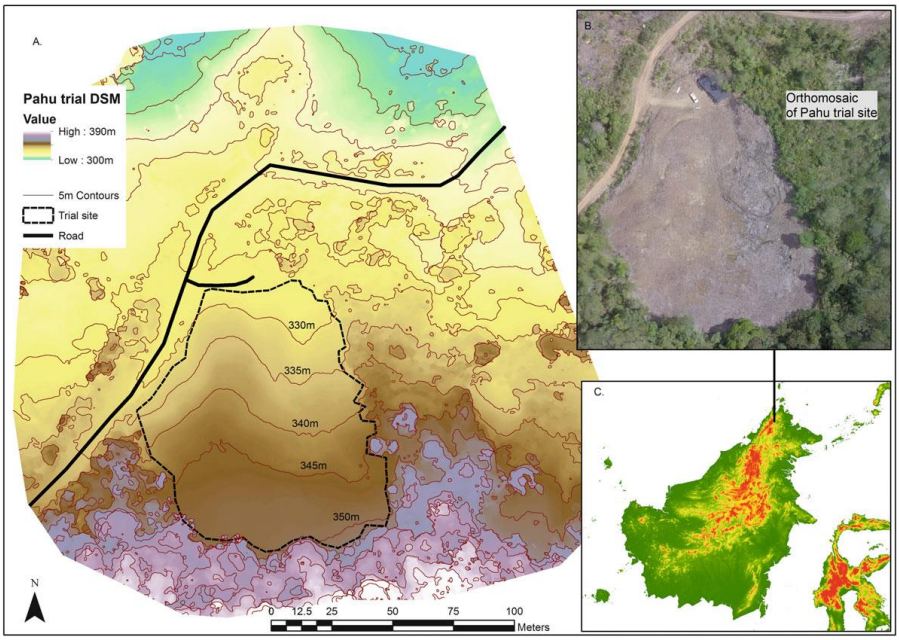

Figure 31: Large-scale field site for tropical Ni agromining demonstration in Sabah, Malaysia (Nkrumah *et al.*, 2021)

Harvested *O. chalcidica* biomass has been shown to have the potential to recover Ni through pyrometallurgical and hydrometallurgical treatments (Laubie *et al.*, 2021). Biomass differs significantly from conventional metal ores in its high organic carbon content. High contents of Ca, Mg, and K are also typical of plant biomass, and minor impurities such as Cl and P are present (Laubie *et al.*, 2021). Three approaches were experimentally evaluated for Ni recovery.

The very first approach was to feed the dry biomass to a traditional smelter (Li *et al.*, 2003), which causes practical issues of dusting, reaction of alkaline compounds with the refractory liners of the smelter, and Ni losses through recombination with impurities. The second approach consists of ashing the biomass, and use hydrometallurgical techniques to leach nickel from the ash, purify it from other compounds in solution and recover it by precipitation (hydroxides, salts). Direct leaching with either water or an extracting agent is the third approach. However, nickel solubilizes with substantial amounts of organic matter (short length carboxylic acids, histidine) that hamper simple purification through precipitation (Guilpain *et al.*, 2018). Successful attempts to recover Ni following this route have therefore required solvent extraction for purification before electroplating (Barbaroux *et al.*, 2011).

Another option is to collect and purify the carboxylic acids bearing the nickel such as, then purify them from other metals using an ion exchanger (Guilpain, 2018).

The ashing route has been the most promising: the advantages include energy generation during combustion, organic matter destruction, and concentration of the elements. Emphasis has been put in producing high-value compounds for the industry such as double salts (*e.g.*, $(NH_4)_2Ni(SO_4)_2 \cdot 6H_2O$ (ANSH)) to increase the economic viability of the process (Figure 32). Briefly, the process involves water washing of the ash to remove K, sulfuric acid leaching of the ash to solubilize Ni, neutralization of the leachate with $Ca(OH)_2$ to precipitate iron hydroxide, NaF addition to precipitate MgF_2, concentration by evaporation before ammonium sulfate addition to form insoluble ANSH (Barbaroux *et al.*, 2012; Zhang *et al.*, 2016).

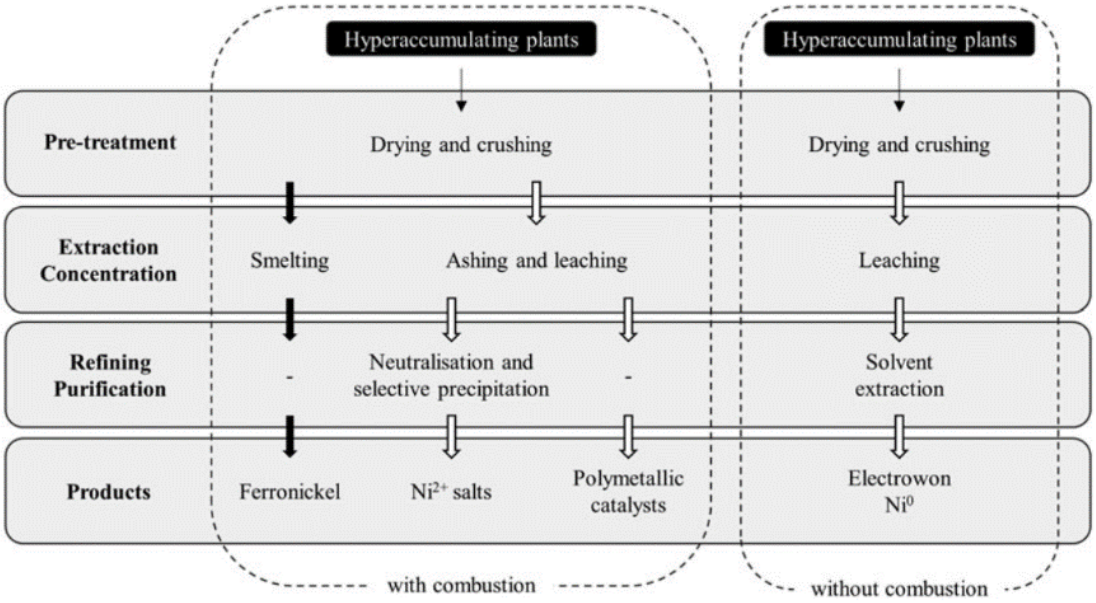

Figure 32: General flow sheet of hyperaccumulator treatment to obtain Ni and Ni compounds (Laubie *et al.*, 2021)

These processes are still being improved and developed for the manufacture of products of industrial interest. Several researchers from the University of Lorraine have created a company, called Econick, to implement the agromining process.

The potential impacts of the agromining chain for Ni were assessed in a LCA (Rodrigues *et al.*, 2016). The representative scenario was the cultivation of *O. chalcidica* onto serpentine soils in Albania, followed by ashing, and the production of Ni salts from the ash. It appears that agromining has the positive effect of reducing land erosion, and improving the fertility of soils. Heat recovery from biomass ashing can greatly benefits the process by substituting energy produced via fossil fuels. Hence, the study demonstrated that agromining was an opportunity to develop new agricultural practices that favorably preserve the environment and strategic resources such as nickel.

1.3.4 RE Hyperaccumulators and recovery processes

1.3.4.1 Hyperaccumulators

For REEs, the identification of REE-accumulating species is ongoing. To date, only two species are listed in the hyperaccumulator database (Reeves *et al.*, 2018) (www.hyperaccumulators.org): *Dicranopteris linearis* (Wang *et al.*, 1997) (Figure 33a) and *Pronephrium simplex* (Figure 33b) (Lai *et*

al., 2005). Both belong to the pteridophyte group. The above-mentioned HAs hyperaccumulate only the light fractions of REEs with a significant negative Ce anomaly.

Typical concentrations for *D. linearis* are 1 000 µg.g^{-1} La, 600 µg.g^{-1} Nd, 200 µg.g^{-1} Ce, 200 µg.g^{-1} Pr (Chour *et al.*, 2018; Liu *et al.*, 2021; W. Liu *et al.*, 2019b). *D. linearis* could also be classified as an Al-hyperaccumulator, with concentration ranging up to 4 170 µg.g^{-1} in fronds (Chour *et al.*, 2018; Liu *et al.*, 2019). *D. linearis* (formerly known as *D. dichotoma*) is a pioneer fern that grows on acidic soils of China, and populations have been reported in contaminated mining sites in ionic clay regions (Liu *et al.*, 2021). Its ability to naturally colonize such degraded ecosystems make it an attractive choice for RE agromining. Nevertheless, appropriate farming trials are required to estimate its agromining potential.

Figure 33: Photos of the two reported REEs hyperaccumulators. (a) *Dicranopteris linearis* (Liu *et al.*, 2021) and (b) *Pronephrium simplex* ("*Pronephrium simplex* fact sheet No. 612")

Figure 34: Photo of *Phytolacca americana* growing on mine tailings in Jiangxi province (Liu *et al.*, 2021)

Other plants have been reported to contain significant amounts of REEs in foliage, such as *Phytolacca americana* (∑REEs in foliage: 1 040 µg.g^{-1} (Liu *et al.*, 2021; Yuan *et al.*, 2018)) (Figure 34), but are not classified as hyperaccumulators. Though, they could be interesting to consider for agromining due to their higher biomass production. *P. americana* is a perennial herb and its superior root development

could help prevent erosion and scavenging REEs deeper in the soil, compared to the fern. Individuals have been reported to be able to grow at mining sites in the Jiangxi region (Liu *et al.*, 2021). Finally, its ability to grow in temperate climate is another advantage to consider in expanding RE agromining to other regions.

Pot cultivation trials using bare tailing soil and amended soil revealed the importance of the nature of the amendment (Liu *et al.*, 2020). A mixture of pig manure and woody dust, as well woody biochar, significantly boosted biomass growth but prevented REE accumulation. REE availability was significantly reduced but the mechanisms were not assessed. The best results in terms of REE phytoextraction (REE biomass concentration multiplied by biomass weight) were obtained using the lowest dose of woody biochar. When no amendment was used, plant growth was totally inhibited. Further research is needed to find the right compromise to maintain REE mobility while providing key nutrients to the plant.

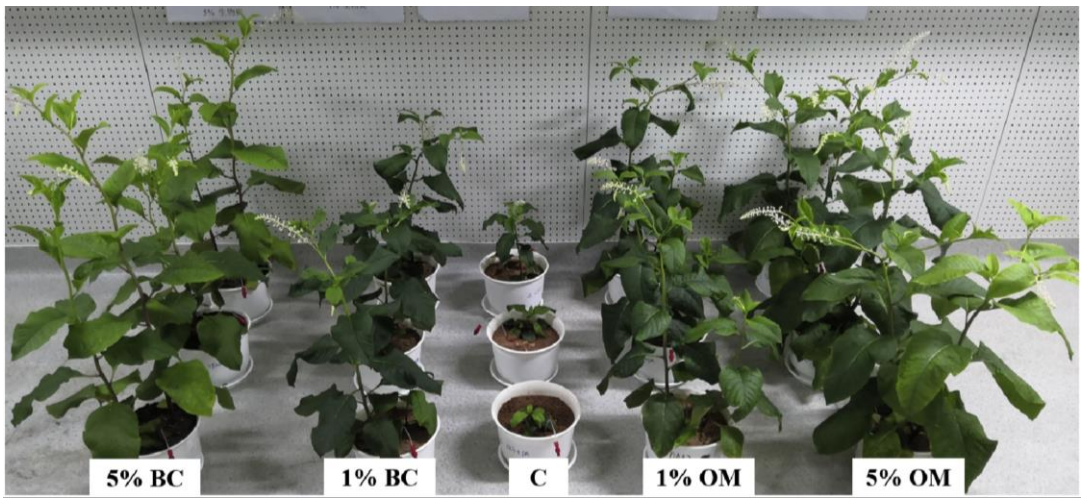

Figure 35: Pot experiments conducted to test the effect of amendment on phytoextraction of REEs with *P. americana*. C, BC, and OM stand for control, biochar, and organic matter (pig manure, and woody dust) treatments respectively. Percents are expressed in mass ratios, dry weight.

1.3.4.2 Process for extracting REEs from hyperaccumulators.

The PhD work of Z. Chour (Chour, 2018) was the first to explore processing routes for REE recovery from the hyperaccumulator *Dicranopteris linearis*. In her work, ground biomass and ash (produced at 550 and 900 °C) were characterized by complementary techniques (SEM-EDS, granulometry, elemental analysis, EDX, thermogravimetric analysis, total carbon), and then extraction routes were explored. Inspired by the nickel recovery process from *O. chalcidica*, three different strategies were conducted to extract and purify REEs (Figure 36).

The first route consisted of the extraction from dried biomass using an aqueous solution (Figure 37) (Chour *et al.*, 2020). The biomass was suspended in an agitated beaker in the presence of different extractants, namely, water, nitric acid, sulfuric acid, EDTA, citric acid, and glutamic acid. Yields higher than 80% could be obtained with strong acids and EDTA.

For further purification, oxalate precipitation was chosen. Dilute concentrations prevented the precipitation of RE oxalates in the nitric media. When using EDTA as the extractant, the decrease in pH resulted in the precipitation of REEs with EDTA. The loss of costly EDTA was unavoidable due to the further calcination step. Oxalate precipitation in sulfuric medium could be successfully conducted with quantitative yields. Calcination of the precipitate led to the formation of an oxide with an estimated

purity of 79%, and the overall yield was estimated at 73%. Thus, it was concluded that extraction with sulfuric acid was the most effective and efficient.

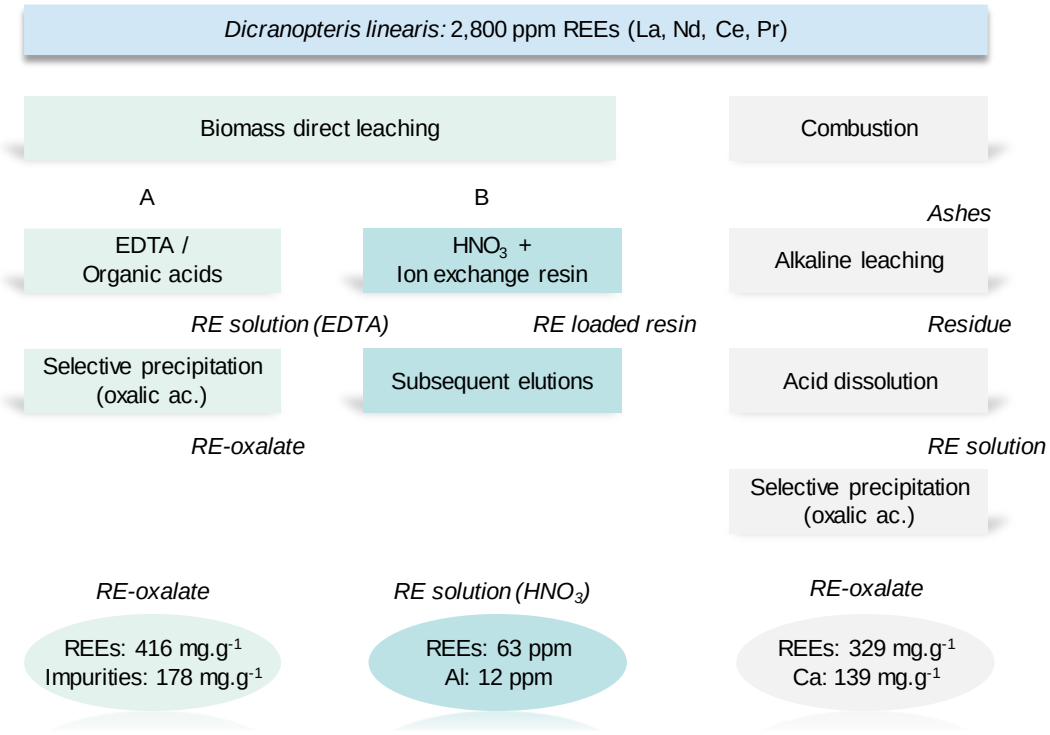

Figure 36: Hydrometallurgical routes explored for REE processing from *Dicranopteris linearis* (Chour, 2018)

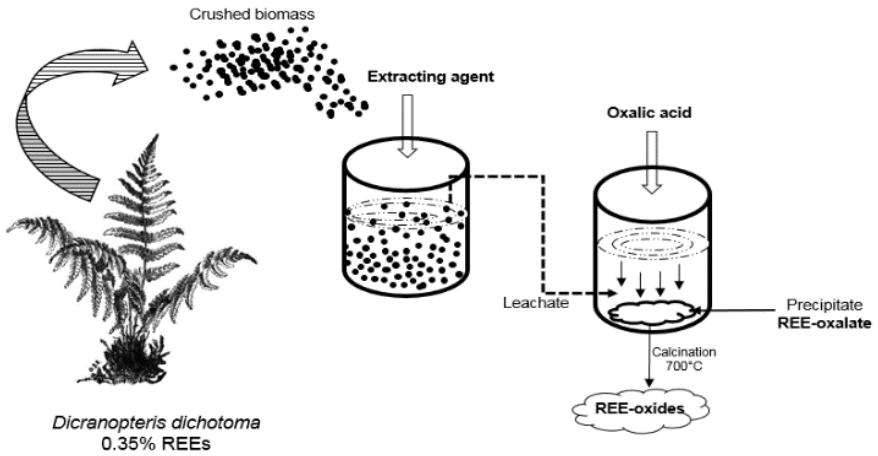

Figure 37: Methodology for direct biomass extraction (Chour, 2018)

Investigations on direct extraction with nitric acid were pursued but intensified thanks to an ion exchange resin. It constitutes the second approach. Strong acid resin beads (AMBERLITE™ IRN77, functional group: sulfonic acid, conditioned with H^+) were placed in a fibrous bag (tea bag), and

extraction was conducted with the biomass suspended in a nitric acid solution (Figure 38). Then, the resin was selectively eluted in a column. A mildly acidic solution (HNO_3 at 0.5 M) selectively eluted divalent and monovalent cations (Ca^{2+}, Zn^{2+}, Na^{+}, K^{+}) and a small part of Al. In a second stage, a stronger nitric acid solution (3 M) eluted the remaining adsorbed trivalent cations (REEs and Al).

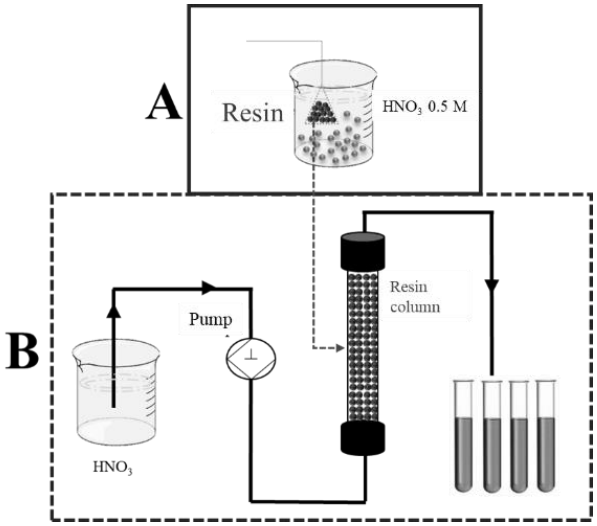

Figure 38: Design of the resin-intensified extraction of the biomass (Chour *et al.*, 2018)

As a result, a solution was produced (∑REE = 63 $mg.L^{-1}$; Al = 12 $mg.L^{-1}$) with an overall recovery yield of 75%. Most of the REE loss occurs during the first resin elution (10% of the REEs), while the intensified leaching of biomass is quantitative thanks to equilibrium displacement. Sulfuric acid was also studied for the elution step but was proven to be considerably less efficient.

The third and last approach entails the ashing of the biomass at 550 °C (Figure 39). As for nickel HAs, this step concentrates the elements of interest, in this case REEs. The concentration factor reached up to 6 (from 3.9 to 22.6 $g.kg^{-1}$ in ∑REE). Also, the high amounts of Si caused the formation of an amorphous, inert glass. This glass is thought to trap the REEs, preventing their recovery upon leaching of the ash with a strong acid.

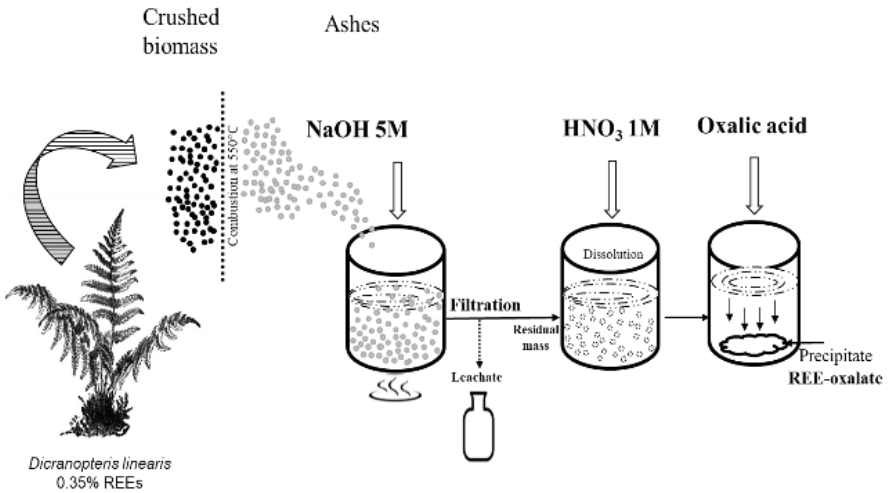

Figure 39: Processing route based on the ashes of *Dicranopteris linearis* (Chour, 2018)

Consequently, alkaline leaching was performed to solubilize Si at high pH using aqueous NaOH. A various set of conditions (temperature, sodium hydroxide concentration, duration) was investigated to find the activation energy of the leaching reaction. Al was also solubilized in significant proportions (65 to 90%) because of the high solubility of $NaAlO_2$ (Bayer, 1888) in alkaline conditions. This step could be performed in less than an hour in the conditions studied. With 5 M NaOH at 80 °C, the behavior of Al is unclear (Figure 40), and further investigations are required to reach 100% Al solubilization.

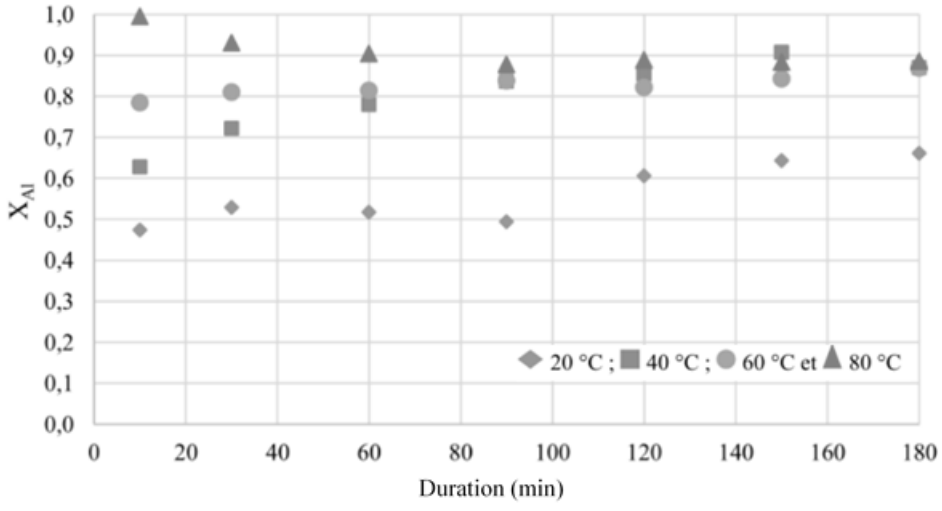

Figure 40: Effect of temperature on the extraction rate of Al by 5 M sodium hydroxide (Chour, 2018)

The solid residue from this step contained the majority of REEs with no detectable loss in the leachate, while the concentration in the solid reached $\sum$[REE] = 59.2 mg.g^{-1}. A nitric acid solution (HNO_3 = 1 M) allowed rapid dissolution of REEs from the residue.

Oxalate precipitation was conducted and a RE-rich solid was produced ([La] = 328.7 mg.g^{-1}). However, Ca co-precipitated in substantial amounts (330 mg.g^{-1}). Further works showed that rinsing the previous residue with water, adjusted to pH 7, could solubilize $CaCO_3$ and thus separate Ca from REEs. Hydroxide precipitation trials were also conducted using the nitric acid solution but resulted in the simultaneous precipitation of Mg and REEs. As a recommendation, the study encouraged the use of resin for purification after alkaline ash leaching.

To conclude, the processing of REE-hyperaccumulator differed strongly from that of Ni-hyperaccumulators (Barbaroux *et al.*, 2012; Zhang *et al.*, 2016). Firstly, the concentrations of the elements of interest were lower: maximum 0.35 wt% of $\sum$REEs in *D. linearis* versus 2 wt% to 2.5 wt% of Ni in *O. chalcidica* or *P. rufuschaneyi* (Bani *et al.*, 2015a; Nkrumah *et al.*, 2019). Additionally, several elements are considered in the case of the REEs, with comparable but different properties and molar masses. In particular, the atomic weights of the REEs (for the lanthanides: 138.9 g.mol^{-1} 175.0 g.mol^{-1}) are two to three times the atomic weight of Ni (58.7 g.mol^{-1}), which decreases even more the molar concentration of REEs relatively to other elements in the plant. The scarcity of REEs in the bio-ore makes the separation from other metals and impurities particularly challenging.

Secondly, in the case of *D. linearis*, the high Si content prevents the acid leaching of ash ([Si] ≈ 14 000 µg.g^{-1} (Chour, 2018)). At very high or very low pH, silica could form a gel in solution or on the reactor walls, which could be a concern (Queneau and Berthold, 1986). Recycling of the alkaline leaching step might also be hampered by silica accumulation. To broaden the knowledge on bio-ore processing, the study of *Phytolacca americana* for REE recovery could be interesting as Si is less

abundant ([Si] ≈ 780 µg.g^{-1}). Aluminum is also a substantial compound of both bio-ores and requires the corresponding separation. However, its separation from REEs is challenging as it readily forms Al^{3+} similarly to the REEs. Al content in both *D. linearis* and *P. americana* is not negligible and could be recovered for valorization.

1.4 Conclusion

The objective of this chapter was to present REEs, their chemistry and their conventional processing in order to frame their behavior in a hydrometallurgical context. An overview of the economic stakes highlights the growing interest for REE-compounds. Little is known about the inherent risks (toxicity, eco-toxicity) of these elements themselves. Processes of extraction, and recovery from primary sources (bastnaesite, monazite, xenotime ore, and ionic clays) have been thoroughly described. Their description and impact assessments (Life Cycle Assessment) reveal that the hydrometallurgical recovery, and most importantly, mining is the main source of concern for environmental damage.

Hence, to mitigate the impacts of mining, there is a need for alternative processing. In a first approach, two routes are possible and described in this report: recycling (*e.g.*, from magnets production swarf, end-of-life products) and the use of secondary sources (industrial waste such as phosphogypsum, bauxite residue, mine tailings). Finally, a third avenue could be relevant in this context: agromining.

By using on-site plants to produce economically valuable compounds (such as REE-compounds), the benefits of phytoremediation could be put into practice to mitigate the environmental impact of former mining sites. Candidate plants, known to be hyperaccumulators, are capable of extracting metals from the soil in extraordinary proportions. Thus, REE recovery from the plants would make site remediation financially viable. Two different candidates are proposed here: the first one, *Dicranopteris linearis* (formerly *D. dichotoma*) is a tropical fern growing on acidic soil. The fronds can contain up to 2 800 µg.g^{-1} of REEs and 4 200 µg.g^{-1} of Al. The second one is *Phytolacca americana*, a perennial herb able to grow in tropical or temperate climates, accumulating up to 1 040 µg.g^{-1} of REEs and 1 100 µg.g^{-1} of Al in its leaves.

Unlike Ni agromining, REE recovery from plants is novel and challenging, as very few studies have yet been conducted (Z. Chour, PhD thesis defended in 2018), and only with *Dicranopteris linearis*. Additionally, the bio-ore grade is lower in the case of REEs, with contents up to 0.39% (total REEs) versus several percent Ni in Ni-HAs plants. Yet, an important exploratory work has been accomplished and several extraction routes have been explored. The processes based on *D. linearis* biomass can be considered developed (Chour *et al.*, 2018, 2020), while the route based on the ash requires more attempts to obtain a purified compound.

Regarding *Phytolacca americana*, no attempts have yet been conducted to recover REEs. This plant strongly differs from the fern in terms of metal composition and most importantly silicon content. Hence, characterization and extraction tests are needed before reproducing the same process. Its lower REE content (not exceeding 1040 µg.g^{-1}) might also hamper the efficiency of the process. Nonetheless, complete chemical and structural characterization of the biomass and ash will pave the way for the design of recovery processes.

The development of a recovery process will follow the steps presented in Figure 41. Initially, the resource containing the REEs will be thoroughly characterized (biomass or ash), separation processes are designed accordingly. The lab-scale implementation will provide insights on the feasibility of the process (selectivity, yields, required reagents). Those collected experimental data will enable

comparison and evaluation of the developed process. Implementation at the lab-scale will also give insights on the key parameters that can be modified to optimize the process. The optimized processes are evaluated again and compared. Criteria are developed and discussed to finally select the best recovery process.

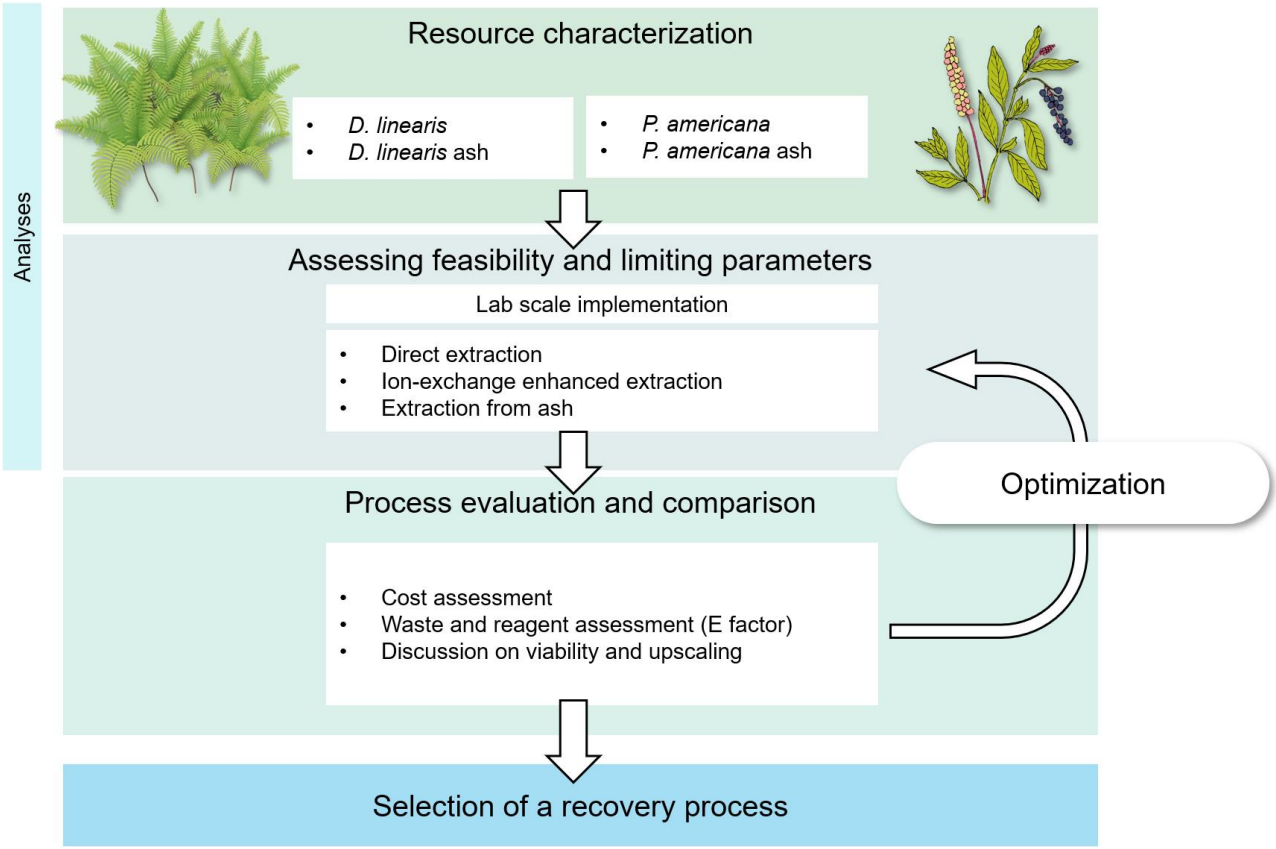

Figure 41: Adopted methodology for the development of a recovery process from REE-hyperaccumulators.

1.5 References

Ali, O.I.M., Osman, H.H., Sayed, S.A., Shalabi, M.E.H., 2011. The removal of some rare earth elements from their aqueous solutions on by-pass cement dust (BCD). J. Hazard. Mater. 195, 62–67. https://doi.org/10.1016/j.jhazmat.2011.08.014

Bani, A., Echevarria, G., Sulçe, S., Morel, J.L., 2015a. Improving the Agronomy of *Alyssum murale* for Extensive Phytomining: A Five-Year Field Study. Int. J. Phytoremediation 17, 117–127. https://doi.org/10.1080/15226514.2013.862204

Bani, A., Echevarria, G., Sulçe, S., Morel, J.L., Mullai, A., 2007. In-situ phytoextraction of Ni by a native population of *Alyssum murale* on an ultramafic site (Albania). Plant Soil 293, 79–89. https://doi.org/10.1007/s11104-007-9245-1

Bani, A., Echevarria, G., Zhang, X., Benizri, E., Laubie, B., Morel, J.L., Simonnot, M.-O., 2015b. The effect of plant density in nickel-phytomining field experiments with *Alyssum murale* in Albania. Aust. J. Bot. 63, 72–77. https://doi.org/10.1071/BT14285

Barbaroux, R., Mercier, G., Blais, J.F., Morel, J.L., Simonnot, M.O., 2011. A new method for obtaining nickel metal from the hyperaccumulator plant *Alyssum murale*. Sep. Purif. Technol. 83, 57–65. https://doi.org/10.1016/j.seppur.2011.09.009

Barbaroux, R., Plasari, E., Mercier, G., Simonnot, M.O., Morel, J.L., Blais, J.F., 2012. A new process for nickel ammonium disulfate production from ash of the hyperaccumulating plant *Alyssum murale*. Sci. Total Environ. 423, 111–119. https://doi.org/10.1016/j.scitotenv.2012.01.063

Bauer, D., Diamond, D., Li, J., Sandalow, D., Telleen, P., Wanner, B., 2010. Critical Materials Strategy (No. 1000846). U.S. Department of Energy, Washington, DC, USA. https://doi.org/10.2172/1000846

Bayer, K.J., 1888. Precipitation of pure $Al(OH)_3$ from sodium aluminate solution by seeding. US Patent US382505.

Bea, F., 2015. Geochemistry of the Lanthanide Elements, in: Proceedings of the XXXV Reunion de La Sociedad Espanola de Mineralogia. Presented at the XXXV Reunion de la Sociedad Espanola de Mineralogia, Huelva, Spain, p. 12.

Benizri, E., Lopez, S., Durand, A., Kidd, P.S., 2021. Diversity and Role of Endophytic and Rhizosphere Microbes Associated with Hyperaccumulator Plants During Metal Accumulation, in: van der Ent, A., Baker, A.J.M., Echevarria, G., Simonnot, M.-O., Morel, J.L. (Eds.), Agromining: Farming for Metals. Springer International Publishing, Cham, pp. 239–279. https://doi.org/10.1007/978-3-030-58904-2_12

Bian, X., Chen, J., Zhao, Z., Yin, S., Luo, Y., Zhang, F., Wu, W., 2010. Kinetics of mixed rare earths minerals decomposed by CaO with NaCl-CaCl2 melting salt. J. Rare Earths 28, 86–90. https://doi.org/10.1016/S1002-0721(10)60268-2

Binnemans, K., Jones, P.T., 2015. Rare Earths and the Balance Problem. J. Sustain. Metall. 1, 29–38. https://doi.org/10.1007/s40831-014-0005-1

Binnemans, K., Jones, P.T., Blanpain, B., Van Gerven, T., Pontikes, Y., 2015. Towards zero-waste valorisation of rare-earth-containing industrial process residues: a critical review. J. Clean. Prod. 99, 17–38. https://doi.org/10.1016/j.jclepro.2015.02.089

Binnemans, K., Jones, P.T., Blanpain, B., Van Gerven, T., Yang, Y., Walton, A., Buchert, M., 2013. Recycling of rare earths: a critical review. J. Clean. Prod. 51, 1–22. https://doi.org/10.1016/j.jclepro.2012.12.037

Binnemans, K., Jones, P.T., Müller, T., Yurramendi, L., 2018. Rare Earths and the Balance Problem: How to Deal with Changing Markets? J. Sustain. Metall. 4, 126–146. https://doi.org/10.1007/s40831-018-0162-8

Bouman, R., van Welzen, P., Sumail, S., Echevarria, G., Erskine, P.D., van der Ent, A., 2018. *Phyllanthus rufuschaneyi*: a new nickel hyperaccumulator from Sabah (Borneo Island) with potential for tropical agromining. Bot. Stud. 59, 9. https://doi.org/10.1186/s40529-018-0225-y

Braconnier, J.-J., Rollat, A., 2010. Method for recovering rare earth elements from a solid mixture containing a halophosphate and a compound of one or more rare earth elements. WO2010118967A1.

Brooks, R.R., Lee, J., Reeves, R.D., Jaffre, T., 1977. Detection of nickeliferous rocks by analysis of herbarium specimens of indicator plants. J. Geochem. Explor. 7, 49–57. https://doi.org/10.1016/0375-6742(77)90074-7

Browning, C., Northey, S., Haque, N., Bruckard, W., Cooksey, M., 2016. Life Cycle Assessment of Rare Earth Production from Monazite, in: REWAS 2016: Towards Materials Resource Sustainability. Presented at the REWAS 2016: Towards Materials Resource Sustainability, Springer, Hoboken, NJ, USA, pp. 83–88. https://doi.org/DOI: 10.1007/978-3-319-48768-7_12

Burges, A., Alkorta, I., Epelde, L., Garbisu, C., 2018. From phytoremediation of soil contaminants to phytomanagement of ecosystem services in metal contaminated sites. Int. J. Phytoremediation 20, 384–397. https://doi.org/10.1080/15226514.2017.1365340

Cannon, H.L., 1960. Botanical Prospecting for Ore Deposits. Science 132, 591–598. https://doi.org/10.1126/science.132.3427.591

Cao, X., Wang, X., Zhao, G., 2000. Assessment of the bioavailability of rare earth elements in soils by chemical fractionation and multiple regression analysis. Chemosphere 40, 23–28.

Chaney, R., 1983. Plant uptake of inorganic waste constituents, in: Parr, J., Marsh, P., Kla, J. (Eds.), Land Treatment of Hazardous Wastes. Noyes Data Corp, Park Ridge, pp. 50–76.

Chaney, R.L., Baker, A.J.M., Morel, J.L., 2021. The Long Road to Developing Agromining/Phytomining, in: van der Ent, A., Baker, A.J.M., Echevarria, G., Simonnot, M.-O., Morel, J.L. (Eds.), Agromining: Farming for Metals. Springer International Publishing, Cham, pp. 1–22. https://doi.org/10.1007/978-3-030-58904-2_1

Chi, R., Tian, J., Li, Z., Peng, C., Wu, Y., Li, S., Wang, C., Zhou, Z., 2005. Existing State and Partitioning of Rare Earth on Weathered Ores. J. Rare Earths 23, 756–759.

Chi, R., Zhou, Z., Xu, Z., Hu, Y., Zhu, G., Xu, S., 2003. Solution-chemistry analysis of ammonium bicarbonate consumption in rare-earth-element precipitation. Metall. Mater. Trans. B 34, 611–617. https://doi.org/10.1007/s11663-003-0031-z

Chour, Z., 2018. Valorisation de terres rares à partir de plantes hyperaccumulatrices (PhD dissertation). Université de Lorraine, Nancy, France.

Chour, Z., Laubie, B., Morel, J.L., Tang, Y., Qiu, R., Simonnot, M.-O., Muhr, L., 2018. Recovery of rare earth elements from *Dicranopteris dichotoma* by an enhanced ion exchange leaching process. Chem. Eng. Process. - Process Intensif. 130, 208–213. https://doi.org/10.1016/j.cep.2018.06.007

Chour, Z., Laubie, B., Morel, J.L., Tang, Y.T., Simonnot, M.O., Muhr, L., 2020. Basis for a new process for producing REE oxides from *Dicranopteris linearis*. J. Environ. Chem. Eng. 103961. https://doi.org/10.1016/j.jece.2020.103961

Chuan, L.M., Zheng, H.G., Zhao, J.J., Wang, A.L., Sun, S.F., 2018. Phosphogypsum production and utilization in China. IOP Conf. Ser. Mater. Sci. Eng. 382, 022099. https://doi.org/10.1088/1757-899X/382/2/022099

Cundy, A.B., Bardos, R.P., Puschenreiter, M., Mench, M., Bert, V., Friesl-Hanl, W., Müller, I., Li, X.N., Weyens, N., Witters, N., Vangronsveld, J., 2016. Brownfields to green fields: Realising wider benefits from practical contaminant phytomanagement strategies. J. Environ. Manage. 184, 67–77. https://doi.org/10.1016/j.jenvman.2016.03.028

Das, G., Lencka, M.M., Eslamimanesh, A., Wang, P., Anderko, A., Riman, R.E., Navrotsky, A., 2019. Rare earth sulfates in aqueous systems: Thermodynamic modeling of binary and multicomponent systems over wide concentration and temperature ranges. J. Chem. Thermodyn. 131, 49–79. https://doi.org/10.1016/j.jct.2018.10.020

Das, N., Das, D., 2013. Recovery of rare earth metals through biosorption: An overview. J. Rare Earths 31, 933–943. https://doi.org/10.1016/S1002-0721(13)60009-5

Davris, P., Balomenos, E., Panias, D., Paspaliaris, I., 2016. Selective leaching of rare earth elements from bauxite residue (red mud), using a functionalized hydrophobic ionic liquid. Hydrometallurgy 164, 125–135. https://doi.org/10.1016/j.hydromet.2016.06.012

De Michelis, I., Ferella, F., Varelli, E.F., Vegliò, F., 2011. Treatment of exhaust fluorescent lamps to recover yttrium: Experimental and process analyses. Waste Manag. 31, 2559–2568. https://doi.org/10.1016/j.wasman.2011.07.004

Duschene, J.-C., 1983. The lanthanides as geochemical tracers of igneous processes: an introduction, in: Sinha, S.P. (Ed.), Systematics and the Properties of the Lanthanides, NATO ASI Series. D. Reidel Pub. Co, Boston : Hingham, MA, U.S.A, pp. 543–560.

Ellis, T.W., Schmidt, F.A., Jones, L.L., 1994. Methods and opportunities in the recycling of rare earth based materials. Presented at the The Metallurgical Society (TMS) conference on high performance composites, Rosemont, IL, USA.

Emsbo, P., McLaughlin, P.I., Breit, G.N., du Bray, E.A., Koenig, A.E., 2015. Rare earth elements in sedimentary phosphate deposits: Solution to the global REE crisis? Gondwana Res. 27, 776–785. https://doi.org/10.1016/j.gr.2014.10.008

European Commission, 2020. Study on the EU's list of critical raw materials - final report. Publications Office of the EU, Luxembourg. https://doi.org/10.2873/11619

Faucon, M.-P., Shutcha, M.N., Meerts, P., 2007. Revisiting copper and cobalt concentrations in supposed hyperaccumulators from SC Africa: influence of washing and metal concentrations in soil. Plant Soil 301, 29–36. https://doi.org/10.1007/s11104-007-9405-3

Feng, X., Long, Z., Cui, D., Wang, L., Huang, X., Zhang, G., 2013. Kinetics of rare earth leaching from roasted ore of bastnaesite with sulfuric acid. Trans. Nonferrous Met. Soc. China 23, 849–854. https://doi.org/10.1016/S1003-6326(13)62538-8

Gavhane, K.A., 2009. Kinetics of Fluid - Particle Reactions, in: Prakashan, N. (Ed.), Chemical Reaction Engineering. Nirali Prakashan, Satara, India, p. 512.

Gonzalez, V., Vignati, D.A.L., Leyval, C., Giamberini, L., 2014. Environmental fate and ecotoxicity of lanthanides: Are they a uniform group beyond chemistry? Environ. Int. 71, 148–157. https://doi.org/10.1016/j.envint.2014.06.019

González, V., Vignati, D.A.L., Pons, M.-N., Montarges-Pelletier, E., Bojic, C., Giamberini, L., 2015. Lanthanide ecotoxicity: First attempt to measure environmental risk for aquatic organisms. Environ. Pollut. 199, 139–147. https://doi.org/10.1016/j.envpol.2015.01.020

Gschneidnerjr, K.A., Daane, A.H., 1988. Chapter 78 : Physical metallurgy, in: Gschneidnerjr, K.A., Eyring, L.R. (Eds.), Handbook on the Physics and Chemistry of Rare Earths. Elsevier, Ames, IA, USA, pp. 409–484. https://doi.org/10.1016/S0168-1273(88)11010-6

Guan, Y., Sun, X., Ren, Y., Jiang, X., 2017. Mineralogy, geochemistry and genesis of the polymetallic crusts and nodules from the South China Sea. Ore Geol. Rev. 89, 206–227. https://doi.org/10.1016/j.oregeorev.2017.06.020

Guilpain, M., 2018. Innovative processes for the recovery of nickel, directly extracted from hyperaccumulator plants (PhD dissertation). Université de Lorraine, Nancy, France.

Guilpain, M., Laubie, B., Zhang, X., Morel, J.L., Simonnot, M.-O., 2018. Speciation of nickel extracted from hyperaccumulator plants by water leaching. Hydrometallurgy 180, 192–200. https://doi.org/10.1016/j.hydromet.2018.07.024

Gupta, C.K., Krishnamurthy, N., 2005. Extractive metallurgy of rare earths. CRC Press, Boca Raton, Fla.

Habashi, F., 2013. Extractive metallurgy of rare earths. Can. Metall. Q. 52, 224–233. https://doi.org/10.1179/1879139513Y.0000000081

Hao, X., Wang, D., Wang, P., Wang, Y., Zhou, D., 2016. Evaluation of water quality in surface water and shallow groundwater: a case study of a rare earth mining area in southern Jiangxi Province, China. Environ. Monit. Assess. 188, 24. https://doi.org/10.1007/s10661-015-5025-1

Haque, N., Hughes, A., Lim, S., Vernon, C., 2014. Rare Earth Elements: Overview of Mining, Mineralogy, Uses, Sustainability and Environmental Impact. Resources 3, 614–635. https://doi.org/10.3390/resources3040614

Harkins, W.D., 1917. The evolution of the elements and the stability of complex atoms. A new periodic system which shows a relation between the abundance of the elements and the structure of the nuclei of atoms. J. Am. Chem. Soc. 39, 856–879. https://doi.org/10.1021/ja02250a002

Hatch, G.P., 2012. Dynamics in the Global Market for Rare Earths. Elements 8, 341–346. https://doi.org/10.2113/gselements.8.5.341

Haxel, G., Hedrick, J., Orris, G., 2002. Rare Earth Elements—Critical Resources for High Technology (No. Fact Sheet 087-02). U.S. Geological Survey.

He, Z., Zhang, Z., Chi, R., Xu, Z., Yu, J., Wu, M., Bai, R., 2017. Leaching hydrodynamics of weathered elution-deposited rare earth ore with ammonium salts solution. J. Rare Earths 35, 824–830. https://doi.org/10.1016/S1002-0721(17)60982-7

He, Z., Zhang, Z., Yu, J., Xu, Z., Chi, R., 2016. Process optimization of rare earth and aluminum leaching from weathered crust elution-deposited rare earth ore with compound ammonium salts. J. Rare Earths 34, 413–419. https://doi.org/10.1016/S1002-0721(16)60042-X

Huot, H., Guo, M.N., Liu, C., Liu, W., Yuan, M., Chen, Y.Y., Zhu, S.C., Wang, Y., Wu, Y.L., Ye, P.X., Chen, J.Q., Séré, G., Watteau, F., Chao, Y.Q., Auclerc, A., Morel, J.L., Tang, Y.T., Qiu, R.L., 2018. Reclamation of ionic rare earth elements (REEs) mine tailings in Southern China, in: 11th Sino-French Workshop - Innovations for the Circular Economy by Recycling Secondary Resources. Presented at the 11th Sino-French Workshop - Innovations for the circular Economy by Recycling Secondary Resources, Sun Yat-sen University, Guangzhou.

Iftekhar, S., Srivastava, V., Casas, A., Sillanpää, M., 2018. Synthesis of novel GA-g-PAM/SiO_2 nanocomposite for the recovery of rare earth elements (REE) ions from aqueous solution. J. Clean. Prod. 170, 251–259. https://doi.org/10.1016/j.jclepro.2017.09.166

Iftekhar, S., Srivastava, V., Sillanpää, M., 2017a. Synthesis and application of LDH intercalated cellulose nanocomposite for separation of rare earth elements (REEs). Chem. Eng. J. 309, 130–139. https://doi.org/10.1016/j.cej.2016.10.028

Iftekhar, S., Srivastava, V., Sillanpää, M., 2017b. Enrichment of lanthanides in aqueous system by cellulose based silica nanocomposite. Chem. Eng. J. 320, 151–159. https://doi.org/10.1016/j.cej.2017.03.051

International Aluminium Institute, 2015. Bauxite Residue Management: Best Practice.

Jaffré, T., 1979. Accumulation du manganèse par les Protéacées de Nouvelle Calédonie. Comptes Rendus Académie Sci. Sci. Nat. 289, 425–428.

Jasinski, S.M., 2019. Mineral Commodity Summaries: Phosphate 2019. U.S. Geological Survey.

Kidd, P.S., Bani, A., Benizri, E., Gonnelli, C., Hazotte, C., Kisser, J., Konstantinou, M., Kuppens, T., Kyrkas, D., Laubie, B., Malina, R., Morel, J.-L., Olcay, H., Pardo, T., Pons, M.-N., Prieto-Fernández, Á., Puschenreiter, M., Quintela-Sabarís, C., Ridard, C., Rodríguez-Garrido, B., Rosenkranz, T., Rozpądek, P., Saad, R., Selvi, F., Simonnot, M.-O., Tognacchini, A., Turnau, K., Ważny, R., Witters, N., Echevarria, G., 2018. Developing Sustainable Agromining Systems in Agricultural Ultramafic Soils for Nickel Recovery. Front. Environ. Sci. 6, 44. https://doi.org/10.3389/fenvs.2018.00044

Kidd, P.S., Monterroso, C., 2005. Metal extraction by *Alyssum serpyllifolium ssp. lusitanicum* on mine-spoil soils from Spain. Sci. Total Environ. 336, 1–11. https://doi.org/10.1016/j.scitotenv.2004.06.003

Kim, C.-J., Yoon, H.-S., Chung, K.W., Lee, J.-Y., Kim, S.-D., Shin, S.M., Lee, S.-J., Joe, A.-R., Lee, S.-I., Yoo, S.-J., Kim, S.-H., 2014. Leaching kinetics of lanthanum in sulfuric acid from rare earth element (REE) slag. Hydrometallurgy 146, 133–137. https://doi.org/10.1016/j.hydromet.2014.04.003

Kim, E., Osseo-Asare, K., 2012. Aqueous stability of thorium and rare earth metals in monazite hydrometallurgy: Eh–pH diagrams for the systems Th–, Ce–, La–, Nd– (PO_4)–(SO_4)–H_2O at 25°C. Hydrometallurgy 113–114, 67–78. https://doi.org/10.1016/j.hydromet.2011.12.007

Koltun, P., Tharumarajah, A., 2014. Life Cycle Impact of Rare Earth Elements. ISRN Metall. 2014, 1–10. https://doi.org/10.1155/2014/907536

Kurvet, I., Juganson, K., Vija, H., Sihtmäe, M., Blinova, I., Syvertsen-Wiig, G., Kahru, A., 2017. Toxicity of Nine (Doped) Rare Earth Metal Oxides and Respective Individual Metals to Aquatic Microorganisms *Vibrio fischeri* and *Tetrahymena thermophila*. Materials 10, 754. https://doi.org/10.3390/ma10070754

Lai, Y., Wang, Q., Yan, W., Yang, L., Huang, B., 2005. Preliminary study of the enrichment and fractionation of REEs in a newly discovered REE hyperaccumulator *Pronephrium simplex* by SEC-ICP-MS and MALDI-TOF/ESI-MS. J. Anal. At. Spectrom. 20, 751. https://doi.org/10.1039/b501766a

Laubie, B., Vaughan, J., Simonnot, M.-O., 2021. Processing of Hyperaccumulator Plants to Nickel Products, in: van der Ent, A., Baker, A.J.M., Echevarria, G., Simonnot, M.-O., Morel, J.L. (Eds.),

Agromining: Farming for Metals. Springer International Publishing, Cham, pp. 47–61. https://doi.org/10.1007/978-3-030-58904-2_3

Leblanc, M., Petit, D., Deram, A., Robinson, B.H., Brooks, R.R., 1999. The phytomining and environmental significance of hyperaccumulation of thallium by Iberis intermedia from southern France. Econ. Geol. 94, 109–113. https://doi.org/10.2113/gsecongeo.94.1.109

Lerat-Hardy, A., Coynel, A., Dutruch, L., Pereto, C., Bossy, C., Gil-Diaz, T., Capdeville, M.-J., Blanc, G., Schäfer, J., 2019. Rare Earth Element fluxes over 15 years into a major European Estuary (Garonne-Gironde, SW France): Hospital effluents as a source of increasing gadolinium anomalies. Sci. Total Environ. 656, 409–420. https://doi.org/10.1016/j.scitotenv.2018.11.343

Leveque, A., Maestro, P., 1993. Terres rares, in: Traité de Génie Chimique, Génie de la réaction chimique. Techniques de l'Ingénieur, pp. 1–15.

Li, C., Zhuang, Z., Huang, F., Wu, Z., Hong, Y., Lin, Z., 2013. Recycling Rare Earth Elements from Industrial Wastewater with Flowerlike Nano-Mg(OH) $_2$. ACS Appl. Mater. Interfaces 5, 9719–9725. https://doi.org/10.1021/am4027967

Li, Y.-M., Chaney, R., Brewer, E., Roseberg, R., Angle, J.S., Baker, A., Reeves, R., Nelkin, J., 2003. Development of a technology for commercial phytoextraction of nickel: economic and technical considerations. Plant Soil 249, 107–115. https://doi.org/10.1023/A:1022527330401

Liang, T., Zhang, S., Wang, L., Kung, H.-T., Wang, Y., Hu, A., Ding, S., 2005. Environmental biogeochemical behaviors of rare earth elements in soil–plant systems. Environ. Geochem. Health 27, 301–311. https://doi.org/10.1007/s10653-004-5734-9

Liu, C., Yuan, M., Liu, W.-S., Guo, M.-N., Zheng, H.-X., Huot, H., Jally, B., Tang, Y.-T., Laubie, B., Simonnot, M.-O., Morel, J.L., Qiu, R.-L., 2021. Element Case Studies: Rare Earth Elements, in: van der Ent, A., Baker, A.J.M., Echevarria, G., Simonnot, M.-O., Morel, J.L. (Eds.), Agromining: Farming for Metals. Springer International Publishing, Cham, pp. 471–483. https://doi.org/10.1007/978-3-030-58904-2_24

Liu, J., Huang, K., Wu, X.-H., Liu, H., 2017. Enrichment of Low Concentration Rare Earths from Leach Solutions of Ion-Adsorption Ores by Bubbling Organic Liquid Membrane Extraction Using N1923. ACS Sustain. Chem. Eng. 5, 8070–8078. https://doi.org/10.1021/acssuschemeng.7b01682

Liu, W., Chen, Y., Huot, H., Liu, C., Guo, M., Qiu, R., Morel, J.L., Tang, Y., 2020. Phytoextraction of rare earth elements from ion-adsorption mine tailings by *Phytolacca americana*: Effects of organic material and biochar amendment. J. Clean. Prod. 275, 122959. https://doi.org/10.1016/j.jclepro.2020.122959

Liu, W., Guo, M., Liu, C., Yuan, M., Chen, X., Huot, H., Zhao, C., Tang, Y., Morel, J.L., Qiu, R., 2019a. Water, sediment and agricultural soil contamination from an ion-adsorption rare earth mining area. Chemosphere 216, 75–83. https://doi.org/10.1016/j.chemosphere.2018.10.109

Liu, W., Zheng, H., Guo, M.N., Liu, C., Huot, H., Morel, J.L., van der Ent, A., Tang, Y., Qiu, R., 2019b. Co-deposition of silicon with rare earth elements (REEs) and aluminium in the fern *Dicranopteris linearis* from China. Plant Soil 1–11. https://doi.org/10.1007/s11104-019-04005-0

Liu, W.-S., Wu, L.-L., Zheng, M.-Y., Chao, Y.-Q., Zhao, C.-M., Zhong, X., Ding, K.-B., Huot, H., Zhang, M.-Y., Tang, Y.-T., Li, C., Qiu, R.-L., 2019. Controls on rare-earth element transport in a river impacted by ion-adsorption rare-earth mining. Sci. Total Environ. 660, 697–704. https://doi.org/10.1016/j.scitotenv.2019.01.076

Louis, P., Messaoudene, A., Jrad, H., Abdoul-Hamid, B.A., Vignati, D.A.L., Pons, M.-N., 2020. Understanding Rare Earth Elements concentrations, anomalies and fluxes at the river basin scale: The Moselle River (France) as a case study. Sci. Total Environ. 742, 140619. https://doi.org/10.1016/j.scitotenv.2020.140619

Luidold, S., Antrekowitsch, H., 2012. Recovery of rare earth metals from waste material by leaching in non-oxidizing acid and by precipitating using sulphates. EP2444507A1.

Luo, X.P., Zou, L.P., Ma, P. long, Luo, C.G., Xu, J., Tang, X.K., 2015. Removing aluminum from a low-concentration lixivium of weathered crust elution-deposited rare earth ore with neutralizing hydrolysis. Rare Met. 36, 685–690. https://doi.org/10.1007/s12598-015-0621-3

Lyman, J.W., Palmer, G.R., 1992. Scrap Treatment Method for Rare Earth Transition Metal Alloys. US Patent 5129945.

Machacek, E., Kalvig, P., 2016. Road map for REE material supply autonomy in Europe. Geological Survey of Denmark and Greenland (GEUS) and D'Appolonia.

Merlot, S., Garcia de la Torre, V.S., Hanikenne, M., 2021. Physiology and Molecular Biology of Trace Element Hyperaccumulation, in: van der Ent, A., Baker, A.J.M., Echevarria, G., Simonnot, M.-O., Morel, J.L. (Eds.), Agromining: Farming for Metals. Springer International Publishing, Cham, pp. 155–181. https://doi.org/10.1007/978-3-030-58904-2_8

Millero, F.J., 1992. Stability constants for the formation of rare earth-inorganic complexes as a function of ionic strength. Geochim. Cosmochim. Acta 56, 3123–3132. https://doi.org/10.1016/0016-7037(92)90293-R

Minguzzi, C., Vergnano, O., 1948. Nickel content of the ash of *Alyssum bertolonii*. Atti Soc Toscana Sci Nat Mem 55, 49–74.

Moore, B.W., 2000. Selective separation of rare earth elements by ion exchange in an iminodiacetic resin. US6093376 (A).

Morel, J.L., Chaineau, C.H., Schiavon, M., Lichtfouse, E., 1999. The Role of Plants in the Remediation of Contaminated Soils, in: Baveye, P., Block, J.-C., Goncharuk, V.V. (Eds.), Bioavailability of Organic Xenobiotics in the Environment. Springer Netherlands, Dordrecht, pp. 429–449. https://doi.org/10.1007/978-94-015-9235-2_22

Morrey, D.R., Balkwill, K., Balkwill, M.J., Williamson, S., 1992. A review of some studies of the serpentine flora of southern Africa, in: Baker, A.J.M., Proctor, J., Reeves, R.D. (Eds.), The Vegetation of Ultramafic (Serpentine) Soils : Proceedings of the First International Conference on Serpentine Ecology, University of California, Davis, 19-22 June 1991. Presented at the the First International Conference on Serpentine Ecology, Andover, England, pp. 147–157.

Morton, J.R., 1969. Method of Separating Yttrium from Rare Earths by Ion Exchange. US3455646 (A).

Müller, T., Friedrich, B., 2006. Development of a recycling process for nickel-metal hydride batteries. J. Power Sources 158, 1498–1509. https://doi.org/10.1016/j.jpowsour.2005.10.046

National Science and Technology Council, 2018. Assessment of Critical Minerals: Updated Application of Screening Methodology.

Navarro, J., Zhao, F., 2014. Life-Cycle Assessment of the Production of Rare-Earth Elements for Energy Applications: A Review. Front. Energy Res. 2, 1–17. https://doi.org/doi:10.3389/fenrg.2014.00045

Nkrumah, P.N., Chaney, R.L., Morel, J.L., 2021. Agronomy of 'Metal Crops' Used in Agromining, in: van der Ent, A., Baker, A.J.M., Echevarria, G., Simonnot, M.-O., Morel, J.L. (Eds.), Agromining: Farming for Metals. Springer International Publishing, Cham, pp. 23–46. https://doi.org/10.1007/978-3-030-58904-2_2

Nkrumah, P.N., Tisserand, R., Chaney, R.L., Baker, A.J.M., Morel, J.L., Goudon, R., Erskine, P.D., Echevarria, G., van der Ent, A., 2019. The first tropical 'metal farm': Some perspectives from field and pot experiments. J. Geochem. Explor. 198, 114–122. https://doi.org/10.1016/j.gexplo.2018.12.003

Norgate, T.E., Jahanshahi, S., Rankin, W.J., 2007. Assessing the environmental impact of metal production processes. J. Clean. Prod. 15, 838–848. https://doi.org/10.1016/j.jclepro.2006.06.018

Oddo, G., 1914. Die Molekularstruktur der radioaktiven Atome. Z. Anorg. Chem. 87, 253–268. https://doi.org/10.1002/zaac.19140870118

Page, M.J., Soldenhoff, K., Ogden, M.D., 2017. Comparative study of the application of chelating resins for rare earth recovery. Hydrometallurgy 169, 275–281. https://doi.org/10.1016/j.hydromet.2017.02.006

Pang, X., Li, D., Peng, A., 2001. Application of rare-earth elements in the agriculture of China and its environmental behavior in soil. J. Soils Sediments 1, 124–129. https://doi.org/10.1007/BF02987718

Parhi, P.K., Park, K.H., Nam, C.W., Park, J.T., 2015. Liquid-liquid extraction and separation of total rare earth (RE) metals from polymetallic manganese nodule leaching solution. J. Rare Earths 33, 207–213. https://doi.org/10.1016/S1002-0721(14)60404-X

Pronephrium simplex fact sheet No. 612 (單葉新月) [WWW Document], n.d. . Chai Plant Netw. URL http://hkcww.org/hkplant/readid.php?id=612 (accessed 4.6.19).

Purwadi, I., Gei, V., Echevarria, G., Erskine, P.D., Mesjasz-Przybyłowicz, J., Przybyłowicz, W.J., van der Ent, A., 2021. Tools for the Discovery of Hyperaccumulator Plant Species in the Field and in the Herbarium, in: van der Ent, A., Baker, A.J.M., Echevarria, G., Simonnot, M.-O., Morel, J.L. (Eds.), Agromining: Farming for Metals. Springer International Publishing, Cham, pp. 183–195. https://doi.org/10.1007/978-3-030-58904-2_9

Qi, D., 2018. Extraction of Rare Earths from RE Concentrates, in: Hydrometallurgy of Rare Earths: Extraction and Separation. Elsevier, pp. 1–185.

Queneau, P.B., Berthold, C.E., 1986. Silica in Hydrometallurgy: An Overview. Can. Metall. Q. 25, 201–209. https://doi.org/10.1179/cmq.1986.25.3.201

Ramasamy, D.L., Repo, E., Srivastava, V., Sillanpää, M., 2017. Chemically immobilized and physically adsorbed PAN/acetylacetone modified mesoporous silica for the recovery of rare earth elements from the waste water-comparative and optimization study. Water Res. 114, 264–276. https://doi.org/10.1016/j.watres.2017.02.045

Redling, K., 2006. Rare Earth Elements in Agriculture with Emphasis on Animal Husbandry (PhD dissertation). Ludwig-Maximilians-Universität, Munich.

Reeves, R.D., Baker, A.J.M., Jaffré, T., Erskine, P.D., Echevarria, G., van der Ent, A., 2018. A global database for plants that hyperaccumulate metal and metalloid trace elements. New Phytol. 218, 407–411. https://doi.org/10.1111/nph.14907

Reeves, R.D., Brooks, R.R., 1983. Hyperaccumulation of lead and zinc by two metallophytes from mining areas of Central Europe. Environ. Pollut. Ser. Ecol. Biol. 31, 277–285. https://doi.org/10.1016/0143-1471(83)90064-8

Reeves, R.D., Schwartz, C., Morel, J.L., Edmondson, J., 2001. Distribution and Metal-Accumulating Behavior of *Thlaspi caerulescens* and Associated Metallophytes in France. Int. J. Phytoremediation 3, 145–172. https://doi.org/10.1080/15226510108500054

Rodrigues, J., Houzelot, V., Ferrari, F., Echevarria, G., Laubie, B., Morel, J.-L., Simonnot, M.-O., Pons, M.-N., 2016. Life cycle assessment of agromining chain highlights role of erosion control and bioenergy. J. Clean. Prod. 139, 770–778. https://doi.org/10.1016/j.jclepro.2016.08.110

Ronda, C.R., 1995. Phosphors for lamps and displays: an applicational view. J. Alloys Compd. 225, 534–538. https://doi.org/10.1016/0925-8388(94)07065-2

Rosenkranz, T., Hipfinger, C., Ridard, C., Puschenreiter, M., 2019. A nickel phytomining field trial using *Odontarrhena chalcidica* and *Noccaea goesingensis* on an Austrian serpentine soil. J. Environ. Manage. 242, 522–528. https://doi.org/10.1016/j.jenvman.2019.04.073

Roskill, 2016. Rare Earths: global industry, markets and outlook to 2026. Roskill Ltd, London, UK.

Rumble, J.R., 2019. CRC handbook of chemistry and physics: a ready-reference book of chemical and physical data. CRC Press, Boca Raton, Fla.

Rychkov, V.N., Kirillov, E.V., Kirillov, S.V., Semenishchev, V.S., Bunkov, G.M., Botalov, M.S., Smyshlyaev, D.V., Malyshev, A.S., 2018. Recovery of rare earth elements from phosphogypsum. J. Clean. Prod. 196, 674–681. https://doi.org/10.1016/j.jclepro.2018.06.114

Saad, R.F., Kobaissi, A., Machinet, G., Villemin, G., Echevarria, G., Benizri, E., 2018. Crop rotation associating a legume and the nickel hyperaccumulator *Alyssum murale* improves the structure and biofunctioning of an ultramafic soil. Ecol. Res. 33, 799–810. https://doi.org/10.1007/s11284-017-1526-4

Sadri, F., Nazari, A.M., Ghahreman, A., 2017. A review on the cracking, baking and leaching processes of rare earth element concentrates. J. Rare Earths 35, 739–752. https://doi.org/10.1016/S1002-0721(17)60971-2

Schreiber, A., Marx, J., Zapp, P., Hake, J.-F., Voßenkaul, D., Friedrich, B., 2016. Environmental Impacts of Rare Earth Mining and Separation Based on Eudialyte: A New European Way. Resources 5, 32–44. https://doi.org/10.3390/resources5040032

Schulze, R., Lartigue-Peyrou, F., Ding, J., Schebek, L., Buchert, M., 2017. Developing a Life Cycle Inventory for Rare Earth Oxides from Ion-Adsorption Deposits: Key Impacts and Further Research Needs. J. Sustain. Metall. 3, 753–771. https://doi.org/10.1007/s40831-017-0139-z

Sheldon, R.A., 2017. The E factor 25 years on: the rise of green chemistry and sustainability. Green Chem. 19, 18–43. https://doi.org/10.1039/C6GC02157C

Sheldon, R.A., 2007. The E Factor: fifteen years on. Green Chem. 9, 1273. https://doi.org/10.1039/b713736m

Sheldon, R.A., 1992. Organic synthesis; past, present and future. Chem. Ind. 903–906.

Sneller, F., Kalf, D., Weltje, L., Van Wezel, A., 2000. Maximum permissible concentrations and negligible concentrations for rare earth elements (REEs). National Institute of Public Health and Environment, Bilthoven, Netherlands.

Spedding, F.H., Fulmer, E.I., Butler, T.A., Gladrow, E.M., Gobush, M., Porter, P.E., Powell, J.E., Wright, J.M., 1947. The Separation of Rare Earths by Ion Exchange.1 III. Pilot Plant Scale Separations. J. Am. Chem. Soc. 69, 2812–2818. https://doi.org/10.1021/ja01203a063

Spedding, F.H., Jaffe, S., 1954. Conductances, Solubilities and Ionization Constants of Some Rare Earth Sulfates in Aqueous Solutions at 25°. J. Am. Chem. Soc. 76, 882–884. https://doi.org/10.1021/ja01632a073

Spedding, F.H., Powell, J.E., 1960. Method of separating rare earths by ion exchange. US2956858 (A).

Spedding, F.H., Voigt, A.F., 1951. Rare earth separation by adsorption and desorption. US2539282 (A).

Sterckeman, T., Ouvrard, S., Leglize, P., 2011. Phytoremédiation des sols, in: Bioprocédés dans les domaines de l'énergie et de l'environnement, Bioprocédés. Techniques de l'Ingénieur, pp. 1–10.

Takaya, Y., Yasukawa, K., Kawasaki, T., Fujinaga, K., Ohta, J., Usui, Y., Nakamura, K., Kimura, J.-I., Chang, Q., Hamada, M., Dodbiba, G., Nozaki, T., Iijima, K., Morisawa, T., Kuwahara, T., Ishida, Y., Ichimura, T., Kitazume, M., Fujita, T., Kato, Y., 2018. The tremendous potential of deep-sea mud as a source of rare-earth elements. Sci. Rep. 8, 5763. https://doi.org/10.1038/s41598-018-23948-5

Técher, D., Grosjean, N., Sohm, B., Blaudez, D., Le Jean, M., 2020. Not merely noxious? Time-dependent hormesis and differential toxic effects systematically induced by rare earth elements in *Escherichia coli*. Environ. Sci. Pollut. Res. 27, 5640–5649. https://doi.org/10.1007/s11356-019-07002-z

Tian, J., Chi, R., Yin, J., 2010. Leaching process of rare earths from weathered crust elution-deposited rare earth ore. Trans. Nonferrous Met. Soc. China 20, 892–896. https://doi.org/10.1016/S1003-6326(09)60232-6

Tisserand, R., Nkrumah, P.N., Ent, A.V.D., Matsain Buang, Sukaibin Sumail, Erskine, P.D., Echevarria, G., 2018. The first tropical 'Metal Farm' : Methodology of nickel biogeochemical cycle study. Presented at the Thematic school: the cycle of metals, Université de Lorraine, Nancy, France. https://doi.org/10.13140/rg.2.2.24040.72962

Tostevin, R., Shields, G.A., Tarbuck, G.M., He, T., Clarkson, M.O., Wood, R.A., 2016. Effective use of cerium anomalies as a redox proxy in carbonate-dominated marine settings. Chem. Geol. 438, 146–162. https://doi.org/10.1016/j.chemgeo.2016.06.027

Trost, B.M., 1991. The atom economy--a search for synthetic efficiency. Science 254, 1471–1477. https://doi.org/10.1126/science.1962206

Vahidi, E., Navarro, J., Zhao, F., 2016. An initial life cycle assessment of rare earth oxides production from ion-adsorption clays. Resour. Conserv. Recycl. 113, 1–11. https://doi.org/10.1016/j.resconrec.2016.05.006

Vahidi, E., Zhao, F., 2018. Assessing the environmental footprint of the production of rare earth metals and alloys via molten salt electrolysis. Resour. Conserv. Recycl. 139, 178–187. https://doi.org/10.1016/j.resconrec.2018.08.010

Vahidi, E., Zhao, F., 2017. Environmental life cycle assessment on the separation of rare earth oxides through solvent extraction. J. Environ. Manage. 203, 255–263. https://doi.org/10.1016/j.jenvman.2017.07.076

van der Ent, A., Baker, A.J.M., Reeves, R.D., Chaney, R.L., Anderson, C.W.N., Meech, J.A., Erskine, P.D., Simonnot, M.-O., Vaughan, J., Morel, J.L., Echevarria, G., Fogliani, B., Rongliang, Q., Mulligan, D.R., 2015. Agromining: Farming for Metals in the Future? Environ. Sci. Technol. 49, 4773–4780. https://doi.org/10.1021/es506031u

van der Ent, A., Baker, A.J.M., Reeves, R.D., Pollard, A.J., Schat, H., 2013. Hyperaccumulators of metal and metalloid trace elements: Facts and fiction. Plant Soil 362, 319–334. https://doi.org/10.1007/s11104-012-1287-3

van der Ent, A., Echevarria, G., Pollard, A.J., Erskine, P.D., 2019. X-Ray Fluorescence Ionomics of Herbarium Collections. Sci. Rep. 9, 4746. https://doi.org/10.1038/s41598-019-40050-6

Volokh, A.A., Gorbunov, A.V., Gundorina, S.F., Revich, B.A., Frontasyeva, M.V., Chen Sen Pal, 1990. Phosphorus fertilizer production as a source of rare-earth elements pollution of the environment. Sci. Total Environ. 95, 141–148. https://doi.org/10.1016/0048-9697(90)90059-4

Wang, Y.Q., Sun, J.X., Chen, H.M., Guo, F.Q., 1997. Determination of the contents and distribution characteristics of REE in natural plants by NAA. J. Radioanal. Nucl. Chem. 219, 99–103. https://doi.org/10.1007/BF02040273

Weng, Z.H., Jowitt, S.M., Mudd, G.M., Haque, N., 2013. Assessing rare earth element mineral deposit types and links to environmental impacts. Appl. Earth Sci. 122, 83–96. https://doi.org/10.1179/1743275813Y.0000000036

Xiao, Y., Huang, L., Long, Z., Feng, Z., Wang, L., 2016. Adsorption ability of rare earth elements on clay minerals and its practical performance. J. Rare Earths 34, 543–548. https://doi.org/10.1016/S1002-0721(16)60060-1

Xiao, Y., Liu, X., Feng, Z., Huang, X., Huang, L., Chen, Y., Wu, W., 2015. Role of minerals properties on leaching process of weathered crust elution-deposited rare earth ore. J. Rare Earths 33, 545–552. https://doi.org/10.1016/S1002-0721(14)60454-3

Xiao, Y.-F., Feng, Z.-Y., Hu, G.-H., Huang, L., Huang, X.-W., Chen, Y.-Y., Li, M.-L., 2015. Leaching and mass transfer characteristics of elements from ion-adsorption type rare earth ore. Rare Met. 34, 357–365. https://doi.org/10.1007/s12598-015-0481-x

Yang, X.J., Lin, A.J., Li, X.L., Wu, Y.D., Zhou, W.B., Chen, Z.H., 2013. China's ion-adsorption rare earth resources, mining consequences and preservation. Environ. Dev. 8, 131–136. https://doi.org/10.1016/j.envdev.2013.03.006

Yuan, M., Guo, M.-N., Liu, W.-S., Liu, C., van der Ent, A., Morel, J.L., Huot, H., Zhao, W.-Y., Wei, X.-G., Qiu, R.-L., Tang, Y.-T., 2017. The accumulation and fractionation of Rare Earth Elements in hydroponically grown Phytolacca americana L. Plant Soil 421, 67–82. https://doi.org/10.1007/s11104-017-3426-3

Yuan, M., Liu, C., Liu, W.-S., Guo, M.-N., Morel, J.L., Huot, H., Yu, H.-J., Tang, Y.-T., Qiu, R.-L., 2018. Accumulation and fractionation of rare earth elements (REEs) in the naturally grown *Phytolacca americana* L. in southern China. Int. J. Phytoremediation 20, 415–423. https://doi.org/10.1080/15226514.2017.1365336

Zaichick, S., Zaichick, V., Karandashev, V., Nosenko, S., 2011. Accumulation of rare earth elements in human bone within the lifespan. Metallomics 3, 186–194. https://doi.org/10.1039/C0MT00069H

Zapp, P., Marx, J., Schreiber, A., Friedrich, B., Voßenkaul, D., 2018. Comparison of dysprosium production from different resources by life cycle assessment. Resour. Conserv. Recycl. 130, 248–259. https://doi.org/10.1016/j.resconrec.2017.12.006

Zhang, B., Liu, C., Li, C., Jiang, M., 2014. A novel approach for recovery of rare earths and niobium from Bayan Obo tailings. Miner. Eng. 65, 17–23. https://doi.org/10.1016/j.mineng.2014.04.011

Zhang, H., Feng, J., Zhu, W., Liu, C., Xu, S., Shao, P., Wu, D., Yang, W., Gu, J., 2000. Chronic Toxicity of Rare-Earth Elements on Human Beings : Implications of Blood Biochemical Indices in REE-high Regions, South Jiangxi. Biol. Trace Elem. Res. 73, 1–18. https://doi.org/10.1385/BTER:73:1:1

Zhang, X., Laubie, B., Houzelot, V., Plasari, E., Echevarria, G., Simonnot, M.-O., 2016. Increasing purity of ammonium nickel sulfate hexahydrate and production sustainability in a nickel phytomining process. Chem. Eng. Res. Des. 106, 26–32. https://doi.org/10.1016/j.cherd.2015.12.009

Zhang, Z., Du, Y., Gao, L., Zhang, Y., Shi, G., Liu, C., Zhang, P., Duan, X., 2012. Enrichment of REEs in polymetallic nodules and crusts and its potential for exploitation. J. Rare Earths 30, 621–626. https://doi.org/10.1016/S1002-0721(12)60101-X

Zhu, G., Chi, R., Shi, W., Xu, Z., 2003. Chlorination kinetics of fluorine-fixed rare earth concentrate. Miner. Eng. 16, 671–674. https://doi.org/10.1016/S0892-6875(03)00129-8

Zhu, W., Xu, S., Shao, P., Zhang, H., Wu, D., Yang, W., Feng, J., Feng, L., 2005. Investigation on Liver Function Among Population in High Background of Rare Earth Area in South China. Biol. Trace Elem. Res. 104, 1–8. https://doi.org/10.1385/BTER:104:1:001

Zhu, W., Xu, S., Zhang, H., SHAO, P., WU, D., YANG, W., FENG, J., 1996. Investigation on the intelligence quotient of children in the areas with high REE background (I)--REE bioeffects in the REE-high areas of southern Jiangxi Province. Chin. Sci. Bull. 41, 1977–1981.

Chapter 2: Materials and methods

This chapter aims at listing the materials (e.g., plants, reagents) as a basis for the development of the process. The scientific tools, methods and analytical techniques are described to render the research reproducible. The relevance of the methods is emphasized in the light of the novelty and complexity of the matrices. This chapter gives a general view of the employed approach along with its inherent limits.

2.1 Plant samples

The plants collected in this work are *Dicranopteris linearis* (previously known as *Dicranopteris dichotoma*), sometimes abbreviated as *D. linearis* or *D.l*, and *Phytolacca americana* abbreviated as *P. americana*, or *P.a.*

All experiments were conducted with natural plant material, either cultivated or naturally grown (wild). No synthetic plants, or ash, or any sub product was produced to substitute the hyperaccumulators. This strategy aims at proposing only realistic processes. It has the drawback to depend upon the natural variability of the biomass in terms of composition and resource availability (logistics required to produce or collect the plants).

D. linearis bulks were all naturally grown, collected between 2016 and 2018 from a formerly mined site in the Dingnan county, Jiangxi Province (China, GPS: 24°57'17.63" N 115°05'33.55" E) (Figure 42). Only the above-ground fraction of the plant was collected, which mostly consisted of the pinnae. All samples were dried before storage, either sun-dried or at 70 °C at least 48 h.

The tailings hosting *D. linearis* can be described as a very eroded soil, acidic (pH_{water} = 4.5), sandy loam (3-5 wt % clay, 60-80 wt % sand) with a high bulk density (1.3 – 1.5 $g.cm^{-3}$). This soil material was characterized prior to this thesis (Huot *et al.*, 2018).

The soil had a relatively high cation-exchangeable concentration of Al (2.1 10^{-2} $mol.kg^{-1}$), and a low nutrient content (total organic content 0.1 %, total nitrogen 0.01%). It results from intense tropical weathering of granites, and the more recent heap leaching (the site was abandoned between 2003 and 2011) using saline solutions (the reader is referred to the first chapter for the extraction techniques used for RE production).

The fern *D. linearis* dominated the patches of bare tailings, revealing its high adaptability considering the low fertility of the substrate. Individuals also dominated the understory of pines (*Pinus massoniana* and *Cunninghamia lanceolata*), where it developed a higher biomass (Figure 43). Two bulks are considered within this work, solely constituted of fronds. The bulk DL5A, and DL6A, were collected in November 2017 and December 2018, respectively. They represented a variety of individuals collected at the former mining site and each bulk weighted approximately 5 kg (dry biomass).

Figure 42: Satellite photo of the sampling site in South China. The blue pointer indicates the site where *D. linearis* shoots were collected. Satellite photo credit: Google Earth, CNES / Airbus, 2018. Map: Wikimedia Commons.

Figure 43: Photos of wild *D. linearis* growing on abandoned mine tailing (a), and pine understory at the same site (b).

Phytolacca americana individuals were absent from the mining site, but specimens were observed in the surrounding area (Figure 44). The sampling sites where wild individuals were collected were not thoroughly characterized. The bulks collected and the corresponding sampling site are listed in Table 12.

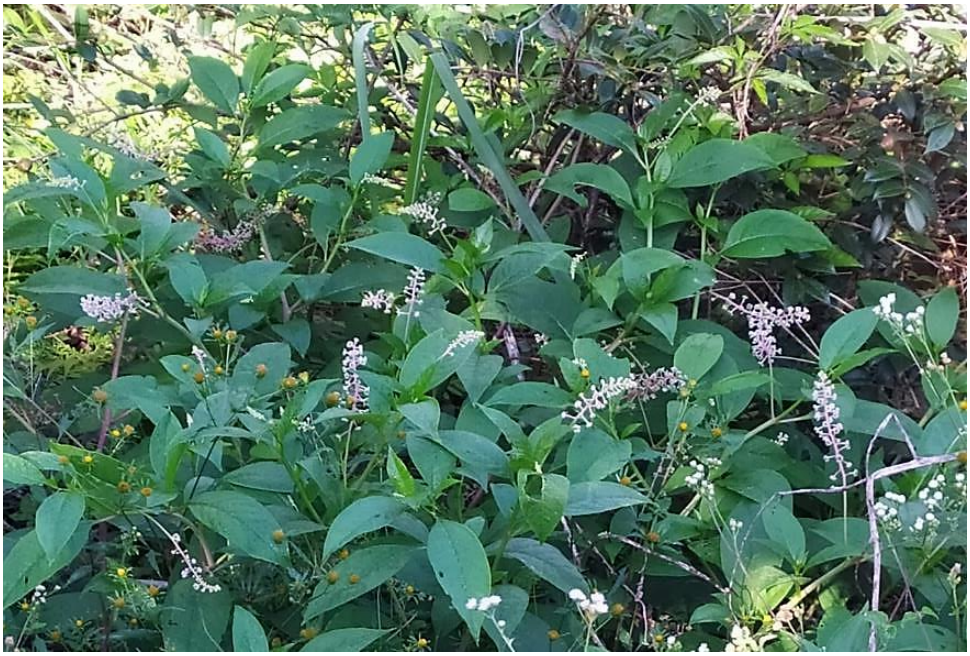

Figure 44: *Phytolacca americana* plants corresponding to bulk PA4

Table 12: Sample characteristics of the different wild *P. americana* collected in Dingnan county (Jiangxi Province, China)

Bulk	Soil type	Surrounding vegetation	Location name	Sampling date	Latitude	Longitude
PA0	Amended tailing	Abundant	"Tea tree mountain"	2018-08	24°59'22.80" N	115°02'42.90"E
PA2	Sandy	Poor	"Brick Yard"	2019-08	24°59'17.80" N	115°02'38.70"E
PA3	Amended tailing	Abundant	"Pear trees"	2019-08	N/D	N/D
PA4	N/D	Abundant	"Garden"	2019-09	24°49'28.00" N	115°01'49.60"E

Phytolacca americana is more easily domesticated than *D. linearis*, and some cultivated shoots were considered in this work, kindly provided by Prof. Jean Louis Morel. In order to produce plant material for processing experiments, cultivated shoots were grown onto RE spiked substrate in pot experiments (n=4 pots). Representative elements were chosen to spike the media as nitrates: La, Ce, Sm, Gd, Yb, and Y. The substrate was composed of a mixture of sand, and topsoil from a garden (Ap horizon) in a 1:1 volume ratio, to which a solution of RE nitrate was mixed. The concentration of the spiking solution was adjusted so that the bulk concentration of REEs in the substrate was 1 $g.kg^{-1}$ (∑REEs), each element in equimolar concentration.

Using that spiked substrate, three bulks of *P. americana* were grown, one during 2019 (Figure 45 (a)), two during 2020 (Figure 45 (b) and (c)). The biomass produced and references for the bulks are given in Table 13. For each harvest, the aerial parts of the 4 pots were collected, dried, and mixed to constitute a bulk. For reference, shoots grown in Prof. Morel's garden (non-spiked substrate) were also collected and prepared for characterization (Figure 45 (d)). Because the level of REEs later determined in the shoot was very low (<10 $\mu g.g^{-1}$), the soil was not characterized, assuming that REE mobility was extremely low.

Within the frame of the REEcovery project, shoots of *P. americana* were cultivated hydroponically at the Interdisciplinary Laboratory for Continental Environments (LIEC). Cultivation conditions were similar to that of Grosjean *et al.*, (2019), except that the selected REEs were Y, La, and Nd at a constant concentration of 33 µmol.L^{-1} for each element. Four shoots were cultivated, and harvested after 6 weeks. The dried leaves of the 4 shoots constituted the bulk PA_Hy_1 (Table 13). Cultivation conditions, and soil characterization were considered beyond the scope of this thesis. Indeed, the main purpose was only to produce plant material containing substantial amounts of REEs.

Table 13: *Phytolacca americana* cultivated bulks used in this thesis and their characteristics

Bulk	Cultivation	Substrate	Collect date
PA_G_1	Open field	Garden	2019-10
PA_G_2	Open field	Garden	2020-05
PA_G_3	Open field	Garden	2020-07
PA_Pots_1	Pots	Spiked substrate	2019-10
PA_Pots_2	Pots	Spiked substrate	2020-05
PA_Pots_3	Pots	Spiked substrate	2020-07
PA_Hy_1	Hydroponics	Nutrient solution	2020-04

Figure 45: *P. americana* shoots grown on spiked substrates (a,b,c), corresponding to bulks PA_Pots_1, 2, and 3, respectively, and *P. americana* grown in the field on a natural soil garden. Photos: Jean Louis Morel

2.2 Analyses

Most of the analyses conducted in this thesis were aimed at determining the elemental composition of a sample. The composition data, in combination with the mass measurements, enable the establishment of mass balances through the process. The other analyses used in this thesis are also described below.

2.2.1 Sample preparation

Like any environmental sample, plant material (fresh or dry biomass, ash) requires preparation prior to analyses. For example, ICP-OES (Inductively Coupled Plasma - Optical Emission Spectroscopy) is a modern and convenient technique to determine the content of trace elements in a sample, but it can only be used onto a clear aqueous solution. The total conversion of the environmental sample to a sample which can be analyzed is crucial and should not be overlooked (Figure 46).

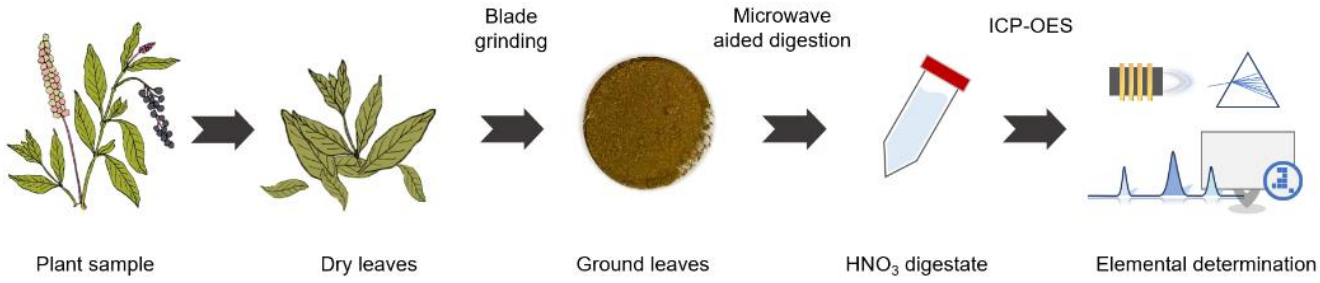

Figure 46: Sample preparation flow in the case of the determination of the elemental composition of dry leaves.

Once collected, the fresh biomass was dried to a constant weight to prevent the apparition of mold and minimize sample moisture. Prior to both analyses and processing, the dried biomass was ground using blade grinders so that particles reached dimensions ≤ 1 mm.

Prior to trace element determination through ICP-OES, plant subsamples were suspended in HNO_3 (0.1 g in 5 mL of 68 wt % HNO_3) in borosilicate glass tubes. The suspensions underwent microwave-aided digestion for 30 min at 230 °C and 80 bar pressure using a single-chamber microwave (Milestone Ultrawave). This technique permits the full oxidation of the organic matter into carbon dioxide, and the dissolution of all trace elements. After cooling to room temperature, the solutions were made up to volume (50 mL) in volumetric flasks with deionized water. The subsamples were all digested at least in triplicates unless otherwise mentioned. At least two blank sample tubes were introduced in the digestion chamber, allowing for the digestion of 15 tubes at one time.

The plant ash sample followed a route more suited to samples with high silica content, known as alkaline fluxing. Alkaline fluxing is a preparative technique used to fully solubilize refractory materials such as soil samples, cements, ceramics, etc. It permits the dissolution of silica, which would otherwise remain solid and form a gel in pure HNO_3 after microwave digestion, possibly retaining trace elements in the solid phase. Alkaline fluxing is the modern substitute for hydrofluoric acid, which is considered too dangerous. The other silicated solids, treated or produced in the process (described in the following chapters) followed the same preparation method prior to trace element determination. The procedure was also adapted to *D. linearis* plant samples, to specifically determine its Si content.

The technique consists of mixing solid subsamples (0.05 g) with alkaline salts (called fluxes) $LiBO_3$ (1.97 g) and LiBr (0.03 g) in a platinum crucible, and heating the mixture at high temperature (1050 °C) for 12 min. The hot melt is poured into a PTFE beaker containing a nitric acid solution (10 % v/v). Magnetic stirring quickly dissolves the melt, and the solution is made up to volume (200 mL) in volumetric flask using deionized water. The procedure is automated from heating the melt to dissolving it by using a dedicated oven (LeNeo Claisse). Subsamples were treated at least in triplicate unless mentioned otherwise, and blank samples were introduced every 10 samples.

Ash used in this thesis followed the same preparation protocol as in Chour's PhD work (Chour, 2018). Ground dry fronds of *D. linearis* were placed in refractory plate (ceramic), the thickness of the layer of ground biomass never exceeded 1 cm to permit oxygen penetration. The batch endured a thermal treatment in oxidizing atmosphere (air), for 3 h at 550 °C in a programmable muffle furnace. The combustion temperature was chosen based on previous results as it was demonstrated that higher combustion temperature (900 °C) yielded ash where REEs were less available for extraction (Chour, 2018). When the oxidation was observably incomplete (*i.e.* appearance of black coal instead of grey to white ashes), the powder was manually agitated with a spatula, and the batch went through a second combustion cycle to make sure that oxidation was complete. After combustion, the furnace was kept slightly opened so that cooling was achieved within 2 h.

Ground leaves of *P. americana* underwent the same thermal treatment. Additionally, combustion batches at 900 °C were conducted. In this case, the temperature gradually increased in the over a ramp of 5 $°C.min^{-1}$ before maintaining the setpoint temperature for 2 h.

2.2.2 Trace element determination: ICP-OES

Inductively coupled plasma optical emission spectroscopy (or ICP-OES) is a common analytical technique to determine trace element content in a liquid sample. In most cases, the liquid sample is an aqueous solution, acidified by a mineral acid (HNO_3 in this work) forming the matrix[1]. The analytes are the trace elements in solution, in the form of dissolved cations or anions. The apparatus can be decomposed into several parts as described in Figure 47.

The sample introduction system (1) consists of an automated sampler, which feeds the nebulizer via a peristaltic pump. The sample is dispersed by an argon (Ar) flow in the nebulizer to form a mist in the cyclonic chamber. The largest droplets are evacuated via the bottom of the chamber and drained. Only a tiny fraction of the aerosol, formed by the smallest drops, flows through the torch.

In the torch (2), induction coils generate an intense radiofrequency field which sustains a plasma of Ar at around 10 000 K. The plasma provides sufficient energy to evaporate the solvent and excite the atoms to higher energy states (excited states). The return from excited state to more stable state (electronic transition) is accompanied by the emission of photons (or ray) with quantified energy characteristic of the transition and the element.

The wavelength and intensity of this emitted rays are quantified by an optical system (3) (mirrors and polychromator) and a detector (charge coupled device, or CCD, in this case). The plasma can be observed perpendicular to the torch (radial view), or along its axis (axial view). The radial view is more suited to observe intense rays, while the axial view enables the collection of lower intensity rays. The

[1]Aqueous basic matrices, and organic matrices can also be analyzed, but are outside the frame of this thesis.

combination of both views permits concentration determination over a wide range of concentrations and elements.

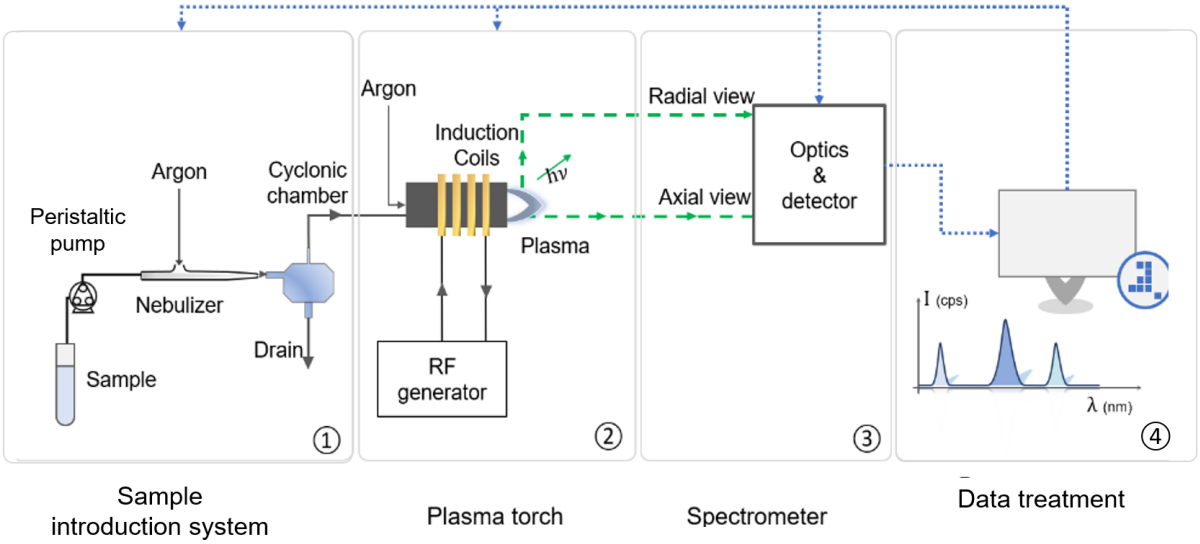

Figure 47: Schematic view of the ICP-OES instrumentation

The signal processing electronics and operation software allow the data treatment (4). For a given ray, the emitted light is directly proportional to the analyte concentration. Hence, the collected intensities are compared to standards following equipment calibration to the concentration of the analyte.

In this thesis, the instrument was a Thermo iCAP 6000, operated with Qtegra software. Instrument calibration was conducted by external calibration: a sequence of samples with known concentration of analyte (standards) are analyzed to draw a calibration curve (line). PlasmaCAL® custom standards (SCP Science) were used to compose a composite standard containing all required analytes in a 3 wt% of HNO_3 matrix.

Two solutions were used for selected trace elements (Al, Co, Cu, Fe, Pb, Mn, Mg, Ca, P, S, Ni, Na, Zn, initially at 1 000 $mg.L^{-1}$ for each element), and for the REEs (Y, Sc, and all 14 lanthanides except Pm, at 100 $mg.L^{-1}$), while the calibration for Si was done separately using a Si standard solution (1 000 $mg.L^{-1}$). The optimized method (after selection of the best wavelength, best dynamic ranges) permits the analysis of samples containing between 0.05 and 10 $mg.L^{-1}$ for trace elements and Si, and between 0.025 and 5 $mg.L^{-1}$ for REEs. Exceptions are Ce and S for which quantification limit was estimated at 0.1 $mg.L^{-1}$.

The selected wavelengths are exposed in Table 14. When liquid samples were from alkaline fluxing, a separate range of standards was used. The standards were prepared in a matrix containing 5 wt% HNO_3 and 1 $g.L^{-1}$ $LiBO_2$ to match the samples matrix and compensate for matrix interferences.

For a given liquid sample, each measurement was repeated three times. Quality checks were performed during the analyses every 10 samples using a known standard solution prepared separately to monitor instrument drift. External recalibration was performed when the quality control deviated by more than 10 % for any analyte.

Table 14: Analytical parameters selected for the routine analysis of liquid samples

Element	Wavelength (nm)	View	Element	Wavelength (nm)	View
La	333.749	Axial	Al	396.152	Radial
Ce	535.353	Axial	Ca	393.366	Radial
Pr	390.844	Axial	Fe	259.940	Axial
Nd	378.425	Axial	K	769.896	Axial
Sm	330.639	Axial	Mg	279.553	Radial
Eu	381.967	Axial	Mn	257.610	Radial
Gd	310.050	Axial	Na	589.592	Radial
Tb	350.917	Axial	Ni	231.604	Axial
Dy	353.170	Axial	P	178.766	Axial
Ho	345.600	Axial	Pb	182.205	Axial
Er	323.058	Axial	S	190.029	Axial
Tm	342.508	Axial	Zn	206.200	Axial
Yb	328.937	Axial	Si	251.611	Axial
Lu	307.760	Axial			
Y	324.228	Axial			

2.2.3 Elemental analysis of H, C, N, S, O, and Cl

Additional analyses were performed on dry biomass and ash to determine their content of the elements H, C, N, S, O, and Cl. As discussed below, these data can be useful to predict thermodynamic values resulting from biomass combustion. Additionally, Cl and S are volatile elements that easily convert to acidic gases, that can be a source of atmospheric pollution if not adequately treated.

To conduct the analysis of the five elements cited, the Microcube Vario elemental analyzer (Elementar) was used (Figure 48). The apparatus can be operated in three different configurations: (a) for HNCS, (b) O, and (c) Cl determination. The equipment consists of a series of ovens (combustion chamber, reduction chamber, pyrolysis chamber) to convert the sample into the simplest gases (H_2, CO_2, N_2, H_2O, SO_2, HCl). The ovens are packed-bed quartz columns, packed with either copper metal or oxide catalyzing the desired reaction. The packing, temperature and arrangement of the columns depend on the configuration (either a, b or c). In all cases, the gas products are separated on an absorbing column (as in a gas chromatography) and finally detected by a thermal conductivity detector (also known as katharometer).

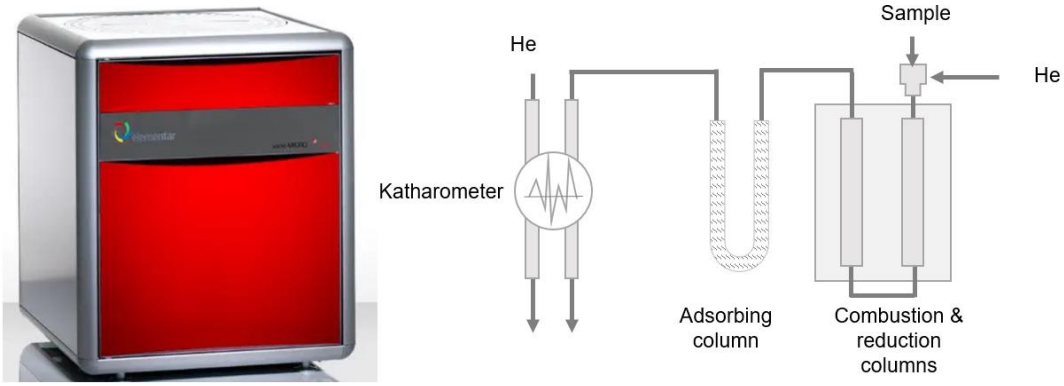

Figure 48: Photography of the Vario Microcube (Elementar) and schematic representation of the configuration used for HCNS determination.

Before introduction, the sample is put in the form of a dry, finely ground solid and packed in a folded tin boat ((a) and (c)) or a silver boat. The sample is prepared using a high-precision scale (Microscale, Mettler-Toledo) as its mass should be between 1 and 5 mg. Instrumental calibration was conducted using BBOT (2,2'-(2,5-thienediyl)bis[5-(2-methyl-2-propanyl)-1,3-benzoxazole]) for HCNS, benzoic acid for O, and methylene blue (3,7-bis(dimethylamino)phenothiazin-5-ium chloride) for Cl. The calibration line was established prior to the analyses and a coefficient correction was made every 5 samples using the appropriate standard.

The constructor's varioEA software was used to operate the instrument and collect the data. Mass concentrations were obtained by converting the area of the detected peaks to the corresponding analyte mass, and dividing by the sample mass.

2.2.4 Scanning Electron Microscopy with Energy Dispersive Spectroscopy

Scanning electron microscopy (SEM) is a technique to observe the topography of solid surfaces. It can be used to collect data on the size and shape of particles, but also to visualize the structure and texture of a given material. The apparatus consists of a probe that fires electrons at the sample, which re-emits secondary electrons of lower energy that hit a detector. The collected signal is amplified and a 2D image is generated. To re-emit electrons, the surface must be electron conductive, so the samples are coated with a gold/palladium alloy under vacuum.

Scanning electron microscopes are often coupled to an energy dispersive spectrometer (EDS) to take advantage of the electron field already present. Atoms hit by the electron beam access an excited state of energy, and the return to their ground state is accompanied by the emission of a photon of high energy (X-ray). The energy of the collected photons is characteristic of the atom; hence energy spectra can be interpreted to deduce the elemental composition of the surface.

In this work, a JEOL-JSM-6490LV was used to observe the morphology of treated or produced solids (combustion, leaching, reprecipitation).

2.2.5 Thermogravimetric analysis

Thermogravimetric analysis (TGA) is the dynamic measurement of the mass of a sample during a thermal treatment. A small amount of sample (*ca.* 10 mg) is placed in a refractory crucible (typically, alumina) resting on the plate of high precision balance. The whole is heated gradually inside a temperature-controlled oven, while an inert (N_2) or reactive (air) gas continually flushes the gaseous

products. The weight measured corresponds to the solid mass of the remaining sample. Temperatures can range up to more than 1 100°C.

This technique is particularly useful to monitor solid/gas reactions occurring at high temperature (*e.g.*, combustion). Additionally, mass balances can be done to measure the hydration numbers of crystalline solids. In this work, TGA was used to determine the hydration number of the final products (rare-earth carbonate). It also provided insight into the ash fraction remaining after combustion under ideal conditions. Indeed, the small amounts of sample are less subject to anaerobic reactions than in larger ovens.

Data for *P. americana* biomass were collected using a TG 209F1 Libra (Netzsch) in Guangzhou, between 30 and 900 °C under an air flux. Replicates were conducted at three heating rates (5, 15, and 30 °C.min^{-1}). The TGA2 (Mettler Toledo) was used in Nancy for data collection of the rare earth carbonate product. Samples underwent the thermal treatment in air

To determine the hydration number x, the reactions (11) and (12) were assumed complete at 900 °C.

$$Ln_2(CO_3)_3 \cdot xH_2O_{(s)} \rightarrow Ln_2(CO_3)_{3(s)} + xH_2O_{(g)} \quad (11)$$

$$Ln_2(CO_3)_{3(s)} \rightarrow Ln_2O_{3(s)} + 3CO_{2(g)} \quad (12)$$

Evaporation of hydration water and carbonate decomposition were assumed to be complete at 900 °C, hence, the conservation of the quantity of matter of Ln is given by:

$$n(Ln_2(CO_3)_3 \cdot xH_2O) = n(Ln_2O_3) \Leftrightarrow \frac{m_0}{2M_{Ln} + 3M_{CO_3} + xM_{H_2O}} = \frac{m_f}{2M_{Ln} + 3M_O} \quad (13)$$

where m_0 and m_f are the sample mass in g at 30 and 900 °C, respectively, M_{Ln} the average molar weight of the main lanthanide in presence (152.3 g.mol^{-1}), M_{CO2}, M_O and M_{H2O} the molar weight of CO_3, O, and H_2O.

Equation (14) was used to determine x:

$$x = \left(\frac{1}{M_{H_2O}}\right) * \left[\left(\frac{m_0}{m_f}\right) * (2M_{Ln} + 3M_O) - \left(2M_{Ln} + 3M_{CO_3}\right)\right] \quad (14)$$

2.2.6 Infrared characterization

Fourier transform infrared spectroscopy (FTIR) is a spectroscopic technique based on the absorption of infrared photons that excite the vibrations of molecular bonds. A spectrum of characteristic bands is produced that can be used as a fingerprint to help identify and characterize the sample. It can be used in transmission or reflectance.

In this work, solid rare earth carbonates were characterized by an attenuated total reflectance instrument (ATR) using the Alpha P (Brucker) equipped with a diamond tip. Each sample was scanned 32 and the spectra were averaged from 4 000 to 360 cm^{-1} at a resolution of 4 cm^{-1}.

2.2.7 X-ray powder diffraction

X-ray diffraction (XRD) is a non-destructive analysis technique for the identification and determination of the different crystalline forms present in a solid. It allows to determine the precise

positions / arrangements of atoms in a crystal. X-ray beams strike the crystal and cause the light beam to diffract in several specific directions.

For powders, the sample is scanned over a range of 2θ angles (Figure 49). Hence, all possible directions are examined and result in a diffractogram (XRD pattern). Minerals have a unique XRD pattern reflecting their crystalline arrangement. Diffractograms of unknown samples are compared to reference patterns from a database, and the crystalline phases in presence can be identified with a detection limit of approximately 2% for mixtures (in mass).

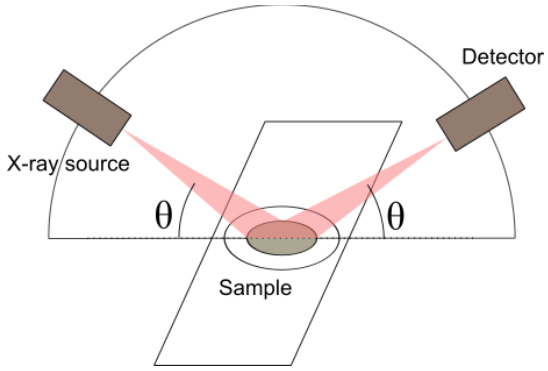

Figure 49: Schematic representation of a powder X-ray diffractometer

The analyses were carried out using the Bruker D8-Advance diffractometer equipped with a cobalt probe ($\lambda Co_{K\alpha}$ 1.79 Å) and a linear detection (LynxEye). The generator power was set by a voltage of 35 kV and 45 mA. Scans were run between 3 and 90°(2θ) with a step size of 0.03° (2θ) and a collection time of 3 s per point. Crystalline phases were identified using the Powder Diffraction File of the International Diffraction Data Centre (PDF-02).

The carbonate precipitates were subject to X-ray fluorescence when using the cobalt probe, generating a high background noise. Thus, additional measurements were run using a copper probe ($\lambda Cu_{K\alpha}$ 1.54 Å). In this case, the generator power was set by a voltage of 40 kV and 40 mA. Diffractograms were collected between 5 and 60° (2θ) with a step size of 0.025° (2θ) and a collection time of 3 s per point. Measurements and interpretations were conducted at the Laboratoire interdisciplinaire des environnements continentaux (LIEC, CNRS-Univ. Lorraine).

2.2.8 Note on sample replicates

Averaged values of empirical results are expressed all along this manuscript to account for natural variability of biomaterial or experimental errors. In this case, the number n of averaged values are noted close to the result (*e.g.*, n=...). Standard deviations (SD) are displayed to provide the reader with an order of magnitude of the scattering of the values. Standard deviation is computed with the n-1 method, to account for estimation bias:

$$\mathrm{SD} = \sqrt{\frac{\sum_i (x_i - \bar{x})^2}{n-1}} \qquad (15)$$

Where SD is the standard deviation, x_i the individual results, $\bar{x}$ the average, and n the number of replicates.

2.3 Tools

2.3.1 Estimations of the calorific power of biomass

The lower heating values (LHV) and higher heating values (HHV) are key data representing how much heat can be recovered from combustion. Those data can be either directly measured in a dedicated apparatus (*e.g.*, calorimeter), or predicted with existing correlations using elemental concentration of C, H, N, and O of the proposed fuel (Boie, 1953; Gumz, 1931). The correlations proposed by Gumz (Equation (1)) and Boie (Equation (2)) were successfully applied to various types of biomass, including hyperaccumulator biomass in recent studies (Hazotte *et al.*, 2020).

$$\mathrm{HHV} = 35.160\ w_C + 116.225\ w_H - 11.090\ w_O + 6.280\ w_N + 10.465\ w_S \quad (16)$$

$$\mathrm{HHV} = 34.03\ w_C + 124.31\ w_H - 9.836\ w_O + 6.278\ w_N + 19.09\ w_S \quad (17)$$

Where HHV is the higher heating value in $MJ.kg^{-1}$, and w_C, w_H, w_O, w_N, w_S the carbon, hydrogen, oxygen, nitrogen and sulfur contents of the dry biomass, respectively in wt %. The difference between HHV and LHV is that the LHV accounts for the evaporation of the water contained in the fuel, while HHV does not. Because a same type of fuel contains varying amount of moisture, it is useful to compare HHVs between different types of fuel (*e.g.*, wood vs. grass).

Oppositely, LHV reflects the experimental amount of heat that can be recovered from a fuel by combustion, accounting for its moisture content. The LHV is sometimes called net calorific value (NCV) or lower calorific value (LCV). The heat spared in the evaporation of water is estimated, and LHV can be derived from HHV using Equation (3) (ISO, 2017).

$$\mathrm{LHV} = \mathrm{HHV} - 212.2 * w_H - 0.8 * [w_O + w_N] \quad (18)$$

Where LHV is expressed in $MJ.kg^{-1}$, and w_H, w_O, w_N, hydrogen, oxygen and nitrogen contents of the biomass, analyzed as received before combustion, respectively in wt %.

2.3.2 Design of experiment

The design of experiment (DoE) methodology allows us to best organize the tests that accompany scientific research or industrial studies (Goupy, 2017). With the DoE, the maximum amount of information is obtained with the minimum of experiments. For this, it is necessary to follow mathematical rules and adopt a rigorous approach (i.e., “designs”). Numerous designs have been developed over the last decades and covering them all would be outside the frame of this work. The composite design allows one to draw a response surface model, where a response (*e.g.*, yield) is the result of combination of the parameters (*i.e.*, a model). Firstly, the experimental domain is defined by setting the parameters and their limits (*e.g.*, T_{min} and T_{max}). The parameters are normalized, so that the extremities of the domain correspond to -1 and +1 values. Trials are conducted at the extremities of the experimental domain and in the center. The model is completed by “star” points, slightly outside the domain (Figure 50).

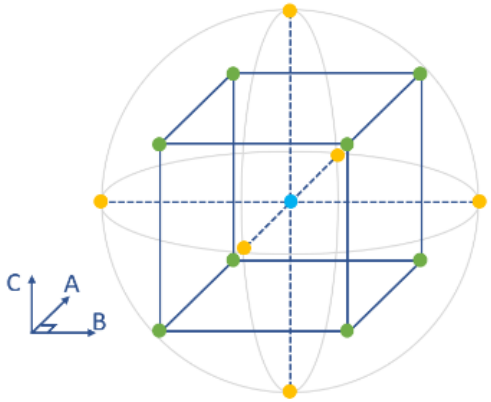

Figure 50: Schematic representation of the central composite design. The blue point is the center of the design (0,0,0); the green points are the cube points or factorial points; and the yellow points are the star points.

The DoE methodology was applied for alkaline ash leaching, using temperature, duration and soda concentration as parameters. The Design Expert 11 software (Stat-ease, Inc.) was used to prepare the experiments and treat the data.

2.3.3 Chemical equilibrium modelling

Aqueous solutions resulting from ash treatment contained numerous anionic and cationic species due to the variety of elements needed by the plant. According to the solvent interaction theory (SIT), each species interacts chemically with each other and with the solvent, resulting in chemical reactions (acid-base, oxidoreduction, precipitation, complexation, *etc.*), which can be modelled by a chemical equilibrium. The reaction described by equation (19) is an example.

$$xA^{m+} + yB^{n-} \leftrightarrow \left(A_xB_y\right)^{(x*m-y*n)} \tag{19}$$

The equilibrium is governed by the mass action law depending on a single constant (usually noted K), depending on the temperature:

$$K(T) = \frac{a\left(A_xB_y\right)^{(x*m-y*n)}}{a(A^{m+})^x * a(B^{n-})^y} \tag{20}$$

Where:

- $a\left(A_xB_y\right)$ represents the activity of A_xB_y
- $a(A^{m+})$ represents the activity of A^{m+}
- $a(B^{n+})$ represents the activity of B^{n-}

More generally, for a chemical reaction defined by:

$$\sum_i m_iA_i = 0 \tag{21}$$

The chemical equilibrium constant is:

$$K = \prod_i a(A_i)^{m_i} \quad (22)$$

The activity of a species is linearly linked to the species concentration via an activity coefficient (generally noted as γ_i).

$$a(A_i) = \gamma_i * [A_i] \quad (23)$$

Models have been developed to estimate these coefficients as a function of the solution ionic strength and temperature (Table 15) (Debye and Hückel, 1923; Davies, 1962; Helgeson, 1969; Truesdell and Jones, 1973).

Table 15: Activity coefficient models for electrolyte in aqueous solutions and their validity range.

Model	Equation	Validity
Debye-Hückel (simplified)	$\log(\gamma_i) = -Az_i^2\sqrt{I}$	$I < 10^{-2.3}$ mol.L^{-1}
Davies	$\log(\gamma_i) = -Az_i^2\left(\frac{\sqrt{I}}{1+\sqrt{I}} - 0.30 * I\right)$	I < 0.5 mol.L^{-1}
Truesdell-Jones	$\log(\gamma_i) = -Az_i^2\left(\frac{\sqrt{I}}{1+Ba_i^0\sqrt{I}}\right) + b_i * I$	I < 1 mol.L^{-1}
B-dot (Hegelson)	$\log(\gamma_i) = \log(\gamma_i) = -Az_i^2\left(\frac{\sqrt{I}}{1+Ba_i^0\sqrt{I}}\right) + \dot{B} * I$	I < 3 mol.L^{-1}

Where z_i is the charge of the ion, a_i^0 and b_i are coefficients characteristic of the ion, and $\dot{B}$ is the deviation function. A and B are functions of the temperature T and dielectric constant ε:

$$A = 1.82\ 10^6 * (\varepsilon T)^{-\frac{3}{2}};\ B = 50.3 * (\varepsilon T)^{-\frac{1}{2}}$$

At 25 °C in water: A = 0.05085 mol$^{-0.5}$.L$^{0.5}$ and B =3.281 10^{-9} mol$^{-0.5}$.L$^{0.5}$.m^{-1}. The reader is referred to the previously cited references for full model description.

When few species are involved, concentrations at equilibrium might be calculated by hand. However, the superposition of numerous molecules and ionic species in solution requires more computational power to correctly predict the aqueous concentration.

Chemical equilibrium modelling computational software fulfills this purpose. Extensive data sets can be considered, and even multiple phase reactions can be implemented. In this study, the computational code CHESS (standing for CHemical Equilibrium with Species and Surfaces) was run (van der Lee and De Windt, 2002). Its graphical interface JCHESS and the default database, adapted from the EQ3/6 version 8 was used (Wolery and Jarek, 2003). To account for the high ionic strength, the activity coefficients were computed using the implemented B-dot equation (Helgeson, 1969).

At higher ionic strength, the SIT theory accuracy decreases and the Pitzer equations (Pitzer and Kim, 1974), based on a different thermodynamic approach, are more accurate. However, calculations require more data input (additional coefficients per electrolyte) which are not as readily available as for SIT

theory. Accurately predicting the behavior of the process solutions and suspensions was outside the frame of this thesis.

Chemical equilibrium modelling was used as a complementary tool to guide the understanding of the reactions involved.

2.4 Experimental setups

2.4.1 Alkaline leaching setup

To conduct the alkaline leaching of *D. linearis* ash, a soda solution of desired concentration was prepared with NaOH pellets and water, on the same day that the leaching was conducted. The lukewarm solution was then heated in a three-neck round-bottom flask (borosilicated glass, 250 – 1000 mL) by using an oil bath (Figure 51). The temperature of the solution was monitored via a glass thermometer, inserted through a side neck. When the solution reached the set temperature, the desired quantity of ash was subsequently added through a funnel using the other side neck, and a small amount of soda solution was used to rinse the neck and flask walls. All along the experiment, agitation was maintained by the mean of a magnetic stirrer.

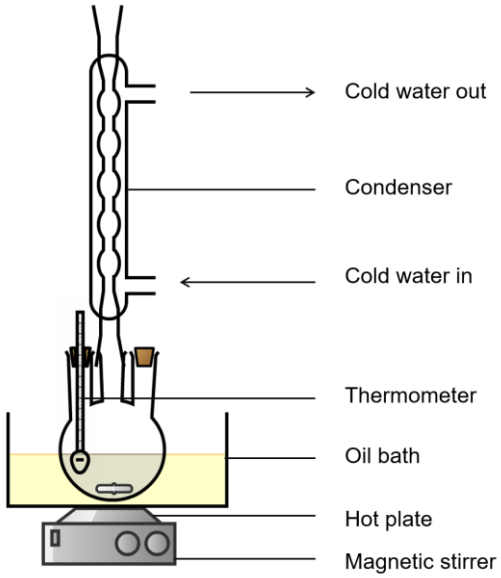

Figure 51: Alkaline leaching setup and apparatus

After the set duration, the flask is removed from the oil bath, and cooled by running water on its walls, until the medium temperature drops below 60 °C. The medium is then immediately vacuum-filtered using glass microfiber filters (GF/C, Whatman ®, $\emptyset_c \approx 1.2$ µm). The mass of leachate is measured by measuring the weight of the Büchner flask before and after filtration.

In the initial trials, the remaining solid was not rinsed and collected for drying at 80 °C (at least 24 h), before mass measurement and further processing. After the rinsing trials were conducted, the solid was rinsed on the filter, using a predetermined quantity of hot (60 °C) deionized water, collected and stored at 80 °C. Prior to further processing (either the recovery process or analyses), dry solids were ground in planetary ball mill for 10 min at 200 RPM (PM100, RETSCH, agate balls and bowl).

After cooling to room temperature, the alkaline leachate is stored in plastic (polyethylene, PE) air-tight container.

2.4.2 Selective extraction

After alkaline leaching, REEs are contained in the solid phase. They are subsequently extracted using an acidic solution in controlled conditions. Progressive extractions were conducted in order to minimize reagent usage and most importantly, assess if a selective extraction is feasible, *i.e.*, extract REEs while certain impurities stay in the solid phase.

Firstly, 0.15 g of dry treated ash, were suspended in 50 mL of deionized water and the pH was progressively diminished. To do so, an automatic titrator (METTLER-Toledo T5) equipped with a pH probe (Mettler), and a HNO_3 solution (0.1 M) were used (Figure 52). Prior to each day of experiment, the probe was calibrated with pH buffers (4, 7, and 10 at 20°C). Sample temperature was monitored using a glass thermometer, and input in the automatic titrator for temperature compensation. Temperature variations never exceeded 3 °C.

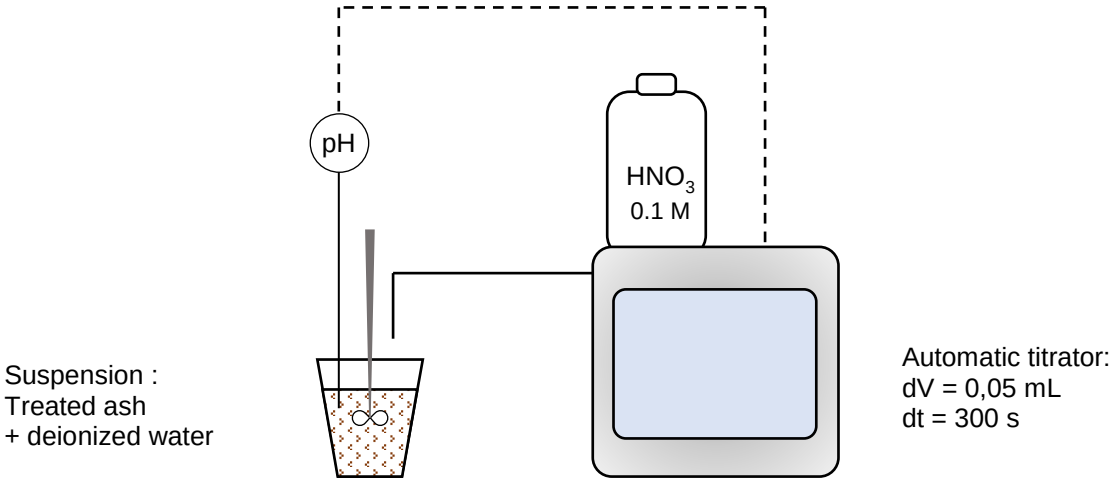

Figure 52: Apparatus used to assess the feasibility of a selective extraction from *D. linearis* treated ash

Small acid volume increments (ΔV = 0.05 mL) were added over large and fixed time increments (Δt = 300 s), to ensure that equilibrium was reached at every step. The experiment was stopped when pH 2 was reached. Throughout the experiment, suspension aliquots (0.5 mL) were sampled, syringe-filtered (Phenomenex, regenerated cellulose, 0.45 µm), and properly diluted prior to elemental analysis (ICP-OES).

Later on, the same setup was used to leach the treated ash at constant set pH value. The automatic titrator was configure to adjust the pH with a tolerance of ± 0.1. Trials were conducted to measure the required time to reach the equilibrium for a given pH value (4.7 in this case). Over 10 h, an aliquot was sampled every hour, syringe-filtered, diluted and analyzed via ICP-OES.

Afterward, the duration was set to 6 h and different pH values for extraction were explored (4.5, 4.6, and 4.7). For each pH value, the experiment was conducted at least in duplicate.

Finally, the influence of the S/L ratio in the alkaline leaching step was monitored. The different solids produced (treated ash) endured the same procedure, and the acid consumption after 6 h was noted.

For every experiment, the added volume of the HNO_3 solution was noted. For each collected sample, the current pH at which it was collected was noted, as well as duration, and acid consumption.

At the end of all the extractions, the suspension was vacuum-filtered using a Büchner flask and microfiber filters (GF/C, Whatman ®, $\emptyset_c \approx 1.2$ µm). The mass of leachate (sometimes called pregnant leach solution, PLS), was carefully measured for mass balance calculations purposes, and its elemental composition was determined after proper dilution via ICP-OES.

2.4.3 Precipitation

The precipitant, NH_4HCO_3 in its solid form (Sigma-Aldrich, reagent grade) was dissolved in deionized water to obtain a 1 M solution. A predetermined amount of precipitating solution was progressively added (1 $mL.min^{-1}$), by the mean of the same pH titrator (Figure 53). Along additions, pH and conductivity were measured. Conductivity of the suspension was measured by the mean of a bench conductimeter and a conductivity cell (Mettler).

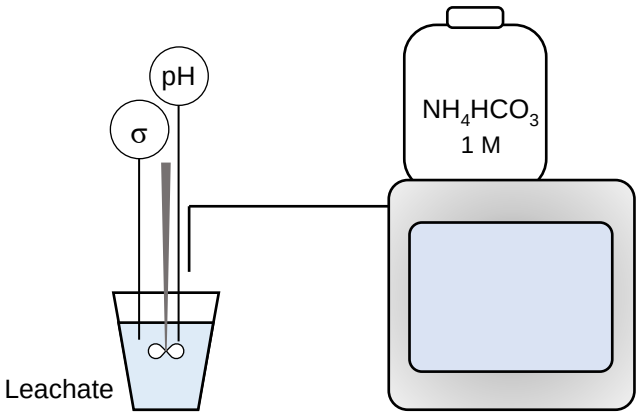

Figure 53: RE carbonate precipitation setup

To promote crystal growth, suspensions were transferred to an air-tight PE container (400 mL), fastened onto an orbital shaking plateau, and placed in a thermostatic shelf at 40 °C for 24 h. After cooling to room temperature, suspensions were vacuum-filtered on a Büchner funnel, using regenerated cellulose filters (D. Dutscher, $\emptyset_c \approx 0.3$ µm).

The fine powder of RE carbonate was carefully collected and placed to dry at 80 °C for 24 h prior to characterizations (TGA, ATR-FTIR, powder XRD). Impurity and RE contents were assessed by dissolving a known mass of the RE carbonate in an ultra-pure HNO_3 solution (Optima™, Fisher scientific) in disposable PE tubes, and analyzed by ICP-OES.

This chapter precisely described the materials, tools, and analytical procedures that have been conducted in this thesis. The reader will be referred to this chapter for the generic procedures. More specific methods (e.g., experimental conditions for a given separation, specific mass balance, etc.) will be described in the appropriate chapter.

As a direct application of the methods described, and to provide some base results, the next chapter will present the resource (plants) used in this thesis.

2.5 References

Boie, W., 1953. Fuel technology calculations. Energietechnik 3, 309–316.

Chour, Z., 2018. Valorisation de terres rares à partir de plantes hyperaccumulatrices (PhD dissertation). Université de Lorraine, Nancy, France.

Davies, C.W., 1962. Ion association. London.

Debye, P., Hückel, E., 1923. The theory of electrolytes. I. Lowering of freezing point and related phenomena. Phys. Z. 24, 185–206.

Goupy, J., 2017. Introduction aux plans d'expériences: avec applications. Dunod, Paris.

Grosjean, N., Le Jean, M., Berthelot, C., Chalot, M., Gross, E.M., Blaudez, D., 2019. Accumulation and fractionation of rare earth elements are conserved traits in the *Phytolacca* genus. Sci. Rep. 9, 18458. https://doi.org/10.1038/s41598-019-54238-3

Gumz, W., 1931. Feuerungstechnisches Rechnen, Monographien zur Feuerungstechnik. Springer-Verlag Berlin Heidelberg, Leipzig. https://doi.org/10.1007/978-3-662-36727-8

Hazotte, C., Laubie, B., Pacault, S., Dufaud, O., Simonnot, M.-O., 2020. Evaluation of the performance of nickel hyperaccumulator plants as combustion fuel. Biomass Bioenergy 140, 105671. https://doi.org/10.1016/j.biombioe.2020.105671

Helgeson, H.C., 1969. Thermodynamics of hydrothermal systems at elevated temperatures and pressures. Am. J. Sci. 267, 729–804. https://doi.org/10.2475/ajs.267.7.729

Huot, H., Guo, M.N., Liu, C., Liu, W., Yuan, M., Chen, Y.Y., Zhu, S.C., Wang, Y., Wu, Y.L., Ye, P.X., Chen, J.Q., Séré, G., Watteau, F., Chao, Y.Q., Auclerc, A., Morel, J.L., Tang, Y.T., Qiu, R.L., 2018. Reclamation of ionic rare earth elements (REEs) mine tailings in Southern China, in: 11th Sino-French Workshop - Innovations for the Circular Economy by Recycling Secondary Resources. Presented at the 11th Sino-French Workshop - Innovations for the circular Economy by Recycling Secondary Resources, Sun Yat-sen University, Guangzhou.

ISO, 2017. ISO 18125:2017 - Solid biofuels — Determination of calorific value.

Pitzer, K.S., Kim, J.J., 1974. Thermodynamics of electrolytes. IV. Activity and osmotic coefficients for mixed electrolytes. J. Am. Chem. Soc. 96, 5701–5707. https://doi.org/10.1021/ja00825a004

Truesdell, A.H., Jones, B.F., 1973. WATEQ – A computer program for calculating chemical equilibria of natural waters, Resources Investigations Report. USGS, Reston, VA.

van der Lee, J., De Windt, L., 2002. CHESS Tutorial and Cookbook. Updated for version 3.0 (Users Manual No. Nr. LHM/RD/02/13). Fontainebleau, France.

Wolery, T.W., Jarek, R.L., 2003. Software user's manual. EQ36 Version 8, 376.

Chapter 3: Resource characterization

The aerial parts of the HAs, or their ash, are bio-materials concentrated in REEs. In a perspective of resource recovery, they can be considered as "bio-ores". This chapter aims at providing an in-depth characterization of them. And just as with conventional ores, prospecting how much bio-ore is available is essential.

Firstly, the agronomic characteristics of the plants are introduced and compared. Secondly, the physicochemical properties of the biomass and its ash are described, as well as the REE content. Thirdly, the expectable metal yield per hectare per year is estimated, and suitable recovery processes are suggested depending on the ore composition. To conclude, the most appropriate hyperaccumulator is selected based on the discussed results.

3.1 Agronomic characteristics of the considered plants

Even though agromining is a novel concept, established agronomic practices are known to improve the quantity and quality of the bio-ore (Kidd *et al.*, 2018; Nkrumah *et al.*, 2019, 2021). For agromining, the most important characteristic of an agrosystem is the metal yield. The metal yield is defined as the quantity of metal extracted per hectare for a crop year. It can be deduced by knowing the biomass yield and the metallic content of the plant.

To date, no field trials to cultivate REE hyperaccumulators have been reported in the literature. To frame and foresee the development of RE agromining, previously established data regarding the growth and cultivation of hyperaccumulators, are reported in this section. The collection and curation of the available data discussed here intend to provide a reliable metal yield for both plants.

3.1.1 Intended type of field

The mined and stripped soils of South China are potential targets of RE agromining. They are the leftovers of REE exploitation and are highly subject to erosion (the reader is referred to the first chapter). The environmental benefits of agromining and ecosystem services (biodiversity, land erosion minimization) are maximum there (Pons *et al.*, 2021; Rodrigues *et al.*, 2016). The available surface is large, built in terraces, and its fertility is low so that they do not compete with food production systems.

In most sites, REE extraction is not complete. Liu *et al.* reported that the tailing concentration ranged up to 1039 $mg.kg^{-1}$ and averaged 392 ±225 mg kg^{-1}, (n=15), as total REEs. In all analyzed samples, the ion exchangeable fraction represented more than 50% (Liu *et al.*, 2019a). Hence, a significant portion remains available to plants.

A representative composition of the tailing soil, sampled from the abandoned mining site (Table 16) was provided by Hermine Huot (Huot *et al.*, 2018). The material is characterized by its high bulk density, low pH, poor nutrient content (C, N) and low Ca/Mg molar ratio. All these characteristics render the substrate generally unfavorable for spontaneous vegetation installation, except for pioneer species (*e.g.*, *D. linearis*).

Table 16: Physico-chemical properties of the soil (tailings) of the abandoned mining site (Huot *et al.*, 2018)

Major elements		**Physico-chemical properties**	
Si (wt %)	33	pH_{H2O}	4.5
Al (wt %)	8.8	$C_{org,tot}$ (%)	0.1
K (wt %)	4.7	N_{tot} (%)	0.01
Fe (wt %)	2.2	Main minerals	Quartz, Feldspars, Micas
Ca ($mg.g^{-1}$)	1 442	Texture	Sandy loam (3-5% clay; 60-80% sand)
Mg ($mg.g^{-1}$)	851	Bulk density	1.3 – 1.5 $g.cm^{-3}$

3.1.2 Contrasted agronomic management and expected biomass yield

Dicranopteris linearis and *Phytolacca americana* are both able to accumulate REEs, Mn and Al. They can grow on the acidic soils in the surroundings of the mining area in South China. A part from that, they form a quite opposed pair of plant species.

To consider agromining, it is necessary to foresee the implantation of the first individuals in the field. In theory, the establishment of *D. linearis* should not be an issue, as it is a pioneer species: "it can endure strong solar radiation, high temperatures, acidity, infertile soil, and drought, and can also thrive in humid environments" (Russell *et al.*, 1998). However, in practice, data regarding the cultivation of *D. linearis* are sparse. Clones obtained by cuttings from surrounding wild individuals can be planted (Yang *et al.*, 2021). Difficulties may emerge when trying to conduct genetic selection, as sexual reproduction occurs *via* the germination of dispersed spores, which is difficult to control.

Wild individuals can colonize bare tailings, but as reported with wild species, *D. linearis* thrives in the understory of pines, and was observed in the field to grow in association with *Miscanthus* (Chen and Chen, 2020; Liu *et al.*, 2017). Fertilization with inorganic amendments could be considered, as wild individuals responded favorably to nutrient presence in the soil, especially N (Li *et al.*, 2013). Artificial irrigation can be avoided as the plant is highly resistant to drought.

Inoculation with micro-organisms (bioaugmentation) has provided promising results with Ni-HAs, increasing the Ni concentration in the plant, and increasing total biomass (Benizri *et al.*, 2021; Kidd *et al.*, 2018). Efforts are currently ongoing to identify and test the effects of plant growth-promoting-rhizobacteria (PGPR), or fungi (*e.g.*, arbuscular mycorrhizal fungi) to boost REE accumulation (Hu *et al.*, 2019; Jalali *et al.*, 2020; Jalali and Lebeau, 2021).

Their harvest can be conducted by cutting the oldest pinnae (fronds), known to contain the most REEs (Liu *et al.*, 2019). Standing litter, or dead pinnae still in place, is also a source of REEs and should not be disregarded (Liu, 2019, personal communication). The amount of total pinnae biomass measured was $636 \pm 144.g\ m^{-2}$ (n=3 patches, of 1 m² quadrats), which translates to 6 $t.ha^{-1}$ for patches growing directly on the tailing (Figure 54).

Figure 54: Patches used for biomass yield measurements. Photos: Wenshen Liu

Chen and Chen (2020), established that the optimal strategy was to clip (cut off the aerial parts) once every two years for wild individuals. This duration would be sufficient to let the patches almost fully replenish (vegetation cover of 92%). By doing so, **the annual yield for *D. linearis* pinnae biomass would be around 3 t.ha^{-1}.y^{-1}**

In contrast, *P. americana* seedlings can be grown in greenhouse and implanted individually. The literature suggests that it cannot be directly sown due to poor seedling vigor (Campbell and Adamson, 1986). As recalled in the first chapter, recent pot experiments have demonstrated that amending the tailing substrate is required to enable growth (Liu *et al.*, 2020). A low dosage of biochar (1% v/v) appears to be the best solution. *P. americana* thrives in moist soils, and a long drought must be avoided (Dumas, 2011; Schnitzler *et al.*, 2007). Hence, artificial irrigation should be considered.

The entire shoot can be harvested, even if the leaves are the only organ concentrated in REEs. The plant develops a rhizome which enables the plant to return after cutting. The species is considered invasive in Europe (Dumas, 2011; Schnitzler *et al.*, 2007), and even if the plant is common in South China, harvesting before fructification is the safest option.

Past field trials were conducted in the USA in order to produce phenolic compounds with *P. americana* (Campbell and Adamson, 1986). Interesting data were collected, especially regarding the expected biomass yield. In their experiment, plant density ranged from 1.2 to 3.6 plant.m^{-2}, and N-P-K fertilizer was applied extensively (112, 49 and 47 kg.ha^{-1}). In the best setting, plant density had no impact on dry matter biomass yield which was 6 t.ha^{-1} in the first year, and 13 t.ha^{-1} in the following year. The leaf mass fraction was measured at about 25% of the total biomass. **Hence the expectable yield of leaves would be about 3.25 t.ha^{-1}.** It should be noted that the study was conducted in Experiment, Georgia, where the climate is comparable to Jiangxi (humid subtropical). Even if pedologic conditions may differ between the two sites, the order of magnitude of the biomass yield can be approximated.

3.2 Physical and chemical characterization of the bio-ores

3.2.1 The fronds of *D. linearis*

The pinnae fraction (the leafy part of the fern "blades", or "fronds") of *D. linearis* is the only part of interest for metal recovery. It has been reported that REE concentration is ten times higher in the pinnae than in the rhizome (*i.e.*, the "stolon") (Shan *et al.*, 2003). As a consequence, the biomass samples used for process assays consisted solely of the pinnae fraction.

The pinnae themselves can be further refined, by removing the ligneous parts of the blade (*e.g.*, rachis and stipe) (Figure 55). This was done at the laboratory scale to test the absence of REE in the ligneous parts (Table 17). The bulk DL5AT was constituted of the ligneous parts of the fronds from bulk DL5A, the remaining formed the DL5AF. For the DL6A bulk, entire pinnae were ground at the pilot scale (on the GISFI experimental platform).

Figure 55: Representative samples of bulks DL5AT (left) and DL5AF (right)

The separation of the ligneous parts was relevant as REE concentrations were negligible for the DL5AT bulk. At the pilot scale, it might be useful to sieve the ground biomass to remove the ligneous parts, which does not contain REEs.

Oppositely, REE concentration values in DLA5F and DL6A bulks exceeded the hyperaccumulation threshold of 1 $mg.g^{-1}$ ∑REEs. The main elements accumulated were LREEs: La, Ce, Pr, and Nd. Because the study of the trace elements distribution was not the objective of this work, the analysis was not pushed further to determine the concentration of less abundant elements (*e.g.*, the HREEs, Sc). The reader is referred to previous work for REE distribution patterns.

The measured values are consistent with the team's previous batch of processed plants, in which concentrations ranged from 1.7 to 3.9 $mg.g^{-1}$ (Chour, 2018). Variations can be attributed to individual

variability, access to more or less available REE pools, and frond age, among other parameters (Liu *et al.*, 2019b).

Table 17: Elemental composition of the *D. linearis* dry biomass bulk used in this thesis. The "stems" bulk represents a mixture of the ligneous parts of the fern frond (*i.e.*, rachis and stipe). The limit of quantification (LQ) was 0.005 $mg.g^{-1}$ for REEs and 0.05 $mg.g^{-1}$ for Na.

Bulk name	DL5AT	DL5AF	DL6A	Liu *et al.* 2019b
Collection date	nov-17	nov-17	dec-18	
Type	"stems"	pinnae	pinnae	pinnae
REEs concentrations ($mg.g^{-1}$)				
∑REEs	0.14 ± 0.01	1.69 ± 0.08	2.31 ± 0.29	0.4 – 2.7
La	0.06 ± 0.01	0.73 ± 0.02	0.83 ± 0.11	
Ce	0.01 ± 0.00	0.28 ± 0.01	0.55 ± 0.07	
Pr	0.01 ± 0.00	0.15 ± 0.01	0.21 ± 0.03	
Nd	0.03 ± 0.00	0.33 ± 0.02	0.50 ± 0.06	
Sm	<LQ	0.05 ± 0.02	0.08 ± 0.01	
Gd	<LQ	0.04 ± 0.00	0.04 ± 0.01	
Dy	<LQ	0.03 ± 0.00	0.02 ± 0.00	
Y	<LQ	0.08 ± 0.00	0.06 ± 0.01	
Trace and common elements concentrations ($mg.g^{-1}$)				
Al	0.17 ± 0.01	3.59 ± 0.21	3.64 ± 0.45	1.9 – 5.9
Ca	0.19 ± 0.03	1.43 ± 0.12	1.41 ± 0.20	
Fe	0.03 ± 0.00	0.22 ± 0.04	0.17 ± 0.06	
K	1.24 ± 0.03	8.04 ± 0.60	4.44 ± 0.56	
Mg	0.08 ± 0.00	0.69 ± 0.03	0.74 ± 0.04	
Mn	0.11 ± 0.00	0.58 ± 0.01	0.91 ± 0.05	
Na	<LQ	<LQ	<LQ	
P	0.03 ± 0.00	0.32 ± 0.01	0.21 ± 0.02	
Pb	0.05 ± 0.01	0.15 ±0.01	0.07 ± 0.01	
S	0.16 ± 0.02	1.25 ± 0.08	1.78 ± 0.20	
Zn	0.03 ± 0.01	0.07 ± 0.01	0.04 ± 0.01	
Si	0.45 ± 0.06	8.58 ± 0.54	7.42 ± 0.72	1.2 – 12.0
Cl	0.11 ± 0.17	0.06 ± 0.11	0.62 ± 0.11	
Main elements concentration (%, dry weight)				
C	49.5 ± 0.2	48.0 ± 0.4	48.3 ± 0.5	
O	44.8 ± 0.6	40.1 ± 0.2	42.5 ± 0.8	
H	5.99 ± 0.04	5.78 ± 0.07	5.83 ± 0.03	
N	0.22 ± 0.05	0.96 ± 0.10	0.82 ± 0.05	

While the usual major elements (Ca, Mg, K) are found in plant tissues at typical concentrations, Al concentrations stand out with unusually high values: the hyperaccumulation threshold of 2.9 $mg_{Al}.g^{-1}$ defined for tropical plants is exceeded (Metali *et al.*, 2012). When considering its separation from REEs, Al can be a source of issues as it forms trivalent cation in solution (He *et al.*, 2016; Wang *et al.*, 2020).

Attention should also be paid to the Si concentration, almost negligible in the stems, but at relatively high concentration in the pinnae (up to 1 wt %). Issues can arise when extracting metals from Si-rich ores, especially when using acids as extractants. Silicone gel formation in the pulp, limiting the mass transfer, is a common issue for silicate minerals (Queneau and Berthold, 1986).

In fact, the very issue was faced and discussed in earlier works, with the direct extraction of REEs from ground *D. linearis* pinnae (Chour *et al.*, 2020). It was concluded that an acidic solution cannot flow freely enough through a packed bed of biomass: silica is readily extracted and forms a gel inhibiting mass transfer. To counteract this effect, biomass must be suspended in large volumes of solution.

Finally, the combustion of the bio-ore is considered. Hence, particular attention must be paid to certain elements. Energy recovery from biomass combustion is a key benefit of the process. The amount of energy that can be recovered can be estimated by correlations using the concentrations of C, H, O, N, and S (See Chapter 2, section 2.3.1). The higher heating values (HHV) estimated by Gumz and Boie correlations applied to the composition of the DL6A bulk are 19.1 and 19.6 $MJ.kg^{-1}$, respectively. Values obtained for the DL5A bulk are similar (19.2 and 19.7 $MJ.kg^{-1}$).

Regarding the lower heating value (LHV), equation (18) yields an average LHV of 19.3 $MJ.kg^{-1}$. This value, very close to the HHV highlights the low water content of the plant. The obtained values are 30 % higher than those of water hyacinth (HHV = 14.6 $MJ.kg^{-1}$), used for energy production (Munjeri *et al.*, 2016). Yet, they are 6 % inferior to Pinus wood pellets or wheat straws (HHV *ca.* 20.4 $MJ.kg^{-1}$) used for household heat production (ISO, 2017). Finally, they compete relatively well with European Ni hyperaccumulators (*O. chalcidica, L. emarginata, B. coddii*, HHV 16-17 $MJ.kg^{-1}$) (Hazotte *et al.*, 2020).

Other elements that require particular attention when considering biomass burning, are volatile elements that can generate atmospheric pollution. Acidic gases can be formed by the incomplete oxidation of N (generating NOx compounds), or the release of SOx, and HCl. The elemental measurements of Cl and S, each below 2 $mg.g^{-1}$, and N below 1.5 wt.%, indicate that the biomass could be a suitable biofuel according to the NF 444 QHP standard (NF label). However, they slightly exceed the values recommended by other authors for Cl and S (< 1 $mg.g^{-1}$) and N (<0.6 wt.%) (Obernberger *et al.*, 2006).

Other potential air contaminants that may be released during combustion are volatile metals (Cd, Zn, Pb). The detected levels of Zn (40 – 60 $mg.kg^{-1}$) are above the typical range for biofuels (10 – 25 $mg.kg^{-1}$), while the levels of Pb (50 – 150 $mg.kg^{-1}$) are several orders higher than in other biofuels (0.1 – 2 $mg.kg^{-1}$) (Obernberger *et al.*, 2006). Cadmium determination was not undertaken in this work, as detection levels are most likely too high with the present analytical methods. Attention should be payed to these elements, Pb especially, if a recovery process including a combustion step was to be upscaled. Measures to limit the emissions of these metals (fine particle collection, temperature control) must be put into practice.

3.2.2 Ash from *D. linearis* fronds

The ash produced at 550 °C was a light grey powder of low density (Figure 56) (apparent density of 0.05 $g.cm^{-3}$).The ash fraction (defined as the mass of ash produced divided by the mass of material burned) was 5.7 ± 0.6 % (n = 6, DL6A bulk). The apparent density of the uncompacted ash was 0.2 $g.cm^{-3}$. Hence, a small amount of ash occupies a large volume. If ash transportation from the production site to the refining site was considered, it could be of interest to compact the ash.

The particle size was determined in earlier works and the volume weighted mean diameter size was around 395 µm (Chour, 2018, unpublished). Because only a small proportion of fine particles are produced (d_{10} > 80 µm), respiratory hazards should be minimum when handling the ash.

Figure 56: Ash of *D. linearis* (bulk DL6A) in its ceramic crucible

After complete oxidation, the ash is a purely mineral material. The main elements encountered in its composition are given in Table 18. Ash composition reflects that of the biomass, as most of the analytes considered here are not volatile below 600 °C. The Si, Al, and K contents particularly stand out. Assuming that Si is in the SiO_2 form, it would represent 42 to 52% of the ash weight. In the view of recovering REEs by hydrometallurgical methods, Si could act as a problematic impurity throughout the process. Fouling of the reactor surface, or gel formation are common issues when processing silicate minerals, and more particularly amorphous silica (Queneau and Berthold, 1986).

As expected, the elements of interest were concentrated, with REEs representing up to 4 wt. % of the ash mass (metallic form). Using an average molar weight of 140.4 $g.mol^{-1}$, and a generic formula for the rare-earth oxide (REO) form: Ln_2O_3 (where Ln is a REE) they would represent 3.5 – 4.6 wt. % of the sample mass as REO, which is close to the Bayan Obo mine tailing content: *ca.* 5.4 wt % (Zhang *et al.*, 2014).

This content is higher than typical values found for coal fly ash (CFA): 0.03 – 0.4 wt. % (Hower *et al.*, 1999; Kolker *et al.*, 2017; Tang *et al.*, 2019), phosphogypsum: 0.1 – 0.4 wt. % (Rychkov *et al.*, 2018; Wang *et al.*, 2010), or bauxite residue: 0.1 – 0.3 wt. % (Davris *et al.*, 2016; Wagh and Pinnock, 1987), while those industrial process residues are considered for REE recovery (Binnemans *et al.*, 2015).

An attempt to determine the phases in presence was formerly conducted by powder XRD (Chour, 2018). The ash proved to be mainly amorphous, even if the presence of crystalline quartz (SiO_2) was detected. The precise nature and formation mechanism of this amorphous phase were not identified. Yet,

the abundance of Si is likely to yield amorphous glass, as has been observed for other Si-rich biomass ashes (*e.g.*, rice straws) (Thy *et al.*, 2006; Vassilev *et al.*, 2013). Despite their potential for energy production, the determination of the phases present in the ash of other ferns has not yet been published.

It appears that CFA has similar content of Al and Si that *D. linearis* ash (Al: 80 – 160 $mg.g^{-1}$,Si: 131 – 241 $mg.g^{-1}$) (Taggart *et al.*, 2016). In this case, several studies determined that REEs were excluded from the crystalline phases of the CFA and dispersed in the aluminosilicate vitreous phase (Kolker *et al.*, 2017; Stuckman *et al.*, 2018). As will be discussed later, it will be assumed that REEs are scattered in the amorphous phases of the fern ash in a similar fashion.

Table 18: Elemental composition of the *D. linearis* ash bulks used in this thesis. Values are mean ± standard deviation over n=3 digested samples (alkaline fluxing). n.d.: not determined.

Bulk name	DL_Ash_5A	DL_Ash_6A
Collection date	Nov-17	Dec-18
Type	Pinnae - Ash	Pinnae - Ash
REE concentrations ($mg.g^{-1}$)		
∑REEs	29.8 ± 0.2	38.4 ± 0.7
La	12.8 ± 0.1	13.3 ± 0.2
Ce	3.1 ± 0.01	8.8 ± 0.2
Pr	2.5 ± 0.01	3.6 ± 0.1
Nd	7.7 ± 0.01	8.6 ± 0.1
Sm	1.4 ± 0.01	1.6 ± 0.01
Gd	0.7 ± 0.01	0.6 ± 0.01
Dy	*n.d.*	0.3 ± 0.01
Y	1.1 ± 0.1	1.0 ± 0.1
Trace and major element concentrations ($mg.g^{-1}$)		
Al	58.5 ± 2.1	75.8 ± 8.5
Ca	22.4 ± 0.5	21.5 ± 1.1
Fe	3.3 ± 0.1	14.2 ± 0.5
K	*n.d.*	86.7 ± 1.6
Mg	11.5 ± 0.5	14.4 ± 0.1
Mn	11.4 ± 0.1	16.4 ± 0.2
Na	0.5 ± 0.1	0.5 ± 0.3
P	3.3 ± 0.1	4.1 ± 0.1
S	8.7 ± 0.2	8.0 ± 0.3
Si	185.5 ± 1.1	226.7 ± 1.0
Cl	*n.d.*	2.7 ± 0.1

3.2.3 The herbaceous plant *P. americana*

Trace and major elemental concentrations in the above-ground parts of *P. americana* were determined (Table 19). The elemental determination H, C, N, O, and Cl, was not conducted for bulks PA2 to PA4 for logistical reasons. The bulk PA1 was not dried properly and was subsequently subject to mold, so it

was not analyzed. The leaves were more easily ground than the fronds, and formed a fine powder (Figure 57).

Figure 57: Ground leaves of *P. americana* (bulk PA4) in the grinder.

The leaves always contained more REEs than the stems and fruits, as illustrated by the composition of the stem sample in Table 19, which is consistent with the literature (Yuan *et al*. 2017, 2018). Hence, only the concentration of foliar REEs is displayed for bulks PA2 to 4. Attempts to determine REE levels in the rhizome of the cultivated shoots were undertaken (PA_Pots_1 to 3), but concentrations were below the limit of detection (LD) of the method (0.005 $mg.kg^{-1}$ dry weight, for every element).

The REE levels reported in the leaves of *P. americana* are inferior to those of *D. linearis* by an order of magnitude. They are within the range of typical values reported for wild individuals collected in the same area: 0.2 – 1.1 $mg.g^{-1}$ (Yuan, 2018; Yuan *et al.*, 2018). The proportion of accumulated Y in regard to REEs was higher than for *D. linearis*, consistently with the observations of Yuan *et al.* (2017).

The hyperaccumulation threshold value of 1 $mg.g^{-1}$ ∑REEs was not reached in any of the available samples. Therefore, members of the REEcovery research project attempted to grow individuals with a higher leaf concentration. However, cultivation conditions were less favorable than for wild-type individuals, and REE foliar concentrations were lower in all samples (the reader is referred to Annex I for the elemental concentrations in the leaves of the cultivated shoots).

The following factors are thought to influence REE accumulation: the available concentration of REEs in the substrate, which depends on REE total concentration, their speciation, soil pH (Yuan, 2018; Yuan *et al.*, 2017, 2018; Liu *et al.*, 2020). Recently, it has been proposed that phosphorus deficiency could favor REE accumulation (Liu *et al.*, 2021).

With these aspects well-considered, it remains possible that the same growing conditions mimicking the natural growing area could be found, yielding individuals with REE foliar concentration superior to 1 $mg.g^{-1}$. With this perspective in mind, further characterization of the bio-ore was pursued.

Table 19: Elemental composition of *P. americana* dry biomass bulks used in this thesis. Values are mean ± standard deviation over n=3 digested samples. Elemental concentrations of elements with an asterisk are purely indicative, as they were comprised between LQ and LD. LD was 0.005 $mg.g^{-1}$ for REEs and 0.05 $mg.g^{-1}$ for Fe. n.d.: not determined.

Bulk name	PA0	PA0	PA2	PA3	PA4
Type	Wild- Stems	Wild- Leaves	Wild- Leaves	Wild- Leaves	Wild- Leaves
			REE concentrations ($mg.g^{-1}$)		
∑REEs	0.087 ± 0.006	0.191 ± 0.005	0.140 ± 0.010	0.278 ± 0.017	0.379 ± 0.017
La	0.023 ± 0.001	0.026 ± 0.001	0.019 ± 0.001	0.029 ± 0.002	0.022 ± 0.001
Ce*	0.017 ± 0.000	0.020 ± 0.000	0.018 ± 0.001	0.022 ± 0.003	0.008 ± 0.001
Pr*	0.009 ± 0.001	0.013 ± 0.001	0.009 ± 0.001	0.015 ± 0.001	0.012 ± 0.001
Nd*	0.018 ± 0.002	0.034 ± 0.001	0.019 ± 0.001	0.050 ± 0.003	0.043 ± 0.002
Sm*	<LD	0.013 ± 0.000	0.007 ± 0.000	0.016 ± 0.000	0.017 ± 0.001
Gd*	<LD	0.009 ± 0.000	0.008 ± 0.000	0.016 ± 0.000	0.024 ± 0.001
Dy*	*n.d.*	<LD	<LD	0.011 ± 0.000	0.024 ± 0.001
Y	0.011 ± 0.000	0.062 ± 0.001	0.038 ± 0.002	0.092 ± 0.006	0.171 ± 0.009
			Trace and major elements concentrations ($mg.g^{-1}$)		
Al	0.33 ± 0.02	1.16 ± 0.03	0.90 ± 0.10	1.14 ± 0.08	0.74 ± 0.04
Ca	2.00 ± 0.09	4.64 ± 0.05	20.59 ± 0.78	20.21 ± 1.04	12.40 ± 0.34
Fe	<LD	<LD	<LD	<LD	<LD
K	26.91 ± 0.98	21.18 ± 0.36	*n.d.*	*n.d.*	*n.d.*
Mg	1.16 ± 0.01	3.01 ± 0.02	9.15 ± 0.28	11.81 ± 0.60	14.19 ± 0.58
Mn	0.31 ± 0.01	1.05 ± 0.10	1.60 ± 0.10	1.35 ± 0.13	1.38 ± 0.04
Na	*n.d.*	*n.d.*	0.14 ± 0.02	0.15 ± 0.01	0.16 ± 0.02
P	1.56 ± 0.01	2.86 ± 0.04	2.28 ± 0.03	2.72 ± 0.04	3.73 ± 0.03
S	1.04 ± 0.02	3.41 ± 0.04	4.28 ± 0.05	3.65 ± 0.03	4.71 ± 0.06
Si	0.64 ± 0.07	0.78 ± 0.03	0.09 ± 0.01	0.12 ± 0.01	0.10 ± 0.01
Cl	0.07 ± 0.06	3.74 ± 0.31	*n.d.*	*n.d.*	*n.d.*

The elemental composition of *P. americana* leaves differs significantly from that of *D. linearis*: major elements contents (Ca, Mg, K) are superior, as well as S and Cl elements. This observation is consistent with the available literature regarding herbaceous species (Vassilev *et al.*, 2013).

Another element worth mentioning is P. The concentration in leaves (1.6 – 3.7 $mg.g^{-1}$) is tenfold higher than in fronds of *D. linearis* (0.2 – 0.3 $mg.g^{-1}$). As described in the first chapter, REEs have a high affinity for phosphate anions, forming insoluble precipitates. Their very high stability may hamper the recovery process, when it comes to extracting (*i.e.*, solubilizing) the REEs before purification. As an illustration, the hydrometallurgical process designed to recover REEs from those compounds (monazite, xenotime) involves an alkaline cracking step (concentrated NaOH, T > 160 °C) to convert them to hydroxides (Chapter 1, equation (2)), prior to the actual extraction (Habashi, 2013).

As a Mn hyperaccumulator, *P. americana* also accumulates more Mn (1.0 – 1.4 $mg.g^{-1}$) than *D. linearis* (0.6 – 0.9 $mg.g^{-1}$), although its maximum observed concentration of 32 $mg.g^{-1}$ was far from being attained (Pollard *et al.*, 2009). Another contrasting point was the lower Si content of *P. americana* leaves, not exceeding 0.8 $mg.g^{-1}$ (*vs*. more than 7 $mg.g^{-1}$ for *D. linearis* fronds) which has a practical

advantage. As it will be emphasized later, the presence of Si in hydrometallurgical processes tends to cause scaling, complicates filtration, and cause mass transfer issues due to gel formation (Queneau and Berthold, 1986).

The Al content was on average 72 % inferior to that of the fern. In a first approach, this inferior Al content appears to be an advantage when comparing the two plants, as in solution, Al^{3+} generally behaves in a similar fashion than REEs (also forming trivalent cations). Therefore, the separation of Al and REEs will be easier if there is overall less Al input to the process. However, on a second approach the amount of Al relative to the REE input should be considered. The average Al/REE molar ratio is *ca.* 21 for the perennial herb, and *ca.* 9 for the fern. Since REEs have been shown to be taken up by *P. americana* through the same physiological channels as Al (Yuan *et al.*, 2017), it is unlikely that the Al/REEs ratio will decrease if the plant accumulates more REEs.

Table 20: C, O, H, and N contents of the PA0 bulks.

Bulk name	PA0	PA0
Type	Wild-Stems	Wild-Leaves
Major elements concentration (%, dry weight)		
C	40.6 ± 0.5	44.1 ± 0.1
O	44.5 ± 0.1	38.2 ± 1.2
H	5.3 ± 0.1	5.7 ± 0.1
N	2.0 ± 0.2	3.7 ± 0.1

Finally, to improve the REE concentration of the bio-material, leaf combustion is considered (Table 20). In the same perspective as beforehand, the H, C, N, S, O, and Cl contents were determined. The potential for energy recovery from *P. americana* leaves can be quickly assessed in the same way as described previously. Gumz and Boie correlations yield a HHV of 15.6 and 16.2 $MJ.kg^{-1}$ for stems, respectively, as for the leaves: 18.1 and 18.6 $MJ.kg^{-1}$. These values are inferior to those for fern (approx. 19.5 $MJ.kg^{-1}$) regarding the stems, and slightly inferior for the leaves.

The S and Cl concentrations exceeded the threshold values of 2 $mg.g^{-1}$ of NF 444 (Marque NF), hence the need to take precautions to prevent acidic gaseous emissions (HCl, SOx). The nitrogen content is also superior to that of the fern, with the N content of 3.7 % exceeding the recommended value of 1.5 %. As for volatile metals (Cd, Zn, Pb), all concentrations fell below the detection limits of the analytical method (*ca.* 5 $mg.kg^{-1}$). It is therefore unlikely that they are of concern during the combustion step.

3.2.4 Ash from *P. americana* leaves

The ash from *P. americana* leaves produced at 550 and 900 °C differed visually (Figure 58). The ash yield at 550 °C was 16.2 ± 0.8 % (n=3) and 5 ± 1 % (n=3) at 900 °C. The first type of ash was a grey powder with an apparent bulk density of 0.2 $g.cm^{-3}$. Major and trace element determination was conducted after alkaline fluxing (Table 21).

At 550 °C, REEs are not volatile, and were concentrated by the operation, reaching up to 1.63 $mg.g^{-1}$ total REEs (0.19 $mg.g^{-1}$ previously). This content is similar to that of phosphogypsum for example (0.1 – 0.2 %). As for the other elements, K concentration particularly stood out, constituting more than 30 % of the sample mass. This observation was consistent with the XRD observation which revealed that

fairchildite ($K_2Ca(CO_3)_2$) was the main crystalline phases (See Annex 2). This phase is typical of biomass ash from herbaceous biomass (Vassilev *et al.*, 2013).

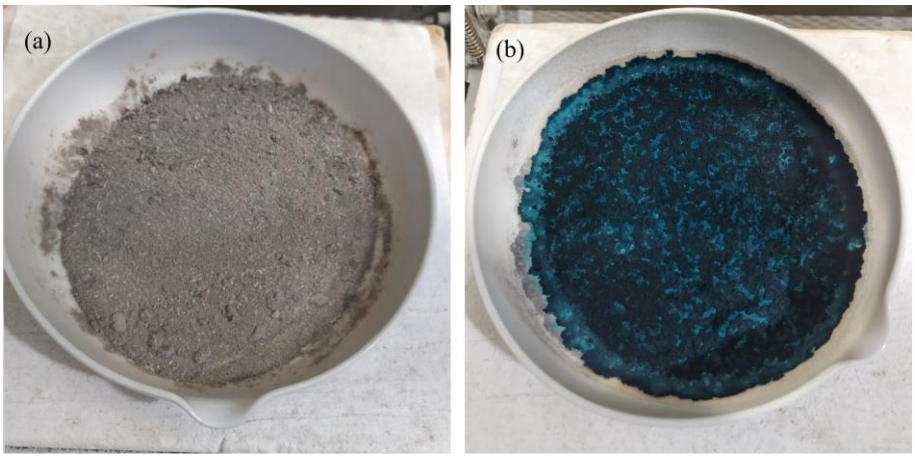

Figure 58: *P. americana* leaf ash produced at 550 °C (a) and 900 °C (b) in ceramic crucibles

One could note that Ce was not detected within the analytical range, while it was detected in the leaves. The sample preparation method accounts for that apparent anomaly, as the sample must be enough diluted so that the flux concentration ($LiBO_2$) does not exceed 1 $g.L^{-1}$ prior to ICP. This results in higher detection limits for samples processed by the alkaline fluxing method.

The ash produced at 900 °C was hard, agglomerated, and strongly adhered to the ceramic plate (Figure 58). It was not possible to recover enough material for major and trace element determination (via alkaline fluxing and ICP OES).

It was assumed that potassium salts were the main constituents of the material, and it was decided to wash the ash with deionized water to dissolve these salts. The ash indeed reacted, generating a deep blue and strongly alkaline solution (pH >12) (Figure 59). The washed ash was now a light-brown solid. The solution turned green after a few minutes, then purple. During the last color change, a brown precipitate appeared.

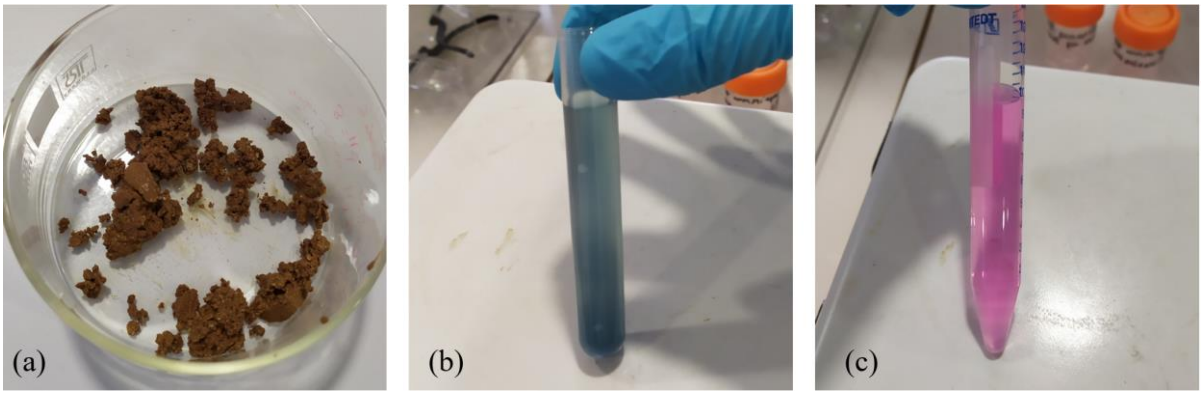

Figure 59: (a) *P. americana* leaf ash (900 °C) washed with deionized water. (b) Wash water immediately after washing, and (c) several minutes later (filtered).

Table 21: Elemental composition of the *P. americana* ash bulks used in this thesis. Values are the mean ± standard deviation over n=3 digested samples (alkaline fluxing). DL was 0.05 $mg.g^{-1}$ for REEs and 0.5 $g.^{-1}$ for Na. n.d.: not determined.

Bulk name	PA0	PA0
Collection date	Nov-17	Nov-17
Type	Leaves – Ash 550 °C	Leaves – Ash (900 °C), washed
REE concentrations ($mg.g^{-1}$)		
∑REEs	1.63 ± 0.52	3.82 ± 0.25
La	0.21 ± 0.06	0.46 ± 0.01
Ce	<DL	0.17 ± 0.05
Pr	0.12 ± 0.03	0.30 ± 0.03
Nd	0.61 ± 0.16	0.84 ± 0.05
Sm	0.09 ± 0.02	0.42 ± 0.03
Gd	0.07 ± 0.02	0.17 ± 0.03
Dy	<DL	0.12 ± 0.00
Y	0.47 ± 0.12	1.07 ± 0.01
Trace and major element concentrations ($mg.g^{-1}$)		
Al	9.7 ± 2.54	49.58 ± 0.6
Ca	29.4 ± 7.54	82.91 ± 0.7
Fe	2.2 ± 0.64	6.0 ± 0.1
K	328 ± 27	158.2 ± 1.0
Mg	21.1 ± 5.2	54.3 ± 0.7
Mn	7.9 ± 1.9	7.5 ± 0.2
Na	<DL	<DL
P	18.1 ± 4.4	16.9 ± 0.3
S	7.5 ± 6.0	1.4 ± 1.8
Si	15.4 ± 5.2	124.2 ± 1.0
Cl	*n.d.*	*n.d.*

Those reactions are beyond the scope of this work (REEs probably played no role in them given their low concentration), and they were not thoroughly investigated. However, one can assume that the high K and Mn contents of the ash are at the heart of them. Indeed, Mn can form highly oxidized compounds when heated in the presence of alkali. Deep blue, green and violet complexes can be attributed to respectively Mn (V), Mn (VI) and Mn (VII). Lastly, the precipitation of a light brown solid is likely to be MnO_2. Indeed, manganate (Mn (VI): MnO_4^{2-}) is known to disproportionate to permanganate (Mn (VII): MnO_4^-) and manganese (IV) oxide (Equation (24)).

$$3MnO_4^{2-} + 2H_2O \rightarrow 2MnO_4^- + MnO_{2(s)} + 4HO^- \quad (24)$$

This reaction was previously reported and used as a proxy for the determination of Mn content in Mn-hyperaccumulator leaves (*Musanga cecropiodes, Musa paradisiaca*) by colorimetric titration (Offem and Edet, 1989).

After washing, the remaining solid contained REEs at the appreciable concentration of 3.8 $mg.g^{-1}$ ∑REEs as well as significant amounts of Si, K and other alkalis (Ca, Mg).

3.3 Combined characteristics: perspectives for a sustainable process

3.3.1 Expectable yield per hectare per year

At the beginning of the chapter, it was established that the biomass yield for *D. linearis* fronds, and *P. americana* leaves would be respectively 3.00 and 3.25 $t.ha^{-1}.y^{-1}$. The second part of the chapter confirmed that only fronds and leaves are concentrated enough in REEs for a recovery process. The typical REE content was estimated, detailed by each element. The most notable REEs for *D. linearis* are La, Ce, Nd, and Pr, and a total concentration of 2.0 ± 0.4 $mg.g^{-1}$ (∑REEs) while for *P. americana* these are Y, Nd, and La and a total concentration of 0.25 ± 0.10 $mg.g^{-1}$(∑REEs).

Natural variation among individuals, sample location and access to variable REE available pools, plant age, are determining factors among others for REE concentration in the bio-ore. Hence, aforementioned values will constitute the reference scenario to calculate the metal yield.

A more optimistic scenario will be developed based on the maximum observed concentration: 3.89 $mg.g^{-1}$ for *D. linearis* fronds (Chour *et al.*, 2020) and 1.04 $mg.g^{-1}$ for *P. americana* leaves (Yuan *et al.*, 2018). In this scenario, it will be assumed that optimized cultivation conditions permit maximal hyperaccumulation, to levels observed in the nature. For simplicity, the repartition of REEs is the same independently of the scenario. The detailed metal yield for each element and total REEs is shown in Table 22.

In the best, optimistic scenario with *D. linearis*, the total metal yield would be around **12 $kg_{REEs}.ha^{-1}.y^{-1}$**. The same order of magnitude was obtained in 2005 with Ni HAs (25 kg_{Ni} $ha^{-1}.y^{-1}$), before optimizing the cultivating conditions (NPK fertilization, weed management, plant density) (Bani *et al.*, 2007). Thanks to best agronomic practices the metal yield now reaches 112 kg_{Ni} $ha^{-1}.y^{-1}$, which suggest that proper field management could further improve the amount of extracted REEs (Bani *et al.*, 2015b).

With regard to *P. americana*, in the best case, the metal yield is **3.4 $kg_{REEs}.ha^{-1}.y^{-1}$** which remains 50 % inferior to the reference one for *D. linearis*. Even if the biomass yield is higher for *P. americana*, the total REE concentration is not high enough to compensate.

The first chapter highlighted the difference of prices between each REE. For example, several orders of magnitude separate the selling price of Dy_2O_3 (295 $USD.kg^{-1}$) and Y_2O_3 (3.3 $USD.kg^{-1}$) (prices retrieved from the Institut Seltene Erden website (http://www.institut-seltene-erden.de/) as of 18 December 2020). The economic contribution of each element is thus different and must not be neglected.

The oxide prices as of December 2020 (tabulated in the first chapter), and previously established metal yield (converted to oxide yield) are used to compute the maximum potential income (Table 23). Oxide purity, market fluctuations, and sales agreement condition (shipping, location of the sold material) have

varying impacts on the product price. Prices were taken for the same month, with the same terms of sale ("Ex Works", rather than "Free-On-Board"), and purity was chosen to be as close to 99.5% as possible.

Table 22: Expectable metal yield for the reference and the optimistic scenario for the two considered HA species.

	P. americana	*P. americana*	*D. linearis*	*D. linearis*
Scenario	reference	optimistic	reference	optimistic
	Metal yield ($kg.ha^{-1}.y^{-1}$)			
La	0.08	0.33	2.34	4.55
Ce	0.05	0.23	1.25	2.42
Pr	0.04	0.17	0.54	1.05
Nd	0.12	0.50	1.25	2.42
Sm	0.04	0.18	0.20	0.38
Gd	0.05	0.20	0.12	0.23
Dy	0.04	0.17	0.08	0.15
Y	0.30	1.25	0.21	0.41
∑REEs	0.80	3.38	6.00	11.67

Table 23: Maximum potential income computed for the different scenarios.

	P. americana	*P. americana*	*D. linearis*	*D. linearis*
Scenario	reference	optimistic	reference	optimistic
	Maximal potential income ($USD.ha^{-1}.y^{-1}$)			
La	0.3	1.4	9.8	19.0
Ce	0.5	2.3	12.3	24.0
Pr	2.4	9.9	32.4	62.9
Nd	10.9	45.7	113.1	220.0
Sm	0.1	0.4	0.4	0.8
Gd	1.5	6.3	3.9	7.5
Dy	14.0	59.1	25.6	49.7
Y	1.1	4.7	0.8	1.6
∑REEs	30.8	129.9	198.2	385.6

For *D. linearis*, the highest contribution was from Nd, followed by Pr and Dy, with Nd accounting for 57% of the potential income. The three elements constituted more than 85% of the total value. For *P. americana*, the first element was Dy followed closely by Nd. Altogether, the best scenario was again the *D. linearis* optimist scenario with potential income of 385.6 $USD.ha^{-1}.y^{-1}$.

To put things in perspective, the maximum potential income using Ni HAs can be estimated in a similar fashion. The metal yield of 25 $kg_{Ni}\ ha^{-1}.y^{-1}$ (value in 2005) would be converted to an oxide yield of 32 $kg_{NiO}.ha^{-1}.y^{-1}$. With the oxide price of 22 $USD.kg^{-1}$ (NiO, 99,5 %, as of October 2021), the potential income would be *ca.* 704 $USD.ha^{-1}.y^{-1}$. Of course, this value has to be multiplied by 4 when considering the current metal yield of the field (*ca.* 105 $kg_{Ni}\ ha^{-1}.y^{-1}$) (Bani *et al.*, 2015a).

3.3.2 Expectable process based on the bio-ore characteristics

The two plants differ in terms of composition, and the design of a recovery process should be adapted to consider the specific features of each material (plant species, plant or ash, ash combustion temperature).

For example, the REE concentration in fern fronds (up to 3.8 $mg.g^{-1}$) is high enough to contemplate a direct extraction procedure. This procedure was covered in details earlier by the team (Chour, 2018; Chour *et al.*, 2020).

An enrichment step through combustion can also be useful to take advantage of the fairly high HHV of the fronds for energy recovery purposes, and concentrate the elements of interest. The presence of Pb requires the ash to be produced at the lowest possible temperature to limit atmospheric releases. The main challenge resides in the great stability of the ash owing to Si rich amorphous phases. This challenge will be addressed in details in the next chapter.

For *P. americana*, the REE content is too low (in our case, averaging 0.25 $mg.g^{-1}$) for a direct extraction and REEs are likely to be drowned in impurities (Al, P, Mn). In particular, the co-extracted P could instantly precipitate REEs and render them unavailable for solubilization.

In contrast, the reactivity of the ash formed at 900 °C might be of use. By leaching the ash with water, a Mn-rich and highly alkaline solution was produced. The possibility to easily recover a manganese compound can only enhance the process viability. Owing to its high K content, the alkalinity of the solution can also be of great use, for example in converting REEs from their phosphate form to their hydroxide form.

3.4 Summary

This chapter has exposed how different the two species considered for RE agromining are, as well as their derived bio-ores. Their main features have been detailed earlier in this chapter and are summarized here (Table 24).

From the previous analysis, it appears that some potential arises from *P. americana* agromining, with an easy Mn recovery process. Additionally, its Dy content, at current market prices, makes it an appealing hyperaccumulator. However, in comparison with *D. linearis*, the lower REE content in its leaves, does not make up for its slightly higher biomass yield. Calculations using the average concentration of REEs estimate the potential annual income to 30 $USD.ha^{-1}.y^{-1}$, which is unambiguously too low to develop hydrometallurgical recovery processes.

Optimization of the cultivation conditions is necessary to consider the plant as an alternative source of REEs. In regards to current knowledge, substrate elaboration (through optimal amendment nature and dosage) and genetic selection appear as the main perspectives for higher accumulation (Liu *et al.*, 2020).

Contrastingly, greater REE concentration favors the fern for the design of a recovery process. The magnitude of the biomass yield is also sufficient to foresee potential income through the yield of Nd and Pr. Issues regarding its cultivation (not domesticated), should not be overlooked. In exchange, they are compensated by high adaptability, hardiness, and growth speed of the fern. Costs related to plant collection are also diminished by less frequent harvestings.

For these reasons, the recovery process detailed in this work will now focus on *D. linearis*.

Table 24: Summary of the bio-ore characteristics in terms of production, composition, reactivity and agromining potential.

		D. linearis	***P. americana***
Biomass production	Cultivation	– Wild – Autonomous	– Domestic – Optimization mandatory – Irrigation
	Harvest	Every 2 years	Twice a year
	Biomass yield	3.00 $t.ha^{-1}.y^{-1}$	3.25 $t.ha^{-1}.y^{-1}$
Agromining key numbers	[REE]	2.0 $mg.g^{-1}$ Up to 3.9 $mg.g^{-1}$	0.25 $mg.g^{-1}$ Up to 1.0 $mg.g^{-1}$
	Metal yield	6.0 $kg_{REE}.ha.y^{-1}$ Up to 11.7 $kg_{REE}.ha.y^{-1}$	0.8 $kg_{REE}.ha.y^{-1}$ Up to 3.4 $kg_{REE}.ha.y^{-1}$
	Potential Income	200 $USD.ha.y^{-1}$ Up to 385 $USD.ha.y^{-1}$	30 $USD.ha.y^{-1}$ Up to 130 $USD.ha.y^{-1}$
Process perspectives	Target elements	Nd, Pr	Nd, Dy
	Combustion & heat recovery	– Low Cl, N, S – High Pb – HHV *ca.* 19.3 $MJ.kg^{-1}$	– High Cl, N, S – Low Pb – HHV *ca.* 18.3 $MJ.kg^{-1}$
	Ash characteristics	Stable	Stable (550 °C) or fused and reactive (900 °C)
	Subproducts considered	Al	Mn

Before assessing the agromining viability using D. linearis *fronds or ash, recovery processes must be explored and designed. Plenty of experimental data has been collected previously regarding the direct extraction of REEs with mineral acids or organic extractants using the fronds (Chour, 2018; Chour et al., 2020, 2018). The ash processing pathway offers different benefits and drawbacks, but data is still lacking on the chemical mechanisms at play.*

Clarification of these mechanisms, and improvements regarding energy and reagent consumption are required to minimize the economic and environmental cost of the process, are the main objectives of the next chapter. The second aim of the following chapter is to propose the best possible recovery process using the ash of D. linearis *fronds, and obtain a dataset for the economic and environmental evaluation in the final chapter of this manuscript.*

3.5 References

Bani, A., Echevarria, G., Sulçe, S., Morel, J.L., 2015a. Improving the Agronomy of *Alyssum murale* for Extensive Phytomining: A Five-Year Field Study. Int. J. Phytoremediation 17, 117–127. https://doi.org/10.1080/15226514.2013.862204

Bani, A., Echevarria, G., Sulçe, S., Morel, J.L., Mullai, A., 2007. In-situ phytoextraction of Ni by a native population of *Alyssum murale* on an ultramafic site (Albania). Plant Soil 293, 79–89. https://doi.org/10.1007/s11104-007-9245-1

Bani, A., Echevarria, G., Zhang, X., Benizri, E., Laubie, B., Morel, J.L., Simonnot, M.-O., 2015b. The effect of plant density in nickel-phytomining field experiments with *Alyssum murale* in Albania. Aust. J. Bot. 63, 72–77. https://doi.org/10.1071/BT14285

Benizri, E., Lopez, S., Durand, A., Kidd, P.S., 2021. Diversity and Role of Endophytic and Rhizosphere Microbes Associated with Hyperaccumulator Plants During Metal Accumulation, in: van der Ent, A., Baker, A.J.M., Echevarria, G., Simonnot, M.-O., Morel, J.L. (Eds.), Agromining: Farming for Metals. Springer International Publishing, Cham, pp. 239–279. https://doi.org/10.1007/978-3-030-58904-2_12

Binnemans, K., Jones, P.T., Blanpain, B., Van Gerven, T., Pontikes, Y., 2015. Towards zero-waste valorisation of rare-earth-containing industrial process residues: a critical review. J. Clean. Prod. 99, 17–38. https://doi.org/10.1016/j.jclepro.2015.02.089

Campbell, T.A., Adamson, W.C., 1986. Effect of population density on agronomic performance and chemical yields in pokeweed, *Phytolacca americana*. Biomass 9, 113–123. https://doi.org/10.1016/0144-4565(86)90115-0

Chen, Z.Q., Chen, Z.B., 2020. Clipping strategy to assist phytoremediation by hyperaccumulator *Dicranopteris dichotoma* at rare earth mines. Int. J. Phytoremediation 1–10. https://doi.org/10.1080/15226514.2020.1725870

Chour, Z., 2018. Valorisation de terres rares à partir de plantes hyperaccumulatrices (PhD dissertation). Université de Lorraine, Nancy, France.

Chour, Z., Laubie, B., Morel, J.L., Tang, Y., Qiu, R., Simonnot, M.-O., Muhr, L., 2018. Recovery of rare earth elements from *Dicranopteris dichotoma* by an enhanced ion exchange leaching process. Chem. Eng. Process. - Process Intensif. 130, 208–213. https://doi.org/10.1016/j.cep.2018.06.007

Chour, Z., Laubie, B., Morel, J.L., Tang, Y.T., Simonnot, M.O., Muhr, L., 2020. Basis for a new process for producing REE oxides from *Dicranopteris linearis*. J. Environ. Chem. Eng. 103961. https://doi.org/10.1016/j.jece.2020.103961

Davris, P., Balomenos, E., Panias, D., Paspaliaris, I., 2016. Selective leaching of rare earth elements from bauxite residue (red mud), using a functionalized hydrophobic ionic liquid. Hydrometallurgy 164, 125–135. https://doi.org/10.1016/j.hydromet.2016.06.012

Dumas, Y., 2011. Que savons-nous du Raisin d'Amérique (Phytolacca americana), espèce exotique envahissante ? Synthèse bibliographique. Rendez-Vous Tech. ONF 48–57.

Habashi, F., 2013. Extractive metallurgy of rare earths. Can. Metall. Q. 52, 224–233. https://doi.org/10.1179/1879139513Y.0000000081

Hazotte, C., Laubie, B., Pacault, S., Dufaud, O., Simonnot, M.-O., 2020. Evaluation of the performance of nickel hyperaccumulator plants as combustion fuel. Biomass Bioenergy 140, 105671. https://doi.org/10.1016/j.biombioe.2020.105671

He, Z., Zhang, Z., Yu, J., Xu, Z., Chi, R., 2016. Process optimization of rare earth and aluminum leaching from weathered crust elution-deposited rare earth ore with compound ammonium salts. J. Rare Earths 34, 413–419. https://doi.org/10.1016/S1002-0721(16)60042-X

Hower, J.C., Ruppert, L.F., Eble, C.F., 1999. Lanthanide, yttrium, and zirconium anomalies in the Fire Clay coal bed, Eastern Kentucky. Int. J. Coal Geol. 39, 141–153. https://doi.org/10.1016/S0166-5162(98)00043-3

Hu, R., De Junet, A., Béguiristain, T., Leyval, C., 2019. Transfer mechanism of rare earth elements (REEs) from soil to plants by arbuscular mycorrhizal (AM) fungi. Presented at the Labex21 Annual Workshop, Nancy, France, pp. 42–43.

Huot, H., Guo, M.N., Liu, C., Liu, W., Yuan, M., Chen, Y.Y., Zhu, S.C., Wang, Y., Wu, Y.L., Ye, P.X., Chen, J.Q., Séré, G., Watteau, F., Chao, Y.Q., Auclerc, A., Morel, J.L., Tang, Y.T., Qiu, R.L., 2018. Reclamation of ionic rare earth elements (REEs) mine tailings in Southern China, in: 11th Sino-French Workshop - Innovations for the Circular Economy by Recycling Secondary Resources. Presented at the 11th Sino-French Workshop - Innovations for the circular Economy by Recycling Secondary Resources, Sun Yat-sen University, Guangzhou.

ISO, 2017. ISO 18125:2017 - Solid biofuels — Determination of calorific value.

Jalali, J., Gaudin, P., Capiaux, H., Ammar, E., Lebeau, T., 2020. Isolation and screening of indigenous bacteria from phosphogypsum-contaminated soils for their potential in promoting plant growth and trace elements mobilization. J. Environ. Manage. 260, 110063. https://doi.org/10.1016/j.jenvman.2020.110063

Jalali, J., Lebeau, T., 2021. The Role of Microorganisms in Mobilization and Phytoextraction of Rare Earth Elements: A Review. Front. Environ. Sci. 0. https://doi.org/10.3389/fenvs.2021.688430

Kidd, P.S., Bani, A., Benizri, E., Gonnelli, C., Hazotte, C., Kisser, J., Konstantinou, M., Kuppens, T., Kyrkas, D., Laubie, B., Malina, R., Morel, J.-L., Olcay, H., Pardo, T., Pons, M.-N., Prieto-Fernández, Á., Puschenreiter, M., Quintela-Sabarís, C., Ridard, C., Rodríguez-Garrido, B., Rosenkranz, T., Rozpądek, P., Saad, R., Selvi, F., Simonnot, M.-O., Tognacchini, A., Turnau, K., Ważny, R., Witters, N., Echevarria, G., 2018. Developing Sustainable Agromining Systems in Agricultural Ultramafic Soils for Nickel Recovery. Front. Environ. Sci. 6, 44. https://doi.org/10.3389/fenvs.2018.00044

Kolker, A., Scott, C., Hower, J.C., Vazquez, J.A., Lopano, C.L., Dai, S., 2017. Distribution of rare earth elements in coal combustion fly ash, determined by SHRIMP-RG ion microprobe. Int. J. Coal Geol. 184, 1–10. https://doi.org/10.1016/j.coal.2017.10.002

Li, X.F., Chen, Z.B., Zheng, L.D., Zhang, X.Y., Li, R.L., 2013. Responses of *Dicranopteris dichotoma* growth to environmental factors in eroded red-soil region of Southern China. Bull. Soil Water Conserv. 33, 33–37. https://doi.org/10.13961/j.cnki.stbctb.2013.03.038

Liu, C., Liu, W.-S., van der Ent, A., Morel, J.L., Zheng, H.-X., Wang, G.-B., Tang, Y.-T., Qiu, R.-L., 2021. Simultaneous hyperaccumulation of rare earth elements, manganese and aluminum in *Phytolacca americana* in response to soil properties. Chemosphere 282, 131096. https://doi.org/10.1016/j.chemosphere.2021.131096

Liu, L., Wang, X.D., Wen, Q., Jia, Q.Q., Liu, Q.J., 2017. Interspecific associations of plant populations in rare earth mining wasteland in southern China. Int. Biodeterior. Biodegrad. 118, 82–88. https://doi.org/10.1016/j.ibiod.2017.01.011

Liu, W., Chen, Y., Huot, H., Liu, C., Guo, M., Qiu, R., Morel, J.L., Tang, Y., 2020. Phytoextraction of rare earth elements from ion-adsorption mine tailings by *Phytolacca americana*: Effects of organic material and biochar amendment. J. Clean. Prod. 275, 122959. https://doi.org/10.1016/j.jclepro.2020.122959

Liu, W., Guo, M., Liu, C., Yuan, M., Chen, X., Huot, H., Zhao, C., Tang, Y., Morel, J.L., Qiu, R., 2019a. Water, sediment and agricultural soil contamination from an ion-adsorption rare earth mining area. Chemosphere 216, 75–83. https://doi.org/10.1016/j.chemosphere.2018.10.109

Liu, W., Zheng, H., Guo, M.N., Liu, C., Huot, H., Morel, J.L., van der Ent, A., Tang, Y., Qiu, R., 2019b. Co-deposition of silicon with rare earth elements (REEs) and aluminium in the fern *Dicranopteris linearis* from China. Plant Soil 1–11. https://doi.org/10.1007/s11104-019-04005-0

Marque NF, AFNOR, Marque NF 444 "Biocombustibles solides" , https://marque-nf.com/categories/genie-climatique/nf-biocombustibles-solides-nf444/ (accessed 8.24.21)

Metali, F., Salim, K.A., Burslem, D.F.R.P., 2012. Evidence of foliar aluminium accumulation in local, regional and global datasets of wild plants. New Phytol. 193, 637–649. https://doi.org/10.1111/j.1469-8137.2011.03965.x

Munjeri, K., Ziuku, S., Maganga, H., Siachingoma, B., Ndlovu, S., 2016. On the potential of water hyacinth as a biomass briquette for heating applications. Int. J. Energy Environ. Eng. 7, 37–43. https://doi.org/10.1007/s40095-015-0195-8

Nkrumah, P.N., Chaney, R.L., Morel, J.L., 2021. Agronomy of 'Metal Crops' Used in Agromining, in: van der Ent, A., Baker, A.J.M., Echevarria, G., Simonnot, M.-O., Morel, J.L. (Eds.),

Agromining: Farming for Metals. Springer International Publishing, Cham, pp. 23–46. https://doi.org/10.1007/978-3-030-58904-2_2

Nkrumah, P.N., Tisserand, R., Chaney, R.L., Baker, A.J.M., Morel, J.L., Goudon, R., Erskine, P.D., Echevarria, G., van der Ent, A., 2019. The first tropical 'metal farm': Some perspectives from field and pot experiments. J. Geochem. Explor. 198, 114–122. https://doi.org/10.1016/j.gexplo.2018.12.003

Obernberger, I., Brunner, T., Bärnthaler, G., 2006. Chemical properties of solid biofuels—significance and impact. Biomass Bioenergy, Standarisation of Solid Biofuels in Europe 30, 973–982. https://doi.org/10.1016/j.biombioe.2006.06.011

Offem, J.O., Edet, O.S.O., 1989. Spectrophotometric determination of manganese based on thermally produced manganese (VI) compounds in plant ash. J. Agric. Sci. 112, 427–431. https://doi.org/10.1017/S0021859600085890

Pollard, J., Stewart, H., Roberson, C., 2009. Manganese Hyperaccumulation in *Phytolacca americana* L. from the Southeastern United States. Northeast. Nat., Proceedings of the Sixth International Conference on Serpentine Ecology 16, 155–162.

Pons, M.-N., Rodrigues, J., Simonnot, M.-O., 2021. Life Cycle Assessment and Ecosystem Services of Agromining, in: van der Ent, A., Baker, A.J.M., Echevarria, G., Simonnot, M.-O., Morel, J.L. (Eds.), Agromining: Farming for Metals. Springer International Publishing, Cham, pp. 75–98. https://doi.org/10.1007/978-3-030-58904-2_5

Queneau, P.B., Berthold, C.E., 1986. Silica in Hydrometallurgy: An Overview. Can. Metall. Q. 25, 201–209. https://doi.org/10.1179/cmq.1986.25.3.201

Rodrigues, J., Houzelot, V., Ferrari, F., Echevarria, G., Laubie, B., Morel, J.-L., Simonnot, M.-O., Pons, M.-N., 2016. Life cycle assessment of agromining chain highlights role of erosion control and bioenergy. J. Clean. Prod. 139, 770–778. https://doi.org/10.1016/j.jclepro.2016.08.110

Russell, A.E., Raich, J.W., Vitousek, P.M., 1998. The ecology of the climbing fern *Dicranopteris linearis* on windward Mauna Loa, Hawaii. J. Ecol. 86, 765–779. https://doi.org/10.1046/j.1365-2745.1998.8650765.x

Rychkov, V.N., Kirillov, E.V., Kirillov, S.V., Semenishchev, V.S., Bunkov, G.M., Botalov, M.S., Smyshlyaev, D.V., Malyshev, A.S., 2018. Recovery of rare earth elements from phosphogypsum. J. Clean. Prod. 196, 674–681. https://doi.org/10.1016/j.jclepro.2018.06.114

Schnitzler, A., Hale, B.W., Alsum, E.M., 2007. Examining native and exotic species diversity in European riparian forests. Biol. Conserv. 138, 146–156. https://doi.org/10.1016/j.biocon.2007.04.010

Shan, X., Wang, H., Zhang, S., Zhou, H., Zheng, Y., Yu, H., Wen, B., 2003. Accumulation and uptake of light rare earth elements in a hyperaccumulator *Dicropteris dichotoma*. Plant Sci. 165, 1343–1353. https://doi.org/10.1016/S0168-9452(03)00361-3

Stuckman, M.Y., Lopano, C.L., Granite, E.J., 2018. Distribution and speciation of rare earth elements in coal combustion by-products via synchrotron microscopy and spectroscopy. Int. J. Coal Geol. 195, 125–138. https://doi.org/10.1016/j.coal.2018.06.001

Taggart, R.K., Hower, J.C., Dwyer, G.S., Hsu-Kim, H., 2016. Trends in the Rare Earth Element Content of U.S.-Based Coal Combustion Fly Ashes. Environ. Sci. Technol. 50, 5919–5926. https://doi.org/10.1021/acs.est.6b00085

Tang, M. cheng, Zhou, C.C., Pan, J.H., Zhang, N.N., Liu, C., Cao, S.S., Hu, T.T., Ji, W.S., 2019. Study on extraction of rare earth elements from coal fly ash through alkali fusion – Acid leaching. Miner. Eng. 136, 36–42. https://doi.org/10.1016/j.mineng.2019.01.027

Thy, P., Jenkins, B.M., Lesher, C.E., Grundvig, S., 2006. Compositional constraints on slag formation and potassium volatilization from rice straw blended wood fuel. Fuel Process. Technol. 87, 383–408. https://doi.org/10.1016/j.fuproc.2005.08.015

Vassilev, S.V., Baxter, D., Andersen, L.K., Vassileva, C.G., 2013. An overview of the composition and application of biomass ash. Part 1. Phase–mineral and chemical composition and classification. Fuel 105, 40–76. https://doi.org/10.1016/j.fuel.2012.09.041

Wagh, A.S., Pinnock, W.R., 1987. Occurrence of scandium and rare earth elements in Jamaican bauxite waste. Econ. Geol. 82, 757–761. https://doi.org/10.2113/gsecongeo.82.3.757

Wang, L., Long, Z., Huang, X., Yu, Y., Cui, D., Zhang, G., 2010. Recovery of rare earths from wet-process phosphoric acid. Hydrometallurgy 101, 41–47. https://doi.org/10.1016/j.hydromet.2009.11.017

Wang, Y.D., Li, J.H., Gao, Yan, Yang, Y., Gao, Yang, Xu, Z.F., 2020. Removal of aluminum from rare-earth leaching solutions via a complexation-precipitation process. Hydrometallurgy 191, 105220. https://doi.org/10.1016/j.hydromet.2019.105220

Yang, L., Huang, Y., Lima, L.V., Sun, Z., Liu, M., Wang, J., Liu, N., Ren, H., 2021. Rethinking the Ecosystem Functions of Dicranopteris, a Widespread Genus of Ferns. Front. Plant Sci. 11, 581513. https://doi.org/10.3389/fpls.2020.581513

Yuan, M., 2018. Mechanism of rare earth elements (REEs) uptake, translocation and fractionation in *Phytolacca americana* (PhD dissertation). Sun Yatsen University, Guangzhou, China.

Yuan, M., Guo, M.-N., Liu, W.-S., Liu, C., van der Ent, A., Morel, J.L., Huot, H., Zhao, W.-Y., Wei, X.-G., Qiu, R.-L., Tang, Y.-T., 2017. The accumulation and fractionation of Rare Earth Elements in hydroponically grown *Phytolacca americana* L. Plant Soil 421, 67–82. https://doi.org/10.1007/s11104-017-3426-3

Yuan, M., Liu, C., Liu, W.-S., Guo, M.-N., Morel, J.L., Huot, H., Yu, H.-J., Tang, Y.-T., Qiu, R.-L., 2018. Accumulation and fractionation of rare earth elements (REEs) in the naturally grown *Phytolacca americana* L. in southern China. Int. J. Phytoremediation 20, 415–423. https://doi.org/10.1080/15226514.2017.1365336

Zhang, B., Liu, C., Li, C., Jiang, M., 2014. A novel approach for recovery of rare earths and niobium from Bayan Obo tailings. Miner. Eng. 65, 17–23. https://doi.org/10.1016/j.mineng.2014.04.011

Chapter 4: Development of a recovery process using the ash of *D. linearis*

This chapter presents the experimental approach conducted to recover the REEs from *D. linearis* ash. The production of a marketable compound is the main goal of the agrominer. Overcoming the stability of the ash, separation of the most problematic impurity (Al), and minimizing reagent consumption, are the three main challenges described and met. The study of the limiting mechanisms at play throughout the process allow for implementation of improvements. At the same time, experimental data is collected in view of upscaling.

4.1 Introduction

As discussed in the first chapter, several approaches have been tested to recover nickel from HA biomass. A great deal of knowledge has been acquired regarding the treatment of this novel type of resource, referred to as bio-ore. So far, the most advanced and promising extraction process begins with the combustion of the biomass. In an attempt to generalize agromining recovery processes, the ash route for the recovery of REEs from *D. linearis* has been investigated.

The following advantages of this first step are emphasized:

- heat recovery for energetic integration,
- drastic concentration of the element of interest,
- removal of organic carbon.

Given that the plant has absorbed atmospheric CO_2, this simple operation enables heat recovery without overall carbon emission. Heat can be input into the process if downstream extraction or purification steps require heating. Another possible application would be to provide heating to the operating building, as it is currently the case on the GISFI platform.

Ashing drastically concentrates the elements of interest by factors ranging from 10 to 20, thus reducing the mass flux early in the process, which is always desirable (Houzelot *et al.*, 2017; Laubie *et al.*, 2021).

In terms of chemistry, the biomass is completely transformed into a mineral matrix. Organic matter is volatilized as CO_2 above 500 °C, although alkali minerals fix some of the carbons as carbonate (*e.g.*, $CaCO_3$) (Houzelot *et al.*, 2017). The recovery of elements of interest is no longer affected by the organic molecules present in the plant. Indeed, diverse, and sometimes unidentified organic molecules render the treatment and understanding of aqueous solutions complicated (Guilpain *et al.*, 2018).

Yet, it is worth mentioning that ashing is not a perfect operation. Temperature, air input, and gas composition must be controlled to ensure that combustion is maximized (lowest amounts of CO as

possible) (Hazotte *et al.*, 2020). Undesirable amounts of nitrogen oxide (NOx) sulfur oxide (SOx), and other acidic gases (HCl) can also appear in the gas phase, reflecting plant composition (Sommersacher *et al.*, 2012). Such emissions should be prevented and minimized. In the presence of volatile metals (*e.g.*, Zn, Cd, Pb), bag filters must be used (Houzelot *et al.*, 2017). Regulatory and logistical issues may arise when considering the transportation of ashes, which may be regarded as hazardous waste (Laubie *et al.*, 2021).

Finally, even though the ash chemistry is simplified by the absence of organic matter, new challenges emerge. In the case of this work, the high contents of Al and Si in the plant are converted into a stable aluminosilicate vitreous phase. The nature of this phase prevents a direct and simple extraction. This fact was illustrated by poor recovery values when digesting the ash in concentrated HNO_3 (65 wt%) at 230 °C, 80 bar for 30 min. Under these harsh conditions, REE recovery values barely attained 60 % (Chour, 2018).

To make the most of the above-mentioned advantages, a process using the ash of *D. linearis* was designed to recover the REEs. The design also benefitted from the team expertise working with other HAs ash (Ni, Zn, Cd). Two main goals are primarily set for this process:

1- Develop a strategy to overcome the challenge posed by the stability of the ash (*i.e.* the aluminosilicate glass matrix) and improve it. Achieving high extraction rates for the REEs will be crucial in this context.

2- The success of the extraction process will also rely on its selectivity. The second main challenge identified for the purification of the REEs from the elements is the presence of Al. In acidic solutions, aluminum behaves in the same fashion as the REEs, forming a trivalent cation. This property makes Al the main impurity in REE-produced compound at the mining stage in South China. The separation is all the more challenging as Al is more abundant than REEs in the plant: the sum of the concentration of the REEs in the ash ($2.2\ 10^{-4}$ mol.g^{-1}) is ten times lower than the Al concentration ($2.4\ 10^{-3}$ mol.g^{-1}). Selectivity will be sought and emphasized throughout the design of operational units.

The pioneering work accomplished in the framework of Z. Chour's PhD thesis has paved the way for such a process. The strategy of leaching the ash in concentrated hot soda solution ("alkaline leaching") permits to solubilize Al and Si, to break the vitreous matrix and to separate a significant part of Al from REEs. The subsequent leaching of the remaining solid in 1M HNO_3 yielded high RE extraction rates, confirming the effectiveness of the strategy.

Additionally, recent attempts to recover REEs from coal fly ash (CFA) produced at thermal power plants, have resulted in similar REE extraction. As discussed in the first chapter, CFA can be considered an alternative source of REEs. Interestingly, this material is similar to *D. linearis* ash, with high contents of Al and Si (Taggart *et al.*, 2016). Direct extraction using strong acids yield low extraction rates (on average 30%) for the same reason. Processes involving alkaline pre-treatment (*e.g.*, alkaline leaching, sintering with $NaCO_3$) have resulted in higher extraction rates than for single acid extractions (King *et al.*, 2018; Taggart *et al.*, 2018; Tang *et al.*, 2019).

The following chapter aims at describing a novel process for the production of RE carbonates using *D. linearis* ash. Results and operating conditions are discussed for each step (Figure 60).

Figure 60: The three main operations described in this chapter

The results of the alkaline leaching experiments conducted in the frame of this thesis are presented, with the goal of clarifying the influence of the operating parameters and delineating the limits of the operation. The chapter also describes the extractions conducted on the treated ash, aiming to minimize reagent consumption and to be as selective as possible.

The precipitation of RE-carbonates is described. Carbonates have the advantage to be a directly salable compounds (they are the raw material for REEs separation and refining), they can be precipitated with low-cost reagents, and with the proposed route, they are produced in their almost pure form.

Two main modifications from the basic process are finally discussed: the increase of the solid to liquid ratio (S|L) in the alkaline leaching step and the influence of pH in the extraction step.

4.2 Alkaline leaching of ash

4.2.1 Maximizing Al dissolution

As mentioned earlier, alkaline ash leaching aims at (i) removing the maximum amount of Al from the ash, and (ii) destroying the aluminosilicate glassy matrix to render the REEs available for extraction. Preliminary experiments conducted by Chour (2018), presented in the first chapter, proved the effectiveness of the treatment. However, we chose to modify operating conditions to improve the removal rate (or "extraction yield", X_{Al} (Eq. 1)) of Al, and try to improve it beyond 90 %. An attractive option to study the influence of parameters and to quickly optimize a chemical process step is the design of experiment (DoE) methodology. The concept of DoE is to conduct a minimum of experiments, carefully designed, in order to obtain the maximum information on the influence of each parameter on a chosen response signal. Empirical models can be quickly drawn up without having to implement a sophisticated physico-chemical model. This methodology was chosen to complement the preliminary experiments in order to find the conditions under which Al was fully removed from the ash.

To do so, a central composite design was chosen to obtain a surface response curve, where Al extraction yield is the response. Three factors were chosen: (i) temperature, ranging from 75 to 90 °C, (ii) NaOH concentration, ranging from 4.8 to 7.2 M, and extraction duration, ranging from 13 to 44 min. Preliminary experiments were considered to define ranges for each parameter. The Al extraction rate was computed each time using either the Al concentration in the aqueous phase (25), or the remaining content of Al in the solid (26).

$$X_{Al} = 100 * \frac{V * [Al]_{t,(aq)}}{[Al]_{0(s)} * m_{0,ash}} \quad (25)$$

X_{Al} is the removal rate (in %), $[Al]_{t,(aq)}$ is the measured aqueous concentration of Al (in M), V the reaction volume (in L), $[Al]_{0(s)}$ the Al concentration in the ash prior to alkaline leaching (in $mol.g^{-1}$), $m_{0,ash}$ the mass of the leached ash.

$$X_{Al} = 100 - 100 * \frac{[Al]_{t,(s)} * m_{t,ash}}{[Al]_{0(s)} * m_{0,ash}} \quad (26)$$

X_{Al} is the removal rate (in %), $[Al]_{t,(s)}$ is the measured concentration of Al in the leached solid (dry, in mol.g^{-1}), $m_{t,ash}$ is the mass of the leached solid (dry, in g), $[Al]_{0(s)}$ the Al concentration in the ash prior to alkaline leaching (in mol.g^{-1}), $m_{0,ash}$ the mass of the leached ash.

Since no model could be drawn when using aqueous Al concentration, and time was not a significant parameter, it was decided to use the remaining Al content in the solid to compute the extraction rate (25).

The influence of NaOH concentration and temperature on the Al extraction rate fitted a two-factor interaction model acceptably (R^2=0.8917) (Figure 61, Equation (27)).

$$X_{Al} = 93.45 + 0.634 \times T^* + 1.39 \times [NaOH]^* + 0.6732 \times T^* \times [NaOH]^* \quad (27)$$

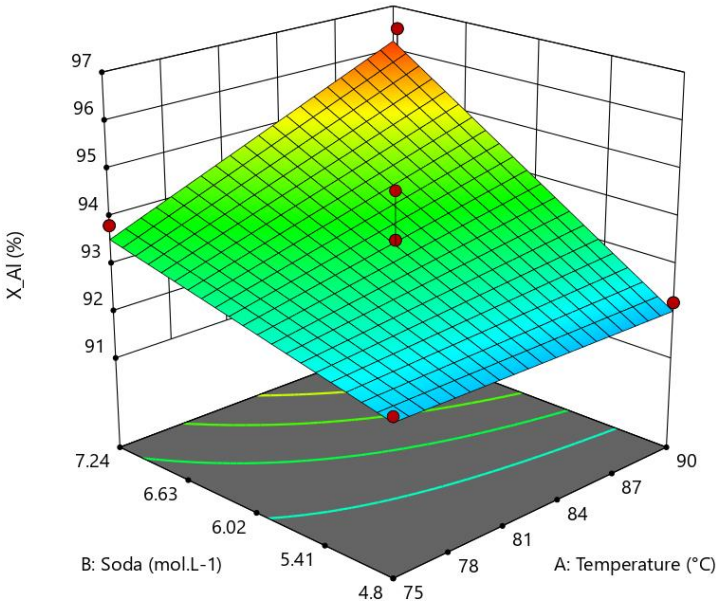

Figure 61: Representation of the surface response of X_{Al} against the operating parameters for the alkaline ash leaching step. The solid/liquid ratio was kept constant at 5 g.L^{-1}.

Here, X_{Al} is the extraction rate of Al in %, T* is the normalized temperature (dimensionless), [NaOH]* is the normalized soda concentration. The parameters are normalized to their range for data processing according to equation (28).

$$X^* = \frac{2\,X}{X_{max} - X_{min}} - \frac{X_{max} + X_{min}}{X_{max} - X_{min}} \quad (28)$$

For example, -1 for temperature would correspond to the minimum temperature of the range considered, *i.e.* to 75 °C. Normalization enables us to compare the effect of the parameters between them, by comparing the corresponding coefficients in the model equation. Hence, it can be observed that – relatively to the range considered – the soda concentration had more impact than the temperature,

as 1.39 is greater than 0.634. The interaction of soda and temperature had a positive effect, as shown by the positive interaction coefficient of 0.6732.

Equation (27) translates into equation (29) where the parameters are input in their usual units for practical purposes: X_{Al} in %, T in °C, and [NaOH] in M.

$$X_{Al} = 111.55 - 0.3643 \times T - 5.013 \times [NaOH] + 0.0748 \times T \times [NaOH] \quad (29)$$

In accordance with the preliminary experiments, the harsher the conditions, the more Al was solubilized. This is indeed consistent with the fact that $NaAlO_2$ solubility increases with temperature, and alkalinity (Peng *et al*. 2018a). Yet, the experiments were considered unsatisfactory because the increase in Al extraction rate was limited in comparison to the great quantity of reagent added.

4.2.2 Mechanism limiting the dissolution of Al

The extraction rate did not exceed 100% as expected. Because Al is a problematic impurity, it was considered crucial to maximize its extraction. Subsequent experiments were conducted to assess what the limiting mechanism was for Al dissolution.

Understanding this mechanism could have been facilitated by the identification of the Al bearing phase in the ash. However, as mentioned earlier, the ash was mainly amorphous. Consequently, examination of X-ray diffraction (XRD) patterns, the usual technique for identifying solid phases, was not conclusive.

An indirect approach was chosen: the speciation of Al was inferred, and a thermodynamic data was used to predict its solubility. The CHESS software was used to compute the equilibrium of a model solution at 60, 75 and 90°C with 1 M NaOH. Regarding Al, the same quantity present in 1 g of ash (2.4×10^{-3} mol) was input as Al hydroxide. Aqueous concentrations were converted to extraction rates using equation (25) and plotted against pH.

Calculations predict its total dissolution mainly as $NaAlO_{2(aq)}$ above pH 12.5 (Figure 62). However, when the pH varied, the reaction was observed to be strongly pH sensitive around the operating point. Temperature decrease could lead to less dissolved Al than expected. Cooling before filtering the hot suspension could have a deleterious effect.

In addition, a decrease in alkalinity during the reaction might also prevent the full dissolution of Al. The conversion of SiO_2 to its alkaline forms $NaSiO_3$ or Na_2SiO_4 would consume soda, resulting in a loss of alkalinity and a pH decrease. However, the stoichiometric excess – at least 1 mol of NaOH *vs.* 41 mmol SiO_2 – must be sufficient to maintain high alkalinity. The other elements present in the solid: K, Ca, and Mg, are most likely in their alkaline form after ashing (either as oxide or carbonates). Hence, they should not reduce the overall alkalinity.

The second possibility was the absorption of atmospheric carbon, which was estimated more likely. Indeed, the alkaline solution was stirred in contact with the atmosphere. The chemical reaction could decrease the pH, following equation (30):

$$CO_{2(g)} + 2HO^-_{(aq)} \rightarrow CO^{2-}_{3(aq)} + H_2O \quad (30)$$

To clarify the influence of this phenomenon, the leaching experiment was performed again with the addition of bubbled N_2 in the reactor, and the results were compared with the control experiments, performed under the same conditions with bubbled air. After leaching, the resulting concentration of Al in the solid did not differ from one experiment to the other (Figure 63). The remaining Al concentrations

were 29.0 ± 1.2 mg.g^{-1} and 30.0 ± 1.7 mg.g^{-1}, for the leaching performed under N_2 and air bubbling conditions, respectively. Hence, the absorption of CO_2 is not the limiting parameter for Al extraction.

The only noticeable difference was in the Mn concentration, which had a higher residual concentration for the experiment performed under air flux. This result is attributed to more oxidizing conditions, favoring the precipitation of oxidized forms of Mn, solid brown MnO_2. The leachates were colorless in this case, while under anaerobic conditions, solutions presented a light pink coloration which might be attributable to soluble Mn.

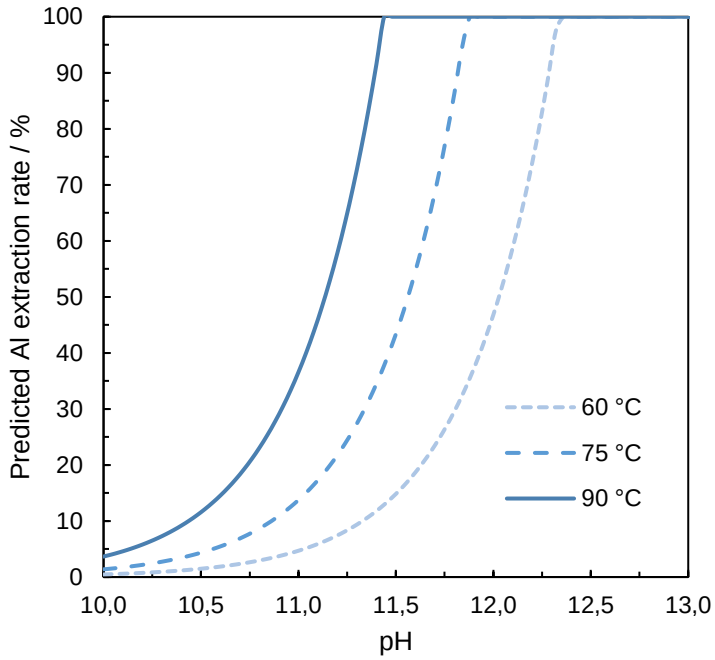

Figure 62: Predicted Al extraction of rate for the alkaline leaching step (CHESS). The initial solid aluminum concentration is 340 mg.L^{-1}, corresponding to the average input amount of Al with 5 g.L^{-1} of ash.

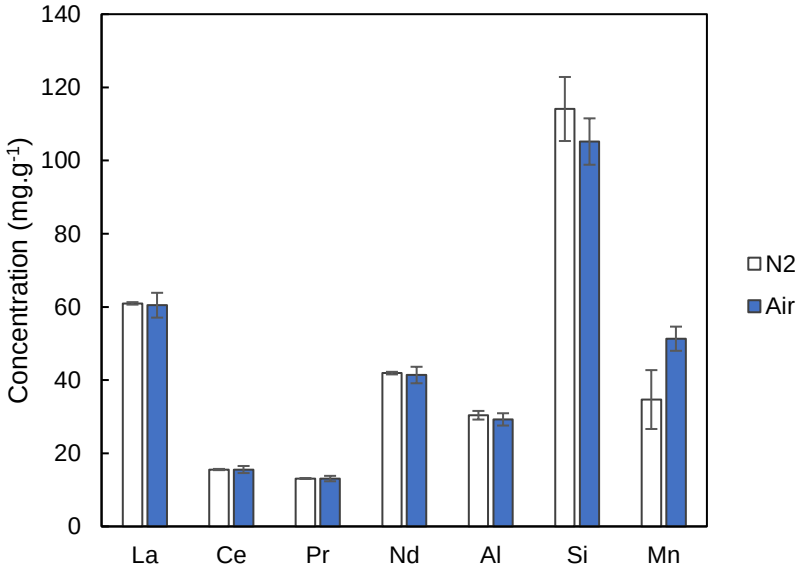

Figure 63: Concentrations in the residual solid after alkaline leaching. Experiments conducted at 80°C, [NaOH] = 6 M, for 10 min. Error bars indicate standard error, computed over n=3 replicates.

Since it was determined that atmospheric carbon absorption was not the limiting factor, the precipitation of an insoluble compound during the extraction was suspected. Indeed, the formation of solid Al-bearing phase cannot be excluded due the important amount of dissolved solids. This phenomenon is well-known in the Bayer process, where heat exchangers and tanks are subject to important scaling. The scale is formed by the precipitation of Al with impurities, dissolved silica being the major one. Two main phases are involved: sodalite and cancrinite (identical stoichiometry: $Na_8[AlSiO_4]_6X_2 \cdot nH_2O$, X=1/2 CO_3^{2-} ,1/2 SO_4^{2-} , Cl^-, OH^-), with cancrinite forming at higher temperatures (> 120 °C) (Armstrong, 1999; Barnes *et al.*, 1999; Hind *et al.*, 1999). Precipitation of the sodalite phase cannot be excluded.

Yet, other insoluble compounds could have been formed. In Bayer plants again, dissolved silica is often precipitated using $Ca(OH)_2$ to form $Ca_3Al_2(SiO_4)_n(OH)_{(12-4n)}$ (Whittington, 1996). Because Ca is a major constituent of the ash (2.2 wt%), the precipitation of calcium aluminosilicate cannot be overlooked. Sodalite, cancrinite and other calcium aluminosilicate are called desilication products (DSP). They are modern subjects of study in the optimization of Bayer refining plants (Peng *et al.*, 2018b, 2018a; Vaughan *et al.*, 2019).

In our case, the precise identification of a single precipitated compound was not achieved. The study of X-ray diffraction patterns suggests the formation of minerals analogous to biotite $KMgSi_3AlO_{10}(OH)_2$, microcline $KAlSi_3O_8$, or hydrotalcite $Mg_6Al_2CO_3(OH)_{16} \cdot 4H_2O$ (Figure 64). A high background noise, most likely due to small particle size or poor crystallinity, prevents a clear-cut interpretation. Hence the result of phase identification must be taken with great care. In any case, it is clear that the major impurities such as K, Mg, and Si play a key role in the formation of insoluble forms of aluminum.

Alkaline leaching experiments conducted by other research on a similar material (CFA), are in good agreement with the above findings. As mentioned previously, *D. linearis* ash is related to CFA to some extent. Li and co-workers (2014) used a similar method to solubilize the aluminosilicate matrix, by using even more concentrated NaOH (40 wt%) in hydrothermal conditions (230 – 260 °C). The formation of a zeolitic compound ($1.33Na_2O \cdot 0.67CaO \cdot Al_2O_3 \cdot 2SiO_2 \cdot H_2O$) was found to keep the extraction rate of Al below 91% (Li *et al.*, 2014). Other authors reported an extraction yield of 92% when using 45 wt% NaOH at 280 °C (Yang *et al.*, 2014). Although CFA contains higher amounts of Al than *D. linearis* ash, these findings support the hypothesis that Al removal is limited by the re-precipitation of insoluble forms.

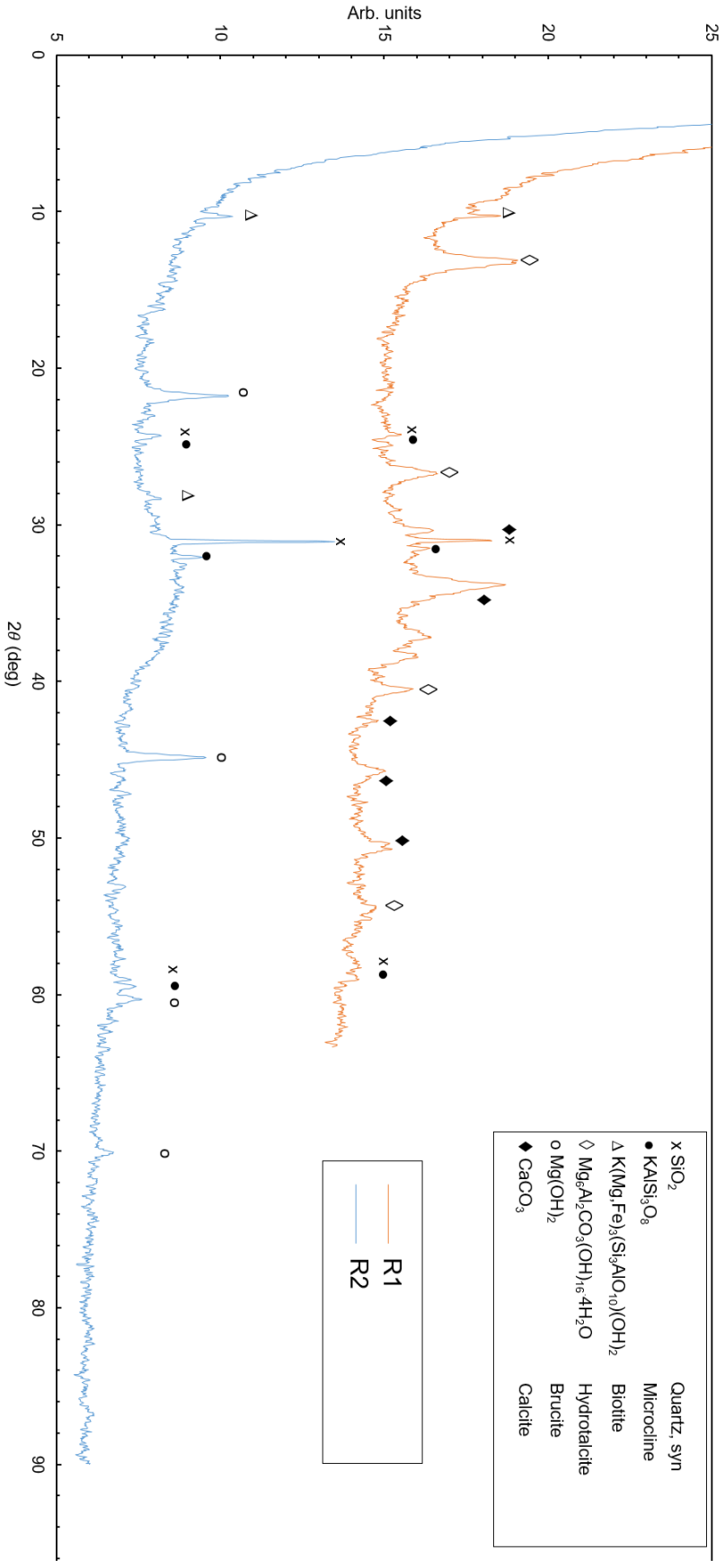

Figure 64: X-ray diffraction patterns of ash leached in 6 M NaOH at 80 °C for 2 h. R1 refers to the leached ash after drying at 80 °C for 24 h. R2 refers to the same solid, rinsed with deionized water in the column (see following section) and dried at 80 °C for 24 h.

4.2.3 Effect and design of the rinsing step

After alkaline leaching, the resulting product is an alkaline solid. When dried, this solid was visibly hygroscopic, and suspected to contain a significant quantity of NaOH. The elemental analysis conducted by ICP-OES is presented in Table 25.

Table 25: Composition of leached ash after alkaline leaching, before and after rinsing. Values were averaged over 4 solids obtained in the design of experiments. The "rinsed" values correspond to the solids obtained after the column rinsing experiment after 35 BV, corresponding to a solid to liquid ratio of 20 g/L. The detection limit (DL) for Pb is estimated to be below 0.001 mmol.g^{-1}.

Average concentration in the leached ash (mmol g^{-1} ± SD)		
Element	Unrinsed (n=4)	Rinsed (n=3)
Na	7.44 ± 0.10	0.44 ± 0.10
Al	0.41 ± 0.03	0.97 ± 0.07
Ca	1.18 ± 0.66	3.47 ± 0.40
Fe	0.09 ± 0.01	0.21 ± 0.03
K	0.15 ± 0.01	0.20 ± 0.01
Mg	0.66 ± 0.07	1.71 ± 0.14
Mn	0.30 ± 0.04	0.76 ± 0.03
P	0.04 ± 0.02	0.10 ± 0.02
Si	0.91 ± 0.10	2.56 ± 0.15
Pb	<DL	<DL
ΣREEs	0.42 ± 0.09	0.99 ± 0.10

It quickly appeared that this solid could be rinsed in deionized water to remove adsorbed NaOH, and decrease its alkalinity before the extraction of REEs in acidic media. In an effort to reduce water consumption, experiments were engaged to determine the minimum quantity of water required.

A predetermined quantity of dried and ground solid was placed in a column. Deionized water was circulated from the bottom to the top at a constant flow rate, while pH and conductivity of the effluent were monitored (Figure 65).

The high pH values (above 12) measured in the effluent confirmed the alkalinity of the solid. The rinsing step required at least 16 bed volumes (corresponding to 68 mL) for the pH and conductivity values to reach a steady state. The resulting solid remained alkaline at the end of the experiment (pH 11.2).

The packed column represented a mass of 2.8 g of dried leached ash. A rough estimation of the volume of water required is thus 24.3 mL per g of dried residue, corresponding to 12.1 mL of water per g of leached ash. Hence, a minimum quantity of water was estimated.

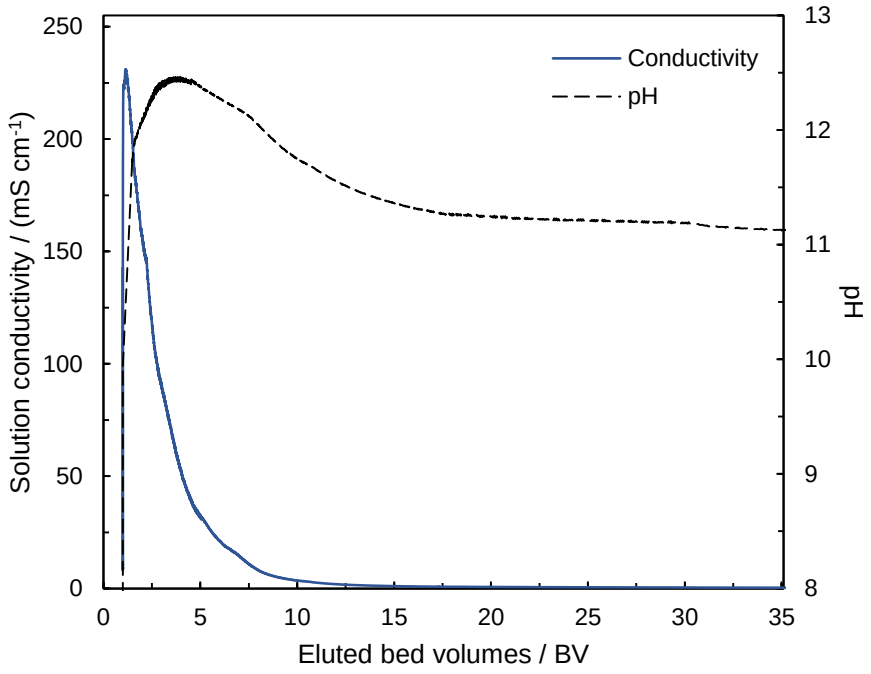

Figure 65: Conductivity and pH of the effluent from the leached ash column

The composition of the effluent was investigated (Figure 66). It appeared that minor impurities such as Pb, Zn and Fe were quickly eluted and their concentration rapidly fell below the detection limits. Conversely, the major elements Na, Si, K, and Al were released in significant proportions over the elution, while Ca – another major constituent of the solid – remained mostly solid. Differences in the observed behaviors suggest that a solid composed of Al, Si, K, and Al is being dissolved. This supports the formation of an insoluble compound in alkaline conditions during the alkaline leaching step. It must also be noted that REEs were below the detection limits in the effluent (each element $<10^{-6}$ M).

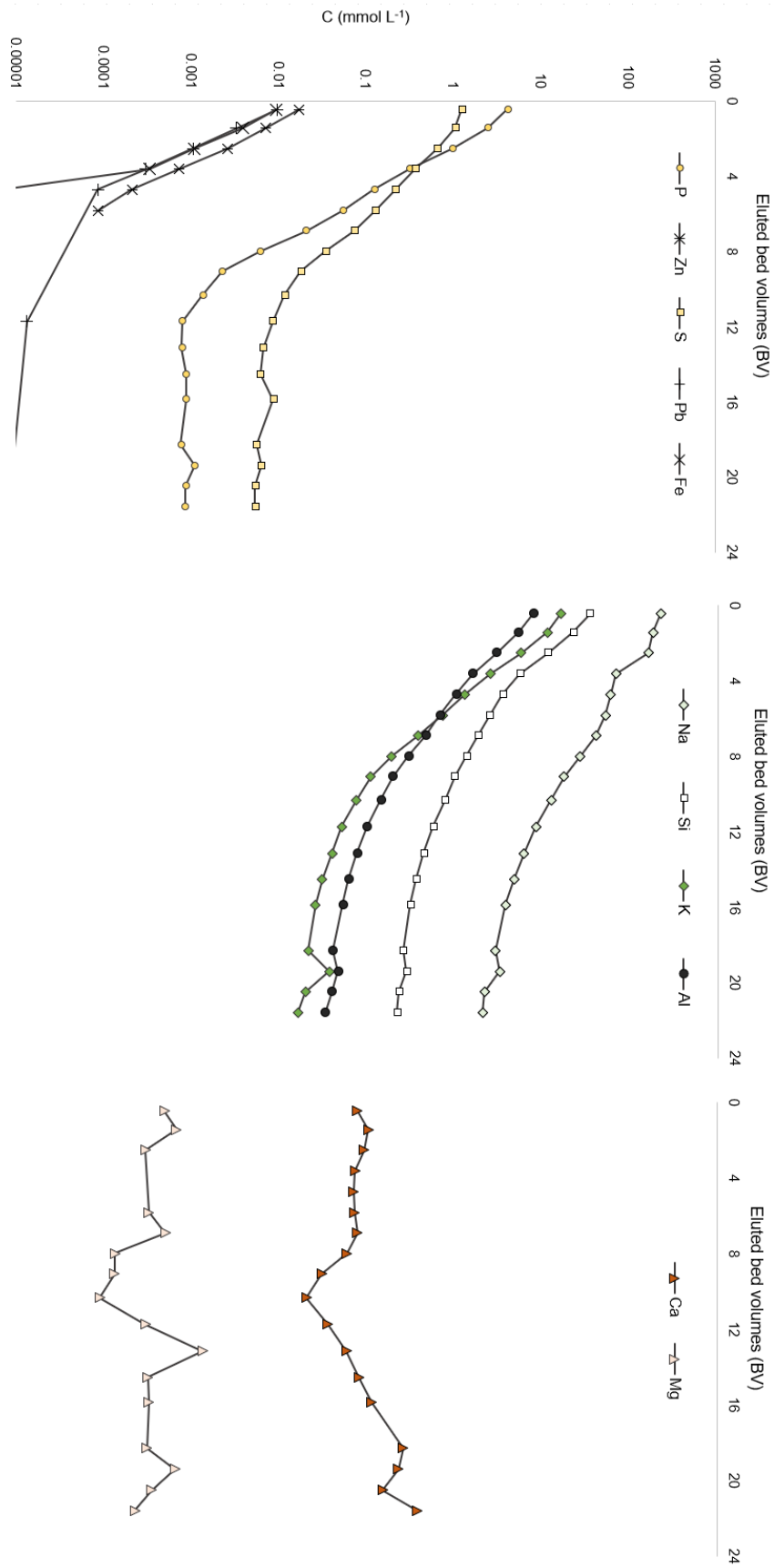

Figure 66: Composition of the rinsing effluent. Aqueous concentrations are expressed in mM and represented in log-scale.

4.3 Selective dissolution of REEs

REE extraction or dissolution, is the main step of the process. Nitric acid (HNO_3) was selected as an extractant. It is a strong acid usually used for REE extraction in the mineral industry, or in hydrometallurgical recycling processes (the reader is referred to chapter 1). Additionally, rare earth nitrates are highly soluble (*e.g.*, at 25°C the solubility of $La(NO_3)_3$ reaches 1.5 kg $La(NO_3)_3$ per kg H_2O, (Rumble, 2019)). Hydrochloric acid may also be used.

In an effort to limit reagent usage, the residue obtained after alkaline leaching (rinsed) was suspended in water, and pH was progressively decreased using HNO_3. By monitoring the gradual dissolution of the elements by sampling aliquots and studying the composition of the aqueous phase, we verified if the selective extraction of REEs was possible (Figure 67).

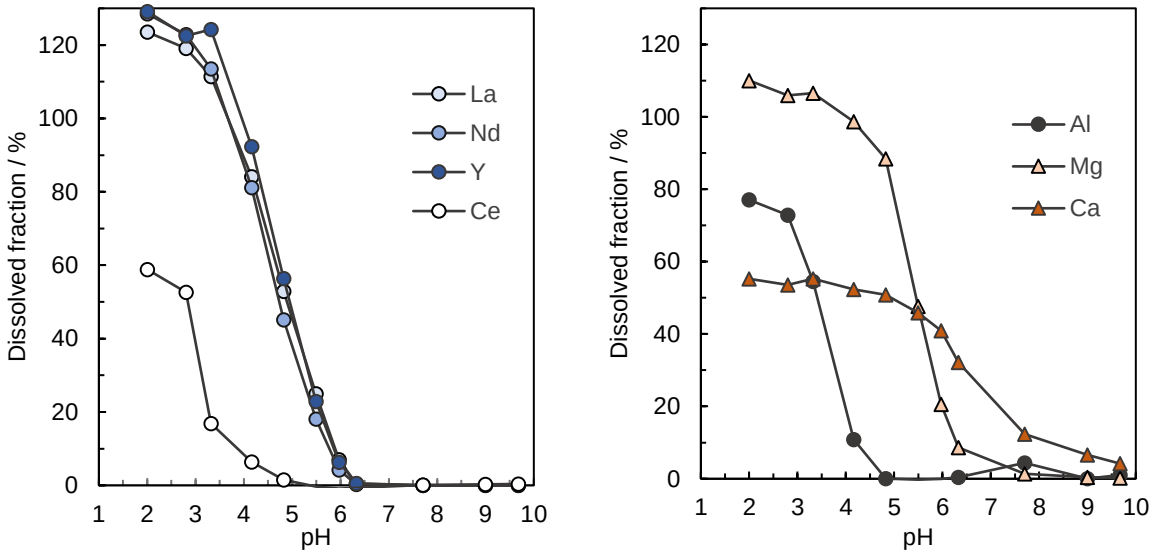

Figure 67: Gradual dissolution of REEs (A) and other major elements (B). The dissolved fraction exceeds 100% most likely because the initial concentration of the solid was underestimated.

The first elements to be released into solution are Ca and Mg, most likely by dissolution of their carbonate forms. Subsequently, the dissolution of REEs occurs starting from pH 6. The REEs behaved consistently, except for Ce, and were fully dissolved at pH 4. The exception regarding Ce can be explained by its valence state. Indeed, as mentioned in the first chapter, Ce (IV) is a possible oxidation state. This form is rather insoluble as CeO_2 is readily formed. The conversion of Ce (III) to Ce(IV) might have been facilitated by the addition of nitric acid, which is an oxidant.

Regarding Al, its dissolution occurred separately, and began between pH 4.8 and 4.0. Hence, it seems possible to selectively dissolve the REEs (except Ce), while keeping Al in the final solid. For the final process, the pH value of 4.8 seemed a suitable target.

The other impurities (*i.e.* Ca and Mg), are less of an issue. Their separation will be addressed in the final step (precipitation of REEs). The target pH appears as a key parameter for both extraction rate of REEs and for the extraction of impurities. Its influence will be discussed on the basis of empirical data in a paragraph below (Influence of the target pH for the extraction of REEs).

To confirm the feasibility of the extraction, additional experiments were conducted. The same equipment (automatic titrator) was used to maintain a target pH in the working suspension. Progressive

additions of concentrated HNO_3 lowered the pH from 11.5 to around 5. Then, the regulation program reduced the flowrate of injected HNO_3 to carefully reach the target pH (here set at 4.8). Upon acid addition, calcium and magnesium carbonate dissolved, releasing carbonate anions (Equation (31)). Around pH 5, carbonate readily formed bicarbonate, consuming a proton (Equation (32)), tending to increase the pH. Regulation maintained a constant pH as carbonates were dissolved.

$$CaCO_{3(s)} \rightarrow Ca^{2+} + CO_3^{2-} \quad (31)$$

$$CO_3^{2-} + H^+ \rightarrow HCO_3^- \quad (32)$$

Here, the dissolution of Ca is used as an example. Other alkaline solid species can be dissolved during this proton-consuming operation (*e.g.*, rare-earth carbonate or hydroxide, magnesium carbonate, the aluminosilicate species formed during alkaline leaching).

The study of the composition of the aqueous phase over time gave insights into the extraction kinetics. The amount of dissolved matter is displayed instead of the aqueous concentration to account for dilution in (Figure 68), calculated as:

$$m_{i(t)} = C_{i,(aq)(t)} * (V_{sol} + V_{ac(t)}) \quad (33)$$

With $m_{i(t)}$ the quantity of matter dissolved of element i (mmol), $C_{i,(aq)(t)}$ the measured concentration of element i (mM), V_{sol} the initial volume of the suspension (L), and $V_{ac(t)}$ the added volume of HNO_3 at time t (L).

The time required to reach equilibrium at constant pH was around 6 h for REEs and Ca. Mg dissolution occurred during the whole experiment, and equilibrium was not reached after 9 h. The amount of aluminum (not shown on the graph) did not exceed 0.02 mmol. In comparison, the total quantity of dissolved REEs reached 1.25 mmol.

From this simple kinetic study, we can conclude that the equilibration times were underestimated in the previous experiment (Figure 67). This means that the actual quantity of REEs that can be recovered at pH 4.8 was underestimated. After 6 h, a significant share of the REEs was dissolved.

The extraction rates reached 56 %, 67 %, 63 % for Pr, Nd, and Y, respectively. The dissolution of La appeared slightly better as 76 % were extracted. As expected, Ce was not released into the solution (measured concentrations were below the detection limit).

It should also be noted that after 6 h of reaction, the extraction rate of the elements of interest barely increases, while Mg dissolution still occurs. Hence, to limit reagent consumption and avoid excessive solubilization of Mg, the extraction duration is set to 6 h for the extraction step.

A possible improvement of this step would be to conduct the extraction at different temperatures to determine the kinetically limiting mechanism and the energy of activation. This would result in finding the optimum temperature to achieve the extraction in a more reasonable time scale (< 2 h). This approach would require considering that the optimal pH value for selective extraction varies with temperature. Degassing of CO_2 might also play a greater role at higher temperatures. This reaction involving complex equilibria (*e.g.*, concomitant reprecipitation of $CaCO_3$) requires great care in the design and the execution of the extraction procedure at mild pH. This approach was considered outside the scope of this thesis but is suggested to improve the extraction step.

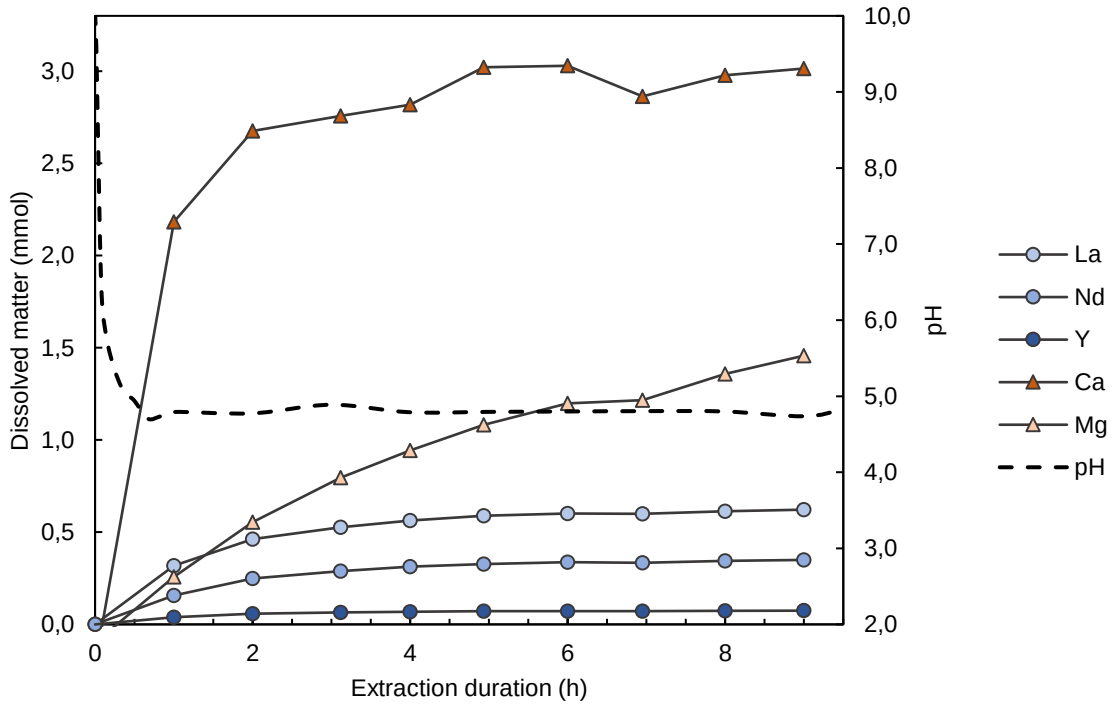

Figure 68: Extraction of the REEs and major elements at constant pH from the concentrated bio-ore (NaOH-treated and rinsed ash)

4.4 Precipitation of rare earth carbonates

4.4.1 Choice of the method and operating parameters

At this point, a solution containing the REEs was obtained after filtration, the total concentration reaching 250 mg.L^{-1}. A number of impurities remain in solution, the major ones being Ca: 173 mg.L^{-1}, Mg: 50 mg.L^{-1}, and Si: 50 mg.L^{-1}, the minor ones being Na: 13 mg.L^{-1} and Mn: 6 mg.L^{-1}. Precipitation is a common option to isolate an element (or a group of elements in this case) in solution. Other purification techniques used in the mineral industry can be contemplated such as ion exchange or solvent extraction.

Regarding ion-exchange, it can be inferred that the total level of impurities is too high, so that Ca and Mg would compete with the individual REEs. The separation may still be possible but inefficient. Solvent extraction might be more suitable for larger amounts of competing impurities. However, it requires the addition of organic solvent, and extracting agent and a separation stage.

In contrast, precipitation requires the addition of a chemical reagent, and the separation is conducted through filtration. Hydroxide precipitation is commonly conducted in hydrometallurgical operations, but other precipitates are possible. In our case, the most convenient form appears to be rare-earth carbonates. Firstly, the solution already contains bicarbonate ions, readily convertible to carbonate. It also means that if hydroxide ions were added to precipitate rare earth hydroxide, they could react with the bicarbonate, yielding carbonate ions, and thus resulting in the co-precipitation of rare earth carbonates anyway. Secondly, the reaction is well known and is the main technique used to precipitate

REEs right after *in situ* leaching in South China. Consequently, the product is already handled by existing refining plants. Selling of the precipitate "as-is" can be directly considered.

Oxalate precipitation is also commonly used for REE isolation and was used by the LRGP team (Chour *et al.*, 2020). Oxalate precipitation is often described as selective. Drawbacks include the cost of the reagent (either as oxalic acid, or as a salt), and the fact that it is condemned to be calcinated to produce the oxide. Oppositely, carbonate salts are comparatively cheaper: 298 USD.t^{-1} vs. 660 USD.t^{-1} for sodium bicarbonate and oxalic acid, respectively (industrial grade, 99%min, Price Market Analysis - Echemi, 2017).

Other insoluble species, but not considered here, are rare earth fluoride or phosphate . They would either be difficult to dissolve back (phosphate), or would involve the addition of HF (hydrofluoric acid), which is too dangerous. Hence, rare earth carbonates were selected as the target precipitates. The target reaction can be described as in equation (10).

$$2Ln^{3+} + 3HCO_3^- \rightarrow 3H^+ + Ln_2(CO_3)_3 \quad (34)$$

Different forms of rare-earth carbonates and allotropes can be formed depending on the operating conditions but also the rare-earth elements. The forms found in the literature are summarized in Table 26.

Table 26: Possible forms of rare earth carbonate in the literature depending on the operating conditions

Crystalline species	Reagent used	Reference
$Ln_2(CO_3)_3 \cdot 8H_2O$ (Lanthanite: La–Nd)	NH_4HCO_3, $NaHCO_3$	(Kim *et al.*, 2018; Nagashima *et al.*, 1973)
$Ln_2(CO_3)_3 \cdot 2(3)H_2O$ (Tengerite: Sm–Tm)	Idem	*Ibid*
$Ln_2(CO_3)_3 \cdot 6H_2O$ (Unique: Yb et Lu)	Idem	*Ibid*
$Lynna(CO_3)_2 \cdot yH_2O$	Na_2CO_3, $NaHCO_3$	(Mochizuki *et al.*, 1974)
$LnOH(CO_3) \cdot yH_2O$ (Hydroxycarbonate)	NH_4HCO_3 & T > 80°C Or extended hydrolysis	(Kim *et al.*, 2018; Nagashima *et al.*, 1973)
$LnO(CO_3) \cdot yH_2O$ (Oxocarbonate)	Results of thermal decomposition	(Kim *et al.*, 2018; Nagashima *et al.*, 1973)

The simple carbonate forms $Ln_2(CO_3)_3$ are referred to as "normal" carbonates in contrast to their hydroxo- forms. The lighter REEs (from La to Nd) tend to form octahydrates ("lanthanite" structure) while the heavier elements form di- or tri- hydrates ("tengerite" structure).

From the literature study, it appears that Na tends to co-precipitate and may even be included in the crystalline structure (Mochizuki *et al.*, 1974; Yu *et al.*, 2020). In order to maximize purity and rare earth total content of the solid, it appears that Na-bearing precipitants should be avoided. The preparation of rare earth carbonate sometimes involves *in situ* hydrolysis of urea under hydrothermal conditions (pressurized vessel, temperature ranging from 50 to 150 °C, one week) (Nagashima *et al.*, 1973). This

method designed for the structural analysis of rare earth carbonate is far from the most practical and easily up scalable.

Eventually, the most suitable reagent appears to be NH_4HCO_3 (ammonium bicarbonate) and was thus selected for this process. The only drawback is the production of a nitrogen-containing effluent. A possibly better solution might be $Mg(HCO_3)_2$, avoiding both crystal incorporation of Na and ammonium discharge. This solution is described in a recent pilot plant experiment (Yu *et al.*, 2020). Because the proposed method involves a preparation specific to their plant, NH_4HCO_3 was chosen for practical purposes.

Regarding the method of preparation, most of the work cited here involves a maturation step. The addition of a maturation step facilitates complete precipitation by maximizing crystal growth. The maturation reactor should be gently mixed to avoid crystal breakage, while maintaining homogenization. Maturation must be done with a constant CO_2 partial pressure (closed vessels), else carbon is released, and normal carbonates hydrolyze to hydroxycarbonates. Temperature has a positive effect on crystal growth kinetics, but also favors hydrolysis. The maturation duration ranges from a few hours to a full day. Arbitrarily, normal carbonates were chosen as the target form.

4.4.2 Efficiency of the precipitation step

The addition of NH_4HCO_3 did not instantly precipitate the REEs. As the first volumes were added, the solution pH quickly increased from 4.8 (the pH at which the dissolution step was conducted) to 6 (Figure 69). Then, pH slowly decreased and stabilized at around pH 5.9. At this moment, the solution became more and more turbid as a white precipitate was formed (Figure 70). The aqueous concentrations of the main REEs gradually diminished as the precipitant was added, attesting to a fast reaction. Because the volume of precipitant added (9 mL) was relatively small compared to the solution (more than 500 mL), dilution could be neglected.

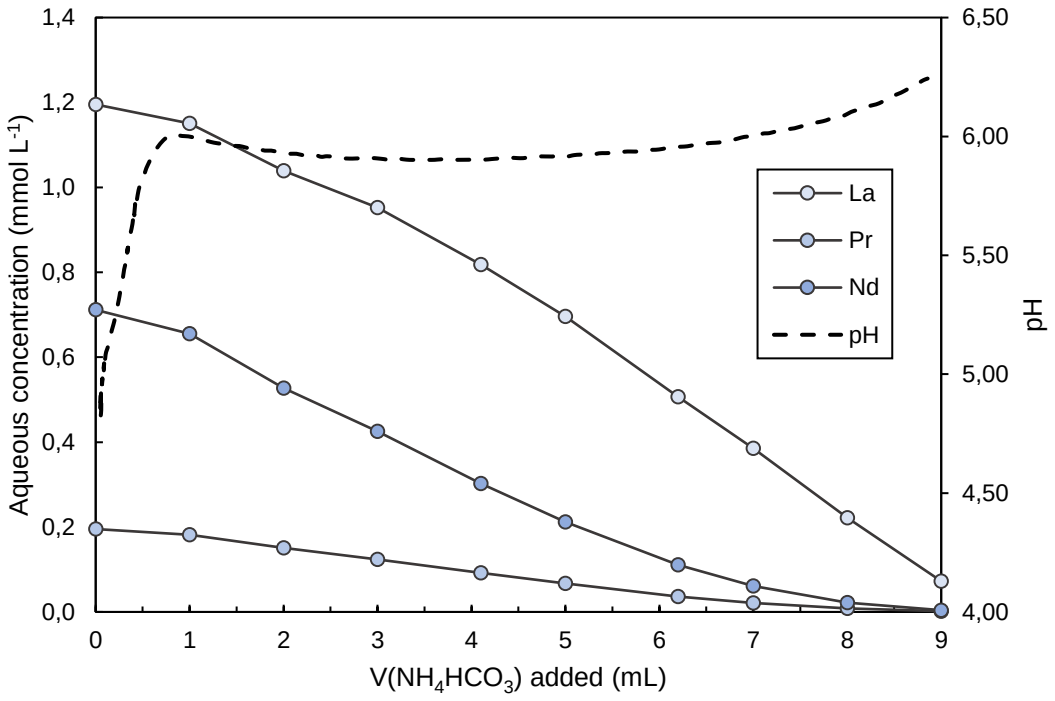

Figure 69: Precipitation of RE carbonates: pH of the suspension and aqueous concentrations of the main REEs *vs.* volume of added precipitant.

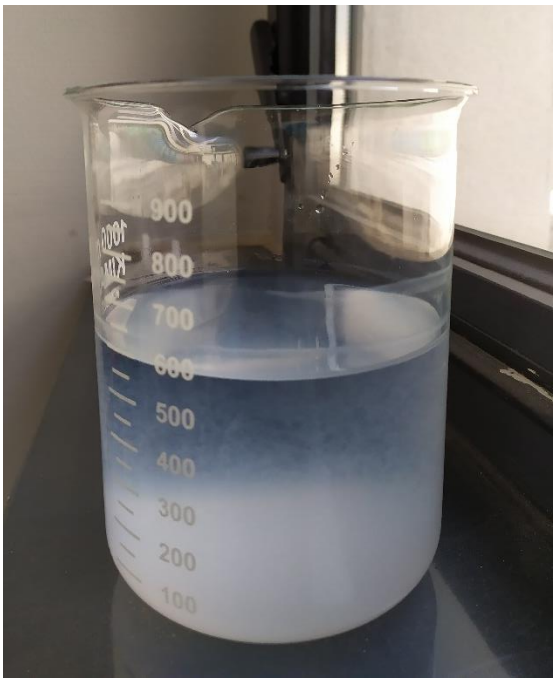

Figure 70: Aspect of the suspension after carbonate precipitation

Measuring the pH of the solution could be a relevant way to monitor the extent of the reaction. Indeed, the precipitation is an acid-base reaction (Equation (10)). When the reaction occurs, the released protons are immediately recaptured by HCO_3^- , forming H_2CO_3 ($H_2O{\cdot}CO_{2(aq)}$) and the pH remains constant. Then, when all the REEs have precipitated, the addition of HCO_3^- simply shifts the H_2CO_3/HCO_3^- equilibrium towards higher pH values. The ammonium cation is too weak an acid to play a role (pKa = 9.25 at 25 °C). Hence, precipitation can be considered complete when the pH reaches a predetermined value. As a recommendation for future process up-scale, the addition of precipitant could be minimized in this way, adapting to varying concentrations of dissolved REEs.

Another possible way to monitor the extent of precipitation is to measure the solution conductivity (Figure 71). During the reaction, electrolytes are added via the addition of precipitant, and removed by the precipitation reaction. Consequently, if the dilution can be neglected, the conductivity varies linearly. Once precipitation is complete, the conductivity can only increase, due to the addition of precipitant. Hence a change in slope of the conductivity curve attests to the end of precipitation. The method is well known and used for chemical titrations. However, it is indirect (a conductivity curve must be plotted, or the first derivative computed) and it requires the precipitant to be added in excess to witness the break in slope.

The maturation step had a positive effect on the precipitation yield as the aqueous concentrations still decreased after 24 h (Table 27). The operation proved to be selective as the main impurities, Ca, Mg, Si, and Mn largely remained in solution. After maturation, the precipitates showed good filterability as vacuum filtration onto cellulose filters (cut-off diameter 2 – 3 µm) was relatively fast.

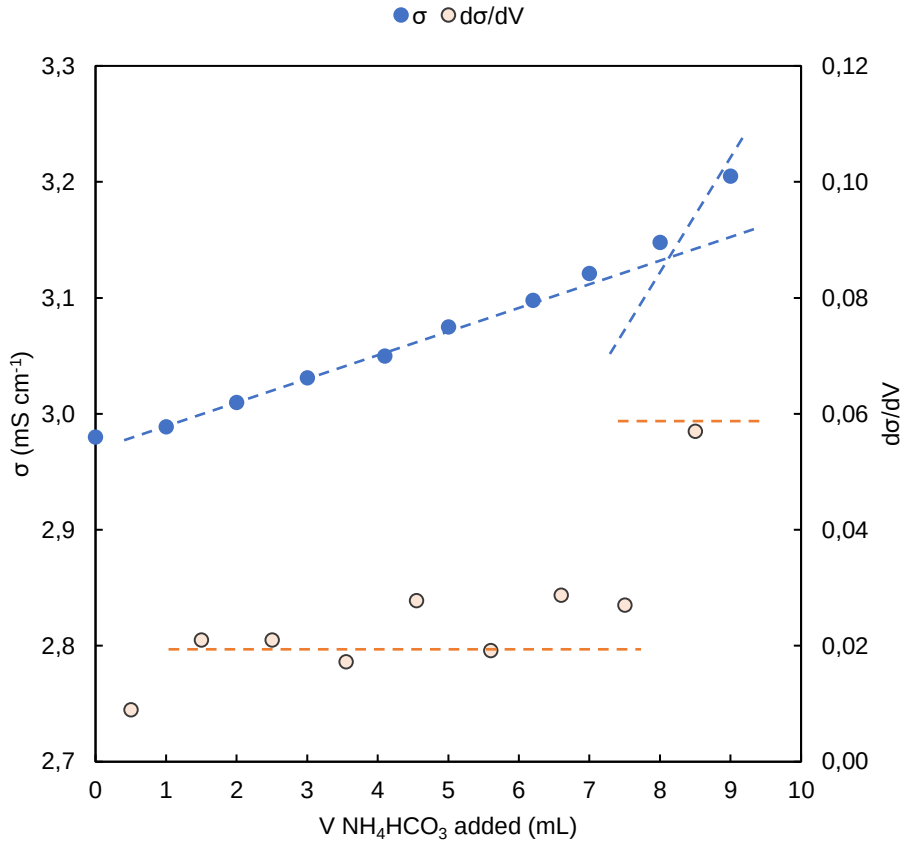

Figure 71: Conductivity of the solution containing the REEs and its first derivative during precipitant addition. Dashed lines are present to guide the eye.

Table 27: Concentrations of the main elements in solution measured by ICP-OES, before and after precipitation

	Initial solution	After precipitation	After crystal maturation (24 h)
Volume (mL)	573	582	582
Element	Aqueous concentration (µM)		
La	1 195 ± 25	72 ± 2	0.72 ± 0.02
Pr	192 ± 4	2.13 ± 0.04	1.42 ± 0.03
Nd	714 ± 15	4.2 ± 0.1	5.5 ± 0.1
Y	146 ± 3	15.7 ± 0.3	3.4 ± 0.1
Ca	4 616 ± 97	4 791 ± 101	4 541 ± 95
Si	2 170 ± 40	2 075 ± 48	1 936 ± 41
Mn	147 ± 3	147 ± 3	144 ± 3
Mg	3 950 ± 83	4 032 ± 85	3 868 ± 81

4.4.3 Product characterization

Infrared spectra of the precipitates were studied to determine the form of the carbonates produced. The spectra collected spectra from the replicates were highly similar and a representative spectrum is presented in Figure 72.

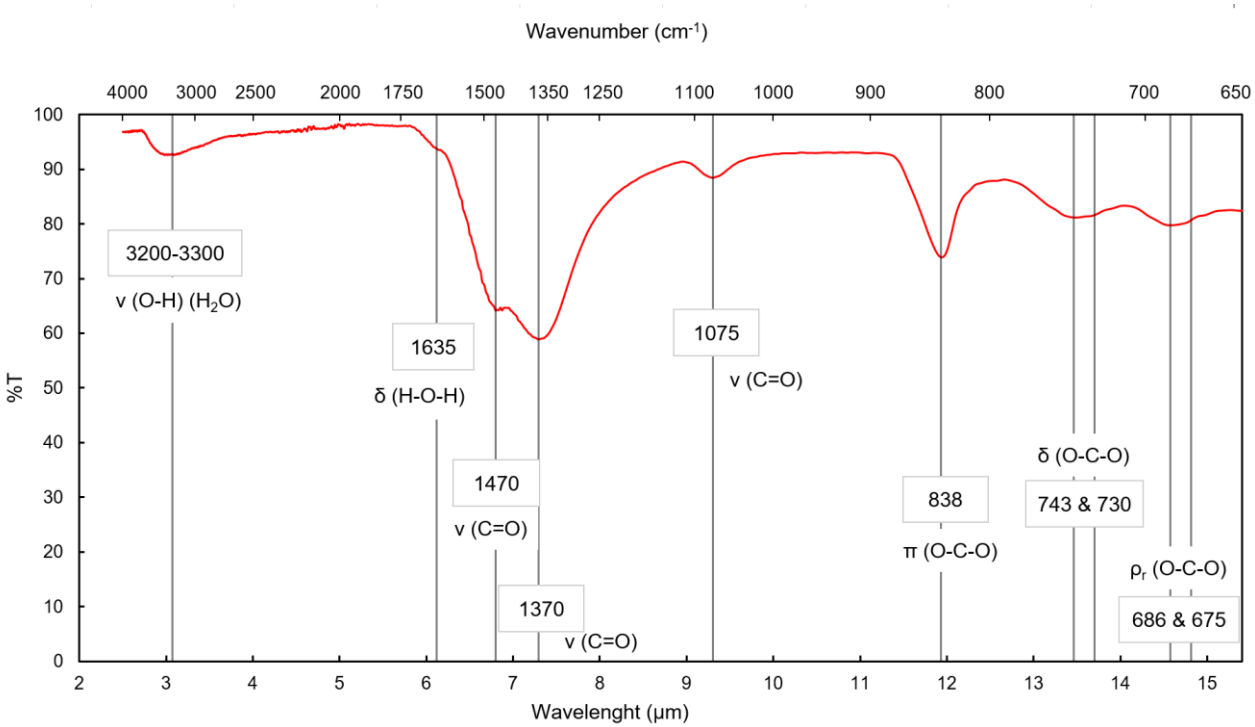

Figure 72: FTIR spectrum of the RE carbonate precipitate and the attribution of vibration bands.

The attribution of the absorption bands was possible using the reference works of Caro *et al.* (1972) and Fujita *et al.* (1962). The vibration of the carbonate ligand is well defined, appearing in the predicted range of wavenumber. Vibrations associated with the metal carbonate bond are not visible, as the strongest is predicted to appear below 400 cm^{-1}. The vibration of hydration water is visible (δ(H-O-H) and ν(O-H)). The absence of an intense band at 3250 cm^{-1} reveals the absence of the hydroxide groups in the solid. Consequently, no hydroxycarbonates were formed. Our results are in good agreement with other recent studies (Lechevallier, 2010; Vallina *et al.*, 2015; Yu *et al.*, 2020).

The X-ray powder diffraction pattern did not permit a clear-cut structural determination due to low signal-to-noise ratio (Figure 73). Yet, the position of the amorphous humps at 18, 30 and 45° matches the one found by Vallina *et al.* (2015). The low signal-to-noise ratio could be due to the small crystallite size and/or poor crystallinity (amorphous phase).

The stability of the amorphous phase was studied in details in other work (Vallina *et al.*, 2015): La aside, rare-earth carbonate tend to be poorly ordered when precipitated at room temperature. By monitoring the turbidity of a saturated solution, the authors measured the lifetime of the amorphous carbonate precursor. They found that the stability of the amorphous precursor increased with increasing ionic potential. The ionic potential is defined as the ratio of the electric charge (z) to the radius (r) of an ion. For REEs, the ionic radius decreases with increasing atomic number (also known as the lanthanide contraction). Hence, the heavier the REE, the more stable the amorphous precursor. This trend observed for La, Nd, and Yb, was later confirmed for Dy.

The phenomenon is also known for Ca^{2+} (ionic potential: 2.02 $Å^{-1}$) and Mg^{2+} (ionic potential: 3.07 $Å^{-1}$): Mg amorphous carbonate is stable for several days while its Ca counterpart has an estimated lifetime of less than 2 min (Navrotsky, 2012; Rodriguez-Blanco *et al.*, 2011). For La and Nd, the estimated lifetimes of the amorphous carbonate precursors are about 9 and 900 min, respectively. If the trend applies for Pr, the third most abundant REE in our precipitate, an even longer lifetime is possible. Hence, 24 h of crystal aging may not be enough to obtain a crystalline compound.

In our case, the crystallinity of the precipitated product is not an issue, as filterability was acceptable and no specification was formulated regarding this criterion. If crystallinity were to be improved, seeding the saturated solution with crystalline rare earth carbonate could be contemplated to favor crystal growth rather than nucleation.

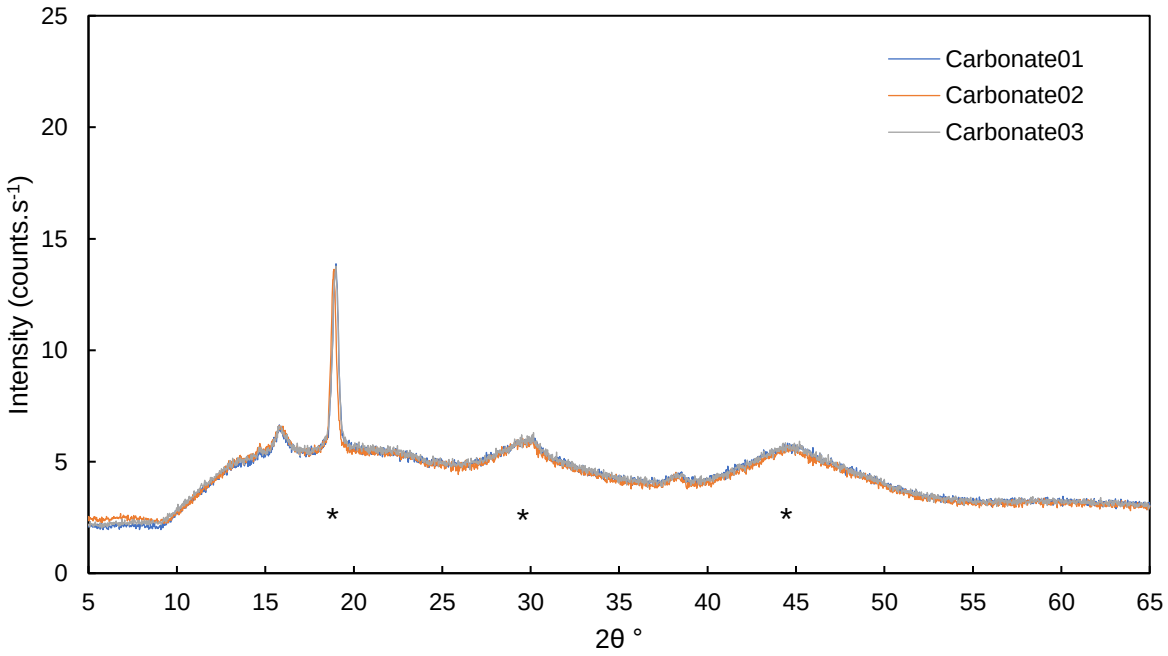

Figure 73: XRD diffraction pattern of the precipitate. Incident beam: Cu Kα (λ=1.54060 Å). Asterisks denote the position of the amorphous humps observed by Vallina *et al.* (2015) from their amorphous neodymium carbonate precursor ("ANC").

To conclude product characterization, thermogravimetric analysis (TGA, Figure 74) was performed to determine the idealized chemical formula of the precipitated compound. Assuming that the thermal decomposition can be summarized as in Equation (11) and is complete, the hydration number x was calculated as described in Chapter 2.

$$(Ln_2(CO_3)_3 \cdot xH_2O)_{(s)} \rightarrow Ln_2O_{3(s)} + 3CO_{2(g)} + xH_2O_{(g)} \quad (35)$$

For the first three replicates, a hydration number of x = 2.1 ± 0.2 was obtained. This number corresponds to the tengerite structure, although, no conclusion can be drawn since the REEs are present in mixture and the crystal structure has not been elucidated by XRD. However, knowledge of x may be of practical interest (*e.g.*, product description).

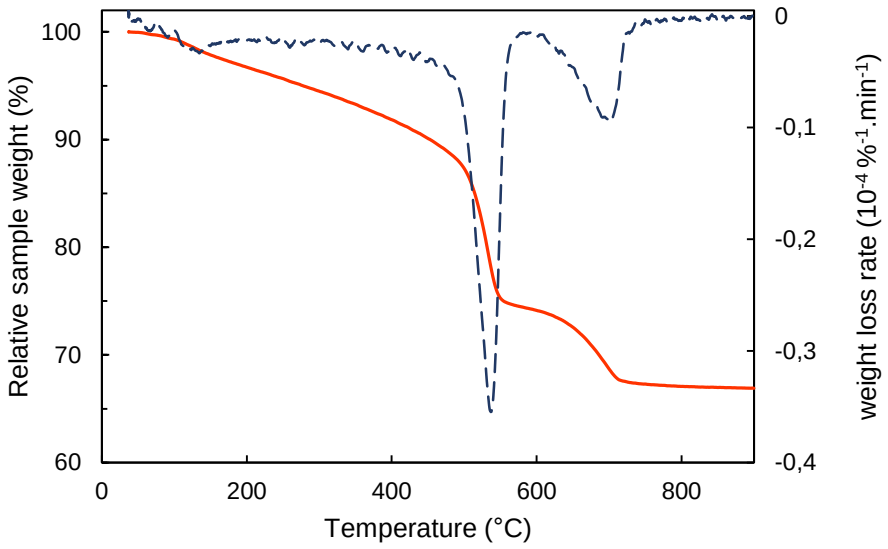

Figure 74: Representative thermogravimetric curve of the produced compound. Curves of the replicates were similar. The continuous line refers to the sample relative weight (reference at 30 °C). The dashed line refers to the weight loss rate, obtained by derivation of the first curve.

Finally, the amount of impurities in the product is low (Table 28). Quantification after HNO_3 digestion revealed that the total amount did not exceed 0.9 % by mass. The purity is thus ≥ 99 %. The concentrations of Pb, Co, and Cu were below the detection limit. The main impurity was Al, confirming that its early removal and separation was crucial.

The main drawback of this precipitation is the time-consuming maturation step, which could be a concern when considering upscaling the process. This finishing step is crucial because it removes the remaining aqueous REE from the solution (Table 27). If the process was to be upscaled, then, a possible substitute for this step could be seeding the leach solution with crystalline rare earth carbonate (Ding *et al.*, 2005; Tilley and Doty, 1985; Zhu *et al.*, 2021).

Table 28: Impurity concentrations in the precipitate. Asterisks indicate that concentrations were below the quantification limit

	Mean concentration (mg g^{-1}) ± SD (n=3)
Al	4.63 ± 0.05
Si	2.51 ± 0.02
Ca	1.289 ± 0.003
Mn	0.175 ± 0.004
Mg	0.110 ± 0.001
Fe	0.076 ± 0.001
Na	0.063 ± 0.002
Ni	0.054 ± 0.004
Zn	0.021 ± 0.001 *
K	0.021 ± 0.002 *
P	0.010 ± 0.000 *
Sum	8.97 ± 0.08

4.5 Process improvements

In the last paragraphs, a process for the production of a semi-finished compound with a minimal purity of 99% has been described (Figure 75). The proof of concept, that REEs can be extracted and isolated from *D. linearis* ash by three relatively simple steps (alkaline leaching, selective extraction, precipitation) has been concretized. Efforts to reduce reagent consumption and increase the product final purity are already integrated and have been discussed.

Figure 75: Process developed for the recovery of REEs from *D. linearis* ash.

However, a mass inventory evidenced that the amount of soda required for the alkaline leaching step was high: 1 kg of NaOH for 1 g of mixed RE carbonate. Aside from environmental consideration, such consumption would render the process uneconomical. Additionally, if the extraction step is selective, it also results in a non-negligible fraction of REEs lost in the solid residue (*ca.* 30-40%).

Hence, new experiments were conducted to improve the process. Two aims were targeted: reduce the consumption of NaOH per gram of REE produced, and increase the extraction yield of REEs.

4.5.1 Influence of the target pH for the extraction of REEs

The extraction step, the operation described in part 3.3., permits the dissolution of REEs while most of the remaining Al stays in the solid phase. The operation is conducted at constant pH by the automatic additions of small volumes of HNO_3 to compensate for carbonate dissolution. As evidenced earlier, the target pH value is crucial. In order to increase the extraction rate of REEs, lower values were attempted (Table 29).

Table 29: Extraction rates of the main elements at different pH values after 6 h of regulation. Experiments were performed at least in duplicates (and n=4 for a target pH 4.8, not including the previous results from part 4.3)

Target pH	4.8	4.7	4.6
	Extraction rate after 6 h (%) ± SD		
La	77 ± 4	79 ± 4	81 ± 4
Ce	1 ± 1	6 ± 1	7 ± 1
Pr	50 ± 2	48 ± 2	58 ± 2
Nd	68 ± 4	71 ± 4	71 ± 4
Sum REEs	63 ± 3	65 ± 3	70 ± 3
REEs - Ce	70 ± 4	72 ± 4	77 ± 3
Al	0.8 ± 0.3	1.6 ± 0.3	15 ± 4
Ca	85 ± 4	72 ± 4	97 ± 4
Fe	0.3 ± 0.1	0.3 ± 0.1	0.1 ± 0.1
Mg	32 ± 2	42 ± 2	57 ± 2
Mn	10 ± 1	10 ± 1	11 ± 1
Si	16 ± 1	15 ± 1	15 ± 1

As expected, extraction rates of REEs improved as the target pH value decreased. However, the changes were small compared to the extraction rate of Al which tended to increase. A more acidic pH also favored the dissolution of other unwanted elements (*e.g.*, Ca, Mg, Mn). This phenomenon was reflected in the composition of the final precipitate (Table 30).

Table 30: Mean concentrations of impurities in the precipitates depending on the extraction conditions. The limit of quantification (LQ) was 0.10 $mg.g^{-1}$

Extraction target pH	4.8	4.7	4.6
	Mean concentration in the solid ($mg.g^{-1}$) ± SD (n=2)		
Al	3.1 ± 0.5	3.0 ± 0.1	3.6 ± 0.1
Si	1.3 ± 1.6	1.0 ± 0.1	1.8 ± 0.1
Ca	0.6 ± 0.4	1.2 ± 0.1	0.8 ± 0.1
K	<LQ	<LQ	<LQ
Fe	<LQ	<LQ	<LQ
Mg	<LQ	<LQ	<LQ
Mn	<LQ	<LQ	<LQ
Na	<LQ	<LQ	<LQ
Ni	<LQ	<LQ	<LQ
P	<LQ	<LQ	<LQ
Pb	<LQ	<LQ	<LQ
Zn	<LQ	<LQ	<LQ
Sum impurities	5.8 ± 2.8	5.3 ± 0.3	6.3 ± 0.3

The amount of impurities in the solid appears to increase with more acidic extraction. Yet, the trend is not drastic as the differences of in concentrations are small, and the interpretation should be cautious. Depending on the application (or buyer's specifications), it might be possible to tune the pH of the extraction step to obtain a more or less pure carbonate compound and maximize extraction. If the specifications were to be higher in terms of purity requirements, additional purification techniques could be put into practice, *e.g.*, re-crystallization.

The compound could be dissolved in fresh solution and precipitated again in a media that is practically free of the main impurities (Al, Si, Ca). However, the need for an ultra-pure compound is unlikely because the compound itself is an intermediate product. Indeed, the refining plants that are able to separate the REEs for their final application can remove trace impurities.

To conclude, the target pH of 4.6 resulted in the precipitation of a compound of acceptable purity (>99%). However, it is foreseen that a more acidic extraction would result in the precipitation of a less pure compound, and the loss of the selectivity of the step.

4.5.2 Effect of solid/liquid ratio

Another improvement regarding the alkaline leaching step, is the study of the effect of the solid/liquid ratio (S|L). By increasing the amount of leached ash and keep using the same quantity of soda solution, the amount of ash processed increases while the amount of reagent used for this step remains constant. Additionally, the initial value of 5 $g_{ash}.L^{-1}$ is relatively small compared to other leaching processes. For example, acid leaching of the ash of Ni HAs is conducted with S/L ratio of 10 to 15 % (by weight), translating to *ca.* 125 to 200 $g.L^{-1}$.

In our case, increasing this parameter leads to increasing aqueous concentrations in the solution (Figure 76). Different behaviors were observed: Si and K were increasingly dissolved when the amount of ash treated increased, in an almost linear trend. Conversely, the concentration of dissolved Al reached a plateau at 25 $g_{ash}.L^{-1}$, confirming again that its release is limited by the solubility of a certain solid phase.

The extraction rate of Al obviously decreased. However, the second important goal for the alkaline leaching step is to destroy the matrix to render the REEs available for extraction. Hence, if Al is leached and then precipitated, the REEs might still be available for extraction.

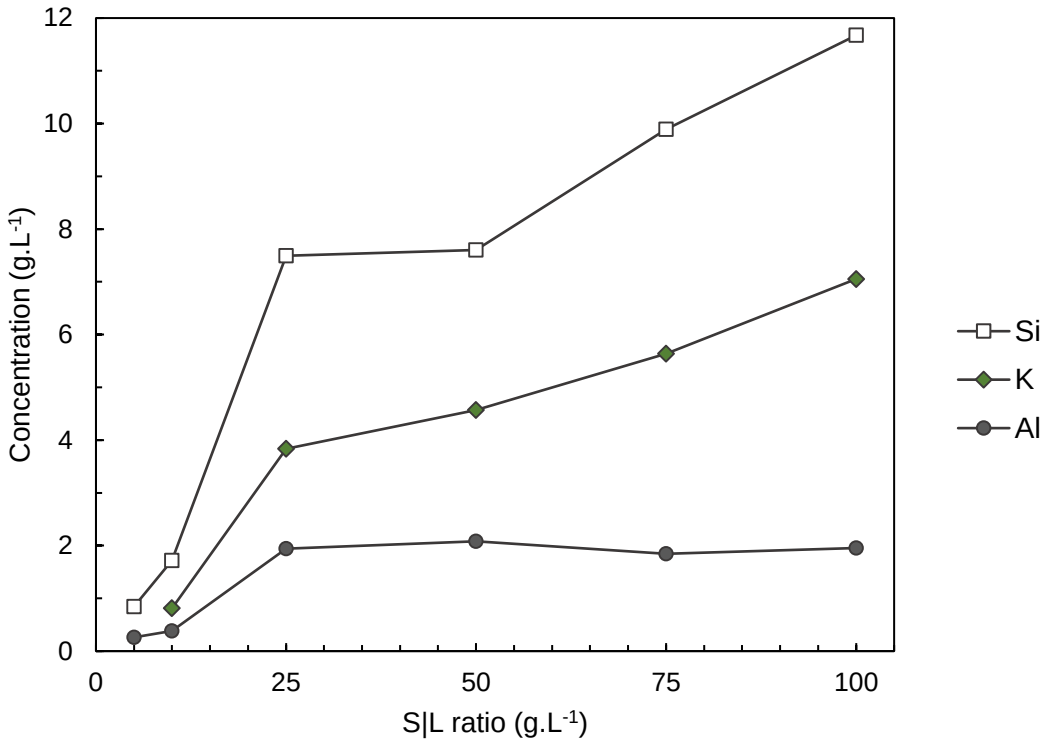

Figure 76: Composition of the alkaline leachate 20 %wt NaOH, 70 °C, 10 min, at various S|L ratios ($g.L^{-1}$)

4.5.3 Consequence on REE availability for extraction

The extraction step was conducted as previously described, using the target pH value of 4.6 using the different solids from the alkaline leaching experiments. The extraction rates are plotted as a function of the S|L ratio of the alkaline leaching step (Figure 77). The rates presented are computed using the different compositions of the solids obtained after alkaline leaching.

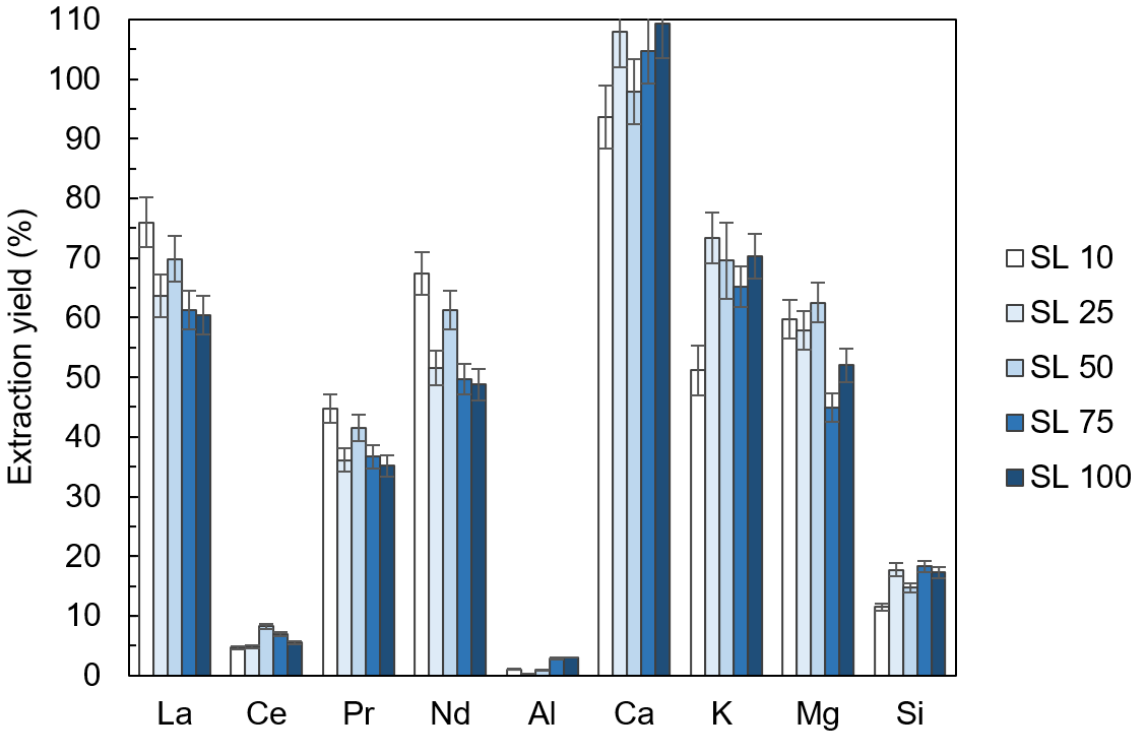

Figure 77: Extraction yields of the main elements from solids obtained under different alkaline leaching conditions

The REEs were increasingly less available for extraction, as shown by the extraction yield of La, decreasing from 75 % to 60 %. The other REEs followed the same trend. Cerium kept behaving in its own fashion, remaining in the solid phase.

Interestingly, Al was increasingly extracted in this step. This trend is slight as the measured aqueous concentration was low (<6 $mg.L^{-1}$), and the extraction yields remained low (<3 %). One possibility could be that as the S|L ratio increases, more and more Al is dissolved and reprecipitated. This new phase is likely to be more reactive than amorphous aluminosilicate glass, and hence more readily extracted.

The calcium extraction yield was the highest, exceeding 100 % due to experimental error. It appears that it is increasingly extracted as the last solid (SL100) gave the highest value. Prior to alkaline leaching, Ca is assumed to be present as carbonate. Earlier, we inferred that it could be converted to $CaSiO_4$ in the presence of soluble Si during the alkaline leaching step. For a given amount of ash treated, a higher S|L ratio means less Ca converted to silicate, and more remains as carbonate. Because $CaCO_3$ is largely more soluble in acidic media than its silicate counterpart, the extraction rate of Ca increases.

4.6 Partial conclusion

A process for the production of an intermediate compound (mixed rare earth carbonate) has been developed using the ash of the hyperaccumulator *D. linearis*. A strategy was successfully developed to overcome the stability of the ash by conducting an alkaline leaching step. The key parameters of this step were assessed (temperature, duration, soda concentration), as well as the mechanisms limiting the dissolution of Al. The influence of the S/L ratio chiefly affected the extraction rate of Al but also the extractability of REEs.

The second central step of the process is the extraction of REEs. It was demonstrated that they could be leached out in mildly acidic conditions (pH *ca.* 4.6), achieving good recovery rates (ranging up to 80%) even at room temperature. The choice of the target pH value had little effect of the extraction rate of REEs, but proved crucial in terms of selectivity.

Finally, the pregnant leach solution was transformed into a mixed rare earth carbonate compound with a high degree of purity. The compound produced was found to be amorphous, but this did not pose practical problems as the solids were easily filtered out.

The feasibility of the process on a laboratory scale was demonstrated and improvements were made to reduce the use of reagents. The process is added to the list of feasible recovery processes from D. linearis. However, its viability (profitability, waste generation, environmental costs) still needs to be assessed. Its performance compared to other recovery process is also to be determined and will be the subject of the next chapter.

4.7 References

Armstrong, J.A., 1999. The investigation of scale formation in the Bayer process (MSc thesis). Loughborough University, Loughborough, UK.

Barnes, M.C., Addai-Mensah, J., Gerson, A.R., 1999. The solubility of sodalite and cancrinite in synthetic spent Bayer liquor. Colloids Surf. Physicochem. Eng. Asp. 157, 101–116. https://doi.org/10.1016/S0927-7757(99)00058-8

Caro, P.E., Sawyer, J.O., Evning, L., 1972. The infrared spectra of rare earth carbonates. Spectrochim. Acta Part Mol. Spectrosc. 28, 1167–1173. https://doi.org/10.1016/0584-8539(72)80088-6

Chour, Z., 2018. Valorisation de terres rares à partir de plantes hyperaccumulatrices (PhD dissertation). Université de Lorraine, Nancy, France.

Chour, Z., Laubie, B., Morel, J.L., Tang, Y.T., Simonnot, M.O., Muhr, L., 2020. Basis for a new process for producing REE oxides from *Dicranopteris linearis*. J. Environ. Chem. Eng. 103961. https://doi.org/10.1016/j.jece.2020.103961

Ding, J., Li, Y., Huang, T., Luo, X., Yang, Y., He, X., 2005. Crystalline neodymium carbonate with lanthanide structure: Preparation, and promoting action of seeding on crystallization. Chin. J. Inorg. Chemsitry 21, 1213–1217.

Fujita, J., Martell, A.E., Nakamoto, K., 1962. Infrared Spectra of Metal Chelate Compounds. VIII. Infrared Spectra of Co(III) Carbonato Complexes. J. Chem. Phys. 36, 339–345. https://doi.org/10.1063/1.1732506

Guilpain, M., Laubie, B., Zhang, X., Morel, J.L., Simonnot, M.-O., 2018. Speciation of nickel extracted from hyperaccumulator plants by water leaching. Hydrometallurgy 180, 192–200. https://doi.org/10.1016/j.hydromet.2018.07.024

Hazotte, C., Laubie, B., Pacault, S., Dufaud, O., Simonnot, M.-O., 2020. Evaluation of the performance of nickel hyperaccumulator plants as combustion fuel. Biomass Bioenergy 140, 105671. https://doi.org/10.1016/j.biombioe.2020.105671

Hind, A.R., Bhargava, S.K., Grocott, S.C., 1999. The surface chemistry of Bayer process solids: a review. Colloids Surf. Physicochem. Eng. Asp. 146, 359–374. https://doi.org/10.1016/S0927-7757(98)00798-5

Houzelot, V., Laubie, B., Pontvianne, S., Simonnot, M.-O., 2017. Effect of up-scaling on the quality of ashes obtained from hyperaccumulator biomass to recover Ni by agromining. Chem. Eng. Res. Des. 120, 26–33. https://doi.org/10.1016/j.cherd.2017.02.002

Kim, P., Anderko, A., Navrotsky, A., Riman, R., 2018. Trends in Structure and Thermodynamic Properties of Normal Rare Earth Carbonates and Rare Earth Hydroxycarbonates. Minerals 8, 106. https://doi.org/10.3390/min8030106

King, J.F., Taggart, R.K., Smith, R.C., Hower, J.C., Hsu-Kim, H., 2018. Aqueous acid and alkaline extraction of rare earth elements from coal combustion ash. Int. J. Coal Geol. 195, 75–83. https://doi.org/10.1016/j.coal.2018.05.009

Laubie, B., Vaughan, J., Simonnot, M.-O., 2021. Processing of Hyperaccumulator Plants to Nickel Products, in: van der Ent, A., Baker, A.J.M., Echevarria, G., Simonnot, M.-O., Morel, J.L. (Eds.), Agromining: Farming for Metals. Springer International Publishing, Cham, pp. 47–61. https://doi.org/10.1007/978-3-030-58904-2_3

Lechevallier, S., 2010. Synthèse et caractérisation de nanoparticules luminescentes à base de lanthanides : vers de nouveaux bio-marqueurs (PhD dissertation). Université de Toulouse, Toulouse, France.

Li, H.Q., Hui, J.B., Wang, C.Y., Bao, W.J., Sun, Z.H., 2014. Extraction of alumina from coal fly ash by mixed-alkaline hydrothermal method. Hydrometallurgy 147–148, 183–187. https://doi.org/10.1016/j.hydromet.2014.05.012

Mochizuki, A., Nagashima, K., Wakita, H., 1974. The Synthesis of Crystalline Hydrated Double Carbonates of Rare Earth Elements and Sodium. Bull. Chem. Soc. Jpn. 47, 755–756. https://doi.org/10.1246/bcsj.47.755

Nagashima, K., Wakita, H., Mochizuki, A., 1973. The Synthesis of Crystalline Rare Earth Carbonates. Bull. Chem. Soc. Jpn. 46, 152–156. https://doi.org/10.1246/bcsj.46.152

Navrotsky, A., 2012. Energetic studies of nanophase and amorphous carbonate minerals, in: Goldschmidt 2012 Conference Abstrac. Presented at the Goldschmidt 2012 Conference, Cambridge University Press, Montreal, Canada, p. 2159. https://doi.org/10.1180/S0026461X00008434

Peng, H., Seneviratne, D., Vaughan, J., 2018a. Role of the Amorphous Phase during Sodium Aluminosilicate Precipitation. Ind. Eng. Chem. Res. 57, 1408–1416. https://doi.org/10.1021/acs.iecr.7b04538

Peng, H., Vaughan, J., Vogrin, J., 2018b. The effect of thermal activation of kaolinite on its dissolution and re-precipitation as zeolites in alkaline aluminate solution. Appl. Clay Sci. 157, 189–197. https://doi.org/10.1016/j.clay.2018.03.002

Price Market Analysis - Echemi [WWW Document], 2017. URL https://www.echemi.com (accessed 4.7.21).

Rodriguez-Blanco, J.D., Shaw, S., Benning, L.G., 2011. The kinetics and mechanisms of amorphous calcium carbonate (ACC) crystallization to calcite, viavaterite. Nanoscale 3, 265–271. https://doi.org/10.1039/C0NR00589D

Rumble, J.R., 2019. CRC handbook of chemistry and physics: a ready-reference book of chemical and physical data. CRC Press, Boca Raton, Fla.

Sommersacher, P., Brunner, T., Obernberger, I., 2012. Fuel Indexes: A Novel Method for the Evaluation of Relevant Combustion Properties of New Biomass Fuels. Energy Fuels 26, 380–390. https://doi.org/10.1021/ef201282y

Taggart, R.K., Hower, J.C., Dwyer, G.S., Hsu-Kim, H., 2016. Trends in the Rare Earth Element Content of U.S.-Based Coal Combustion Fly Ashes. Environ. Sci. Technol. 50, 5919–5926. https://doi.org/10.1021/acs.est.6b00085

Taggart, R.K., Hower, J.C., Hsu-Kim, H., 2018. Effects of roasting additives and leaching parameters on the extraction of rare earth elements from coal fly ash. Int. J. Coal Geol. 196, 106–114. https://doi.org/10.1016/j.coal.2018.06.021

Tang, M. cheng, Zhou, C.C., Pan, J.H., Zhang, N.N., Liu, C., Cao, S.S., Hu, T.T., Ji, W.S., 2019. Study on extraction of rare earth elements from coal fly ash through alkali fusion – Acid leaching. Miner. Eng. 136, 36–42. https://doi.org/10.1016/j.mineng.2019.01.027

Tilley, G.L., Doty, A.W., 1985. Production of rare earth compounds. US4497785A.

Vallina, B., Rodriguez-Blanco, J.D., Brown, A.P., Blanco, J.A., Benning, L.G., 2015. The role of amorphous precursors in the crystallization of La and Nd carbonates. Nanoscale 7, 12166–12179. https://doi.org/10.1039/C5NR01497B

Vaughan, J., Peng, H., Seneviratne, D., Hodge, H., Hawker, W., Hayes, P., Staker, W., 2019. The Sandy Desilication Product Process Concept. JOM 71, 2928–2935. https://doi.org/10.1007/s11837-019-03617-2

Whittington, B.I., 1996. The chemistry of CaO and Ca(OH)2 relating to the Bayer process. Hydrometallurgy 43, 13–35. https://doi.org/10.1016/0304-386X(96)00009-6

Yang, Q.C., Ma, S.H., Zheng, S.L., Zhang, R., 2014. Recovery of alumina from circulating fluidized bed combustion Al-rich fly ash using mild hydrochemical process. Trans. Nonferrous Met. Soc. China 24, 1187–1195. https://doi.org/10.1016/S1003-6326(14)63178-2

Yu, Z., Wang, M., Wang, L., Zhao, L., Feng, Z., Sun, X., Huang, X., 2020. Preparation of crystalline mixed rare earth carbonates by Mg(HCO3)2 precipitation method. J. Rare Earths 38, 292–298. https://doi.org/10.1016/j.jre.2019.05.006

Zhu, D., Chen, Q., Qiu, T., Zhao, G., Fang, X., 2021. Optimization of rare earth carbonate reactive-crystallization process based on response surface method. J. Rare Earths 39, 98–104. https://doi.org/10.1016/j.jre.2020.03.011

Chapter 5:
Viability of RE agromining

The purpose of this chapter is to develop a viability study for RE agromining. To do so, the study background is established, the marketable product is defined, and the recovery processes are designed for pilot scale. A systematic inventory of the processes inputs and outputs (emissions) is conducted to provide two metrics: The E factor, the amount of waste generated and reagent needed per unit of salable product produced; And the economic cost per unit of mass of bio-ore processed. Considering current market prices, the economic viability of the process is estimated, and concentration threshold for REEs in HA biomass is discussed (Figure 78).

5.1 Framework of the study

5.1.1 Geographical setting

In this work, we propose that the field used for RE agromining is the mine tailings in Southern China. As mentioned in the third chapter (Resource Characterization), mine tailings are not suitable for agricultural purposes, subject to intense erosion, and a great surface is available. There is also a favorable incentive from the authorities for ecological restoration of these degraded land. As an illustration, the research team has access to an area of 530 000 ha, currently being restored by active revegetation.

The consecration of one to several hectares for *D. linearis* cultivation and demonstration of RE agromining appears achievable. It has been shown earlier that they provide a favorable habitat for *D. linearis*, as well as an available pool of REEs. The area is located in Dingnan county, Jiangxi Province, (GPS coordinates: 24°57’17.63” N 115°05’33.55” E) and is readily accessible by car.

Even if the field is located in rural area, access to electricity, water, and transportation of supplies (delivery of chemical reagents, shipping of the REE product) should not pose any difficulty. Hence, the processing facility can be located in a nearby area, to limit the transportation of biomass over large distances.

5.1.2 Targeting a marketable product

Ideally, the products obtain from the recovery process should be solids, have a direct application, or be capable of being refined in existing metallurgical plants. High purity (>99 %) RE carbonate as the final product of the process presented in the last chapter fits this purpose.

The processes previously developed for *D. linearis* (Chour *et al.*, 2018, 2020) should also be discussed. First, the direct extraction of REEs from the biomass by sulfuric acid, followed by oxalate precipitation yields a suitable solid product. Additional calcination of the oxalate improves the RE content of the product.

Secondly, the other resin-enhanced extraction yields a very acidic solution (HNO_3, 3 M) loaded with REEs. Neutralization and precipitation would be too costly, considering the high acidity of the solution (3 M) and the relatively low REE concentration (65 $mg.L^{-1}$ ∑REEs). This solution is better suited for

subsequent separation of the REEs, generally conducted by solvent extraction, which is outside the scope of this work.

Two products can therefore be considered: a high purity RE carbonate (>99 %, this work), a RE oxalate or oxide (purity >95 %) (Chour *et al.*, 2020). The RE carbonate is produced via the ash process (ASH process), and the RE oxide via the sulfuric acid extraction process (SULF process).

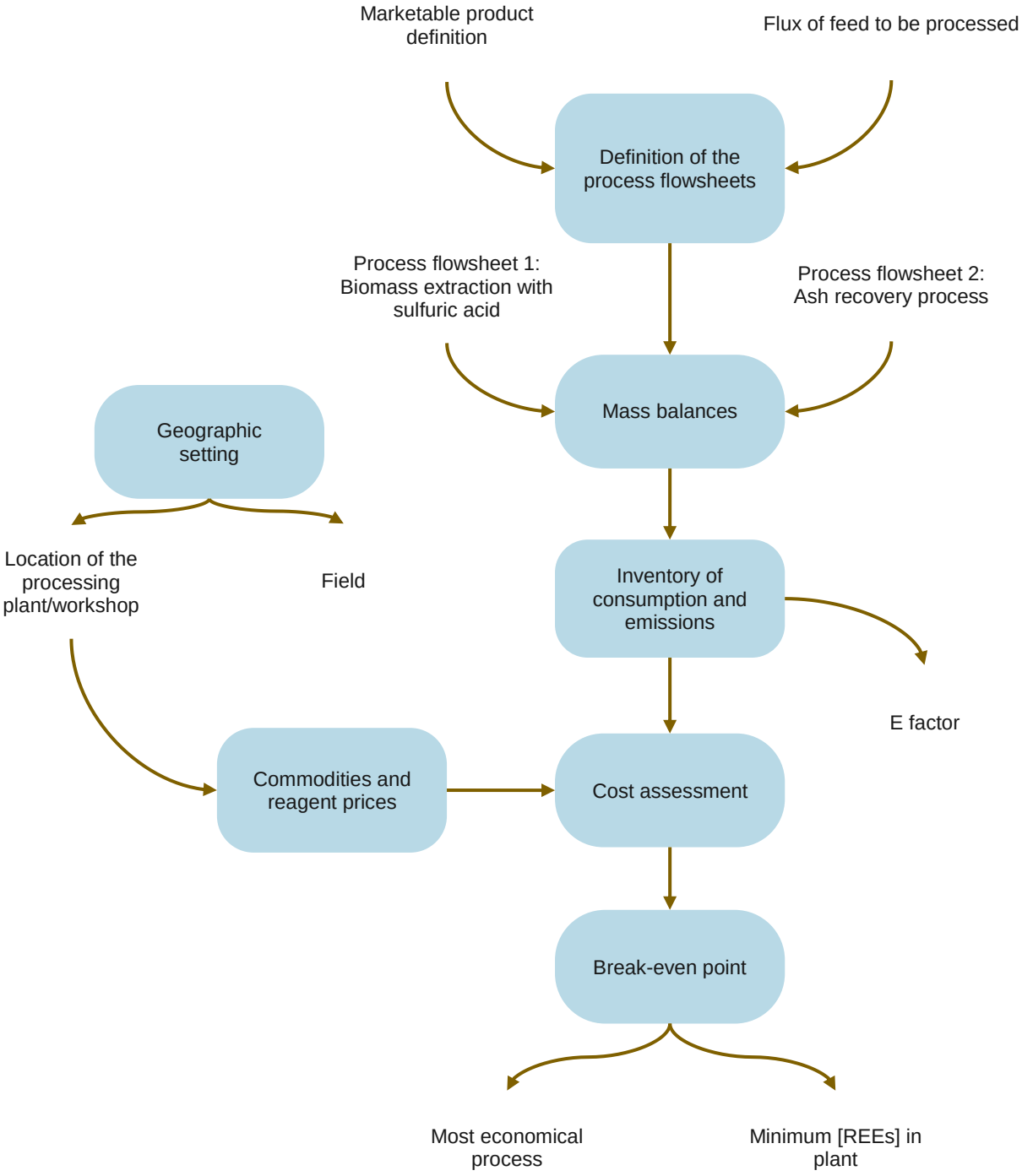

Figure 78: Approach to the proposed economic study

5.2 Pilot scale processes

The flowsheets of the aforementioned processes are represented (Figure 79, Figure 80)

For ease of understanding, the mass flows and operations are represented separately. However, at the pilot scale, some operations can be conducted using the same tank for example.

The basis is the production of a hectare cultivated tailing, generating 3 $t.y^{-1}$ of pinnae. In a first approach, the REE concentration in pinnae will be assumed to be constant and set to 2 $mg.g^{-1}$∑REEs. The repartition of REEs is conserved (in regards to Chapter 3). An average molar weight of 141.2 $g.mol^{-1}$ is used (weighted mean using REE repartition).The mass inventory is conducted for both process, managing the assumptions based on the lab scale processes.

5.2.1 SULF Process

5.2.1.1 Calculation assumptions

For the SULF process (Figure 79), the assumptions are the following:

- No matter is lost during the grinding operation $F_0 = F_1$

For the extraction step:

- The amount of extracting reagent (H_2SO_4) and water depends on the total biomass processed rather than the REE content (variable)
- The aqueous concentration of H_2SO_4 is 0.25 M
- The S/L ratio is 10 % (by weight), higher than published experiments (2 %)
- After filtering the spent biomass, the extraction yield is 80 % for all REEs
- The filtered spent biomass is wet, with a water content of 30%.

For the precipitation step:

- The pH of the pregnant leach solution (F_5) is adjusted to 2.5 using NaOH. To do so, the molar ratio NaOH/H_2SO_4 is 1.5
- The oxalic acid to REEs molar ratio is 3
- The precipitation yield is 100 % for all REEs

Finally:

- The calcination yield is 100 % for all REEs

Using previous assumptions, and readily available physico-chemistry data (*e.g.*, H_2SO_4 density, molar weights, *etc.*)(Rumble, 2019), the mass balance can be computed (Table 31). Calculations were performed in an MS Excel worksheet, with three main parameters: pinnae mass flow input, REE concentration in the pinnae, and extraction S/L ratio.

5.2.1.2 Process outputs and requirements

The main result is the production of 5.6 $kg.y^{-1}$ of a mixed RE oxide. This value is proportional to the pinnae mass flow input, the pinnae REE concentration and the extraction rate.

Another output is the treated biomass, wet, acidic and enriched in sulfate. A prospect for this by-product could be to valorize it as an agricultural amendment. Neutralization could be conducted by

mixing it with lime ($Ca(OH)_2$ or CaO), so that sulfate anions form inert gypsum $CaSO_4 \cdot xH_2O$. Then, the solid mixture can be composted.

The fate of the spent liquor flux should also be examined. The solution inherits significant amounts of Na^+, and SO_4^{2-} from the previous steps. Cooling the solution to precipitate Na_2SO_4 (mirabilite) might be feasible as the solubility of this salt varies greatly with temperature around room temperature (from 281 $g.L^{-1}$ at 25 °C to 62 $g.L^{-1}$ at 5 °C). Depending on the purity of the obtained crystals, a marketable by-product could be obtained.

As for the requirements, process water needs depend on the biomass input and the S/L ratio. For the set values, a consumption of approximately 20 $m^3.y^{-1}$ can be expected. The total mass of chemical reagents needed is about 1 100 $kg.y^{-1}$ mainly consisting of H_2SO_4 and NaOH, the oxalic acid requirements being marginal (9.2 $kg.y^{-1}$).

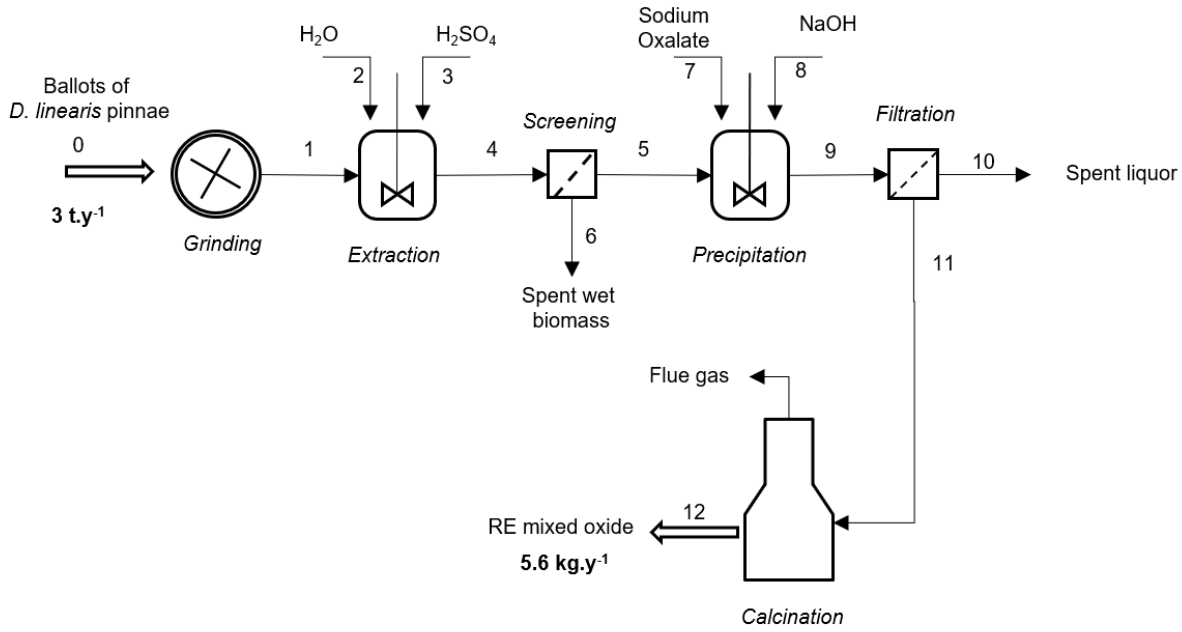

Figure 79: Process flow diagram for the direct extraction of REEs from *D. linearis* biomass (SULF process). Fluxes are numbered according to Table 31.

It is already possible to calculate the environmental factor (E factor), defined as the ratio of the mass of waste to that of the products ((Sheldon, 1992).

Because solvents and water are well recycled in medium scale plants, they are generally not included in E_{factor} calculations. To account for this, water consumption is excluded, but dry biomass is counted as waste, as well as are all chemicals used (ending as dissolved salts).

The E_{factor} is thus:

$$E_{factor} \approx \frac{3\,000 + 1\,100}{5.6} = 732\ \text{kg.}\,\text{kg}^{-1} \quad (36)$$

To reduce the E_{factor}, and thus the process efficiency, the valorization of by-products (as proposed earlier) could add mass to the denominator. Moreover, the addition of recycling loops reduces the overall need for chemical reagents (almost always in excess).

Table 31: Mass flows for the direct extraction process using H_2SO_4 (SULF)

F	Name	Mass flow	REEs		H_2SO_4		Oxalic acid		NaOH		RE oxalate		RE Oxide	
		($kg.y^{-1}$)	($mol.y^{-1}$)	($kg.y^{-1}$)	($mol.y^{-1}$)	($kg.y^{-1}$)	($mol.y^{-1}$)	($kg.y^{-1}$)	($mol.y^{-1}$)	($kg.y^{-1}$)	($mol.y^{-1}$)	($kg.y^{-1}$)	($mol.y^{-1}$)	($kg.y^{-1}$)
0	Pinnae	3 000	42.6	6.0	-	-	-	-	-	-	-	-	-	-
1	Ground pinnae	3 000	42.6	6.0	-	-	-	-	-	-	-	-	-	-
2	Water	19 675	-	-	-	-	-	-	-	-	-	-	-	-
3	H_2SO_4 (95%)	690	-	-	6 683	690	-	-	-	-	-	-	-	-
4	Biomass suspension	23 365	42.6	6.0	6 683	690	-	-	-	-	-	-	-	-
5	Pregnant Leach Solution	19 465	34.0	4.8	6 349	655	-	-	-	-	-	-	-	-
6	Spent wet biomass	3900	8.5	1.2	295	30	-	-	-	-	-	-	-	-
7	Oxalic acid	9.2	-	-	-	-	102	9.2	-	-	-	-	-	-
8	NaOH	401	-	-	-	-	-	-	10 025	401	-	-	-	-
9	RE-oxalate suspension	19 768	34.0	4.8	-	-	51	4.5	-	-	17.0	9.3	-	-
10	Spent liquor	19 759	-	-	-	-	51	4.5	-	-	-	-	-	-
11	RE oxalate (REE_2Ox_3)	9.3	34.0	4.8	-	-	-	-	-	-	17.0	9.3	-	-
12	RE oxide (REE_2O_3)	5.6	34.0	4.8	-	-	-	-	-	-	-	-	17.0	5.6

5.2.1.3 Possible recycling loops

Yet, no recycling has been considered, as it was not explored at the lab scale. However, the optimization of the process must include the recycling of the pregnant leach solution (F_5). After one extraction cycle, the solution is still acidic and could be recycled. Co-extracted Si, organic carbon, and other impurities (Al, K) could cause issues (*e.g.*, gel formation, filter clogging) upon reaching a threshold concentration. A decreasing in the acidity of the extracting solution can be expected, and can be compensated by small additions of acid.

It is suggested that a number of *N* extractions could be performed before reaching the threshold of extraction issues. The mass balance can be easily reperformed by multiplying the extraction S/L ratio in the worksheet by *N*.

Finally, the process design could benefit from oxalate recycling which is a common industrial practice (Habashi, 2013). Precipitated oxalates are digested with NaOH to form RE hydroxides, while sodium oxalate is regenerated (Equation (36)). Later on, the hydroxides are calcinated to form oxides and CO_2 release is thus avoided.

$$Ln_2(C_2O_4)_{3(s)} + OH^- \rightarrow 2Ln(OH)_{3(s)} + 3(C_2O_4)^{2-} \quad (37)$$

The accumulation of Na and SO_4 could be dealt with the precipitation of mirabilite, as suggested earlier.

5.2.2 ASH Process

5.2.2.1 Calculation assumptions

For the ASH process (Figure 80), the assumptions are as follows:

- The ash yield is constant, and set to 5.7 % (see Chapter 3)

During the alkaline leaching step (the reader is referred to Chapter 4)

- The S/L ratio is 50 $g.L^{-1}$ and the soda concentration is 20 % (by weight)
- No REE is lost to the aqueous phase
- The mass of water required for the rinsing step is 12 times the mass of ash
- After alkaline leaching and rinsing, the mass of treated ash (dry) is 0.25 × the mass of ash

During the extraction step:

- Variation in the composition of *D. linearis* does not affect acid consumption
- Even though the operation must be controlled to maintain a constant pH, the acid consumption is set to 7.3 g HNO_3 (1 M solution) per g of treated ash (dry basis):
- The S/L ratio is increased to 30 $g.L^{-1}$ to limit water usage (3 $g.L^{-1}$ in Chapter 4)
- After filtration, the extraction yield is 70 % for all REEs but Ce. Initially, Ce makes up for 15 % of the REE content:
- The mass of final residue was determined experimentally to be 0.58 × the mass of rinsed ash (dry basis):

For the precipitation step:

- The NH_4HCO_3 to REEs molar ratio is 3
- The precipitation yield is 100% for all REEs
- The molecular formula of the carbonate compound is $Ln_2(CO_3)_3 \cdot 2.1H_2O$, and its weighted average molar weight is M=500.2 $g.mol^{-1}$

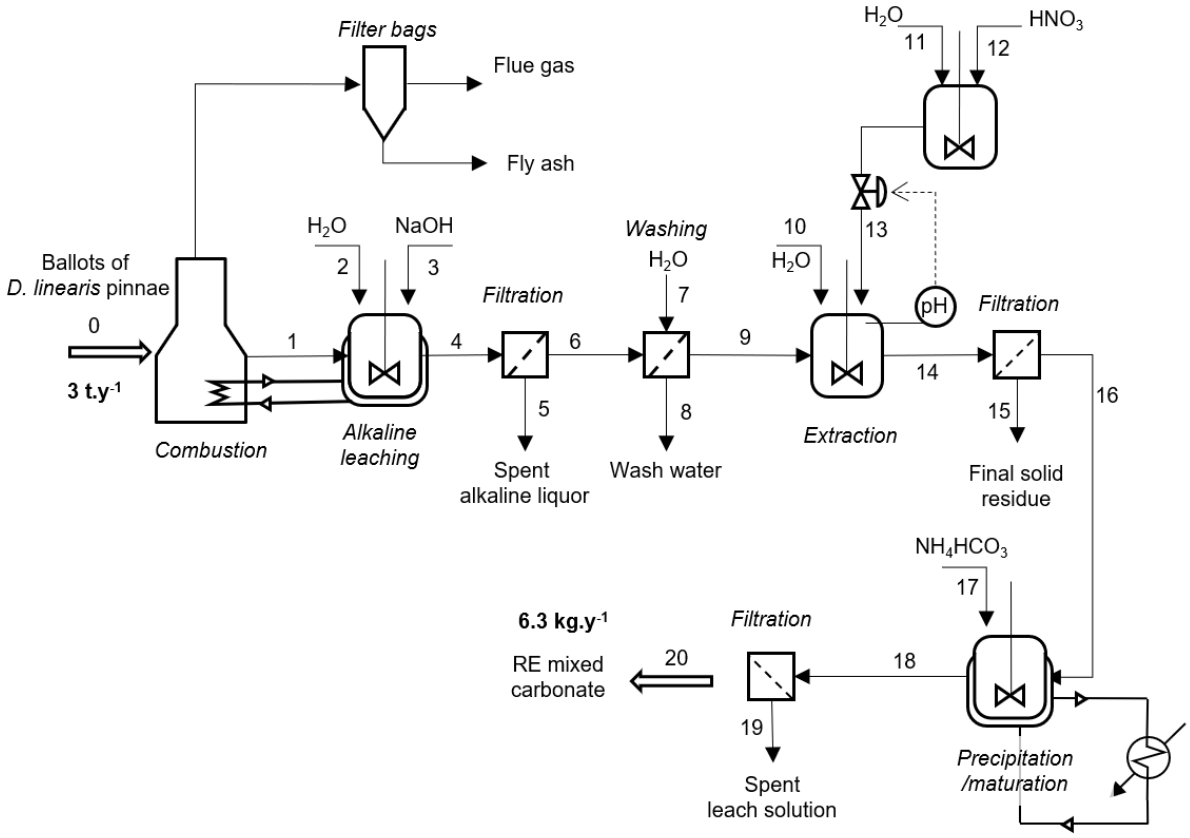

Figure 80: Process flow diagram for the recovery of REEs from the ash of *D. linearis* (ASH process). Fluxes are numbered in regard to Table 32.

Table 32: Mass flows for the ash extraction process (ASH)

F	Name	Mass flow	REEs		NaOH		HNO_3 (1 M)		NH_4HCO_3		RE carbonate	
		($kg.y^{-1}$)	($mol.y^{-1}$)	($kg.y^{-1}$)	($mol.y^{-1}$)	($kg.y^{-1}$)	($mol.y^{-1}$)	($kg.y^{-1}$)	($mol.y^{-1}$)	($kg.y^{-1}$)	($mol.y^{-1}$)	($kg.y^{-1}$)
0	Pinnae	3 000	42.5	6.0	-	-	-	-	-	-	-	-
1	Ash	171	42.5	6.0	-	-	-	-	-	-	-	-
2	Water	3 420	-	-	-	-	-	-	-	-	-	-
3	NaOH	855	-	-	21 375	855	-	-	-	-	-	-
4	Treated ash suspension	4 446	42.5	6.0	-	-	-	-	-	-	-	-
5	Spent alkaline liquor	4 361	-	-	-	-	-	-	-	-	-	-
6	Treated ash	86	42.5	6.0	-	-	-	-	-	-	-	-
7	Wash water clean	2052	-	-	-	-	-	-	-	-	-	-
8	Wash water	2095	-	-	-	-	-	-	-	-	-	-
9	Rinsed ash	43	42.5	6.0	-	-	-	-	-	-	-	-
10	Suspension water	1 425	-	-	-	-	-	-	-	-	-	-
11	Solution Prep. Water	283	-	-	-	-	-	-	-	-	-	-
12	HNO_3 (68 wt.%)	29	-	-	-	-	312	29	-	-	-	-
13	HNO_3 (1 M)	312	-	-	-	-	312	312	-	-	-	-
14	Extraction suspension	1 780	42.5	6.0	-	-	-	-	-	-	-	-
15	Final solid residue	25	17.2	2.4	-	-	-	-	-	-	-	-
16	Pregnant leach solution	1 755	25.3	3.6	-	-	-	-	-	-	-	-
17	NH_4HCO_3	6.0	-	-	-	-	-	-	108	8.6	-	-
18	Carbonate suspension	1 761	25.3	3.6	-	-	-	-	-	-	12.6	6.3
19	Spent leach solution	1 755	-	-	-	-	-	-	-	-	-	-
20	RE mixed carbonate	6.3	25.3	3.6	-	-	-	-	-	-	12.6	6.3

5.2.2.2 Process outputs and requirements

The mass balance of the process is presented in Table 32. The annual production is expected to be about 6.3 kg of mixed RE carbonate. It is important to note that this compound is exempt of Ce because of the extraction procedure. Hence, it is relatively richer in other REEs than the original plant. As an illustration the average REE composition of the carbonate precipitate is presented (Table 33).

Table 33: Average RE composition of the carbonate produced in this thesis. Contents are expressed as oxide to facilitate comparison with other RE concentrates.

RE Oxide	**REO content ± SD (n=7) (%)**
La_2O_3	34.14 ± 2.08
Ce_2O_3	0.75 ± 0.05
Pr_2O_3	5.98 ± 0.22
Nd_2O_3	22.66 ± 1.19
Sm_2O_3	3.51 ± 0.29
Eu_2O_3	0.40 ± 0.03
Gd_2O_3	1.56 ± 0.07
Tb_2O_3	0.20 ± 0.01
Dy_2O_3	0.82 ± 0.03
Ho_2O_3	0.11 ± 0.01
Er_2O_3	0.63 ± 0.04
Tm_2O_3	0.18 ± 0.01
Yb_2O_3	0.11 ± 0.01
Lu_2O_3	0.02 ± 0.01
Y_2O_3	2.72 ± 0.15
∑REO	73.8 ± 4.2

In comparison with the SULF process, the amount of solid waste is far inferior, as the final solid residue is 25 $kg.y^{-1}$ (*vs.* 3900 kg wet biomass). Of course, the main reason is that the biomass is burned, and the organic carbon converted to CO_2. Nonetheless, the fate of the final solid residue, mainly composed of aluminosilicate and $Ce(OH)_2$, should be addressed as 4.3 kg are produced per kg of carbonate. Further characterizations are needed to determine how this by-product can be valorized. This could not be conducted in this thesis as produced volumes were extremely small (<1 g).

The required amounts of water (alkaline leaching solution, rinsing water, and extracting solution) total 7.1 $m^3.y^{-1}$. Hence, without the recycling loops, the water consumption is inferior to that of the SULF process (20 $m^3.y^{-1}$). The amount of chemical reagent needed ($NaOH_{(s)}$, HNO_3 (68 wt%), $NH_4HCO_{3(s)}$) is comparable, totaling 890 $kg.y^{-1}$ (*vs.* 1 100 $kg.y^{-1}$ in the SULF process), with sodium hydroxide making the most of the consumption (855 $kg.y^{-1}$).

It appears that the ASH process is slightly more economical than the SULF process, in terms of water and reagent consumption when comparing mass fluxes. The REE recovery yield is however lower, 70 % for all REEs but Ce, vs. 80 % in the SULF process.

To account for that, the E factor can be computed. Water usage is again excluded from calculations. Carbon dioxide production from the combustion step is not counted as waste because it is returned to the atmosphere after being sequestrated by the plant. Reagents used are counted as waste (eventually ending as disposed salts).

Finally, to allow for comparison, the carbonate product is hypothetically converted to its oxide form, using the values in Table 33. Hence, the annual REO production would be 4.65 $kg.y^{-1}$, consistently inferior to that of the SULF process.

The E factor is thus:

$$E_{factor} \approx \frac{25 + 890}{4.65} = 197\ kg.\,kg^{-1} \quad (38)$$

Because its E_{factor} is lower, the ASH process appears more efficient than the SULF process, generating three times less waste per mass unit of REO produced. Even though, these calculations were performed on the basis of lab-scale experiment, and without the implementation of by-product valorization or recycling loops, they provide quantified data on the process efficiency.

5.2.2.3 Possible recycling loops

Optimization can be sought by recycling some of the solution fluxes. As described in the previous chapter, the wash water (F_7) is an alkaline solution containing diluted amounts of K, Si, Al, Ca, and Mg. It might be recycled as the base matrix for the alkaline solution instead of pure water (F_2). By doing so, the amount of fresh water utilized can be diminished.

In contrast, spent alkaline liquor (F_5) is expected to be more difficult to recycle because of its high dissolved solid content, the most preoccupying being SiO_2. To tackle that issue, the desilication of the solution can be envisaged by adding $Ca(OH)_2$ or $Mg(OH)_2$ or KOH, in a separate tank. In this way, $Ca_3Al_2(SiO_4)_n(OH)_{(12-4n)}$ can be precipitated (Whittington, 1996). With $Mg(OH)_2$ or KOH additions, the previously observed insoluble minerals (biotite $KMgSi_3AlO_{10}(OH)_2$, microcline $KAlSiO_3$) are willingly precipitated while NaOH is kept in solution. Although these are speculative suggestions, desilication is a modern industrial solution for NaOH recycling in contemporary Bayer plants (Peng and Vaughan, 2018; Vaughan *et al.*, 2019).

Attention should be paid to the increase in Pb concentration after each recycling loop. For example, for a solid/liquid ratio of 50 $g.L^{-1}$, Pb concentration in the alkaline liquor was 23 $mg.L^{-1}$ (90% were extracted from the ash). An adapted decontamination of the spent liquors is mandatory. Chemical equilibrium calculations (by CHESS) suggests that $Pb(OH)_3^-$ is the dominant Pb species in concentrated NaOH. The previously cited desilication products (*e.g.*, biotite or microcline) are clay minerals and may be able to retain anionic $Pb(OH)_3^-$ by functioning as ion-exchangers.

Finally, the spent leach solution (F_{19}) is a slightly acidic solution (pH ≈ 6), containing an excess of NH_4HCO_3, and limited amounts of dissolved Mg and Ca. A small fraction of this solution can be used to prepare another batch of precipitating solution (concentrated NH_4HCO_3).

5.2.3 Integration of recycling loops

The implementation of the aforementioned recycling loops must be conducted experimentally, preferably when a pilot setup is available. Mass balance calculations have not been performed given the uncertainties and the feasibility of each proposed loop. Nevertheless, they are exposed in the following flowsheets as a guide for future implementation (Figure 81, Figure 82).

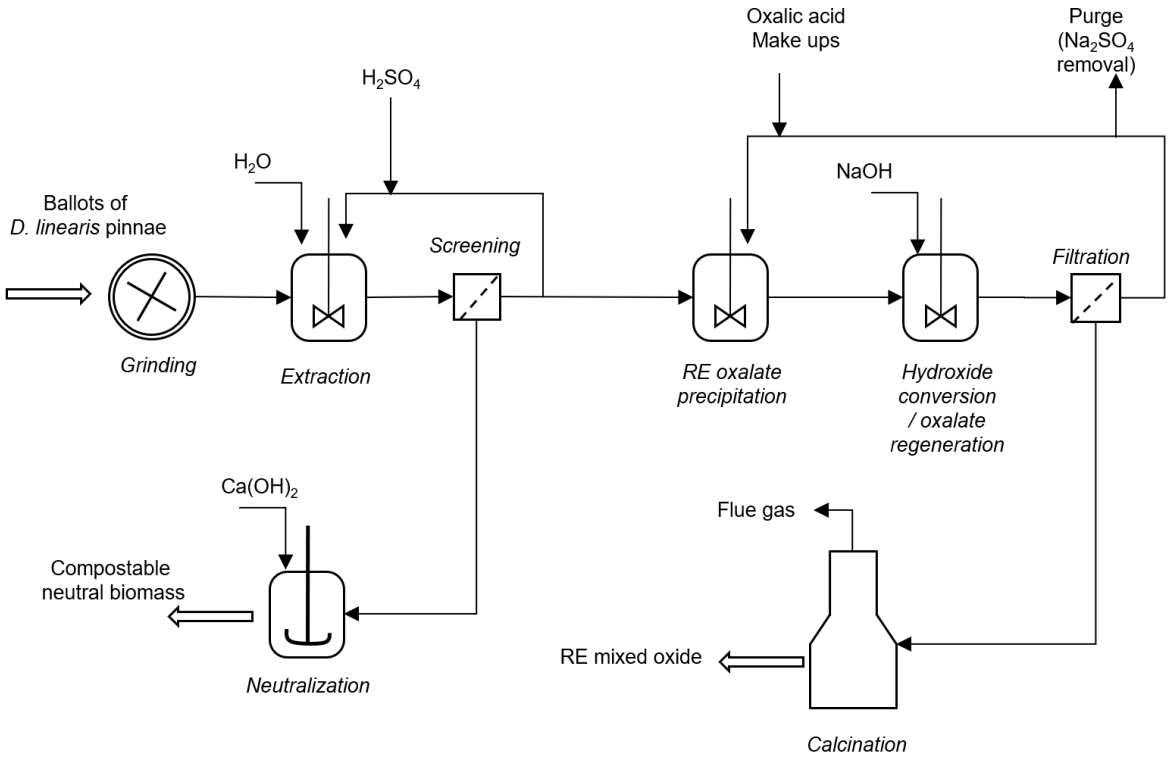

Figure 81: SULF process flowsheet with the proposed recycling loops

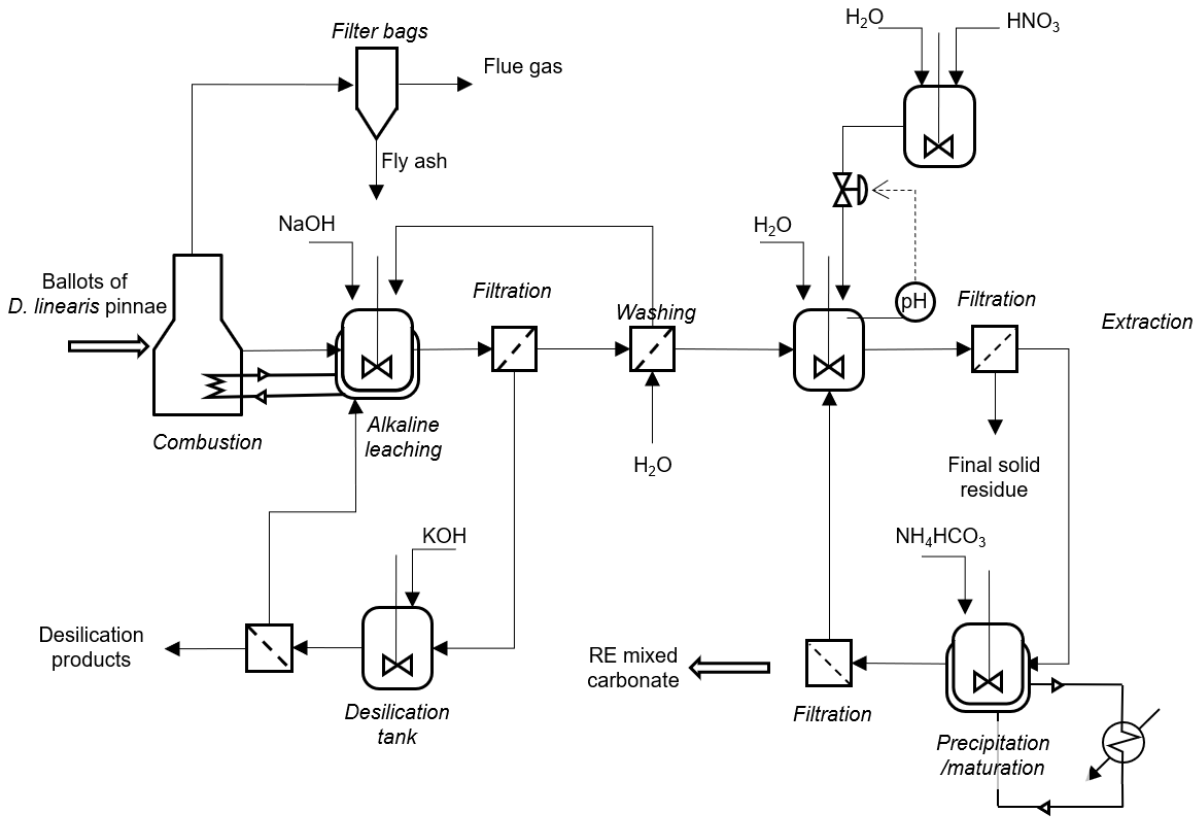

Figure 82: ASH process flowsheet with the proposed recycling loops

5.2.4 Short note on energetic aspects

For the ASH process, the proposed flowsheet suggests using the thermal energy from the combustion step, to reach the temperature of 90 °C in the alkaline leaching tank. Based on one kg of biomass, we demonstrate that the process can be energy self-sufficient.

- The energy released from the combustion of 1 kg of biomass is ~19 MJ (see Chapter 3, section 3.2.1).
- The ash yield being 5.7%, the mass of ash produced is 57 g. Consequently, a volume of 1.2 L is required to conduct alkaline leaching (at 50 $g.L^{-1}$), which translates into a solution mass of 1.4 kg.
- The thermal energy required to reach 90 °C in the alkaline leach tank can be approximated by the energy required for the soda solution at room temperature (20 °C) to reach 90 °C, neglecting the heat transferred to the reactor itself. The energy is thus:

$$E = \Delta H_{\text{soda solution}} = m_{\text{solution}} \times Cp_{\text{solution}} \times \Delta T \quad (39)$$

$$\approx m_{\text{solution}} \times Cp_{H_2O} \times \Delta T \quad (40)$$

$$= 1.4 \times 4.185 \times (90 - 20) = 410 \text{ kJ} \quad (41)$$

The energy required to treat the ash from one kg of biomass constitutes *ca.* 2% of the produced heat. Additionally, the heat released during the dissolution of the NaOH salt was not considered. Hence, even though heat loss is unavoidable through the reactor walls, and heat exchangers are not ideal, the alkaline leaching step can unambiguously beneficiate from the combustion heat.

The crystal maturation step is also conducted above room temperature (40 °C). From the previous calculations, it can be reasonably assumed that the necessary heat is available for this step as well.

Regarding the SULF process, the main energetic consumption resides in the calcination step. Because of the small amount of solid treated (the annual mass of RE oxalate produced is around 9 $kg.y^{-1}$.), the energy consumption will mostly depend on the furnace design, and the number of batches conducted over the year.

5.3 Economic aspects

5.3.1 Estimation of the possible income

The possible annual income (in $USD.y^{-1}$) is the sum of the REO produced ($F_{REO,i}$, in $kg_{REO,i}.y^{-1}$) multiplied by their wholesale price (p_i, in $USD.kg_{REO,i}$).

$$\text{Income} = \sum_i (F_{REO,i} * p_i) \quad (42)$$

Assuming that, aside from the extraction step, there are no losses of REEs in the process, the amount of RE oxide produced ($F_{REO,i}$), is:

$$F_{REO,i} = BM * [REO]_{i,BM} * X_i \quad (43)$$

With, for each REE (i), X_i its individual extraction rate in the process, $[REO]_{i,BM}$ its concentration in the biomass (in $kg_{REO,i}.kg_{biomass}^{-1}$), and BM, the biomass processed (in $kg_{biomass}.y^{-1}$)

The income is thus:

$$\text{Income} = BM * \sum_i ([REO]_{i,BM} * X_i * p_i) \quad (44)$$

For the SULF process, assuming that the extraction yield is the same for each REE (X_{SULF} in this case), and for the ASH process, the extraction yield for Ce is 5 % and 70 % for all other REEs.

Consistent with previous calculations, prices are the ones presented in the first chapter (as of December 2020). The composition of the biomass is the same as that used for mass balances calculations, with average concentration of ∑REEs = 2 $mg.g^{-1}$ = 2.36 10^{-3} $kg_{REO}.kg^{-1}$.

By doing so, the expected revenue from the SULF process is estimated to be 155 $USD.y^{-1}$, and 134 $USD.y^{-1}$ for the ASH process. Similarly to what was exposed in the 3rd chapter, more optimistic concentrations can be expected for *D. linearis*, with contents up to 3.89 $mg.g^{-1}$ (∑REEs). Consequently, the revenue would increase to 302 and 261 $USD.y^{-1}$ for the SULF and ASH process, respectively.

For the ASH process, the heat generated can be converted to electricity and sold, providing additional incomes. Given the relatively small scale of the envisaged production, a more realistic approach would be to substitute traditional combustible with similar characteristics (*e.g.*, wood, straws). Hence, no hypothesis is made about the amount of energy is recovered, converted to electricity, *etc*.

It was stated earlier that wood pellets have a similar higher heating value that *D. linearis* (*ca*. 20 $MJ.kg^{-1}$). Wholesale prices currently varies from 80 to 180 $USD.t^{-1}$ from Chinese suppliers, depending on the type of wood and quality. In this work we will consider that 80 $USD.t^{-1}$ is a reasonable estimation for *D. linearis* biomass destined to energy production. Hence, the corresponding income attributable to combustion would be 240 $USD.y^{-1}$, therefore, the overall revenue for the ASH process would totalize 501 $USD.y^{-1}$.

5.3.2 Commodity and reagent prices

China is major producer and supplier of numerous chemical compounds. For the selected processes, the required reagents and their prices (originally in RMB) are presented in Table 34.

Prices were collected from websites displaying producer prices, do not include shipping (from China), and were converted to USD with a conversion rate of 1 USD = 6.39 RMB (as of November 16, 2021). The quantities ordered were selected to match as closely as possible the amount needed for one year (Table 31, Table 32).

Unless the Al concentrations are challengingly high, it is suggested to use tap water for all solutions and suspensions requirements. The price for tap water for industrial use was reported to be about 4.8 $RMB.t^{-1}$ in September 2021 equivalent to 0.751 $USD.t^{-1}$ (CEIC, 2021).

Table 34: Current prices (as of November 16, 2021) of the reagents required for the selected processes. Prices extracted from www.echemi.com and www.alibaba.com.

Reagent name	Formula	Form	Purity	Order quantity (kg)	Order price (USD)	Unitary price (USD.kg^{-1})
Sodium hydroxide	NaOH	Pellets	Industrial grade (>99%)	1 000	430	0.43
Ammonium bicarbonate	NH_4HCO_3	Powder	Food grade (>99.9%)	25	31	1.25
Oxalic acid	$C_2H_6O_2$	Powder	Reagent grade (>99.5%)	25	113	4.52
Sulfuric acid	H_2SO_4	Liquid	98%	1 000	114	0.11
Nitric acid	HNO_3	Liquid	68%	25	27	1.08
Water	H_2O	Liquid	-	-	-	7.51 10^{-4}

5.3.3 Process cost assessment

The cost of the process obviously depends on the cost of producing the biomass (fertilization, planting, harvesting). At the time being, no field trials have been succeeded for *D. linearis*, hence too much uncertainty remains to provide an acceptable estimate of the biomass related cost. However, the cost attributable to the transformation process itself can be estimated based on previous mass balances.

Using the prices from Table 34 and the mass fluxes from Table 31 and Table 32, the cost of reagents and commodities is estimated for both process (Table 35, Table 37). As described, the annual cost of the SULF process is 308 USD.y^{-1}, and 415 USD.y^{-1} for the ASH process.

Table 35: Reagent and commodities related cost for the SULF process

F	Mass flux name	Mass flux (kg.y^{-1})	Unitary price (USD.kg^{-1})	Cost (USD.y^{-1})
2	Water	19 675	$7.51 \cdot 10^{-4}$	15
3	H_2SO_4 (95%)	690	0.11	76
7	Oxalic acid	9	4.52	42
8	NaOH	401	0.43	172
			Sum	308

Regarding the SULF process, the main expense concerns sodium hydroxide, used for pH adjustment right before oxalate precipitation. A partial neutralization is indeed mandatory to convert oxalic acid into oxalate anions. Sodium hydroxide was used at the laboratory scale because it was conveniently available.

For the pH range considered (from 0.8 to 3), it can be substituted by an alternative cheaper alkali. Common alkalis and their market price are presented for reference (Table 36). Slaked lime ($Ca(OH)_2$) is an industrial commodity, widely available and cheaper than soda (0.150 USD.kg^{-1}). Additionally, for

the same mass of reagent, more hydroxy anions are provided: 370 $kg.y^{-1}$ would be required, instead of 401 $kg.y^{-1}$ NaOH. Because the precipitation of REEs with oxalate is highly selective, industrial grade should be sufficient. By doing so, the cost of partial neutralization would decrease from 172 $USD.y^{-1}$ to 56 $USD.y^{-1}$. This adjustment of the process will be referred to as SULF2.

Essays could be conducted with even cheaper alkali products originating from the circular economy (*e.g.*, biomass ash) to minimize cost and impacts of the process.

Recycling the extraction solution is also expected to cause cost reductions, as H_2SO_4 is the second most important cost of the process. Finally, oxalate being the most expensive reagent, its recycling (even partial) will greatly decrease the associated cost.

In an optimistic scenario where the total concentration of REEs is maximum (3.89 $mg.g^{-1}$ ∑REEs), mass balances are recalculated as well as the process costs. In this case, expenses of sulfuric acid and soda are identical, but the oxalate requirements increase.

The process cost would reach 347 $USD.y^{-1}$, representing a 13 % increase on the one hand. On the other hand, the income would increase to 302 $USD.y^{-1}$, thus reducing the gap between cost and benefits and converging towards profitability. If $Ca(OH)_2$ is used for partial neutralization (process SULF2), profitability of the process is already ensured.

Table 36: Alternative reagents and their prices

Reagent name	**Formula**	**Form**	**Purity**	**Ordered quantity (kg)**	**Order price (USD)**	**Unit price ($USD.kg^{-1}$)**
Potassium hydroxide	KOH	Flakes	Industrial grade (>90%)	400	397	0.99
Sodium carbonate	Na_2CO_3	Powder	Industrial grade (>99%)	1000	358	0.358
Slaked lime	$Ca(OH)_2$	Powder	Industrial grade (>99%)	1000	150	0.150

As for the ASH process (Table 37), the main expense concerns the sodium hydroxide used for the alkaline leaching step. In this case, the alkali cannot be substituted as the goal of this step is to solubilize Al and Si by forming their sodium aluminate form ($NaAlO_2$, $NaSiO_3$) (Habashi, 2016).

Yet, as suggested earlier (5.2.2.3 Possible recycling loops), NaOH recycling is possible at the expense of desilication of the leaching solution (Peng and Vaughan, 2018; Vaughan *et al.*, 2019).

Otherwise, the extraction cost is minimal as dilute HNO_3 is enough to extract the REEs thanks to the process design. Depending on the product desired purity, an even cheaper process can be achieved using sulfuric acid for extraction, and sodium carbonate for precipitation. In this case, after mass balances recalculations, the cost of the tuned ASH process (referred to as ASH2) averages 379 $USD.y^{-1}$.

Table 37: Reagent and commodity costs for the ASH process

F	Mass flux name	Mass flux ($kg.y^{-1}$)	Unit price ($USD.kg^{-1}$)	Cost ($USD.y^{-1}$)
2	Water	3420	$7.51 \cdot 10^{-4}$	3
3	NaOH	855	0.43	368
7	Wash water	2052	$7.51 \cdot 10^{-4}$	1.5
10	Suspension water	1425	$7.51 \cdot 10^{-4}$	1.1
11	Prep. Water	283	$7.51 \cdot 10^{-4}$	0.2
12	HNO_3 (68 wt.%)	29	1.08	31
17	NH_4HCO_3	6	1.25	7
			Sum	415

5.3.4 Overall viability of the process

The cost, income and the difference between cost and income for the described processes were calculated for two REE concentrations in the biomass (Figure 83).

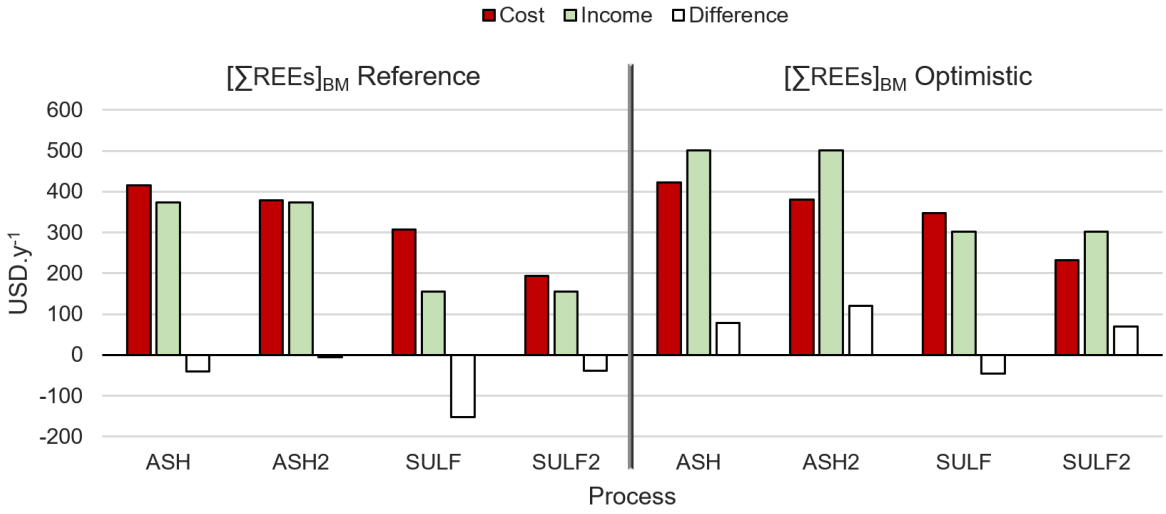

Figure 83: Cost, income, and difference for the considered process in $USD.y^{-1}$ for the 1 ha farm. Influence of REE concentration in biomass ($[REEs]_{BM}$) is illustrated for the reference value ($[\sum REEs]_{BM}$ = 2.0 $mg.g^{-1}$, left-side panel) and the optimistic value ($[\sum REEs]_{BM}$ = 3.9 $mg.g^{-1}$, right-side panel).

In the case where the biomass concentration averages 2.0 $mg.g^{-1}$ ∑REEs, the difference between income and cost is negative for all processes considered. In a more optimistic scenario where the fronds processed are richer in REEs (3.9 $mg.g^{-1}$ ∑REEs), both ASH and ASH2 are profitable, as well as the SULF2 process. In all cases, the ASH2 process is always the most cost-effective.

The ASH processes are the most expensive but are cost-effective due to heat recovery from combustion. The associated incomes permit to exceed the process costs and are required to reach viability. Careful usage of the heat provided is necessary, as the estimated incomes from heat recovery are *ca.* 50% of the earnings. Both processes are the most profitable with a benefit of 79 and 121 $USD.y^{-1}$ for ASH and ASH2 process, respectively.

The SULF process should not be abandoned yet, as several improvements can still be made. The SULF2 process is actually cost effective in the case of REE-rich biomass (benefit of 69 USD.y^{-1}). Additionally, it is by design the simplest and the one which could be implemented most easily.

From the previous calculations, it appears that the concentration in the biomass has drastic effects on the profitability for all considered processes. The concentration for which the net benefit is zero, will be defined as the breakeven concentration. For the four processes, the breakeven concentration was computed (Table 38).

Table 38: Minimum REE concentration in *D. linearis* biomass to achieve profitability (breakeven concentration)

Process	**Breakeven concentration (mg.g^{-1} ∑REEs)**
SULF	>3.89
ASH	2.65
SULF2	2.69
ASH2	2.08

These values can be used as a basis for targeting *D. linearis* populations that will yield profitable bio-ores (biomass or ash). Selective breeding and agricultural practices should be implemented to ensure that the threshold value of *ca.* 2 mg.g^{-1} ∑REEs is exceeded. Below this threshold, extracting REEs with the proposed processes is expected to result in net deficits.

Nevertheless, these values are only valid for *D. linearis*, or any plant with the same typical REE composition (with appreciable proportions of La, Nd, Pr, and Dy). This composition may vary depending on the REEs available to the plant. Additionally, they should be used only as a regional guideline values as they integrate current REO prices, power generation revenues, current reagents and commodities prices in China.

5.4 Partial conclusion

The objective of this chapter was to frame and study the viability of two recovery process from the hyperaccumulator plant *D. linearis* (ASH and SULF). After establishing the geographical and economic context of the process, mass balances were calculated on the basis of experimental values.

Waste production and reagent consumption were quantified based on the annual production of one hectare of land. Even though these process mass balance cannot fully represent the optimized pilot scale process, orders of magnitude in reagent consumption can be derived. It appeared necessary to emphasize the fact that the recovery process will generate waste and consume chemical reagents through the calculation of the E factor (Sheldon, 2017). As described, and without optimizations, and excluding water consumptions, the ASH and SULF process generate 732 and 197 kilograms of waste per kilograms of produced REO, respectively. The E factor is not a commonly available metric for hydrometallurgical processes, and varies greatly depending on the process, target mineral, source, *etc*. To give orders of magnitude, the high pressure acid leaching process for nickel laterites (HPAL) generates up to 100 t of residue per ton of nickel extracted, at the Goro plant in New Caledonia (Ang, 2017). Meanwhile, the Bayer process generates 1 to 2.5 t of bauxite residue per ton of alumina produced (Paramguru *et al.*, 2004).

Hence, further improvements of the developed processes are required, and recycling loops and reagent substitution have been proposed for their implementation. Converting a process waste into a reusable product (*e.g.*, treated acidic biomass to compostable matter) is another way to reduce process impact.

The mass balances having been established, it was possible to calculate the operating costs of the process. It appeared that some reagents could be replaced by cheaper ones, to minimize the economic costs. The two processes proposed (SULF and ASH) were examined, as well as their economic variations (SULF2 and ASH2), to determine their viability. It was concluded that the ASH2 process, is the most economical thanks to the energy generation the combustion step provides. The associated income could reach up to 500 USD.ha.y^{-1}, and 121 USD.ha.y^{-1} with the process costs deduced.

Finally, the influence of the total REE concentration in the biomass was determined to be a fundamental parameter for process profitability. For *D. linearis*, it was demonstrated that a concentration below 2 mg.g^{-1} ∑REEs will result in uneconomic bio-ores, regardless of the considered process. Oppositely, concentrations *ca.* 3.9 mg.g^{-1} will give a profitable recovery process and should be sought. Such concentrations have been previously observed and even higher values have been measured (up to 7 mg.g^{-1}, (Shan *et al.*, 2003)), confirming that the optimistic scenario is realistic.

Active revegetation of abandoned mine tailings using *D. linearis* is the next step to measure the requirements of soil amendments and labor needed for planting and harvesting. We hope that this study can constitute a basis for the implementation of a pilot-scale unit, to further develop process improvements and demonstrate feasibility at field scale.

5.5 References

Ang, C.A., 2017. Green Processing and Waste Valorization: Sulfur Removal and Hematite Recovery from High Pressure Acid Leach Residue for Steelmaking (MSc thesis). University of Toronto.

Chour, Z., Laubie, B., Morel, J.L., Tang, Y., Qiu, R., Simonnot, M.-O., Muhr, L., 2018. Recovery of rare earth elements from *Dicranopteris dichotoma* by an enhanced ion exchange leaching process. Chem. Eng. Process. - Process Intensif. 130, 208–213. https://doi.org/10.1016/j.cep.2018.06.007

Chour, Z., Laubie, B., Morel, J.L., Tang, Y.T., Simonnot, M.O., Muhr, L., 2020. Basis for a new process for producing REE oxides from *Dicranopteris linearis*. J. Environ. Chem. Eng. 103961. https://doi.org/10.1016/j.jece.2020.103961

Global Economic Data, Indicators, Charts & Forecasts | CEIC [WWW Document]. URL https://www.ceicdata.com/en (accessed 12.8.21).

Habashi, F., 2016. A Hundred Years of the Bayer Process for Alumina Production, in: Donaldson, D., Raahauge, B.E. (Eds.), Essential Readings in Light Metals. Springer International Publishing, Cham, pp. 85–93. https://doi.org/10.1007/978-3-319-48176-0_12

Habashi, F., 2013. Extractive metallurgy of rare earths. Can. Metall. Q. 52, 224–233. https://doi.org/10.1179/1879139513Y.0000000081

Paramguru, R.K., Rath, P.C., Misra, V.N., 2004. Trends in Red Mud Utilization – a Review. Miner. Process. Extr. Metall. Rev. 26, 1–29. https://doi.org/10.1080/08827500490477603

Peng, H., Vaughan, J., 2018. Aluminate effect on desilication product phase transformation. J. Cryst. Growth 492, 84–91. https://doi.org/10.1016/j.jcrysgro.2018.04.013

Rumble, J.R., 2019. CRC handbook of chemistry and physics: a ready-reference book of chemical and physical data. CRC Press, Boca Raton, Fla.

Shan, X., Wang, H., Zhang, S., Zhou, H., Zheng, Y., Yu, H., Wen, B., 2003. Accumulation and uptake of light rare earth elements in a hyperaccumulator *Dicranopteris dichotoma*. Plant Sci. 165, 1343–1353. https://doi.org/10.1016/S0168-9452(03)00361-3

Sheldon, R.A., 2017. The E factor 25 years on: the rise of green chemistry and sustainability. Green Chem. 19, 18–43. https://doi.org/10.1039/C6GC02157C

Sheldon, R.A., 1992. Organic synthesis; past, present and future. Chem. Ind. 903–906.

Vaughan, J., Peng, H., Seneviratne, D., Hodge, H., Hawker, W., Hayes, P., Staker, W., 2019. The Sandy Desilication Product Process Concept. JOM 71, 2928–2935. https://doi.org/10.1007/s11837-019-03617-2

Whittington, B.I., 1996. The chemistry of CaO and $Ca(OH)_2$ relating to the Bayer process. Hydrometallurgy 43, 13–35. https://doi.org/10.1016/0304-386X(96)00009-6

Conclusion

The objectives of the thesis, set forth in the introduction have been attained. Firstly, RE agromining in a context of mine tailings restoration was determined to be feasible, as profits emerge from the production of RE compounds. Biomass combustion to recover energy, is primarily important to maximize profits, and minimize the waste produced.

A new transformation process was designed, that factored in the specificity of the biomass ash (Figure 84). The ASH recovery process overcomes the stability the aluminosilicate glass matrix, and yields a marketable compound of high purity (>99.5 %).

At the same time, diminution of the reagents required was put into practice, and further improvements were identified for the pilot scale. Previously developed processes were considered, as the SULF process was evaluated in terms of waste produced per unit of product (E factor) and economic viability.

To date, it appears that the best plant candidate is *D. linearis*. In comparison to *P. americana*, the fern entails many favorable features, among which its pioneer characteristic and higher metal yield (up to 12 $kg_{REEs}.ha.y^{-1}$). In regards to current market price, the potential income could reach up to 385 $USD.ha.y^{-1}$, thanks to the high prices of Nd and Pr. Additionally, low N, Cl, and S content as well as appreciable calorific value (19 $MJ.kg^{-1}$) make it suitable for energy recovery through combustion.

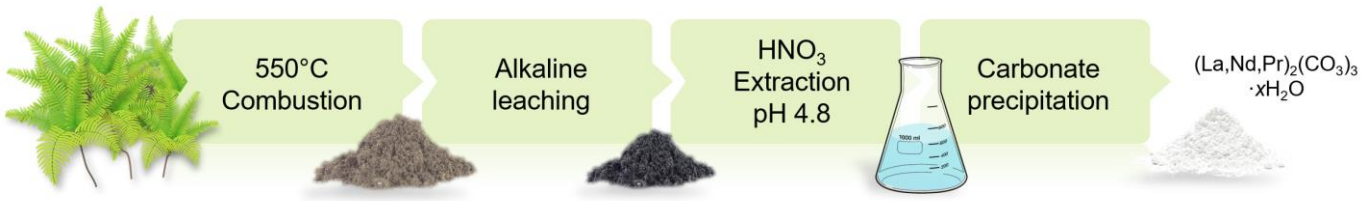

Figure 84: Process developed in this thesis for the recovery of REEs from *D. linearis* ash

The scientific questions established for this work were answered. By means of experimentation, a novel process was designed. A mass balance approach, combined with an economic study, permitted to render two recovery processes more efficient and determined them to be economically viable.

The processing of *D. linearis* ash, did initially appear as a hindrance to the recovery of REEs. However, the integration of heat recovery, in combination with the production of a high-purity compound, makes it a more efficient (lower E factor) and more economic than the processing of dry biomass.

For the selected processes, **the concentration of REEs appeared as the most crucial criterion**, which dictates the viability. A minimal concentration was established to be around 2.1 $mg.g^{-1}$ ∑REEs. This criterion could be altered, depending on the raw material to be processed, as it is based on a typical RE repartition for *D. linearis*. The criterion would be higher if less valuable elements make most of the RE content (*e.g.*, La, Ce, Y). For *D. linearis*, it provides a guiding value to select individuals, and orients cultural practices towards a tangible objective.

This value constitutes a first point of vigilance, but a second vigilance point has been identified. **If possible, candidate hyperaccumulator species should avoid to co-accumulate Al in their aerial parts.** The consumption of reagent (primarily soda) and the purity of the final product are at stake. Taking into account the Al/REEs molar ratio is a new criterion that could shuffle the search for new candidate plants, or guide cultivation practices.

This thesis has demonstrated the importance of the characterization of a complex matrix. Indeed, if the target elements to be extracted are crucial, knowledge of the elements and phases constituting the matrix (99% of the raw material) is just as important. This knowledge allows us to find adapted processes, even when the precise speciation of the target elements is unknown.

This thesis also showed that **finding and identifying the impurities having a chemistry comparable to the target elements (here Al) was essential**. Their early separation permitted to avoid either: the use of expensive selective reagents (oxalate), or a supplementary downstream separation. The early identification of aluminum as a problematic impurity has indeed allowed to obtain high-purity compounds, without having to use a selective reagent (carbonate instead of oxalate).

The use of thermodynamic calculations with an extended database has proven to be a good way to understand the chemistry of concentrated and multi-constituent aqueous solutions (often more than a dozen elements). The precipitation reactions play a determining role and often yield amorphous and arduously identifiable products (large number of elements in presence, X-ray diffractogram difficult to interpret). This approach finds its limits on kinetic aspects which can play a crucial role. Two other notable limitations are the incompleteness of the databases, especially at temperatures different from 25 °C, and the validity of the solvent interaction theory models (used in this thesis) in concentrated solutions (*i.e.*, for $I \geq 1$ M).

In order to quickly lead to the production of a marketable RE-compound, the separation of REEs from each other was not considered during this thesis. As underlined in the literature review, this separation implies advanced separation processes with important investment and size (hundreds of liquid-liquid extraction cells, ion exchange columns of several meters). Nevertheless, **the separation of Ce from other REEs by oxidation of the latter during the extraction phase constitutes a certain progress**. The latter being not economically interesting, the final compound is enriched in the other REEs. Conversely, Ce is concentrated in the final residue, which can either be recovered via an additional process.

For the separation of REEs in the context of agromining, only an approach compatible with small scales can be considered. Emerging modular and compact solutions such as liquid-liquid extraction in milli- or even micro- fluidic (decanter mixer, milli-column) could be part of the solution in the future.

The use of liquid-liquid extraction for ash treatment was not considered for the selective recovery of REEs. There are two reasons for this choice: the use of an organic phase (diluent + extractant) generally involves the use of a hazardous alkylated diluent (typically kerosene in the industry), to allow the solubilization of the extractant, which is often dangerous (tri-butyl phosphate, TBP). The second reason was the assumption that the extractant could not recover the REEs from the amorphous glassy matrix of *D. linearis* ash. As for *P. americana*, the orders of magnitude of REEs concentration in the extracts (8 $mg.L^{-1}$ REEs maximum) were arbitrarily considered too low, a choice which can be discussed.

In a broader context, **this work opens the perspectives of agromining in general**, by proposing concrete solutions and approaches **to address potentially problematic elements** (or elements of interest, depending on the perspective) **such as Al and Si**. Indeed, they have received little attention in the field of agromining. In the event that new hyperaccumulator plants are discovered, of REEs or other elements of interest, the knowledge provided by this thesis could be valorized once again.

Moreover, Al take the same absorption pathways in plants as REEs. Hence, the separation approach proposed here will be benefit for the recovery of REEs from newly discovered hyperaccumulating species.

At present, the Chinese ion-adsorption tailings are a unique opportunity for agromining, because large surface areas are available, REEs are dilute, and most importantly, a large fraction of them are accessible to the plant thanks to the nature of the deposit (adsorbed REEs, acidic soils). Nonetheless, areas in Europe, or in other parts of the world, matching these criteria may not yet have been sufficiently researched.

To conclude, **the approach developed here for either ash, or biomaterial, can find echoes for application to other type of matrices**. The recovery of critical elements in dilute and complex matrices is a recurring challenge for circular economy, in a world where the amount of waste produced keeps increasing while natural resources keep depleting.

Perspectives

On another aspect, convincing field trials need to be conducted to produce the expected biomass. As pointed out in this study, **agronomic challenges also need to be addressed** regarding *D. linearis*. Finding the right strategy for its implantation and multiplication will be a crucial task. Another challenge will reside in finding the best amendment additions (type, quantities) to maximize biomass growth and REE accumulation, while minimizing cultivation costs.

Increasing foliar concentration in known REEs accumulator (*e.g.*, *P. americana*), is a necessary step to bridge the gap of process viability. The foliar concentration value of 2 $mg.g^{-1}$ ∑REEs can serve as a tangible objective to promote accumulation (via amendments, and/or chelating agents), or to select plant individuals.

Regarding separation processes, scientific perspectives reside in the effects of upscaling. For example, keeping a constant quality of ash could be a challenge: unburnt material will bring unnecessary mass and carbon to the alkaline leaching step, resulting in avoidable soda loss. Careful design of the furnace is required to allow for energy recovery, good ash quality, and fly ash collection. Advances from nickel hyperaccumulator ashing should be mobilized as similar challenges are addressed.

Specifically for *D. linearis* ash processing, dealing with large amounts of hydrophobic and voluminous ash (0.05 $g.cm^{-3}$) is a predictable challenge. Indeed, if the ash was to be compacted (for easier transportation and handling and safety), the counterpart would be in a loss of reactivity. Furthermore, in the extraction step, requires a fine control of the pH. This is easily done at the lab scale, but maintaining a constant pH in larger tank with a precision of ± 0.1 could be problematic. Reliable

measurements, precise acid-additions, and homogenous mixing, are minimum requirements, otherwise, the purity of the product could be compromised.

Alternatively, for the SULF process, mass-transfer issues, filters clogging, and scaling due to Si gelification are anticipated hindrances. The co-extraction of organics has also to be considered: actions may be necessary to keep them from being a nuisance to the process, or to recover them as co-products.

Once a demonstrating platform has been built, a deep environmental evaluation could be performed to further legitimate (or disprove) the usefulness of process. **Among the available tools, the life cycle assessment could prove useful, to consider the variety of the services provided by agromining.** The study should consider at least, (i**)** revegetation of the surfaces (limiting erosion, among other ecosystemic services), (ii) energy production, and (iii) production of RE compounds via one process or another (ASH or SULF).

A possible reference scenario providing the same functions, could involve revegetation with commercial herbs (as it currently done), energy biomass, or fiber producing biomass (i). All those scenarios must then be completed by the production of heat (ii), and the production of RE compounds (iii), either from the leftover tailings, or from unmined deposits (by in-situ leaching). It is requisite that the three aspects are covered before comparing to the agromining scenarios which provides them all (Pons *et al.*, 2021).

As indicators, it is suggested to consider at least : primary energy consumed and greenhouse gas emissions (for the energetic aspects), eutrophication (in situ mining entails unavoidable loss of ammonium sulfate in the environment), acidification (combustion), ecotoxicity and human (process reagents and waste), erosion and land-use, and natural resource depletion.

Before assessment, the RE agromining processes must gain maturity to be compared with fully developed and optimized industrial process, both in terms of agronomic practices and the recycling performance of the recovery processes.

The processes described in this thesis, should not refrain research to develop new pathways to treat RE hyperaccumulators differently. For example, processing the plants with biodegrading micro-organisms may address the issue of the acid consumption costs. Indeed, the plant provides all the nutriments required for its own decomposition. With the help of selected communities, a decomposition of the plant in a slightly acidic medium could yield a low-cost leachate, rich in REEs.

Directly marketable and conventional compounds (carbonate, oxalate) were chosen as targets, to provide a realistic process in a limited time frame. However, if applications are to be found for other types of RE concentrates, new processes could be designed. For example, the pyrolysis product of *D. linearis* is a char-rich and reducing agent (Mai *et al.*, 2019). The presence of REEs in such a product could also be useful for catalytic purposes.

To concretize the economic values of the plants, new application can be found or sought. As an illustration, if not considered for the recovery of REEs, the ash of *Phytolacca americana* produced at 900 °C, seems a promising source of easily extractable Mn.

In the same perspective, the ash of the fern could constitute an alternative source of Si. Current trends in SiO_2 recovery from biomass ash involve an alkaline leaching with NaOH, followed by neutralization with a strong acid to precipitate the silica gel (Kalapathy *et al.*, 2000; Yang, 1992). Further acidification could result in the solubilization of the impurities (Al, Mn, Pb). If this process requires experimental work and evaluation, the recovery of SiO_2 appears totally feasible.

At the time being, different degrees of maturity have been attained depending on the element considered for agromining. Recovery processes have been developed for a certain number of elements with the main ones being Ni, Zn, Mn, Au, Cu, Cd, As (Jally *et al.*, 2021). Among all of them, Ni agromining remains the most advanced one thanks to large surface areas cultivated in several parts of the world, and hence important volumes of Ni-rich biomass have been produced and harvested. The high concentration of Ni in the aerial parts (1 to 2 wt.%) seems to be a driver for the development and implementation of the processes in comparison to other elements (generally inferior than 1 wt%).

The development of several cost-effective recovery processes from HAs adds credibility to RE agromining. Improvement of those processes via reagent and solution recycling is the key to further success. Process engineering challenges now need to be addressed at the pilot scale in order to further decrease the amount of reagent used. The sobriety of the processes will chiefly determine the social acceptability of agromining, in a context where the mineral processing industry has left visible environmental impacts.

The implementation of the recovery processes could also be completed by other products from the circular economy. The treatment of similar materials can be envisaged (*e.g.*, coal fly ash): by diversifying the raw materials processed, the production unit could gain in robustness and viability.

The integration of Si recovery appears as an interesting perspective: indeed, it is a recurrent element in the plants. It could even be implemented for Ni hyperaccumulators, after Ni has been extracted from the ash. **The recovery of every component of the plant** (heat, main elements, and metallic elements) should be the most relevant strategy to make the most of the efforts deployed to cultivate and harvest biomass, while minimizing waste issued from biomass itself.

Finally, little attention has been paid to the addition of reagents prior to the combustion step. We have seen that the presence of Mn and K renders the ash of *P. americana* leaves very reactive. What if the mineralogy of the ash of an hyperaccumulator could be changed by addition of a reagent prior to combustion? **Suitable additives must be found in order to render the target elements easily extractable, and conversely unwanted elements more stable.** Addition of other plants (not mandatorily HAs) could help supplement the unit for energetic production, and at the same time shift the ash mineralogy towards a desired composition. Mixing hyperaccumulators of the same element could even mitigate dilution.

Until recently, the study of biomass ash has been passive, considering it only as a by-product of thermal plants, and trying to find a use for them. The diversity and complexity of the phases encountered have since been seen as an obstacle to their valorization - or landfilling. **However, for the agrominer they are an opportunity to, once more, shift paradigms.**

References

Jally, B., Laubie, B., Tang, Y.-T., Simonnot, M.-O., 2021. Processing of Plants to Products: Gold, REEs and Other Elements, in: van der Ent, A., Baker, A.J.M., Echevarria, G., Simonnot, M.-O., Morel, J.L. (Eds.), Agromining: Farming for Metals. Springer International Publishing, Cham, pp. 63–74. https://doi.org/10.1007/978-3-030-58904-2_4

Kalapathy, U., Proctor, A., Shultz, J., 2000. A simple method for production of pure silica from rice hull ash. Bioresour. Technol. 73, 257–262. https://doi.org/10.1016/S0960-8524(99)00127-3

Mai, N.T., Nguyen, N.H., Tsubota, T., Shinogi, Y., Dultz, S., Nguyen, M.N., 2019. Fern *Dicranopteris linearis*-derived biochars: Adjusting surface properties by direct processing of the silica phase. Colloids Surf. Physicochem. Eng. Asp. 583, 123937. https://doi.org/10.1016/j.colsurfa.2019.123937

Pons, M.-N., Rodrigues, J., Simonnot, M.-O., 2021. Life Cycle Assessment and Ecosystem Services of Agromining, in: van der Ent, A., Baker, A.J.M., Echevarria, G., Simonnot, M.-O., Morel, J.L. (Eds.), Agromining: Farming for Metals. Springer International Publishing, Cham, pp. 75–98. https://doi.org/10.1007/978-3-030-58904-2_5

Yang, X., 1992. The method of extraction of highly pure silica in the rice husk. CN1063087A.

Annexes

I. Trace and major element concentration in cultivated shoots: leaves

Bulk name	PA_G_1	PA_G_3	PA_Pots_1	PA_Pots_2	PA_Pots_3	PA_Hy_1
Type	Garden-Leaves	Garden-Leaves	Spiked pots-Leaves	Spiked pots-Leaves	Spiked pots-Leaves	Hydroponics -Leaves
	REEs concentrations (mg.g^{-1}) *Indicative: QL was 0.05 mg.g^{-1} ; DL was 0.005 mg.g^{-1}*					
La	< LD	< LD	<LD	0.007 ± 0.001	< LD	0.007 ± 0.004
Ce	< DL	0.040 ± 0.017	0.023 ± 0.038	0.026 ± 0.014	0.047 ± 0.009	< LD
Pr	< LD	< LD	< LD	< LD	< LD	< LD
Nd	< LD	< LD	< LD	< LD	< LD	0.012 ± 0.004
Sm	< LD	< LD	0.013 ± 0.001	0.007 ± 0.001	< LD	< LD
Gd	< LD	< LD	< LD	0.006 ± 0.001	< LD	< LD
Dy	< LD	< LD	< LD	< LD	< LD	< LD
Y	< LD	< LD	< LD	< LD	< LD	0.017 ± 0.005
	Trace and common elements concentrations (mg.g^{-1}) *QL was 0.5 mg.g^{-1} ; DL was 0.05 mg.g^{-1}*					
Al	0.51 ± 0.06	0.44 ± 0.06	0.88 ± 0.10	0.45 ± 0.05	0.39 ± 0.12	0.10 ± 0.03
Ca	20.79 ± 0.12	24.50 ± 0.97	29.81 ± 0.20	18.33 ± 0.39	29.18 ± 0.62	6.49 ± 0.85
Fe	*0.22 ± 0.01*	*0.15 ± 0.01*	0.59 ± 0.02	*0.25 ± 0.02*	*0.15 ± 0.00*	*0.10 ± 0.12*
K	48.84 ± 0.83	69.36 ± 1.73	29.01 ± 0.45	41.72 ± 0.30	38.59 ± 0.48	24.82 ± 3.27
Mg	14.72 ± 0.28	14.12 ± 0.28	6.40 ± 0.05	10.19 ± 0.09	18.24 ± 0.47	4.87 ± 0.31
Mn	*0.19 ± 0.01*	*0.24 ± 0.01*	*0.19 ± 0.00*	*0.13 ± 0.00*	*0.13 ± 0.01*	*0.08 ± 0.01*
Na	1.91 ± 0.20	2.70 ± 0.13	1.68 ± 0.38	3.45 ± 0.10	2.65 ± 0.35	2.61 ± 0.48
P	2.68 ± 0.03	2.17 ± 0.04	3.68 ± 0.05	3.75 ± 0.02	1.20 ± 0.02	1.30 ± 0.34
S	5.02 ± 0.25	*0.40 ± 0.28*	3.84 ± 0.30	< LD	< LD	< LD
Si	0.97 ± 0.09	0.82 ± 0.03	1.15 ± 0.15	1.10 ± 0.01	0.72 ± 0.08	0.34 ± 0.07
Zn	*0.09 ± 0.02*	< LD	< LD	< LD	< LD	< LD

II. X-Ray powder diffraction of *P. americana* ash

Diffractogram of the ash of *P. americana* leaves, produced at 550°C. Baseline corrected. The main identified phase is Fairchildite ($K_2Ca(CO_3)_2$) (red peaks)

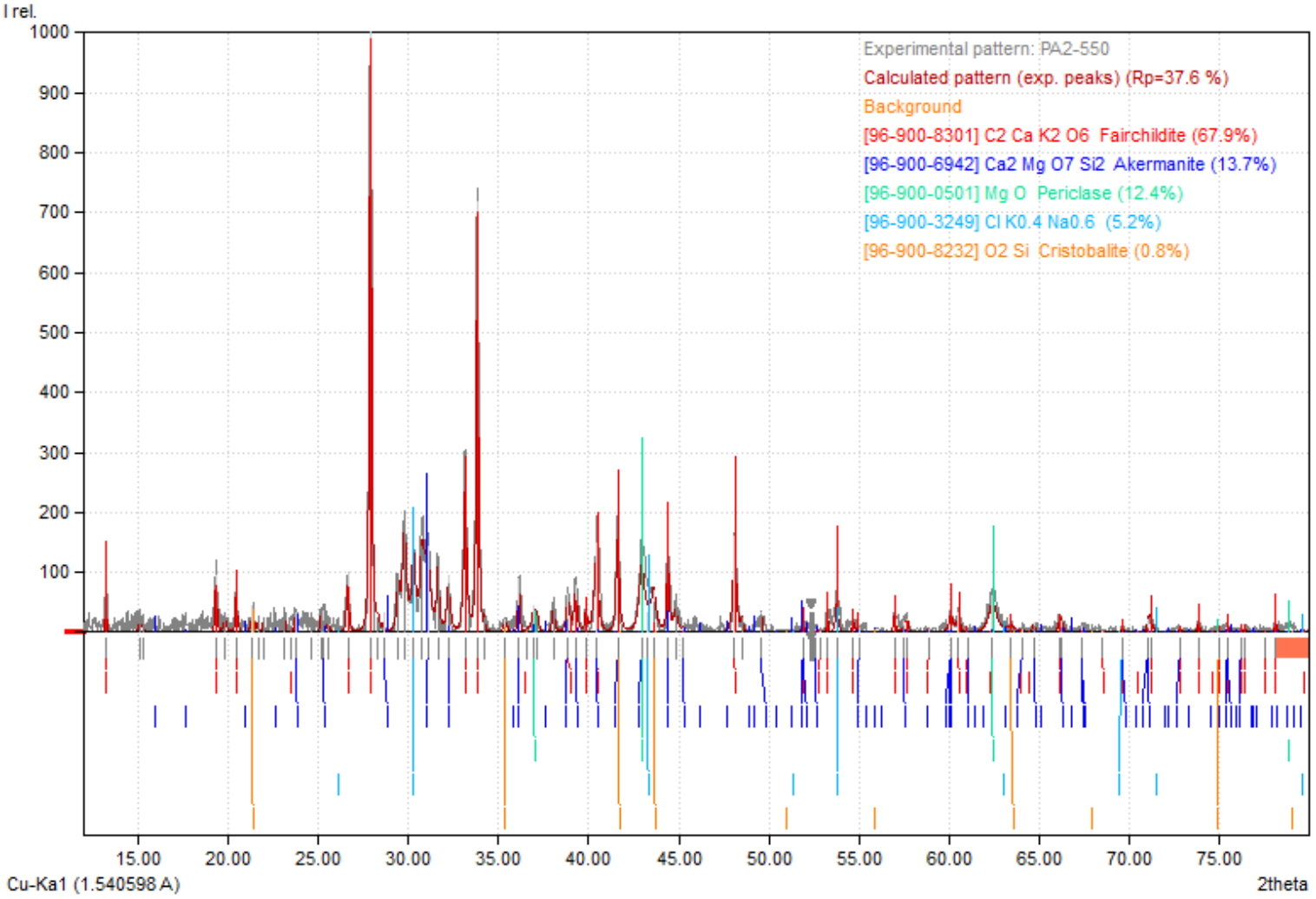

Diffractogram of the ash of *P. americana* leaves, produced at 900°C. The main phase remains unidentified (blue peaks)